STUDIES ON DYNAMICS OF THE EQUATORIAL IONOSPHERE

A Thesis
Submitted For the Degree of
Doctor of Philosophy in the Faculty of Science
BANGALORE UNIVERSITY

By

K.B.RAMESH

INDIAN INSTITUTE OF ASTROPHYSICS
BANGALORE - 560034
INDIA

MARCH 1994

DECLARATION

I hereby declare that the matter contained in this thesis is the result of the investigations carried out by me in Indian Institute of Astrophysics, Bangalore under the supervision of Prof. J. Hanumath Sastri. This work has not been submitted for the award of any degree, Diploma, Associateship, Fellowship, etc., of any university or institute.

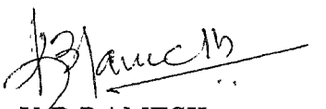

K.B.RAMESH
Candidate

Prof. J. Hanumath Sastri
Research Supervisor

Bangalore - 560034
Date :

ACKNOWLEDGMENTS

It has been a great pleasure and inspiration to have had Prof. J. Hanumath Sastri as my research guide. I am greatly indebted to him for introducing me to the field of Solar-Terrestrial Physics and for orienting my career towards the academic line. His timely suggestions not only in the scientific work but also in the normal course of life stimulated me to carry out this work with him. This thesis would not have been possible without his constant encouragement and invaluable guidance.

I thankfully acknowledge the keen interest shown by Prof. B. C. Chandrasekhara, Prof. N. G. Puttaswamy, and Prof. K. H. Chennappa in the progress of the work. I am grateful to Prof. J.C. Bhattacharyya for his kind encouragement and for allowing me to carry out the thesis work as a part of the research work of the institute. I thank Prof. Ramnath Cowsik, Director, Indian Institute of Astrophysics for providing an excellent environment for research activities in Solar-Terrestrial Physics.

I am grateful to Dr. C. Raghava Reddy, Space Physics Laboratory, Vikram Sarabhai Space Centre, Trivandrum, for useful discussions in the experimental aspects of this thesis work. Grateful thanks are due to Prof. D. R. K. Rao, Indian Institute of Geomagnetism, Bombay, and Dr. V. V. Somayajulu, Space Physics Laboratory, Vikram Sarabhai Space Centre, Trivandrum, for providing the geomagnetic micropulsation data and the VHF backscatter radar data of electrojet irregularities respectively used in the thesis.

The contribution of Mr. J. V. S. Visveswara Rao in acquiring the phase path data which forms a major portion of the work reported in this thesis, is thankfully acknowledged. I had many useful discussions with Mr. H. N. Ranganath Rao. I am extremely thankful to Mr. D. Karunakaran and Mr. K. Sasidharan for introducing me to the ionogram and magnetogram data of Kodaikanal. I thank Mr. S. Ganeshan for his assistance during observations and for digitizing the data and Miss. M. Kasturi Bai for keying in the digitized data on to a storage memory.

My sincere thanks are due to Mr. Baba Verghese for his help in various stages of the programming work and in the text processing during the preparation of the thesis. I take this opportunity to thank Drs. Rangarajan, Mohan Rao, and Mr. Srinivasa Rao for their cheerful encouragement. I thank Dr. R. Kariyappa for his help in university formalities.

I am extremely thankful to Mr. J. S. Nathan for providing the necessary help in the computer center and to Dr. R. Srinivasan and Mr. A.V. Ananth for providing the full time computing facility. Mr. S. S. Gupta, Mr. P. S. M. Aleem and Mr. K. Sundararaman have provided the necessary help during my visits to Kodaikanal. The library facilities provided by Mrs. A. Vagiswari, Mr. H. N. Manjunath and Ms. Christina Louis is thankfully acknowledged. The draughtsmanship of Mr. S. Muthukrishnan can be seen in many of the complicated diagrams. A part of the thesis is typed by Mr. N. Valsalan. Mr. P. N. Prabhakara made xerox copies of the thesis. Mr. D. Kanakaraj bound the copies of the thesis. My thanks are due to all of them.

I extend my sincere thanks to my colleagues in the institute who have helped me in many ways during the course of this thesis work.

Thanks are due to my brother Mr. K. B. Raghavendra Rao for preparing some of the diagrams through "ORCAD" software and for providing necessary support in the day-to-day family affairs during the course of this work. I extend my gratitude to my parents and to every one of my family members for their encouragement.

Simple words cannot express the understanding and cooperation extended by my wife Smt.Bhagya Lakshmi and daughter Shruthi. They deserve a special mention of thanks for their patience and for sacrificing their precious time.

Preface

This thesis focuses on the dynamical behaviour of the equatorial F-region with particular reference to the vertical drifts and its temporal fine structure. Vertical drifts are important in understanding the dynamics of the ionospheric F-region in the vicinity of the dip equator because of the orthogonally oriented zonal electric and earths magnetic field there that cause the vertical drifts. Variation in the vertical drift can be caused by perturbations in electric or magnetic fields or in both. Studies on perturbations in the zonal electric fields, the data of which when analysed in conjunction with the other parameters such as auroral electrojet indices (AE) will give an insight into the magnetosphere-ionosphere coupling processes. Once acquired on large scale the vertical drift data will provide the understanding of its morphological features.

The plan is to identify the physical of processes that cause the small scale structures in the equatorial F-region vertical plasma drifts and to understand the perturbations in vertical drifts that occur in association with magnetospheric substorms. The HF phase path sounder (Doppler radar) is a resourceful groundbased experiment for studying the dynamical behaviour of the ionospheric regions. The author had participated in the installation of the phase path sounder and in the observations. He also made major contributions to the augmentation of the system for multi- height/ multi-frequency recordings and developed the software required for off-line processing of the data on main frame computers such as Mighty Frame II, VAX-11/780. The present thesis is based on data from the phase path sounder experiment and also from the ionosonde. Both these experiments are operated at the equatorial station, Kodaikanal (Dip 3°N) in the Indian equatorial zone.

The thesis consists of six chapters. The present day understanding of some of the F-region processes relevant to the thesis is presented briefly in the first chapter. The details of the phase path sounder experiment, the system design, observational procedure and the method of analysis are presented in the second chapter. The results of the studies made on the basis of the data obtained from the above mentioned experiments in respect of the dynamics of the equatorial

F-region are presented in the 3^{rd}, 4^{th} and 5^{th} chapters. A summary of the results obtained from the present work and the scope for further investigations are presented in the sixth chapter.

This thesis is an outcome of the research work carried out in the area of Solar-Terrestrial Physics at Indian Institute of Astrophysics, Bangalore, India.

LIST OF PUBLICATIONS

1. Doppler frequency fluctuations of lower thermospheric reflections in the equatorial electrojet region, J. H. Sastri, K. B. Ramesh, and J. V. S. V. Rao, **Journal of Atmospheric and Terrestrial Physics, 53, 567-576, 1991.**

2. Origin of short-period (30-300s) Doppler frequency fluctuations of lower F-region echoes in the electrojet region, J. H. Sastri, K. B. Ramesh, V. V. Somayajulu, and J. V. S. V. Rao, **Radio Science, 26, 1403-1413, 1991.**

3. On the nature of substorm- related transient electric field disturbances in the equatorial ionosphere, J. H. Sastri, K. B. Ramesh, and D.Karunakaran, **Planetary Space Science, 40, 95-103, 1992.**

4. Oscillations in F-region Doppler velocity in the dip equatorial region associated with ULF geomagnetic pulsations, J. H. Sastri, K. B. Ramesh, D. R. K. Rao, and J. V. S. V. Rao, **Journal of Atmospheric and Terrestrial Physics, 55, 1271-1276, 1993.**

5. Vertical plasma drifts of nighttime F-region near geomagnetic equator, J. H. Sastri, K. B. Ramesh, and J.V.S.V. Rao, **Proc. 1992 STEP symposium/ COSPAR colloquim No. 5 (ed. M. Teague)** - 1993 (in press).

6. Solar cycle and seasonal variations in F-region vertical drifts over Kodaikanal (Dip 3°N), India, K. B. Ramesh, and J.H. Sastri, Submitted (in January 1994) to **Annales Geophysicae.**

CONTENTS

CHAPTER 1

INTRODUCTION

1.1. THE EARTH'S ATMOSPHERE

The Earth's atmosphere is classified into different regions based on temperature, composition and the dominant physical process. Fig.1.1 illustrates the regions of the atmosphere along with the typical daytime height profile of the neutral gas temperature, and variations of the density of the neutral atmospheric constituents and electron density. Based on the temperature gradient the atmosphere is classified into four main regions. Troposphere is the lowest part of the atmosphere in which the temperature decreases with altitude at $\sim$ 10°K/km upto about 15km. In the stratosphere $\sim$ 15-50 km from the groundlevel the temperature increases with height. This increase in temperature is due to the absorption of solar ultra-violet radiation by ozone with a maximum temperature of $\sim$ 220°K appearing at about 50km. The temperature again decreases with height in the mesosphere. The upper boundary of the mesosphere with a temperature of about 180°K at $\sim$ 80-85 km is the coldest part of the earth's atmosphere. The existence of the temperature minimum is due to the lack of any strong heating mechanism. The temperature again increases in the thermosphere. The high temperature in the thermosphere is due to the absorption of solar ultraviolet radiation from the Sun, while the increase in temperature with altitude above the mesopause is due to the downward molecular conduction of heat. Major heat loss occurs through radiation and transport processes. The neutral gas temperature in the thermosphere approaches an asymptotic value called the exospheric temperature of about 1000-2000°K at altitudes of about 400 km. The exosphere is the region above about 600km where the atmospheric particles follow ballistic trajectories. The atmosphere below about 100 km is relatively uniform in composition due to turbulent mixing and is termed as the homosphere. In the region above 100 km, called the heterosphere turbulence ceases and the distribution of the atmospheric constituents is controlled by molecular diffusion.

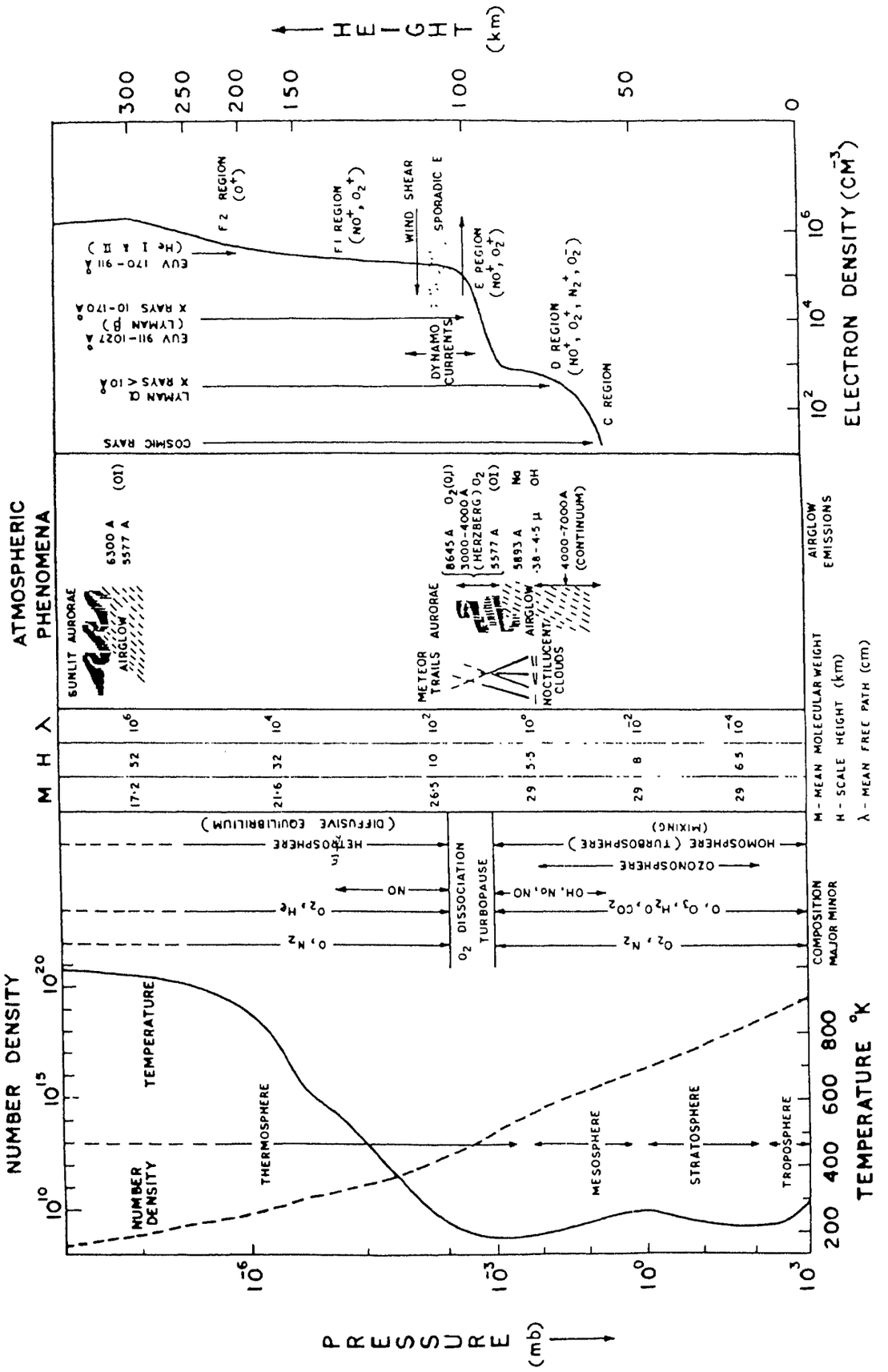

FIG 1·1 EARTH'S UPPER ATMOSPHERE

1.2. THE IONOSPHERE

The interference technique experiments of Appleton and Barnett (1925) and the pulse sounding experiments of Briet and Tuve (1926) proved the existence of a conducting layer in the Earth's upper atmosphere. The ionized region of the Earth's upper atmosphere, where the ions and electrons are present in sufficient quantities to affect the propagation of the radio waves is called the "ionosphere", the name coined by R. Watson-Watt in 1926. The source of ionization in the upper atmosphere is the highly energetic component of the solar electromagnetic radiation. Based on the physical and chemical processes at work the Earth's ionosphere is classified into three main regions; viz., D, E and F-regions. Lyman α, EUV, hard X-rays and cosmic rays are the major sources of D-region ionization. The D-region is the lower most part of the ionosphere and covers the altitude range of $\sim$ 60 to 90 km. The ionospheric E-region, in the altitude range of 90-140 km is formed by the solar EUV and X-rays. The F-region of the ionosphere starts from about 140km. EUV radiation from the Sun is the major source of F-region ionization. The electrons produced during the photoionization processes directly or indirectly combine with ions and a balance is established between the electron-ion pair production and loss processes. Ionized component of the upper atmosphere amounts to only 1% of the concentration of the total neutral gas and therefore constitutes only a weakly ionized plasma. Loss due to transport of ionization also contributes to the equilibrium conditions. The balance equation for the equilibrium electron/ion concentration is given by :

$$\frac{\partial N_{e,i}}{\partial t} = Q - L(N_{e,i}) - \nabla(N_{e,i}V) \tag{1.1}$$

where $N_{e,i}$ is electron/ion concentration, Q, L and V are rate of production of ionization, loss due to chemical processes and the mean drift velocity of the electrons/ions respectively.

The E-region also known as the dynamo region of the ionosphere is basically a chemistry dominated region. The peak of the ionization occurs around 105 km. The rate of electron loss is determined by the dissociative recombination process. E-region does not quite disappear at night. During nighttime the region remains weakly ionized with electron density of about 5 x $10^3/cm^3$ as against $10^5/cm^3$ by day. In the E-region the movement of electrons are governed by the geomagnetic field as their gyration frequency is higher than electron-neutral collision frequency, while the movement of ions is controlled by neutral winds as the ion-neutral collision frequency is higher than their gyration frequency.

Ionosondes have detected patches of ionization in the E-region at altitudes of 100 to 120 km and are termed as sporadic E (Es) layers. Wealth of information on Es is documented in the monograph "Ionospheric sporadic E" edited by Smith and Matsushita (1962). These layers are partially transparent to waves reflected from higher layers. By virtue of the mechanisms through which they form and their diurnal and seasonal behaviour, Es layers have been classified into three types namely 1) auroral 2) temperate and 3) equatorial kinds of sporadic E. Fig. 1.2 shows the occurrence probability of sporadic E against time of the day, and month of the year for the three latitude zones. Higher probability of occurrence of equatorial sporadic E (Esq) during daytime is attributed to the equatorial electrojet irregularities, a daytime phenomena at equatorial latitudes, while the temperate and high latitude types are attributed to the wind-shear mechanism and ionization arising from energetic particles respectively (see Rishbeth and Garriott, 1969).

The F-region of the ionosphere starts at about 150 km. The peak of the F-region occurs anywhere between 200 to 600 km. At these altitudes the movement of ions and electrons are governed by the geomagnetic field as their gyration frequencies are higher than their corresponding collision frequencies with neutral particles. The F region is formed mainly by the photoionization of the atomic oxygen.

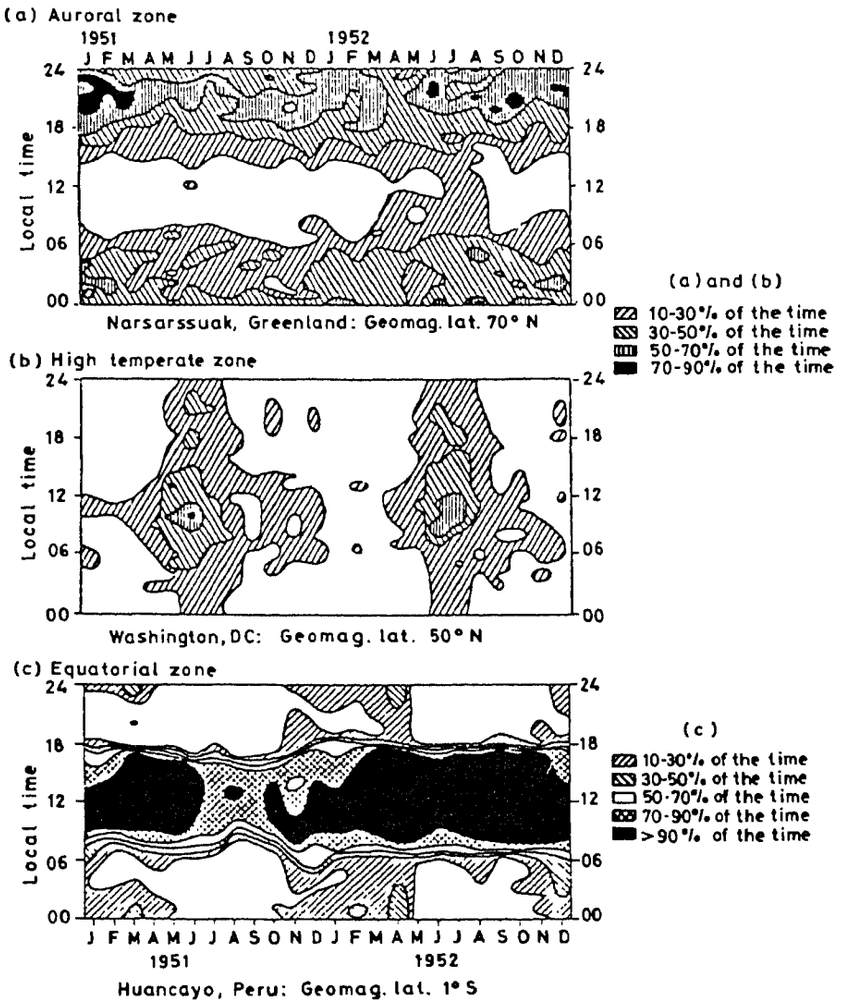

Fig.1.2. Diurnal and seasonal occurrence of three kinds of sporadic-E. (a) The auroral kind maxmizes at night but has no seasonal variation. (b) The temperate kind peaks near noon in summer. (c) The equatorial kind occurs mainly by day but shows no seasonal preference. (After E.K. Smith, NBS Circ. 582, 1957.)

$$O + h\nu \xrightarrow{\lambda = 150-796\ \mathring{A}} O^+ + e \qquad (1.2)$$

The major electron loss process in the F-region is not direct recombination but a two-stage process. In the first stage the O^+ ions exchange charge with molecules such as N_2 or O_2 and in the second stage the molecular ion dissociates by recombining with an electron. Since the molecular concentration is very low at higher altitudes (above F_2 peak) the vertical transport takes over as a dominant loss process over the chemical recombination process. The equilibrium level of F-region, therefore, occurs where the two loss processes are equally important. Since the transport processes are involved in determining the F-region peak, the F-region behaviour deviates from the classical Chapman theory. Plasma diffusion and drifts due to electric fields and neutral winds constitute the basic transport processes. The F-region is thus a dynamics dominated region of the ionosphere. Some important features of the dynamical behaviour of the F-region of the equatorial ionosphere relevant to the present study are presented briefly in the following sections.

1.3. GEOMAGNETIC FIELD VARIATIONS

As a first approximation the geomagnetic field above the earth's surface can be represented by a dipole field, the north and south poles of the dipole being at geographic co-ordinates 79°N, 70°W and 79°S, 70°E respectively. Due to the continuous flow of solar wind across the earth, the geomagnetic field gets confined to a cavity called "magnetosphere". Catastrophic changes seem to occur in the magnetosphere as well as the ionosphere when the north-south component of the interplanetary magnetic field (IMF B_z), which is 'frozen in' to the solar wind plasma, turns southward and merges with geomagnetic field on the day side. Some aspects of the geomagnetic field variations relevant to the present study are briefly described in the following.

1.3.1. Geomagnetic storms

The geomagnetic storm is, in short, a signature of the varying magnetospheric response to the varying conditions of interplanetary space which in turn are caused by the energetic particles emitted from the Sun. Geomagnetic storm often begins with a "sudden commencement". The arrival of the interplanetary discontinuity at the magnetopause causes the sudden compression of the geomagnetic field boundary, and the shock front first gets transmitted by means of hydromagnetic waves, and appears as a storm sudden commencement (ssc) in the H-component of Earth's magnetic field recorded at groundlevel. The rise time of H-value during ssc, which is of the order of 2-5 min, varies with local time of occurrence of ssc. The initial phase follows the ssc. In this phase the rise of H value usually persists for a few hours before it drops back to the pre-storm level. During the main phase the H-value dips down by several hundred gamma ($1\gamma = 10^{-9}$ tesla). This phase of the magnetic storm begins at about the time when the shock driven plasma reaches the magnetosphere. A part of the hot plasma is injected into the trapping region and forms the storm time proton belt constituting the ring current (D_{st}) while some energy is removed from the system in the polar and auroral regions (Auroral Electrojets). The magnetic effects of intense proton belt are seen as a decrease of the horizontal component of the geomagnetic field at low and middle latitudes. The recovery phase representing the gradual decay of the ring current to the pre-storm level follows the main phase in few tens of hours unless a fresh storm intervenes. Quiet time geomagnetic variations, disturbed day geomagnetic variations, morphological features of the geomagnetic storm and related phenomena are widely documented in the literature (see for example the review by Kane, 1976).

1.3.2. Substorms

The phenomenon of magnetospheric substorms is quite complicated. The concept of a violent magnetospheric process termed "substorm" was first introduced by Akasofu and Chapman (1961) while definitions of the time sequence of events associated with

the substorm are first introduced by Akasofu (1964). More refined definition of the magnetospheric substorm is given by Rostoker et al. (1980). A magnetospheric substorm is a transient process initiated on the nightside of the earth in which a significant amount of energy derived from solar wind-magnetosphere interactions is deposited in the auroral ionosphere and in the magnetosphere. Generally substorms occur within one hour after the reversal of the B_z component of the interplanetary magnetic field (IMF) from northward to southward. Beginning of the growth phase is marked by the merging of interplanetary and geomagnetic field lines following the southward turning of IMF B_z. During this phase weak auroral electrojets (predominantly westward electrojet) start appearing in the auroral region. The expansion phase is the interval of time in which the intensity of the auroral electrojets, from their pre-substorm level reaches its maximum. An intense negative (magnetic) bay appears in the midnight sector in the auroral region indicating an overhead westward electrojet which expands northward and westward with intense electron precipitation. A positive (magnetic) bay appears in low latitudes in the midnight sector. (Ijima and Nagata, 1972). In the evening sector of the auroral zone, an eastward electrojet may appear which slowly shifts equatorward. In the recovery phase the intensity of the auroral electrojets returns to pre-substorm level and this process is associated in general with the northward turning of IMF B_z. The southward component of the IMF is generally found to bear a direct and significant relationship with the geomagnetic substorm activity (e.g., Arnoldy, 1971; Foster et al., 1971). Cluster of substorms are generally associated with the main phase of a geomagnetic storm. However substorms do also occur in isolation.

1.3.3. Geomagnetic Pulsations

Another important aspect of the geomagnetic field variations relevant to the present work is the quasi-sinusiodal disturbance patterns that appear in the records of ground- level as well as satellite based magnetometers called the mocropulsations (e.g., Samson et al., 1971; Fukunishi and Lanzerotti, 1974; Cummings et al., 1971). Periodicities as small as 0.2 sec with amplitudes of about 10 mγ and as high as 5 min with

amplitudes of about 100 γ are detected with rapid-run magnetometers, induction coils and in the recordings of the electric currents induced in the ground by variations of the geomagnetic field. The geomagnetic micropulsations are attributed to the hydromagnetic waves (Ultra Low Frequency electromagnetic waves) resonating on geomagnetic field lines (Dungey, 1963). Most of the geomagnetic micropulsations are likely to be generated in the magnetosphere and in interplanetary space (Gul'yel'mi, 1974; Russell and Fleming, 1976). The international scheme of classification for regular or continuous (Pc) and irregular (Pi) micropulsations is reproduced in Table 1.1.

Table 1.1. Micropulsation Classification

Regular/Continuous Pulsations		Irregular Pulsations	
Type	Period Range (sec)	Type	Period Range (sec)
Pc1	0.2 - 5	Pi1	1 - 40
Pc2	5 - 10	Pi2	40 - 150
Pc3	10 - 45		
Pc4	45 - 150		
Pc5	150 - 600		

The regular pulsations are associated with magnetic bays during substorms. Many of these pulsations are similar at magnetically conjugate points, indicating that the magnetosphere is a major influence. Pc1 is attributed to bunches of particles, probably protons oscillating between conjugate points. Pc2-5 are usually explained as various oscillation modes within the magnetosphere. Pc5 is thought to be toroidal oscillation of the whole field line between conjugate points. These oscillations show opposite polarizations in the morning and the evening periods. Details of field line resonance structure of the pulsation signals have been studied theoretically (Southwood, 1974; Chen and Hasegawa, 1974). Several characteristics of the various Pc and Pi pulsations have been given by Orr (1973). The magnetospheric pulsations cause precipitation of electrons in the ionosphere which results in additional ionospheric currents giving micropulsations on the ground.

1.4. THE EQUATORIAL IONOSPHERE

The geomagnetic field configuration shows marked asymmetry at various geographic longitudes. This causes the magnetic dip equator to deviate from the geographic equator to assume a northward position in the Asian sector and southward position in the American sector (Fig. 1.3). The total field intensity in the equatorial region varies markedly between the two longitude sectors. The dynamics of the ionospheric F-region, with which we are mainly concerned, depends greatly on plasma transport due to diffusion along the geomagnetic field lines, electrodynamic drift and neutral winds effects. At equatorial latitudes the planetary scale east-west electric fields generated by the action of tidal winds in combination with the north-south geomagnetic field introduces phenomena such as equatorial electrojet, equatorial ionization anomaly and generation of plasma density irregularities which are unique characteristics of this region of the earth's near-space environment.

1.4.1. The Equatorial Electrojet

The horizontal wind system in the upper atmosphere forces the ions and electrons to move in the direction of the wind. At E-region altitudes the electron gyro frequency exceeds the electron-neutral collision frequency while ion-neutral collision frequency exceeds ion gyro frequency ($\omega_e > \nu_e, \omega_i < \nu_i$). Consequently the ions are carried along with the wind but the electrons move across the wind around geomagnetic field lines. The relative movement of the charges constitutes an electric current, and charge separation produces horizontal electric fields. In the system with electric fields perpendicular to the north-south geomagnetic field that prevails near the magnetic equator, Pedersen currents flow parallel to the component of electric field, and Hall currents in the direction perpendicular to the plane of both electric and magnetic fields. Since the ionosphere has layered structure, the flow of Hall currents above and below the dynamo region (80-140 km) is inhibited. Extreme case of inhibition occurs at the magnetic equator (Cowling, 1933; Martyn, 1948; Cowling and Borger, 1948; Baker & Martyn, 1953 and Sugiura &

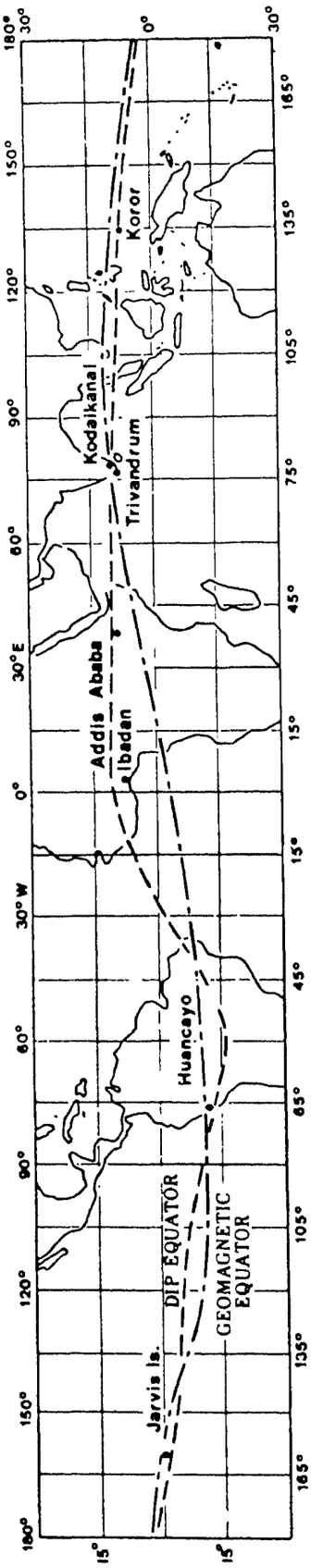

Fig.1.3. Location of geographic, geomagnetic, and dip equators and some of the equatorial magnetic observatories (Figure is from Gupta, 1973)

Cain, 1966) and this results in an enhanced conductivity called Cowling conductivity, parallel to the boundaries and normal to the magnetic field. Chapman (1951) named this ribbon-like enhanced east-west overhead current in the vicinity of the dip equator as "equatorial electrojet" (EEJ). The latitudinal extent of EEJ is about $\pm 3°$ around the dip equator (Knecht and McDuffie, 1962). Near the dip equator the east-west electric field is about 0.5 mV/m and the maximum vertical polarization field (at about 105 km) is of the order of 10-15 mV/m. The maximum east-west electron drift velocity is about 400-600m/s. The drift velocity is westward during day and eastward during night. Basic structure and morphological features of the equatorial electrojet are reviewed by Forbes (1981) and Raghavarao et al.(1988). Near the dip equator EEJ manifest itself as an abnormal increase in the range of the diurnal variation of the H-component of the geomagnetic field (Onwumechili, 1967 and references therein).

Several theoretical models of the equatorial electrojet have been developed and compared with observations. Sugiura and Poros (1969) investigated the longitudinal dependence of the equatorial electrojet due to variations in the main magnetic field and found the electrojet intensity and associated meridional currents to be strongest over Peru and weakest over India. Forbes and Lindzen (1976) investigated the local time, latitude and height structure of the electrojet by taking into account the realistic diurnal and semidiurnal tidal winds which are expected to be present in the electrojet region. Richmond et al. (1976) studied the mid-and low latitude electric field and currents generated by a combination of the diurnal trapped (1, -2) tidal mode modified by ion drag and of the upper propagating semidiurnal (2, 4) mode. Results of this model showed closer agreement with the low and mid-latitude drift data. A comprehensive review of the E-region dynamo theories is given by Richmond (1979). At times, the electrojet was found to reverse its direction giving rise to the phenomenon of "counter electrojet" (Gouin and Mayaud, 1967). CEJ events occur during the forenoon (0600 - 0800 hr LT) as well as in the afternoon hours (1400 - 1800 hr LT) with peak occurrence around 1500 hrs. These events with reverse or weak electric fields are shown to be

caused by semi-diurnal tidal winds, in particular of (2,2) mode with sufficiently high intensity (Takeda and Maeda 1980). Raghavarao and Anandarao (1980, 1987) have shown that a combination of vertical wind at the equator and a meridional wind with shear of opposite polarity on either side of the dip equator would lead to CEJ. Stenning (1989) further suggested that the antisymmetric semi-diurnal tides (solar and lunar) may be important in forming the CEJ on some occasions.

1.4.2. Electrojet Irregularities

Most of the information concerning the physics of the electrojet irregularities has come from the VHF radar measurements performed at the Jicamarca Radar Observatory, Lima, Peru. Rocket observations of electric field and electron density profiles at Thumba (76°56'E dip 0.6°S), India; Punta Lobos (dip 0.5°N), Peru; and Kwajalein Island (167.5°W, dip 8.4°N) have also provided valuable information on the electrojet irregularities (see review of Fejer and Kelley, 1980; Kelley, 1989). Theoretical studies also have contributed extensively to this field of research (see review by Farley, 1985). Some important results of both theoretical and experimental studies regarding electrojet irregularities are presented in the following paragraphs.

The equatorial E-region irregularities are closely associated with the global east-west electric field of dynamo origin which drives the electrojet. Plasma instabilities in the equatorial E-region are produced by the interaction of crossed electric (vertical Hall polarization field) and magnetic field with the vertical plasma gradient in the E-region. The irregularities which are field aligned are present during both day and night. VHF backscatter radar observations have shown the existence of two classes of irregularities, called Type I and Type II in the equatorial electrojet medium. At E-region altitudes electrons move freely under the influence of the geomagnetic field, where as the ions remain practically stationary when compared to electrons because of their collisions with neutrals. If the drift velocity of the electrons relative to ions exceeds the ion-acoustic velocity, the two-stream instability sets in (Buneman, 1963; Farley, 1963) giving rise to

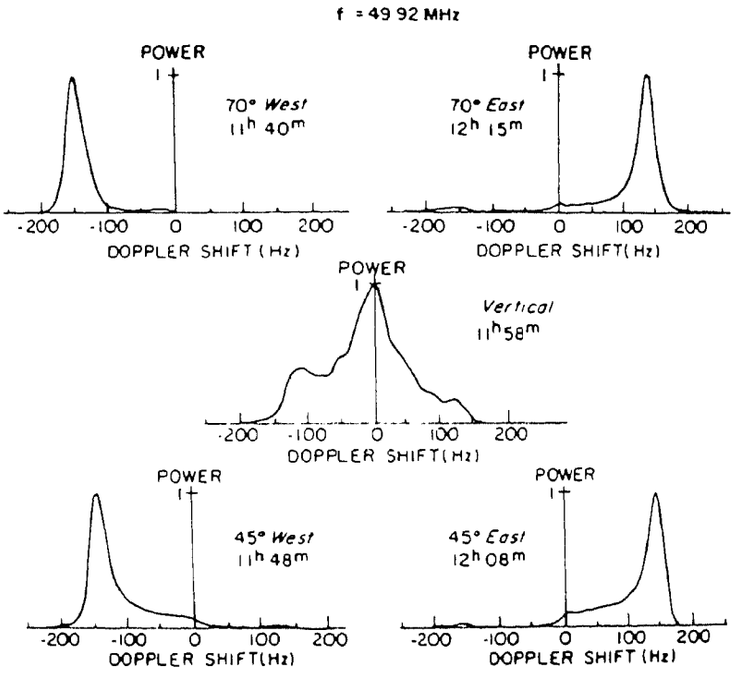

Fig.1.4. Series of Doppler spectra (normalized to a fixed peak) from the equatorial electrojet irregularities at different elevation angles obtained at Jicamarca during a period of relatively strong scattering (After Cohen and Bowles (1967)

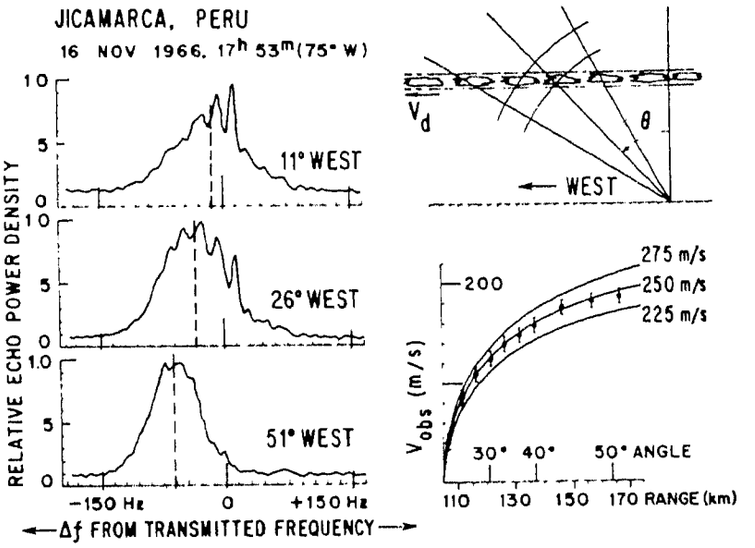

Fig.1.5. Type II spectra measured at 50 MHz simultaneously at different antenna zenith angles. The dashed lines indicate the average Doppler shifts. The geometry of the experiment is shown in the top right panel. The results of the experiment, together with three theoretical curves for which a sine dependence of the average phase velocity with zenith angle was assumed, are shown in the bottom right panel. (After Balsley, 1969)

Type I irregularities. Fig. 1.4 shows the characteristics of Type I irregularities as observed from the Doppler spectra of electrojet irregularities obtained during strong electrojet conditions. Type I irregularities have a narrow spectrum with Doppler shift of 120 $\pm$ 20 Hz (for 50 MHz radar) that correspond approximately to the ion-acoustic velocity ($\sim$ 360 m/s) in the electrojet region. During daytime (nighttime) the Doppler shift of the dominant peak is positive (negative) when the antenna is directed towards the east (west) and negative (positive) when the antenna is looking to the west (east). Therefore the phase velocity of the Type I irregularities has a component in the direction of the electron flow, since during the day (night) the electron flow is westward (eastward). Linear kinetic theory (Farley, 1963) and fluid treatment of the two stream instability (Buneman,1963) have explained the radar observations of 3 m (scale size of Type I) irregularities in EEJ and many other features of the Type I irregularities. Sudan et al (1973) developed the idea that two-stream waves may be generated via a two-step process, in which the driving plasma drift may be governed by that due to a large amplitude wave electric field. This work gained importance in explaining the radar observations of two stream waves perpendicular to current flow and for developing early ideas of plasma turbulence in the electrojet. Numerous theories (e.g., Sleeper and Weinstock, 1972; Sato, 1972; Sudan, 1983) have been developed to explain several intriguing aspects of two stream irregularities, for example, the saturated phase velocities observed with the backscatter radar (Fejer and Kelley, 1980). The theory of Sudan (1983) is also important for developing the idea concerning the evolution of two-stream waves in fully developed plasma turbulence through the advancement of a new nonlinear theory invoking wave induced anomalous diffusion for the saturation of the two stream instability. Theoretical studies involving two-stream waves in the equatorial electrojet have been reviewed by Farley (1985).

During daytime Type II irregularities appear even for small values of the eastward drift velocity (Cohen and Bowles, 1967; Balsley, 1969). The average phase velocity of the Type II irregularities is smaller than the ion-acoustic velocity and is approximately

proportional to the cosine of the radar elevation angle (Balsley, 1969). The spectral width of Type II echoes is much broader than the Type I echoes and is often greater than the mean Doppler shift (Fig. 1.5). Ionosonde and VHF radar measurements have shown that during daytime the irregularities disappear at the times of westward current flow i.e. under counter electrojet conditions (Rastogi, 1972; Fejer et al., 1976; Carter et al., 1976). During nighttime the Type II irregularities are almost always observed except at the time of electric field reversal (e.g., Fejer, et al., 1975; Reddy and Devasia, 1977). Very small electric field is required for the generation of Type II irregularities while a definite electric field threshold is required for the excitation of Type I irregularities. Type II irregularities cover the scale size ranging from about one kilometer to a few meters with amplitudes 5-15% of the ambient electron density (Basu et al., 1977).

At 50 MHz the vertical structure of the electrojet scattering region shows considerable variation between day and night (Fejer et al., 1975). During daytime, when the electron drift velocity is westward, profile show a single echo at altitudes in the height range of 93 and 113 km. During nighttime, irregularities show strong layered structure extending over a wide range of altitude between 90-130 km (Fig. 1.6). Another important contribution to the vertical structure of the electrojet irregularities came from simultaneous measurements of density profiles and density fluctuations (Fig. 1.7) through rocket experiments (Prakash et al., 1972). The results of Indian rocket experiments conducted during daytime showed a strong peak in irregularity amplitude near 106 km with total fluctuation of about 1% in the wavelength range 1-15m. During nighttime the density profile was very irregular (Fig. 1.7) and the most intense signals were in the longer wavelength (30-300m) portion of the spectrum. VHF radar studies of wavelength dependence of electrojet irregularities, have shown that the Type I phase velocity (V_p) increases only to a small extent with decreasing wavelength but that the mean Type II phase velocity is wavelength independent (Balsley and Farley, 1971). At HF frequencies the Type I phase velocity decreases more significantly with increasing wave length, while Type II average phase velocity is independent of frequency (Crochet,

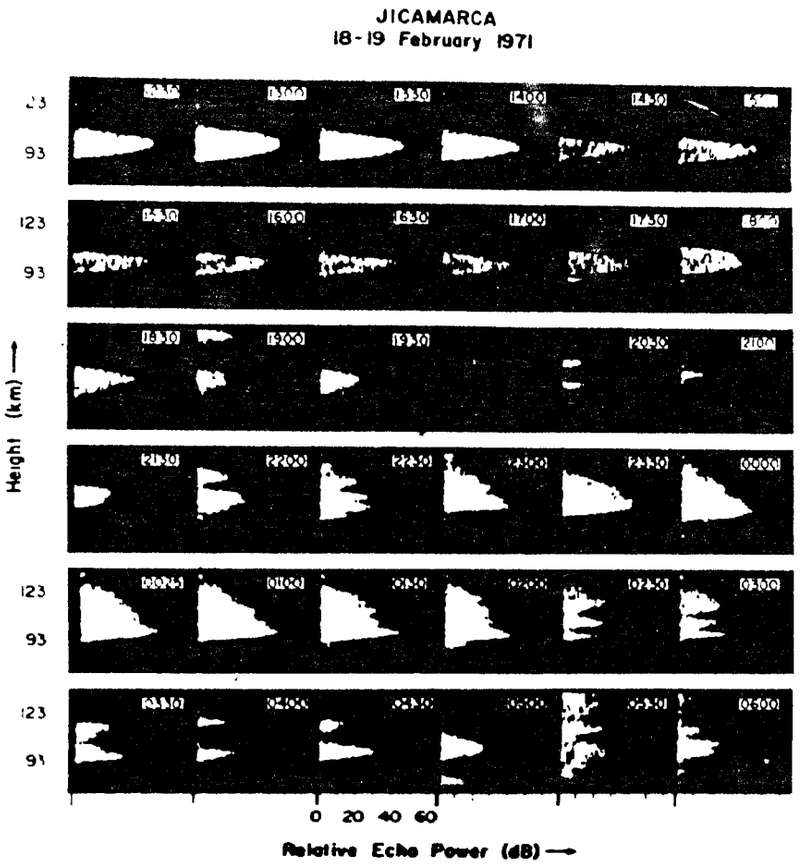

Fig.1.6. Sample of the 50 MHz backscattering power profiles from the electrojet irregularitiies measured with the large vertically directed incoherent scatter antenna at Jicamarca. Spread F echoes contaminated the data between 0450 and 0550 hrs and perhaps at 1900 hrs. (After Fejer et al., 1975)

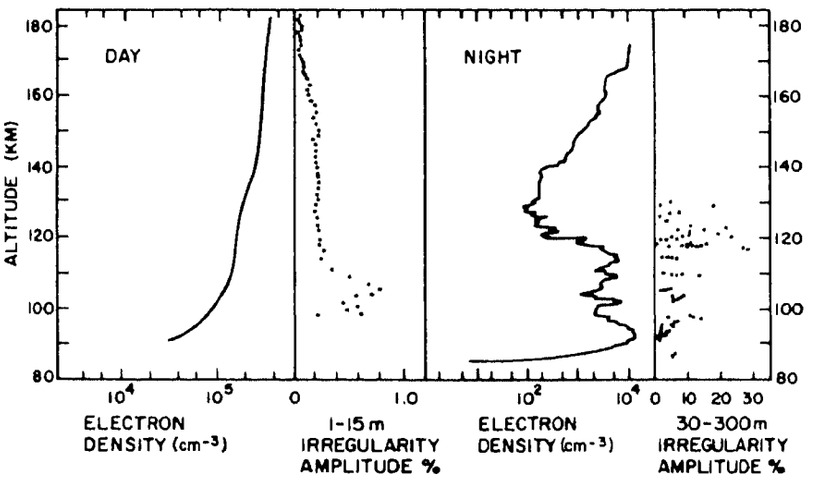

Fig.1.7. Height variations of the electron density and irregularity amplitudes measured at Thumba, India, around noon and midnight. (Adapted from Prakash et al., 1972)

1977; Hanuise and Chrochet, 1977). Experiments (see Farely, 1985) indicated that with increase of the electrojet strength, the electron drift speed increases while the growth time of Type II irregularities decreases. VHF radar observations show that the strength of the irregularities depends quite sensitively on the electron drift (Reddy and Devasia, 1976; Farley 1985). The net effect of an enhancement in electrojet strength is, therefore, an increase in the electron drift speed as well as the strength of the irregularities.

Traces of Sporadic E layers observable regularly in vertical incidence soundings during daylight hours in the vicinity of the dip equator are called equatorial sporadic E (E_{sq}). E_{sq} which is largely transparent to the reflections from higher regions has been shown to be related to the equatorial electrojet (Matsushita, 1951). Type II electrojet irregularities are thought to be responsible for the formation of Esq traces on ionograms at equatorial stations (Balsley et al., 1976b). A variety of observations indicated that the Esq traces disappear during 'counter electrojet' conditions (Hutton and Oyinloye, 1970; Rastogi et al., 1971; Rastogi, 1973).

1.4.3. Equatorial F-region

As mentioned earlier, chemical recombination and plasma transport play a vital role in deciding the equilibrium level of the ionospheric F-region. The efficiency of the chemical recombination loss processes decreases with height as it depends on the molecular concentration of N_2 and O_2. Therefore at F-region altitudes plasma transport plays a major role in electron loss. Plasma diffusion, drifts due to electric fields and neutral winds constitute the basic transport processes. The F-region is thus a dynamics-dominated region of the ionosphere. Assuming that a neutral wind of velocity U is operating in transporting the plasma then the resulting vertical motion of the ions is given by

$$V_z = \frac{U_e cosI(\nu_i/\omega_i) + U_s cosI sinI}{1 + (\frac{\nu_i}{\omega_i})^2} \tag{1.3}$$

where V_z is the resultant vertical motion, ν_i and ω_i are ion-neutral collision frequency and the ion gyrofrequency, U_s and U_e are magnetically southward and eastward components of U and I is the dip angle. The electron drift is negligible compared to ion drift, since $\frac{\nu_e}{\omega_e} \ll \frac{\nu_i}{\omega_i}$, where ν_e and ω_e respectively are the electron-neutral collision frequency and electron gyrofrequency. At F-region altitudes the ion-neutral collision frequency is very small compared to the ion gyro frequency and hence the vertical drift V_z is given by U_s cos I sin I. This expression represents the ineffectiveness of the neutral wind in transporting the plasma in the vertical direction at the dip equator (I = O). Instead, electric fields play a dominant role in the dynamical processes of the equatorial F-region.

During magnetically quiet periods the main sources of ionospheric electric fields are the magnetospheric convection due to the interaction of the solar wind with the earth's magnetic field (solar wind - magnetosphere dynamo), and the circulation of neutral atmosphere across the earth's magnetic field under the influence of tidal winds (ionospheric wind dynamo). The magnetospheric convection dominates at high latitudes while electric fields of the ionospheric wind dynamo origin predominate at mid and low/equatorial latitudes (Mozer, 1973; Richmond et al., 1976). In the vicinity of the dip equator the east-west electric field (E) generated in the E-region dynamo gets mapped to the F-region along the highly conducting field lines and lift the plasma to higher altitudes (Martyn, 1947) in the presence of the horizontal north-south magnetic field (B). The magnitude of the vertical plasma drift is given by $V_z = \frac{EXB}{B^2}$, where V_z is the vertical drift of plasma.

a) Equatorial Ionization Anomaly (EIA)

A major consequence of the plasma transport during daytime and evening hours in the equatorial ionosphere is the formation of the well known Equatorial Ionization

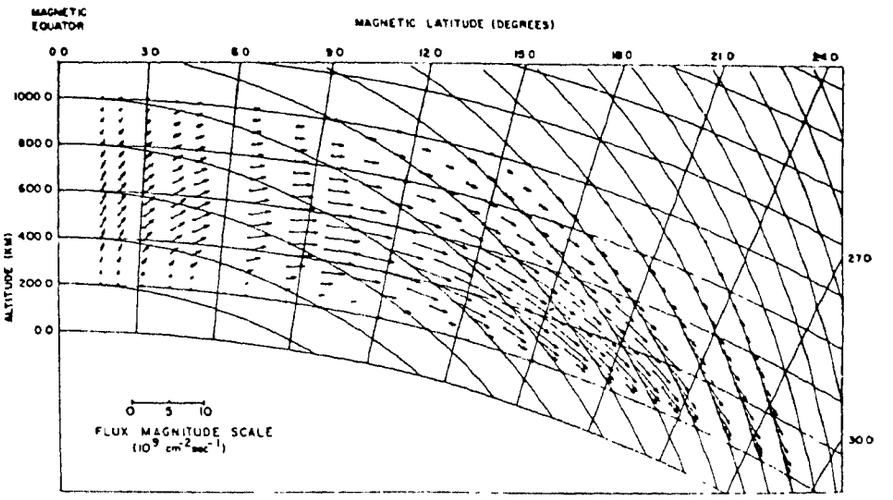

Fig.1.9. Electrodynamic lifting and fountain effect in the equatorial F-region. The upward drift over the magnetic equator is due to an eastward electric field communicated from the E-region. The arrows show the flux of ionization in direction and magnitude. The computation is for noon conditions (W.B. Hanson and R.J. Moffett, 1966)

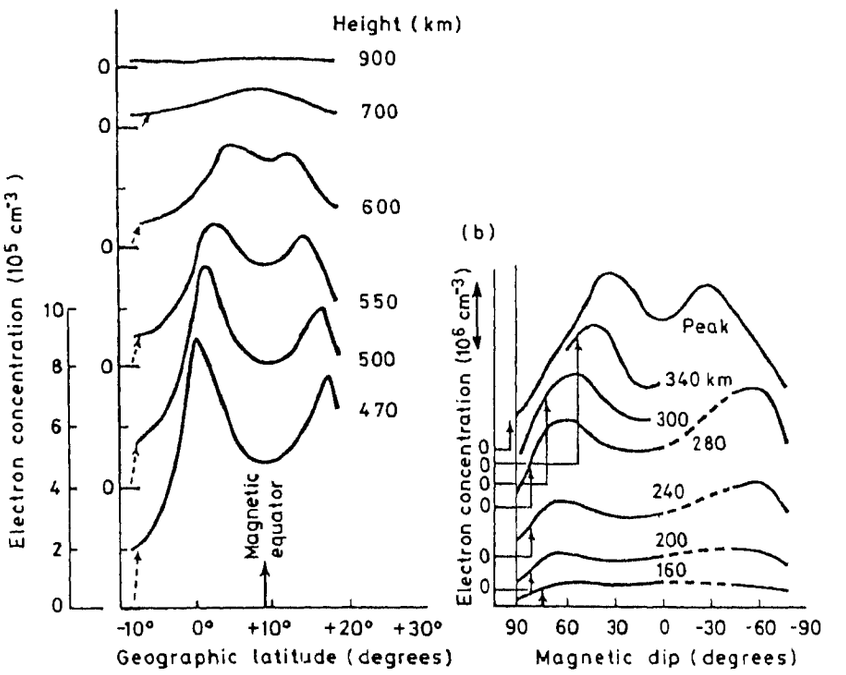

Fig.1.8. Latitudinal variation of electron density across the equatorial anomaly at several altitudes : (a) above h_{hmax} (from topside ionograms); (b) below h_{hmax} (from bottomside ionograms).

Anomaly (EIA), also known as Appleton Anomaly (Appleton, 1946). This phenomenon is characterized by a depression in the F-region ionization densities or "trough" at the equator and two peaks at $\pm$ 20° dip latitude (Fig. 1.8). The formation of the anomaly occurs primarily through the "fountain effect" originally proposed by Martyn (1947). The ionization lifted vertically upwards by an eastward electric field of E-region origin around the dip equator diffuses downwards along the field lines under the influence of gravity and pressure gradient forces, resulting in crests of ionization in north and south of the dip equator and a trough at the dip equator (Fig.1.9) .

Comprehensive description of observation of the equatorial anomaly and the underlying physical processes is given by Moffett (1979). Anderson (1981) reviewed the modelling work with particular reference to the effects of electrodynamic processes on EIA. He has shown that field-aligned plasma diffusion alone cannot produce a large enough anomaly and vertical upward plasma drift is essential for the formation of the anomaly (Fig. 1.10). Longitudinal differences observed in the development of equatorial anomaly (Walker, et al., 1980) and the effects of relative location of geographic and magnetic equators (Fig. 1.3) in American, African and Asian zones on the development of EIA have been reviewed by Walker (1981). Abdu et al.(1990) studied the EIA response to changes in electric fields associated with equatorial electrojet and counter electrojet and the neutral wind effects on the development of EIA during magnetically disturbed conditions. Sastri (1990) comprehensively reviewed the dependence of variability in EIA on the vertical drift (V_z) of F-region plasma around the dip equator and the thermospheric neutral wind field (V_n), particularly the meridional component whose magnitude and direction depend on the global/regional pressure distribution and ambipolar diffusion that depends on neutral density and scale height. The need for coordinated measurements of the parameters of the ionosphere (e.g., V_z) as well as the thermosphere (V_n) using the multi-station/ multi-technique approach to develop reliable data bases for comprehensive understanding of EIA is also highlighted (Sastri, 1990).

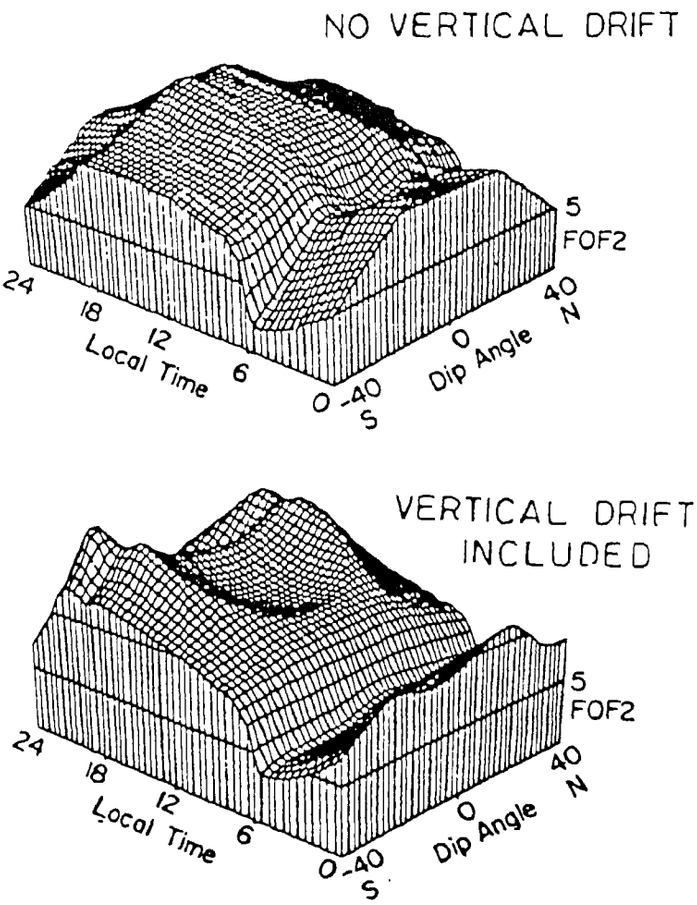

Fig.1.10 Dip angle variation of f_0F_2 as a function of local time obtained from numerical simulation of plasma continuity equation with F-region vertical plasma drift neglected (upper panel) and a realistic drift model included (bottom panel) illustrating the essentiality of vertical plasma drift for the formation of the anomaly. (After Anderson, 1981)

Chan and Walker (1984 a,b) and Sojka and Schunk (1985) both used the electric field model of Richmond et al (1980) in simulating the equatorial ionization anomaly. Semi-empirical model of Anderson et al (1987a) uses six different electric field models which are derived from the measurements of Fejer et al. (1979a) at Jicamarca. Walker and Chan (1989) note that all these electric field models, including that of Richmond et al. (1980), are based on measurements made in the American sector and may not be quite appropriate for the Australian/East Asian longitude zones. This inapplicability was further supported by Fejer et al. (1991) by comparing the Jicamarca vertical drift data with ionosonde data. The recent article by Stenning (1992) reviews the current status and merits and demerits of the different models of low latitude F-region.

b) Equatorial F-region vertical drifts (V_z) and electric fields

In the vicinity of the dip equator the F-region vertical plasma drift (V_z) is a poignant indicator of the effects of crossed zonal electric and magnetic fields and hence is the direct measure of the electric fields. The drifts of the F-region plasma are usually measured using HF, VHF radars and barium cloud releases. Incoherent scatter radar at Jicamarca (11.95°S, 76.87°W, dip 2°N) Radio Observatory provided extensive information on the equatorial F-region vertical drifts. HF ionosondes are also used at times, but at a very low time resolution. HF Doppler radars operated at vertical incidence and ionosondes have been employed to measure the F-region vertical drifts in Indian equatorial zone (e.g., Sastri,1984; Namboothiri et al., 1989; Goel et al., 1990). Rocket release experiments of barium clouds have been used to determine the ionospheric electric fields during twilight periods (e.g., Rieger, 1970; Raghavarao et al., 1987), and also with vector electric field and ion drift measurements on board the dynamics explorer-2 satellite (Aggson et al., 1987; Anderson et al., 1987b; Maynard et al., 1988; Coley and Heelis, 1989). Dynamical processes involving the equatorial electric fields responsible for the equatorial F-region plasma drifts have been reviewed by several authors (e.g., Rishbeth 1977; Fejer 1981; Heelis, 1987; Fejer, 1991). Some of the important results from the literature in respect of the F-region vertical plasma drifts at equatorial latitudes are

presented briefly in the following paragraphs.

i) Observations

The first systematic groundbased measurements of F-region vertical drift velocity (V_z) have been made with the incoherent scatter radar at Jicamarca. These observations revealed that the F-region vertical drifts are upward during day with typical values of the order of 20 ms^{-1} corresponding to an east-west electric field of 0.5mV/m. During nighttime downward drifts are inferred with velocities of the same magnitude as that of daytime (Woodman, 1970). The F-region vertical drifts are nearly independent of height except around the evening reversal periods and during times of fast drift variations (Woodman, 1970; Pingree and Fejer, 1987). Reversal in the drift direction usually occurs 1 to 2 hours after sunset and within 1 hour either before or after sunrise. The variability in V_z is high during sunset times and less during sunrise periods. After sunset an increase in vertical drift is generally observed before the drift reversal and is commonly known as the postsunset or prereversal enhancement. The equatorial vertical plasma drifts shows large day-to-day (Fig. 1.11) seasonal and solar cycle variation (Fig. 1.12) (Woodman, 1970; Fejer et al., 1979a, 1989, 1991). The peak of the prereversal enhancement of vertical drifts (V_{zp}) also shows seasonal, and solar cycle variation and is reported to increase linearly with solar flux during equinox and summer and saturate for high flux levels during southern hemisphere winter (Fejer et al.,1991).

During high magnetic activity conditions the F-region vertical drift and hence the zonal electric field shows significant departures from the quite day pattern (e.g., Fejer et al., 1979b, Gonzales et al., 1979). In contrast, the east-west F-region drifts are not affected by magnetic activity. Vertical drift data of Jicamarca incoherent scatter radar indicated large perturbations in the vertical velocity during daytime as well as nighttime, with more frequent and more severe perturbations in the midnight- early-morning period (Fejer, 1986). These perturbation are usually characterised by decrease and sometimes reversal of drift direction.

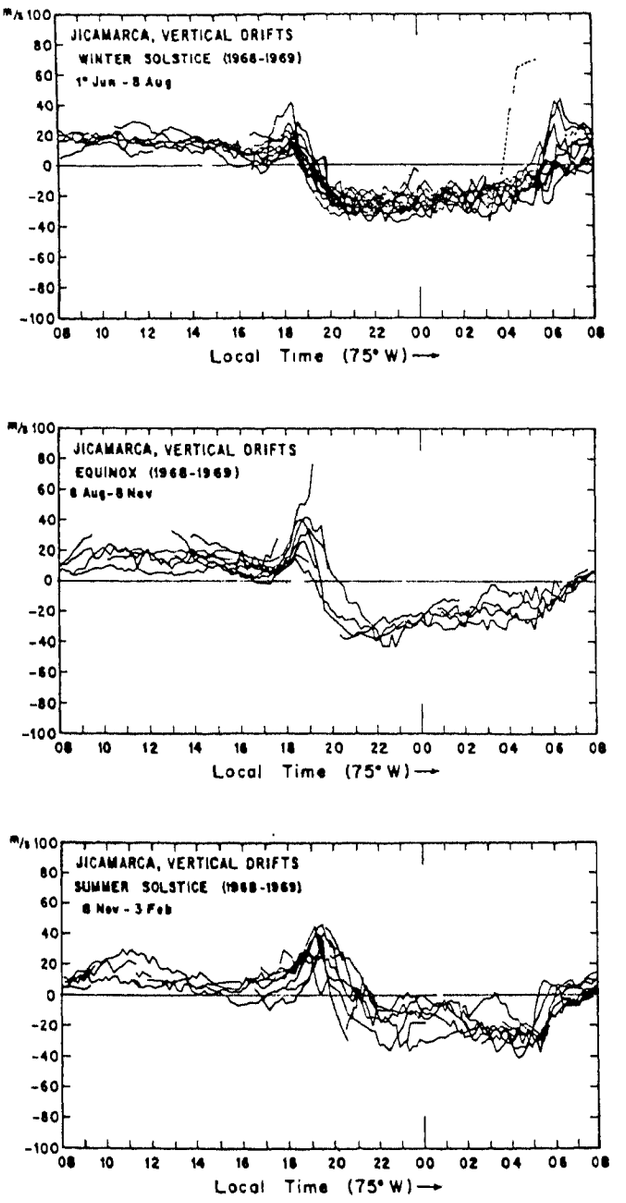

Fig.1.11. Composite pictures showing vertical drifts of F-region over Jicamarca (dip 2°N) for different seasons.

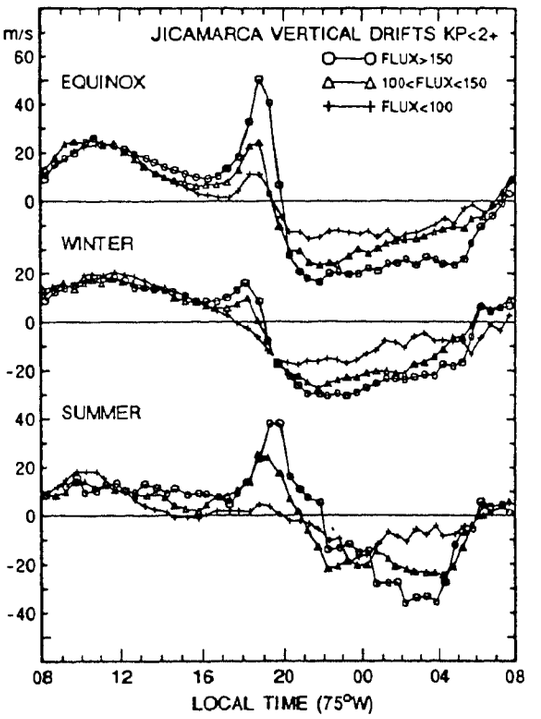

Fig.1.12. Average vertical plasma drifts measured at Jicamarca during equinox (March-April, September-October), winter (May - August), and summer (November - February) for three levels of solar flux.

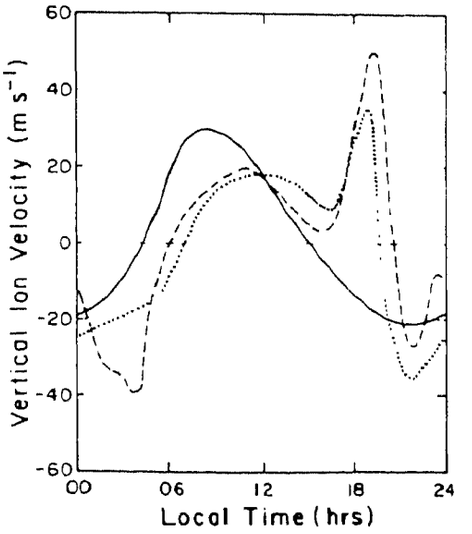

Fig.1.13. Calculated vertical ion drift velocities for several driving wind components. The solid line includes only the tidal-driven E-region dynamo, while the dashed line includes the F-region dynamo as well. Typical measured vertical plasma drifts are indicated by thr dotted line. (After Heelis et al., 1974)

Sastri (1984) and Batista et al.(1986, 1990) used ionosonde observations to study the effects of magnetic activity on vertical plasma drifts in the afternoon-midnight sector and also on the occurrence of equatorial spread-F. The time derivatives of the height of bottomside F-region (h'F) were taken as the vertical drifts and these studies showed that the upward drift velocities near dusk for local winter and summer during magnetically disturbed conditions are in good agreement with the Jicamarca F-region vertical drifts (Fejer et al., 1989). However, Bittencourt and Abdu (1981) pointed out that the ionosonde technique for determining the EXB vertical drift velocities in the equatorial zone works well only when the height of F layer is above about 300km.

Namboothiri et al. (1989) studied the variations of the F-region vertical plasma drift over Trivandrum (8.5°N, 77°E, dip 0.6°S) from HF Doppler observations. Their results indicate an increase of V_{zp} with solar activity consistent with the Jicamarca data. Their results also suggest that V_{zp} decreases as magnetic activity changes from quite to moderate conditions ($A_p \sim$ 15-20), but increase well above the quite time values for high magnetic activity.

ii) Theories

Several workers have examined the plasma drifts and ionospheric currents generated by the E-region dynamo (e.g., Richmond et al., 1976; Forbes and Lindzen, 1976a, b, 1977; Stening, 1977). A comprehensive review of the E-region dynamo theories is given by Richmond (1979). The electric fields of E-region dynamo origin are in fairly good agreement with the equatorial F-region drifts during day, but not during evening and night times. Schieldge et al. (1973) tried to explain the prereversal enhancement of the vertical drifts by adjusting the phase and amplitude of the E-region tidal modes. Forbes and Lindzen (1977) suggested that the disagreement of tidal electric fields and F-region drifts during nighttime is caused by the neglect of the F-region dynamo field.

Rishbeth (1971) suggested that the enhanced electric field responsible for the post-sunset enhancement of F-region vertical drift is actually generated by the F-region dynamo driven by thermospheric winds. These F-region dynamo driven polarization fields can operate only during nighttime as these are shorted out by the large E-region conductivity during daytime. Heelis et al. (1974) and Matuura (1974) showed that the postsunset enhancement in V_z can indeed be produced by F-region dynamo mechanism. Fig. 1.13 shows the numerical simulation of prereversal enhancement by Heelis et al. (1974). However, these models showed strong downward drifts before sunrise which are not commonly observed. Farley et al. (1986) in their rtecent model explained that the constant eastward F-region wind can account for the prereversal enhancement of the equatorial electric fields. They showed that the post sunset enhancement of the F-region vertical velocity (eastward electric field) is a direct consequence of the rapid decrease of the E-region conductivity after sunset compared to that of the F-region. Their model strongly suggests that a number of factors contribute to the prereversal enhancement of V_z and its day-to-day, seasonal, and solar cycle changes. These include the variations in the F-region wind, changes in ratio of E to F region conductivity, E-region dynamo contributions which can be comparable to those of the F-region and the effects of the lack of symmetry between the hemispheres and the noncoincidence of the geographic and dip equators. Farley et al (1986) suggested that the less pronounced prereversal enhancement in V_z during non-equinoctical months, for example, is the effect of such asymmetries which make the sunset effects less abrupt due to differing sunset times in the two hemispheres.

Batista et al. (1986) computed the equatorial F-region vertical drifts using the numerical simulation technique based on the F-region dynamo model. E and F-region electrodynamic coupling is also included in their simulation model. The results of their work shows that the time of occurrence of the evening F-region prereversal peak velocity and its seasonal variation at a station are controlled by the magnetic declination angle at that station, which determines the seasonal variation of the sunset time (and hence

the integrated Pederson conductivity longitudinal gradient) at its magnetic conjugate E layers. They have also shown that the declination angle and the thermospheric winds strongly influence the amplitude of the prereversal peak.

From a comparative study of the evening prereversal enhancements in the F-region ionization drift velocities over two equatorial stations namely Fortaleza (3°S, 38°W, dip 2°S, declination 21°W), Brazil and Huancayo (12°S, 75°W, dip 0.6°N, declination 3°E), Peru in the American sector, Abdu et al. (1981) found many dissimilarities in the seasonal trends, in the time and widths of the prereversal peak. They suggested that the observed dissimilarities arise mainly from the difference in the magnetic field declination angles that causes differences in the conjugate E-region sunset duration and, hence in the F-region polarization electric field development rates at the two stations. Goel et al. (1990) suggested that the increase of the E-region conductivity gradient near dusk from solar minimum to the maximum is also partly responsible for the increase of the prereversal velocity enhancement with solar flux.

Based on the f_oF_2 observations from Interkosmos-19 satellite data, Deminov et al. (1988) suggested that the longitudinal variation of equatorial vertical drift at 14 LT may result from differences in Joule heating due to the change in the intensity of the earth's magnetic field along the equator. Analysis of equatorial vertical drift data from the low inclination AE-E satellite showed excellent agreement with the average diurnal variation measured at Jicamarca (Coley et al., 1990). Ionosonde observations suggest that the longitudinal variation of the F-region vertical drift should be most pronounced in the dusk sector during the solstices (e.g., Fejer et al., 1991). From a detailed study of the electrodynamics of both the undisturbed and the chemically modified postsunset equatorial F-region, Haerandel and Eccles (1992) suggested that the electric fields in the evening sector is a consequence of the effects of the F-region neutral wind dynamo and of the equatorial electrojet. Their work indicates that the equatorial electrojet plays an important role in the evening upward and eastward velocity enhancement.

1.5. NEUTRAL ATMOSPHERE

Neutral composition, neutral temperature and neutral wind field are the important parameters involved in the neutral dynamics at the low/equatorial latitudes. Due to collisions between neutral and ionized particles in a situation where the ions cannot cross geomagnetic field lines, the neutral air experiences a deceleration known as "ion-drag". At F-region heights variation in the plasma densities, therefore, influences the neutral gas dynamics. A strong two-way coupling exists between the neutral and ionized constituents in the ionosphere because the neutral wind also effects the ionization density which inturn, modifies the wind system through ion-drag. Generally the neutral atmospheric models (e.g., Hedin, 1987) are used in conjunction with appropriate empirical models of the ionospheric plasma parameters (e.g., Chiu, 1975) to derive the temperature and neutral circulation pattern. A brief account of some of the input parameters required for modelling purposes are presented in the following paragraphs.

1.5.1. Neutral Composition

The major neutral atmospheric constituents O,O_2 and N_2 in the thermosphere are in diffusive equilibrium and decrease their concentrations exponentially with altitude depending on mass of the species. Several empirical models are available for the prediction of the densities of the neutral atmospheric species as a function of altitude, latitude and local time and for specified levels of geomagnetic and solar activities (e.g., Jacchia, 1977; Hedin, 1987). Global models (for example, Jacchia, 1977; Hedin, 1987) predict very moderate increases of temperature and molecular species (decrease in O/N_2 ratio) at low latitudes at times of severe geomagnetic activity. However, on occasions of severe geomagnetic storms, observations from a network of stations distributed from high midlatitudes to dip equator in the Indian sector exhibited significant and persistent depressions in f_oF_2 during daytime near the dip equator during recovery phase of the storm (Sastri, 1980). These observed anomalous reductions in f_oF_2 (Fig. 1.14) associated with prominent increase in height of F_2 layer in the electrojet region are interpreted as due

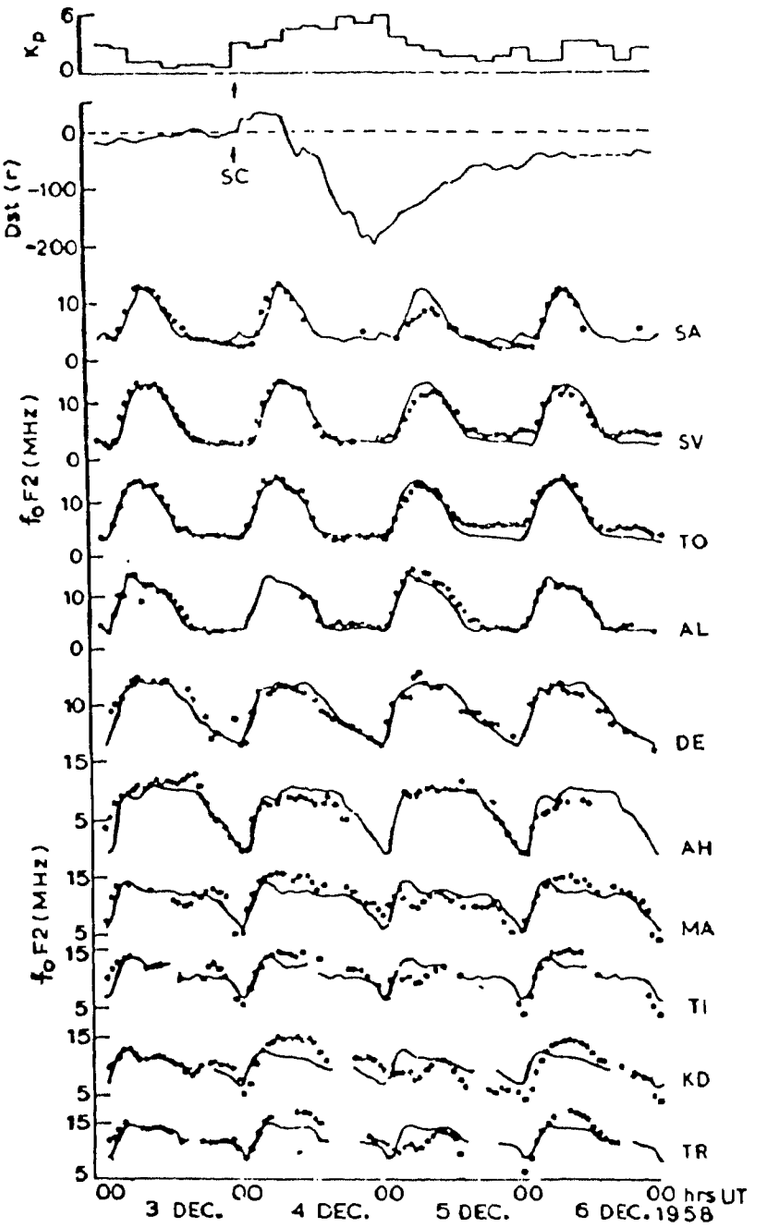

Fig.1.14. Diurnal profiles of f_oF_2 at stations from the dip equator to high latitudes in the Asian sector during the severe geomagnetic storm of December 4-6, 1958. The marked and sustained reductions in daytime f_oF_2 near the dip equator on 5 December that occurred with prominent increases in h_mF_2 are considered as insignia of localised neutral composition changes (decrease in $\frac{O}{N_2}$) caused by the severe storm. (After Sastri, 1980)

to the enhanced loss rate brought about by localized changes in the chemical composition (decrease in O/N_2 ratio). Berger et al. (1988 a,b) reported prominent increase in neutral temperature along with the severe reductions in O/N_2 ratio and this response is interpreted in terms of heat transport from high latitudes through thermal conductivity as well as wave dissipation. These results amply demonstrate the inadequacy of the global models to predict the equatorial neutral atmospheric response to severe geomagnetic storms.

1.5.2. Neutral Winds and Temperatures

Most of the observations and theoretical studies made to-date have concentrated on the neutral dynamics of the mid and high latitudes, and relatively few systematic direct observations of neutral atmospheric parameters are available from low and equatorial latitudes (e.g., Sipler and Biondi, 1978; Burnside et al., 1981; Sipler et al., 1983; Biondi and Sipler, 1985; Meriwether et al., 1986; Biondi et al., 1991; Sahai et al., 1992). Experiments such as the Fabry-Perot interferometer for measurements of the Doppler width and the Doppler shift of 630 nm airglow emissions (e.g., Meriwether et al., 1986; Biondi et al., 1991; Sridharan et al., 1991; Sastri and Rao, 1993), artificial vapour cloud release method (e.g., Desai et al., 1975; Raghavarao et al., 1987) and satellite borne quadrupole mass spectrometer (Wind And Temperature Spectrometer, WATS) (Spencer et al., 1973) are commonly employed for the measurement of winds and temperature in the neutral atmosphere. Recently Krishnamurthy et al. (1990) have used h'F data of two equatorial stations in the same magnetic meridian to derive the nighttime meridional neutral winds at equatorial latitudes.

Neutral winds in the thermosphere play an important role in the plasma transport processes at low and equatorial latitudes. The neutral wind system influences the F-region ionization through its ability to move the ions and electrons along the magnetic field lines. Since plasma transport along the field lines is the second important process in the formation of equatorial ionization anomaly (EIA), the changes brought about by

neutral winds can account for the variability in EIA besides the changes in E X B drift. One example of such neutral wind effects is the asymmetric latitudinal distribution of the two crests of the EIA. This effect which commonly prevails during the solstice months of solar maximum epochs is due to meridional winds caused by the highly asymmetric pressure distributions about the equator, which can transport plasma from the summer hemisphere to the winter hemisphere causing an upward motion of the layer in the summer hemisphere (upwind side) and downward motion in the winter hemisphere (downwind side). Theoretical simulation of this asymmetric feature of the anomaly (Anderson and Roble, 1981) is depicted in Fig. 1.15. Another important aspect of the effect of neutral wind on the anomaly morphology is the pronounced longitudinal differences in the diurnal manifestation of the anomaly from day-to-day and from season-to-season (Walker, 1981). These effects with zonal winds producing motion downward (upward) of ionization during the morning (evening) hours and lowering of ionization crests at the northern summer in east Asia and at the southern summer in American zone are thought to arise because of the regional differences in the geomagnetic declination angle and the relative locations of the geographic and geomagnetic equators respectively (Walker, 1981). In recent times Sahai et al (1990) compared the O_I 630 nm emission intensities obtained from a two channel tilting photometer and the predicted values from SLIM (Semi-empirical Low latitude Ionospheric Model) model (Anderson et al., 1987a) in conjunction with MSIS (Mass Spectrometer Incoherent Scatter) -86 neutral atmospheric model (Hedin, 1987). Their studies showed large discrepancies during high solar activity conditions. They have suggested that the observed discrepancies are due to the over estimation of the F-region peak heights by the SLIM model as the O_I 630nm intensity is strongly dependent on F-region height. The F-region peak height variations are governed primarily by local time behavior of the E X B vertical plasma drifts (Bittencourt and Sahai, 1979) and also by the thermospheric neutral winds whose effects on the F-region peak heights are longitudinal dependent due to the longitudinal differences in the relative positions of the geomagnetic and geographic equators (Bittencourt and Sahai, 1978). Sahai et al (1990), therefore, emphasized the

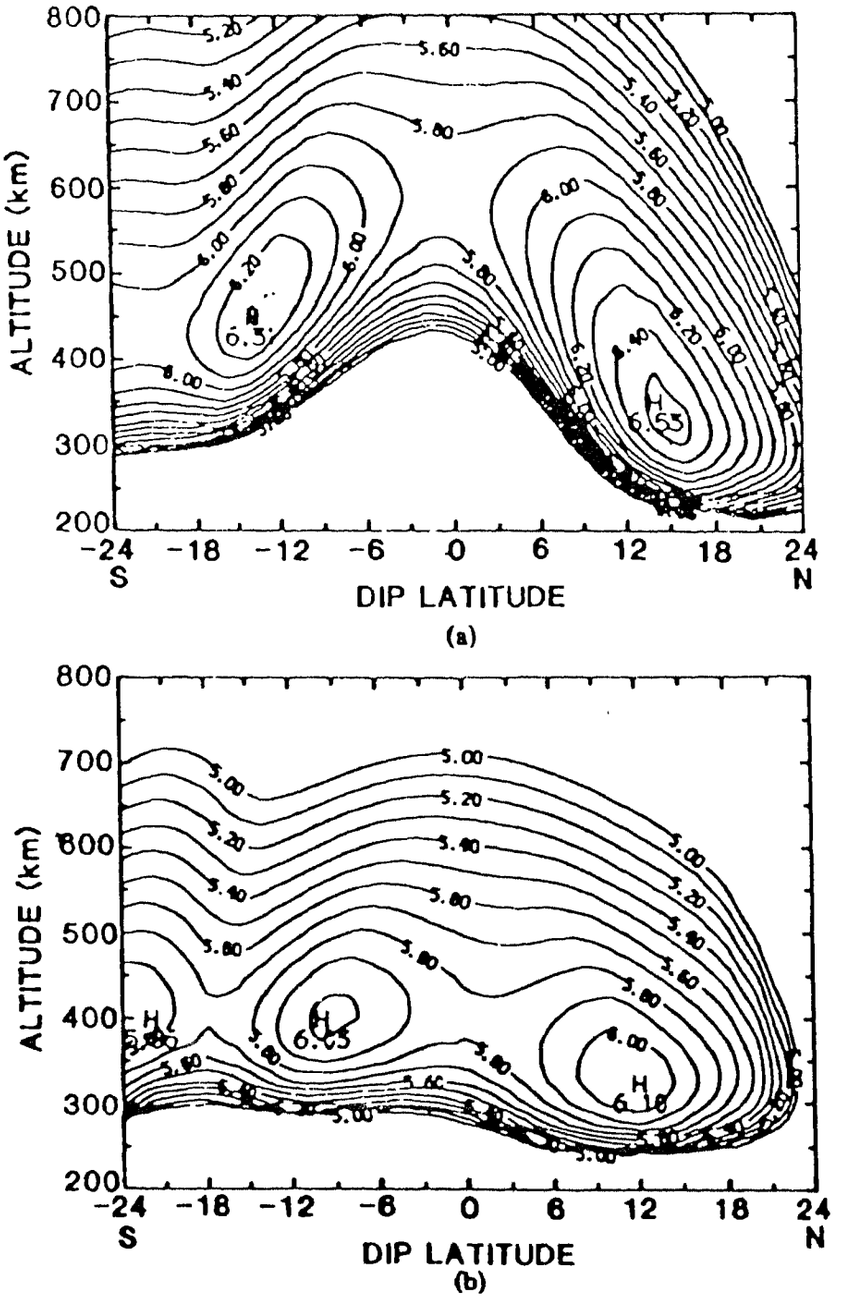

Fig.1.15. Electron density contours (log N_e) for December solstice conditions as a function of altitude and dip latitude at (a) 2000 LT and (b) 2400 LT illustrating the ability of transequatorial winds (south to north) to produce an asymmetric anomaly. The electron densities are obtained from solution of the F-region plasma continuity equation with inputs on neutral temperature and winds from NCAR TGCM. (After Anderson and Rouble, 1981)

necessity of regional models of E X B vertical plasma drift and thermospheric wind to develop a global low latitude ionospheric model. There is, thus, a definite need for the development of the morphological picture of vertical plasma drifts for different longitude sectors in the equatorial zone which can serve as inputs for the regional models. In fact, such an attempt has been made by making use of phase path data of ionospheric F-region reflections obtained at Kodaikanal in the Indian sector and is presented in the fourth chapter of this thesis.

Neutral temperatures estimated from the 630nm night airglow emissions through interferometer technique were found to be in reasonable agreement with the model estimates. Severe enhancements of the measured temperatures from the model estimates were also found under disturbed geomagnetic conditions and sometimes even for quiet condition (Rajaram et al., 1979; Biondi and Meriwether, 1985). While the mechanisms responsible for such enhancements are unknown, the extensive monitoring of neutral temperature is called for, as the enhanced temperatures can influence the global circulation pattern which can affect the characteristics of the EIA through the associated neutral winds and chemical composition changes (Sastri, 1990).

1.6. IONOSPHERIC OSCILLATIONS

Near the dip equator the temporal fine structure in vertical drifts of F-region plasma and hence in the equatorial electric fields are important in understanding the dynamics of the equatorial ionosphere, particularly the magnetosphere - ionosphere coupling processes (e.g., Patel and Lagos, 1985; Earle and Kelley, 1987). Considerable amount of work has been done by several workers on this problem over the past two decades. Some important results relevant to the present study are briefly summerized in this section.

Near the dip equator the east-west electric field, the F-region plasma density and vertical drift are known to undergo changes on short time scales besides the long duration diurnal changes of large amplitudes. Krishnamurthy et al. (1976) have reported

the observation of quasi-periodic fluctuations of the order of few minutes to few tens of minutes ($\sim$ 10-15 min) in the F-region reflections using the HF phase path technique. These observations, however, pertain to the postsunset period and with particular reference to the equatorial spread F. From the spectral studies of 1 min interval ionosonde observations at Kodaikanal, Sastri and Murthy (1977) showed that fluctuations in f_oF_2 with periodicities in the range 5-60 min manifest commonly during daytime. They have suggested that atmospheric gravity waves are the cause of the observed fluctuations in f_oF_2. Measurements of the F-region peak plasma density with the incoherent scatter radar at Arecibo (18°N, 67°W, dip 45°N) also showed the occurrence of small scale fluctuations with the periods in the range 10-20 min (Ganguly & Behnke, 1982). Subbarao and Krishnamurthy (1983) showed the occurrence of $\sim$ 9 min oscillations in the rate of change of phase path of F-region reflections observed simultaneously on two frequencies. They suggested that the fluctuations in the east-west electric field due to internal atmospheric gravity waves at E-region level at the magnetic link latitude of equatorial F-region are communicated to F-region levels leading to quasi-periodic fluctuations in the F-region vertical velocity. They have also observed a downward phase propagation in the F-region and interpreted it as due to the equatorward propagation of the disturbance in the east-west electric fields at the magnetically linked E-region levels.

From the spectral analysis of high time resolution data obtained from incoherent scatter radar at Jicamarca, Peru, Patel and Lagos (1985) showed the presence of significant wave activity in the electron drift velocity (V_e) in the period range 80-125 sec throughout the F-region (200-935 km). The plausible association of these fluctuations in V_e with electrostatic low-frequency drift mode waves and the hydromagnetic mode waves remained unassessed. Earle and Kelley (1987) have carried out spectral analysis of incoherent scatter radar data obtained at three different latitudes to understand the sources of ionospheric electric field fluctuations of periods in the range 1-10 hr. They have identified two distinct sources of these observed fluctuations. At the magnetic

equator, the magnetospheric sources have been suggested as the dominant sources of fluctuations of less than 5 hr for the $K_p > \sim 3$. However at other sites and even for other components (fluctuations with periods > 5hr) at the magnetic equator, atmospheric gravity waves have been suggested as the dominant sources of the electric field fluctuations. Fluctuations with periods ranging from few minutes to several tens of minutes were reported from the spectral studies of the East-West electric fields, inferred from the vertical plasma drifts in the F-region during post sunset hours (Balachandran Nair et al. 1992). They have suggested that the frequently occurring medium-scale gravity waves (Fransis, 1975; Booker, 1979) could be the plausible sources of the observed fluctuations.

The ionospheric variations associated with geomagnetic micropulsation have been observed in the Doppler velocity of ionospheric reflections at both oblique and vertical incidence (e.g., Chan et al., 1962; Devies and Beker, 1966; Duffus and Boyd, 1968, Klostermeyer and Rottger, 1976; Menk et al., 1983; Sutcliffe and Poole, 1984; Watermann, 1987; Jarvis and Gough, 1988; Yamoto et al., 1989, Todd et al., 1989), in total electron content, (Davies and Hartmann, 1976; Okugawa and Davies, 1981), in ionospheric electric fields determined from incoherent scatter radar measurements (Doupnik et al., 1977; Walker et al., 1979; Lathuillere et al., 1981; Glangeaud et al., 1985) and in Doppler shift of HF backscatter radar echoes at oblique incidence (Bourdillon et al., 1989). Chan et al. (1962), Davies and Baker (1966) and Lewis (1967) compared geomagnetic pulsations and long period variations with Doppler shifts of HF radio waves reflected obliquely from the F-layer. Duffus and Boyd (1968) specifically investigated the correlation of ULF geomagnetic pulsations with the ionospheric oscillations observed in the Doppler frequency of HF waves reflected from the F-layer in oblique path. Rishbeth and Garriot (1964) proposed two mechanisms to explain the association of Doppler velocity oscillations with geomagnetic variations. In their "dynamo-motor" theory, the Doppler velocity oscillations were taken to be due to the vertical component of the bulk motion of the ionosphere caused by the E X B drift of plasma associated

with the oscillating electric field in the F-region, that is, the ionospheric "motor" effect. The second mechanism is the motion of the F-layer under the direct influence of magneto-hydrodynamic wave. The later mechanism was supported by the observations of fluctuations in the Doppler frequency of F-region reflections associated with geomagnetic field oscillations (Klostermeyer and Rottger, 1976; Menk et al., 1983). Sutcliffe and Poole (1984) demonstrated that two mechanisms namely the vertical EXB drift of the ionosphere as a whole due to east-west component of the pulsation electric field, and the variation in refractive index of the ionosphere due to the oscillation of the north-south component of the pulsation magnetic field, can account for their observations of oscillations in the ionospheric Doppler velocity.

Poole et al. (1988) show that the mechanism of compression and rarefaction of the plasma associated with the field-aligned component of the pulsation magnetic field can give rise to changes in phase path of ionospheric reflections. Poole and Sutcliffe (1987) have demonstrated that it is this mechanism that is most likely responsible for the pulsations observed in total electron content (TEC) by Okuzawa and Davies (1981). Recent studies showed that the mechanisms proposed by Rishbeth and Garriot (1964) and Poole et al. (1988) play an important role (e.g., Yumoto et al., 1989: Jarvis and Gough, 1988; Tedd et al., 1989). The experimental results available to-date and the model predictions (Sutcliffe and Poole, 1990) indicate that the relationship between ionospheric Doppler Velocity oscillations and groundlevel micropulsations is highly variable and complex, and carefully planned observations are necessary to ascertain the relative role of the various mechanisms for different geophysical situations. A case study made to understand the mechanism(s) responsible for the fluctuations in the Doppler frequency of F-region reflections associated with geomagnetic micropulsation activity, in fact, is presented and discussed in the fourth chapter of this thesis.

1.7. PERTURBATIONS IN THE EQUATORIAL ELECTRIC FIELD

The equatorial F-region vertical drifts, driven by the zonal electric fields show considerable day-to-day variation even during magnetically quiet periods (Fejer et al., 1989). In addition the vertical drifts are strongly affected by magnetic activity (e.g., Fejer et al., 1976, 1979b; Gonzales et al., 1979, 1983). The equatorial zonal electric fields and the perturbations in them are usually studied with direct experimental techniques such as coherent and incoherent radar techniques as well as indirect techniques such as ground based magnetometers and ionosondes. Several experimental studies, based on groundlevel magnetometers, radar observations of plasma waves in the equatorial electrojet, and incoherent scatter radar measurements have demonstrated the effects of high latitude currents on equatorial plasma drifts and currents during disturbed conditions (Onwumechille et al., 1973; Nishida et al., 1966; Matsushita, 1979; Matsushita and Balsley, 1972; Reddy et al., 1979; Gonzales et al., 1979, 1983; Fejer et al., 1979a, 1983, 1990a; Somayajulu et al., 1985, 1987, Viswanathan et al., 1987, Sastri, 1988 a, b). Two channels have been identified for the influence of high latitude current systems on the equatorial/low latitude electric fields, viz, penetration of high latitude electric fields into equatorial region (e.g., Fejer, 1986) and from disturbance dynamo effects (Blanc and Richmond, 1980). Electric field disturbances arising out of these two mechanisms are briefly presented in the following sections.

1.7.1. Effects of Penetration electric fields

Sudden perturbations in the magnetosphere potential across the polar cap often result in short-term (1-2 hour) electric field disturbances propagating almost instantly from high to middle and equatorial/low latitudes. Such effects often occur in association with sudden and prominent transitions in the orientation of the north-south (B_z) component of interplanetary magnetic field (IMF). First observational evidence for the large reversals in the equatorial zonal electric fields in the wake of large and rapid northward reversals of IMF B_z have been reported by Rastogi and Patel (1975), and

subsequently by several others (Patel, 1978; Kane, 1978; Fejer et al., 1979b; Kelley et al., 1979; Gonzales et al., 1979). Studies of Fejer et al (1979b), however, revealed that, not every northward turning of B_z is associated with a reversal in the equatorial electric field. On the other hand, their studies revealed the occurrence of large equatorial electric field reversals in the absence of northward turning of B_z and during steady and large values of southward B_z. The extensive measurements of equatorial electric field made from Jicamarca radar showed that the large equatorial electric field perturbations often coincide with sudden northward turning of IMF B_z (Fejer, 1986). Kelley et al (1979) suggested that a sudden northward turning of IMF B_z causes a temporary imbalance between the convection related charge density and the charge on the inner edge of the magnetosphere, due to the sudden decrease of the convection electric field. Since the time constant for the decay or the build up of ring current charges is greater than several minutes (Vasyliunas, 1972), this imbalance produces a dusk-to-dawn electric field perturbation which then penetrates the plasmasphere giving rise to perturbations in the equatorial electric fields in phase opposition to S_q field pattern. Sastri (1988b) advocated this mechanism of prompt penetration of electric fields into low latitudes by explaining the important role of the variance of the IMF in controlling the efficiency of the mechanism. The frequency of occurrence and the amplitude of the equatorial electric field perturbations associated with northward turning of B_z change considerably with local time (Fejer, 1986).

Most of the anomalous equatorial F-region vertical drift reversals occur at the times of the onset of substorm recovery phase triggered by the rapid northward turning of IMF B_z (Rastogi and Patel, 1975; Fejer et al., 1979b). The polarity pattern of the zonal electric field (vertical drift) perturbation during the substorm recovery phase is westward (downward) by day and eastward (upward) by night, i.e. in phase opposition with the S_q field (Rastogi and Patel, 1975; and Patel 1978). However, transient disturbances in the equatorial zonal electric field in phase with the S_q-field pattern, are also observed in association with the onset of the substorm. The polarity pattern of the disturbed zonal

electric fields at times of onset of substorm triggered by swift southward turning of B_z is eastward by day and westward by night. Several examples of pronounced downward and upward perturbations associated, respectively, with large southward and northward turnings of IMF are presented by Gonzales et al. (1979, 1983) and Fejer (1986). One such example is reproduced in Fig. 1.16. The daytime westward perturbations have typical amplitudes of about 0.3mV/m. The nighttime eastward electric field perturbations have largest amplitudes (up to about 1.5 mV/m) in the post midnight sector and smallest amplitudes between dusk and midnight (Fig. 1.17). Perturbations in equatorial electric fields during times of substorm recovery phase manifest quite frequently. However the daytime eastward and nighttime westward electric field perturbations associated with southward IMF B_z turnings manifest only occasionally with a preference for the midnight noon sector with largest amplitudes just before sunrise (Fejer, 1986). Therefore the response of the equatorial zonal electric field to changes in IMF B_z and substorm activity is quite asymmetric.

1.7.2. Numerical models of penetration electric fields

Several numerical models are available in the literature to experimentally evaluate study the penetration of high latitude electric fields into the middle and low latitude ionosphere (e.g., Nisbet et al., 1978; Kamide and Matsushita, 1981; Senior and Blanc, 1984; Spiro et al., 1988, Zamay, 1989). Senior and Blanc (1984) have presented a detailed model for magnetospheric convection, with latitudinal and local time dependent ionospheric conductivities as well as a time dependent ring current. They have also calculated middle latitude fields generated by sudden increases in the dawn to dusk potential drop. The Rice convection models (Wolf et al., 1986; Spiro et al., 1988), with more accurate description of magnetospheric processes provide more realistic predictions of low latitude electric field perturbations. The models predict correctly that a decrease in convection associated with a rapid northward change of the IMF B_z generates westward electric field perturbations during the day and eastward at night and in particular, the maximum amplitude of the zonal electric field perturbations near the

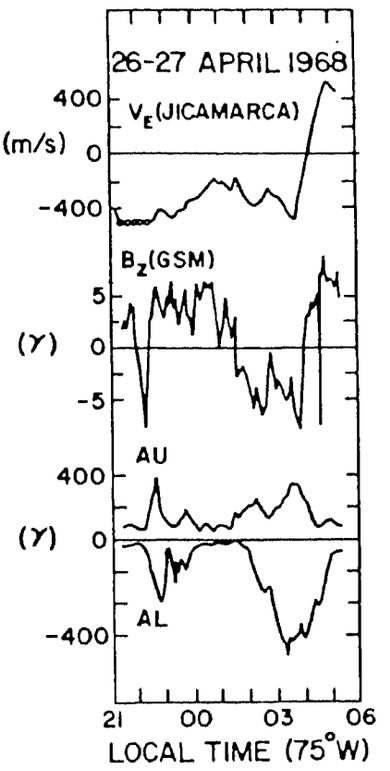

Fig.1.16. An example of near simultaneous reversal of the equatorial electric field (westward drifts or positive V_E) and the IMF B_z at night. Note that the equatorial field reversal is well correlated with substorm recovery.

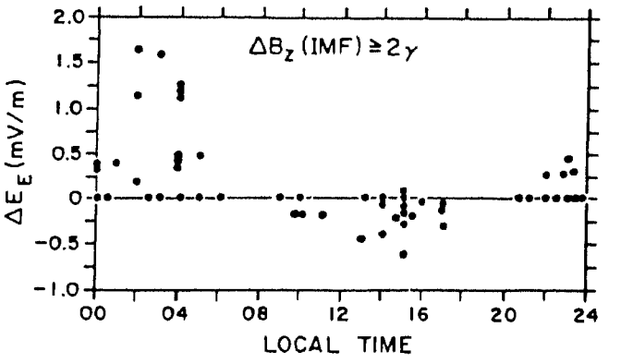

Fig.1.17. Local time dependence of equatorial eastward electric field perturbations associated with northward IMF turnings of 2gammas or greater.

dip equator in the midnight-dawn sector. The predicted latitudinal variation of the zonal perturbation electric fields is also in reasonable agreement with observations (Fejer et al., 1990a, b).

The models, however, cannot reproduce the observed polarity pattern of large electric field disturbance at middle and low latitudes during a substorm (Reddy et al., 1990a, b). Also some of the morphological features of penetration electric fields are not well understood. For example, the models cannot explain the highly asymmetric response of the equatorial zonal electric field to sudden changes in polar cap potential (ϕ_{pc}) i.e., higher sensitivity to decrease in polar cap potential than to increase in polar cap potential. Experiments show that the transient electric field perturbations occur either with an increase in convection at the onset of the substorm in association with southward turning of B_z or with a decrease in convection during the recovery phase of the substorm associated with northward turning of B_z but not both (Fejer et al., 1979). In any typical substorm, however, perturbations associated with both increase and decrease in convection are to be seen. In fact, the calculations of Spiro et al (1988) and Fejer et al (1990b) simulate the effects of a sharp increase in the polar cap potential (ϕ_{pc}) followed by a sharp decrease in a substorm. Fejer (1991) suggest that extensive worldwide electric field measurements are needed to understand the low/equatorial latitude electric field perturbation associated with the substorm phenomenon. The present models also have to take into account self consistently the thermospheric neutral wind, conductivity and magnetospheric effects to predict the realistic situation (Fejer, 1991).

1.7.3. Effects of Disturbance dynamo electric fields

Equatorial ionospheric electric fields are also influenced by the large changes in the global thermospheric circulation due to storm time heating at high latitudes from Joule dissipation of enhanced auroral currents and from particle precipitation (Blanc and Richmond, 1980; Mazaudier et al., 1985). These disturbance dynamo effects propagate equatorward with latitude dependent time delays. Modelling studies showed that the de-

layed ionospheric disturbance dynamo related electric fields can decrease and occasionally reverse the quite time electric field pattern in the vicinity of the dip equator (Blanc & Richmond, 1980, Blanc, 1983). Studies of the behaviour of the equatorial electrojet strength, and of F-region plasma drifts and electron densities following magnetic storms indicate that disturbance dynamo effects can indeed disturb significantly the low latitude ionosphere (Fejer et al., 1983; Sastri, 1988a, 1989, Mazaudier and Venkateswaran, 1990). Recent studies also showed that the disturbance dynamo related electric field perturbations manifest with delays of 12-24 hr with reference to the causative geomagnetic disturbances and with a marked preference for the postmidnight- prenoon local time sector (Fejer et al., 1983, Sastri,1988a, Mazaudier et al., 1985). Groundbased magnetometer and ionosonde observations indicate that delayed equatorial electric field disturbances do not always follow enhanced magnetic activity even in the presence of ionospheric storm effects at mid latitudes (Sastri, 1988a). Fejer (1991) pointed out that other effects such as changes in the chemical composition of mid latitude ionosphere and long period gravity waves may play a role in the occurrence of persistant and delayed electric field disturbances at equatorial latitudes.

1.8. SCOPE OF THE PRESENT THESIS

At equatorial latitudes the vertical plasma drifts caused by the east-west electric field of E-region and F-region dynamo origin play a vital role in the overall dynamics of the F-region. The main aim of the present thesis is to identify the processes that are responsible for some of the small scale structures in the equatorial F-region vertical plasma drifts and to understand the perturbations in them those occur in association with magnetospheric substorms. Data obtained from the HF phase path sounder experiment and the ionosonde operated at the equatorial station, Kodaikanal (10°14′N, 77°29′E, dip 3°N) in the Indian zone form the primary material for the present work.

In the second chapter are presented the details of experimental set-up used for continuous recording of phase path variations of reflections at normal incidence from

discrete regions of the ionosphere.

Phase path (P) observations of ionospheric F-region reflections on 5 MHz probing frequency at Kodaikanal have been made on 116 days during the day light hours between 08-16 IST. Small scale fluctuations (30-600 sec) in $\dot{P}$ are found to manifest at all times during daytime superposed on the long-duration diurnal changes. Detailed study of these small scale (in time and amplitude) perturbations is made to understand their origin and the results are presented in the third chapter.

Measurements of phase path of F-region reflections on 4 MHz during nighttime (1600-0600 IST) were made on 410 nights over the period February 1991 through February 1993 to investigate the nighttime pattern of F-region vertical plasma drift and fluctuations in them. An effort has been made to derive the nighttime average pattern of vertical drift (V_z) and the changes in it from day-to-day, with season and level of solar and magnetic activity and the results are presented in the fourth chapter. The results of an analysis made to understand the mechanisms responsible for the quasi-periodic fluctuation in F-region Doppler velocity, V_D observed on 24 March 1991 in association with groundlevel geomagnetic pulsations (Psc5) are also presented.

Data of height of bottomside F-region (h'F) obtained from 5 minute interval ionograms at Kodaikanal on the night of 29-30 August 1957 indicated a marked perturbation with sudden decrease in h'F followed by a conspicuous increase over a period of 3 hours. A detailed analysis of h'F data in conjunction with the h'F data of two low latitude stations in the Indian longitude sector has been carried out to understand the nature and characteristics of the perturbation which occurred in the wake of isolated substorm activity and the results are presented in the fifth chapter.

In the sixth (final) chapter, a summary of the results and conclusions of the studies on different aspects of the equatorial ionosphere described in the thesis are summarized. The scope for further work on the dynamics of the F-region with the HF Phase Path (Doppler) sounder at Kodaikanal is also presented.

CHAPTER 2

INSTRUMENTATION

2.1 INTRODUCTION

Standard swept-frequency ionosondes are in use since a long time to provide synoptic information on the ionospheric regions. The ionosonde data have, infact, contributed greatly to our current understanding of the structure of the ionosphere and its variability. The ionosonde technique has also been used for the studies of several aspects of ionospheric dynamics such as small scale fluctuations in the F-region electron density (e.g., Nagpal and Gupta, 1973; Sastri and Murthy, 1977), and for the studies of the various aspects of F-region vertical plasma drifts (e.g., Abdu et al., 1981; Batista et al., 1986, 1990; Sastri, 1984, 1988 a, b and Goel et al., 1990). Time derivative of the virtual height of the reflecting layer (h'F) has been used to represent the vertical drift velocity. This procedure of estimating vertical drifts is valid particularly in the nighttime when the effects due to the ionization below the reflection level can be neglected. In fact, based on this technique a study of substorm related equatorial electric field perturbations has been made and presented in the 5th Chapter of this thesis. The ionosonde technique has obvious limitations for studies of ionospheric dynamics. For example the maximum temporal resolution usually available with the ionosondes is 1min and the height of reflection can be scaled to an accuracy of 3-5km. Studies of height fluctuations of much shorter time scales and of small amplitude are therefore not possible with the ionosonde. Continuous monitoring of the vertical drift of the reflecting layer, however, is not possible with ionosonde data. Sophisticated and capital-intensive experiments such as the VHF radars is, however, resourceful for studies of small scale fluctuations in ionospheric electric fields (e.g., Patel and Lagos 1985; Earle and Kelley, 1987), Zonal and vertical plasma drifts (e.g., Woodman, 1970, Fejer et al., 1979a, Fejer et al., 1989, Fejer et al., 1991) and electrojet irregularities and associated phenomena (e.g., Fejer and Kelley, 1980; Kelley, 1989).

Vertical drifts can be estimated to a high accuracy by measuring the time rate of change of phase path of ionospherically reflected HF radio waves at normal incidence. The HF phase path technique similar to one used by Findlay (1951) is a cost effective and resourceful means of studying ionospheric dynamics. It is traditionally used for investigating several aspects of ionospheric dynamics such as medium-scale travelling ionospheric disturbances (MSTIDS) (e.g., Georges, 1968; Pfister, 1971; Reddi and Rao, 1971; Butcher and Joyner, 1972; Schrader and Fraser, 1975; Wadlock and Jones, 1986; Jacobson and Carols, 1989), ionospheric oscillations associated with geomagnetic micropulsations (e.g., Menk et al., 1983; Sutcliffe and Poole, 1984; Watermann, 1987; Yumoto et al., 1989) and energetic geophysical events like severe thunderstorms and earthquakes (e.g., Georges, 1967, 1973; Beker and Davies, 1969; Davies and Jones, 1971, 1973; Prasad et al., 1975; Raju et al., 1981; Tanaka et al., 1984; Okuzawa et al., 1986; Jacobson et al., 1988). It is also employed in recent times to derive information on ionospheric electric field disturbances (e.g., Tsutsui et al., 1984; Kikuchi and Araki, 1985; Kikuchi, 1986; Tsutsui et al., 1988) and the thermospheric wind vector (e.g., Balan et al., 1992). The present work is mainly based on continuous measurements of the phase path of ionospheric reflections at normal incidence made at Kodaikanal. Salient features of the system design and hardware implementation are presented in this Chapter.

The phase path (P) of the ionospheric signal is expressed as

$$P = \int_s \mu ds \tag{2.1}$$

where μ is the phase refractive index given by Appleton-Hartree formula and s is the ray path. Equation (2.1) shows that the time variation of phase path provides information on μ and the height of reflection. In the case of a horizontally stratified ionosphere and for vertical incidence, the phase path is just twice the phase height, and is given by

$$P = 2\int_o^H \mu dh \tag{2.2}$$

where h is the altitude measured from the earth's surface and H is the height of reflection level. From the equation (2.2) it is clear that the changes in phase path can be caused

by the up and down movement of the reflection point and/or due to the changes in phase refractive index along the ray path. For the transmitter and receiver at the same location the time rate of change of phase path is given by

$$\frac{dP}{dt} = p.V_D \tag{2.3}$$

where p is a unit vector in the ray direction and V_D is the Doppler velocity of the reflecting layer. Equation (2.3) is valid when there are no changes in refractive index of the medium below the reflection level due to production and recombination of ionization. The vertical velocity (V_z) of the reflecting layer is then half of the Doppler velocity i.e., changes in single trip ray traverse.

The frequency deviation δf suffered by a wave of frequency f whose phase path (P) is changing with time is given by

$$\delta f = -\frac{f}{c}\frac{dP}{dt} \tag{2.4}$$

where c is the velocity of the wave. From the equation (2.4) it is clear that the HF phase path measurement method is similar to that of HF Doppler measurement method described by Watts and Davies (1960).

Findlay (1951) originally introduced the method for continuous recording of the changes in phase path of the signal reflected from the ionosphere at normal incidence. The phase of the signal received after reflection from the ionosphere is compared with the phase of a reference oscillator which is phase coherent with the transmitted signal. Phase comparison is made at the operating frequency itself. This method was later modified by Reddi and Rao (1967) wherein the phase of the ionospheric signal is compared in the receiver at an intermediate frequency (IF) against that of a stable reference oscillator of frequency differing from IF by about 20 KHz. The reference oscillator is triggered by the transmitter pulse and is thus phase locked with it. The changes in the resultant beat pattern then represent the time variations of the phase of the ionospheric echo with respect to the transmitter pulse. The phase comparison at the IF stage provides the advantage of chosing any required frequency in the HF band for probing the ionosphere.

Also such a system enables simultaneous recording of phase as well as the amplitude of the ionospheric signal. The beat pattern recorded on a photographic film appears as sloping traces, the negative and positive slope traces representing the increase and decrease in phase path changes respectively. This kind of a system was widely used in the past for the studies of Travelling Ionospheric Disturbances (TIDs) (Reddi and Rao, 1971, Srivastava et al., 1971; Vincent, 1972; Butcher and Joyner, 1972; Schrader and Fraser, 1975). Inspite of its high sensitivity, the photographic recording of the beat pattern results in jumps or discontinuities in the phase path records at times of appearance of interference, and renders chunks data useless for analysis (Reddi, 1969; Schrader and Fraser, 1975). Systems that rely on coherent detection are now widely used for continuous recording of the phase path changes of reflections from discrete regions of the ionosphere (Balan et al., 1979; Reddi et al., 1980). Such a system has been developed and used for the present study.

2.2. DESIGN ASPECTS OF THE HF PHASE PATH SOUNDER.

The block diagram of the phase path recording system is shown in Fig 2.1. The system comprises of a frequency synthesizer, a pulse transmitter, receiver(s), logic for inferring sense of changes in phase path, display and analog recording facilities.

Accurate measurements of changes in phase path depend on the stability and the phase coherence of the various frequencies and the timing pulses. If the frequencies required for transmitter and receiver units are generated from different sources then the frequency stability of better than 1 part in 10^9 is required for the maintenance of phase coherence. However frequency standards with a long term stability of 1 part in 10^6 and a short term stability an order of magnitude more have proved to be adequate for measurements of phase path if all the required frequencies are generated from a single source (Reddi et al., 1980). The system (Plate 1) used for present investigations incorporates such a method of direct synthesis of all the required frequencies from a single source.

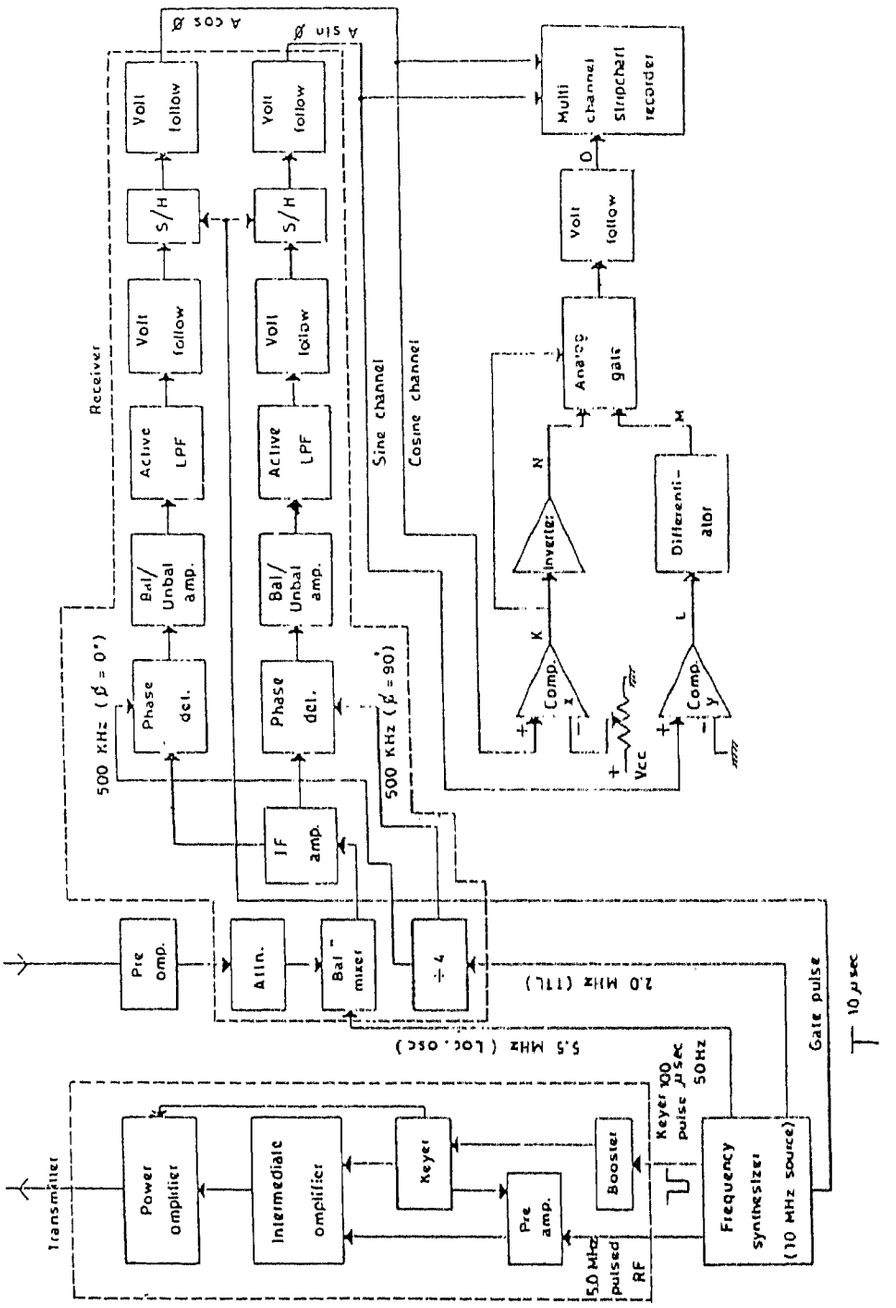

Fig.2.1. Block diagram of the phase path sounder.

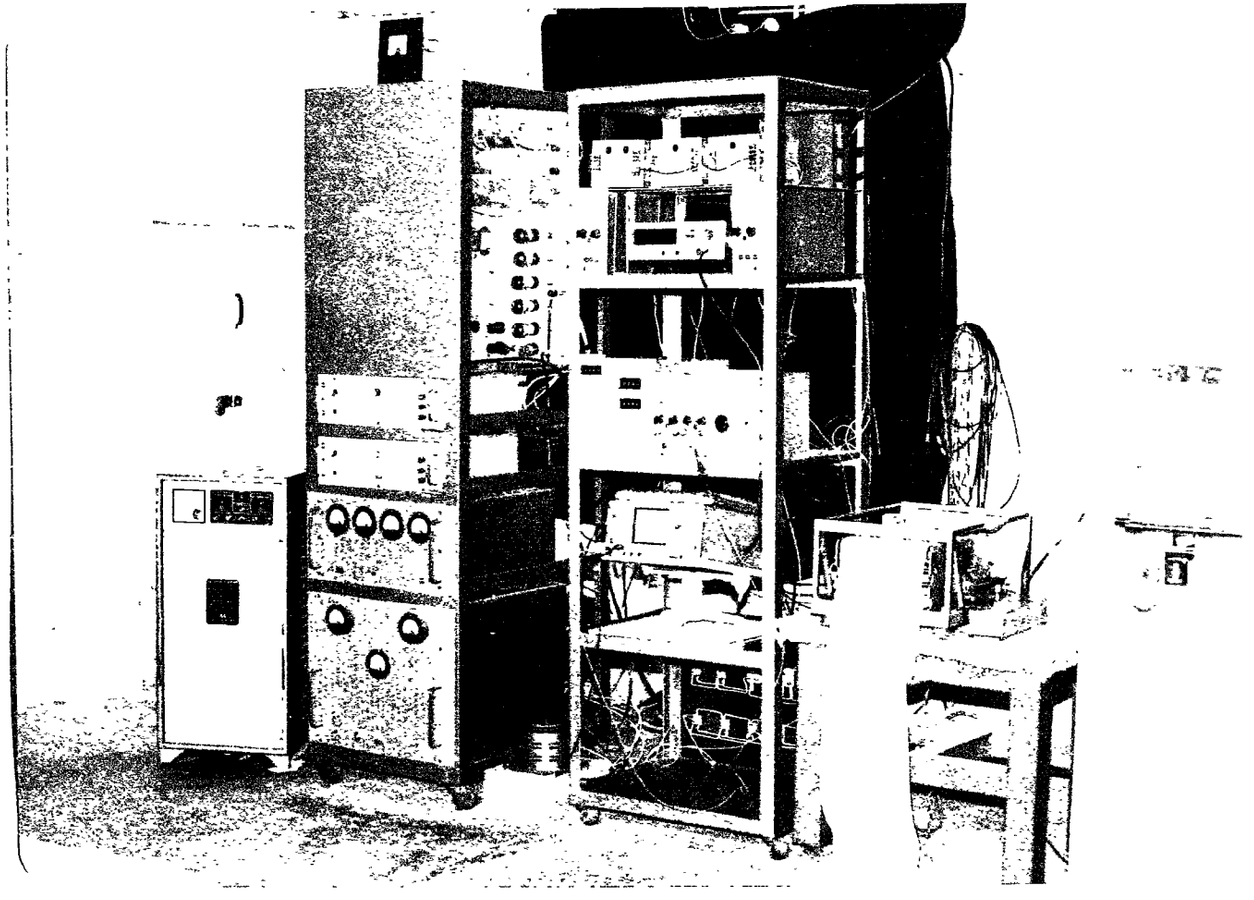

PLATE 1: HF PHASE PATH (DOPPLER FREQUENCY) SOUNDER AT KODAIKANAL OBSERVATORY.

2.2.1. Frequency Synthesizer.

The block diagram of the frequency synthesizer is shown in Fig. 2.2. It employs a 10 MHz temperature-controlled crystal oscillator with long-term stability of 1 part in 10^6 and a short-term stability an order of magnitude more, to synthesize all the signals required for the transmitter and the receiver units. Therefore the transmitter and receiver frequencies are phase locked. A sequence of arithmetical operations are performed on this reference frequency to generate the various other required frequencies. This method of frequency synthesis offers finer resolution and greater spectral purity in the output over the indirect method of synthesizing the required frequencies from different sources. Also the overall stability of the system is directly linked to the reference source.

The output of the 10 MHz master crystal oscillator is frequency divided to get 5 MHz, 2 MHz, 500 KHz, 500 Hz and 50 Hz signals. The 500 Hz and 50 Hz TTL pulses are used in conjunction with logic gates to generate the negative pulse for the transmitter keyer unit and the positive pulse for the delay gate pulse generator. Both the pulses are of 100 μs width with a repetition frequency of 50 Hz (PRF) and occur at the same time. The carrier frequency of 5 MHz for the transmitter is generated by filtering the 5 MHz square waves from the decade scaler chain. 5 MHz and 500 KHz square waves are mixed and then filtered to get 5.5 MHz local oscillator (LO) signal. This signal is fed to the receiver through an attenuator. A conventional four decade counter comparator is used to generate the delay gate pulse of 10 μ sec width for activating the S/H circuits in the receiver. 100 μsec positive transmitter pulse and 100 KHz TTL pulses are used as initiating and clock pulses respectively for the counter comparator logic.

Solid state devices (IC chips and transistors) are exclusively used in the frequency synthesizer unit. The printed circuit board on which the synthesizer unit is wired consists of three parts. The first part is comprised of 10 MHz crystal oscillator, frequency dividers and the logic gates for the generation of the negative and positive Tx pulses, the circuit diagram of which is shown in Fig. 2.3. 7437 quadruple 2 input NAND gate is used as 10

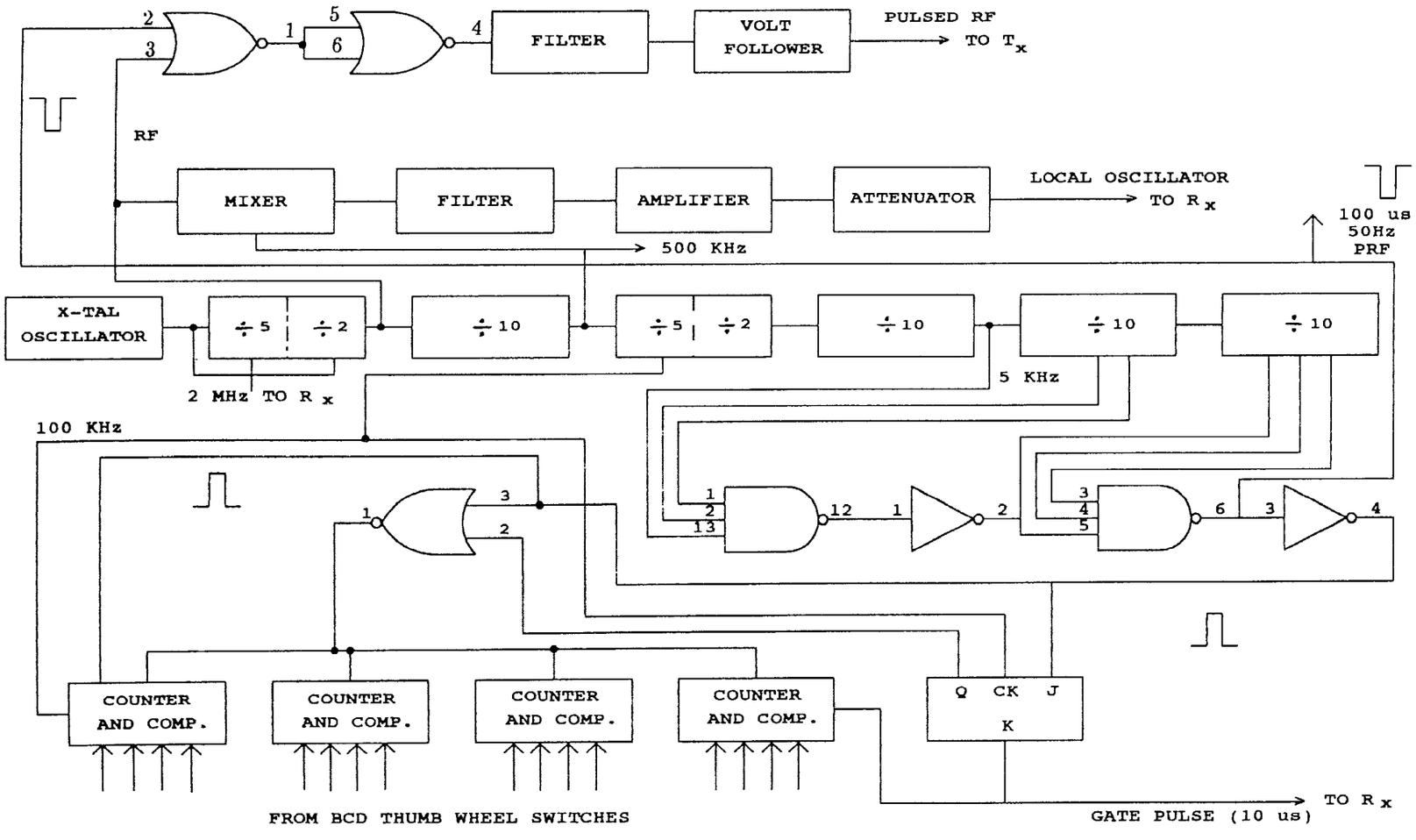

Fig. 2.2. Block diagram of the frequency synthesizer and selective delay gate pulse generator

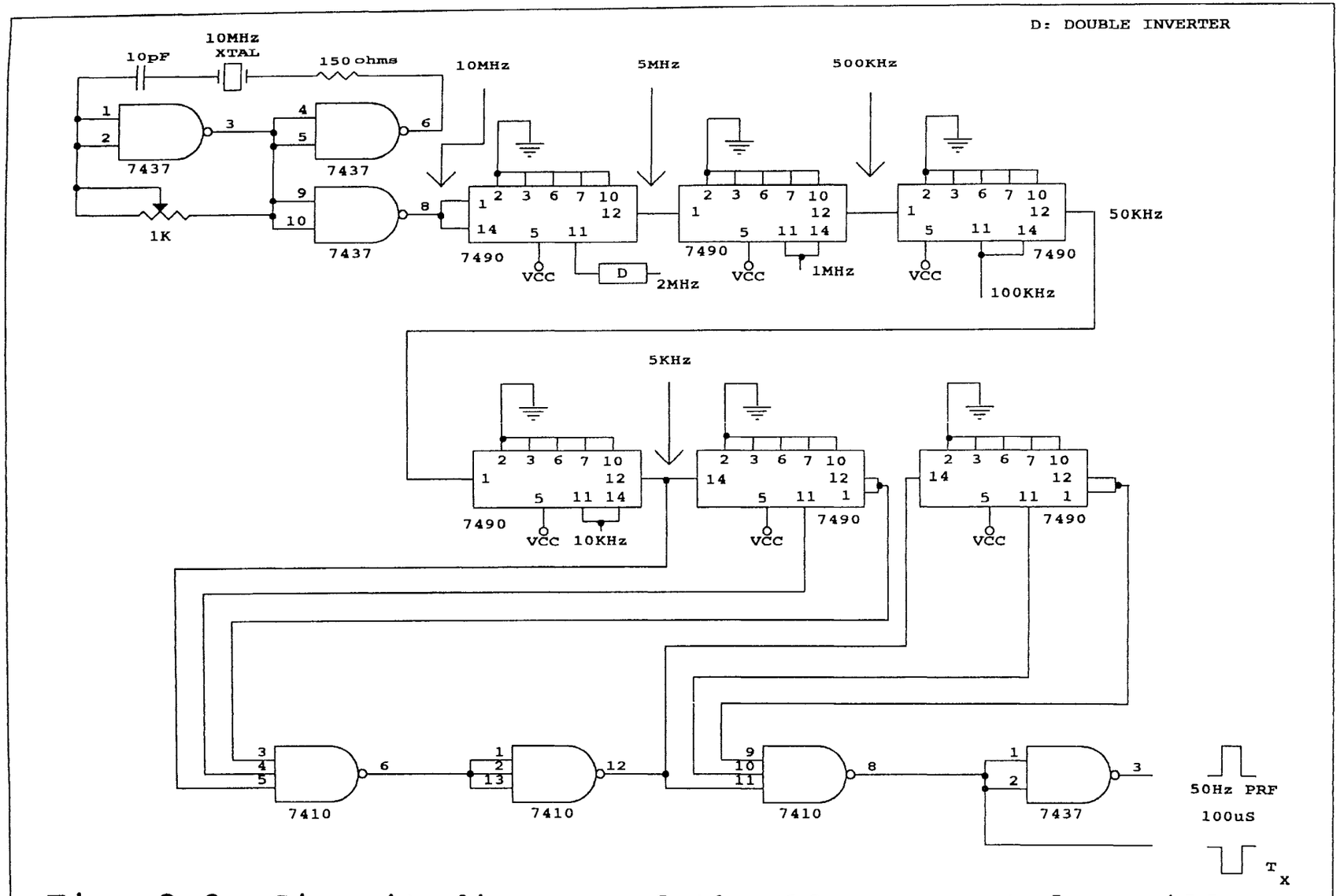

Fig. 2.3. Circuit diagram of the 10MHz crystal oscillator and 5MHz RF and keyer pulse generator

MHz master oscillator with the crystal in its feedback loop. 10 MHz RF is then fed to a string of 7490 decade counters. TTL pulse trains with frequencies of 5 MHz and 500 KHz required for synthesizing the driver signals for Tx and LO for the receiver are taken through double inverters (7404) from appropriate points of the driver chain. 7410 triple input NAND gates are used in association with the last two decade scalers of the driver chain to generate the negative and positive pulses of 100 μsec width and 50 Hz repetition frequency.

Fig. 2.4 shows the delay gate pulse generator circuit. 100 KHz frequency and pulses of 100 μsec width 50 Hz PRF serves as inputs to this circuit. 7485 4-bit magnitude comparators, 7490 decade counters, 7476 J-K flip-flop and 7402 2-input NOR gate constitute the hardware used for the logic designed to generate the gate pulses of 10 μ sec width. Positive Tx pulse initiates the counter. Four thumb-wheel switches together with 7404 inverters generate the program of time delay for the sample and hold (S/H) gate pulse.

The third portion of the synthesizer unit comprises of the 5 MHz and 5.5 MHz (LO) signal generators the circuit of which is shown in Fig 2.5. The 5 MHz square waves are filtered in a Butterworth filter to give a 5 MHz CW signal free from higher harmonics. The 5 MHz CW signal is then taken through a current amplifier stage employing 2N2219A transistor. This signal along with negative Tx pulse is fed to 74128 IC to get the pulse modulated carrier signal. A 2N708 transistor is used to mix the 5 MHz and 500 KHz square waves and the mixer output is filtered in a 3 section Butterworth band pass filter to yield pure 5.5 MHz local oscillator signal. The LO signal is then amplified in a tuned amplifier stage using 2N2219A transistor and is fed to the receiver through an attenuator.

The PCB with frequency synthesizer unit described above is mounted in a well shielded aluminium box with the on-off switch and thumb wheel switches mounted on the front panel. BNC panel receptacles required for supplying signals to other units of the system are mounted on the rear panel. The synthesizer unit with the 10 MHz master crystal oscillator is used for daytime measurements of phase path of ionospheric reflections from

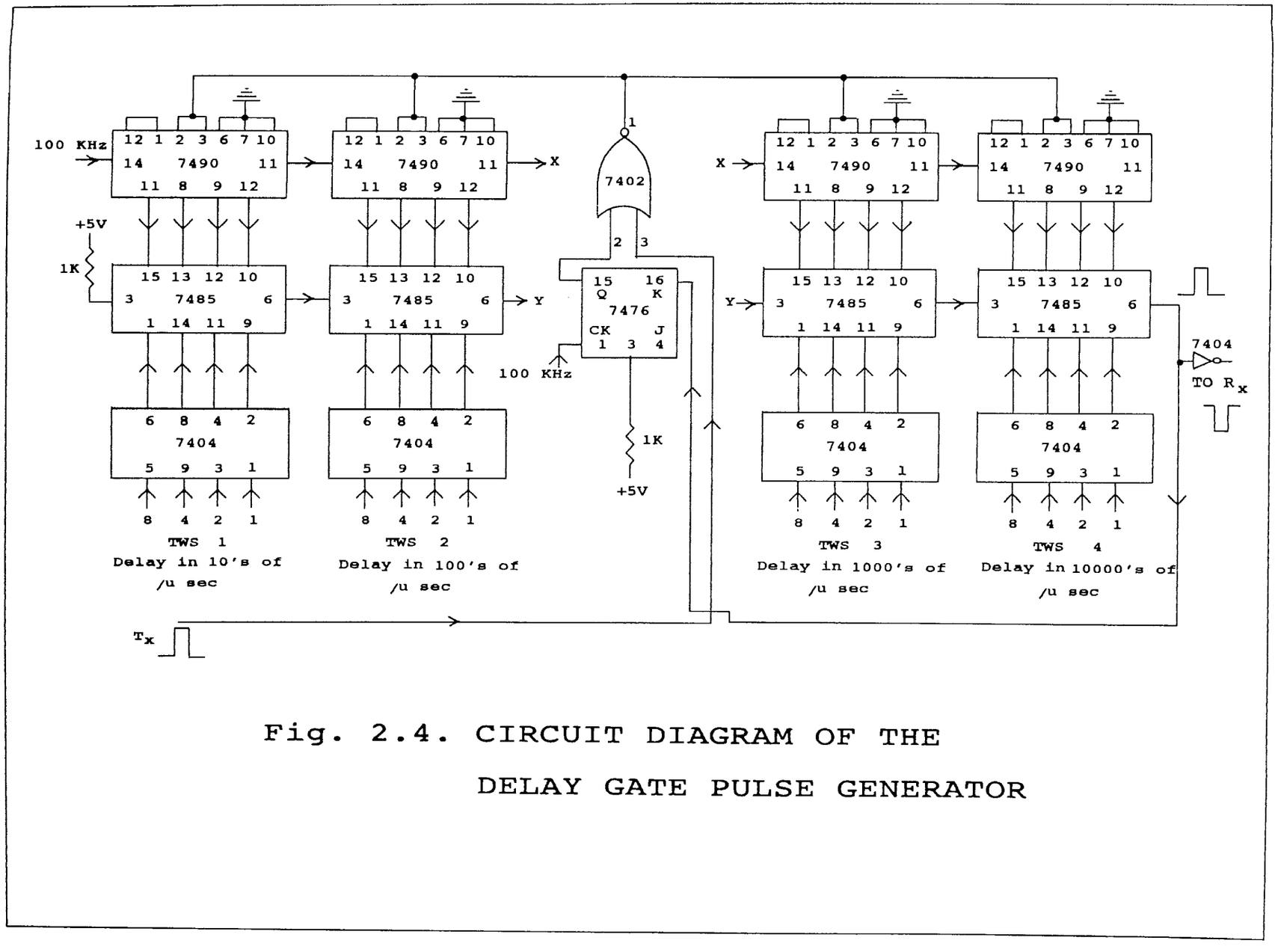

Fig. 2.4. CIRCUIT DIAGRAM OF THE DELAY GATE PULSE GENERATOR

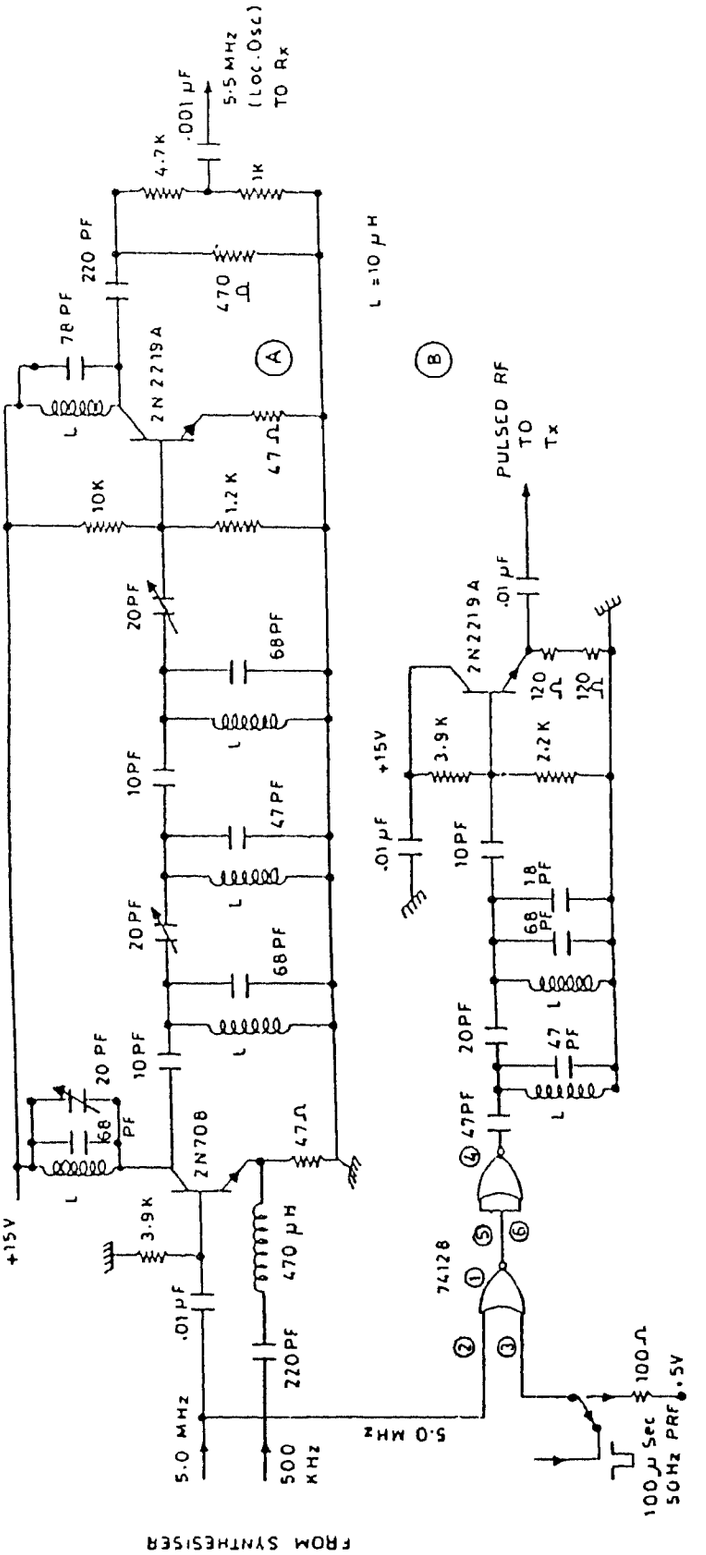

Fig.2.5. Circuit diagram of 5.5 MHz Local Oscillator frequency and 5 MHz pulsed RF generators.

discrete levels. A similar type of unit but with a 16 MHz crystal oscillator is also designed and constructed for the generation of 4 MHz gated *RF* and 4.5 MHz LO to operate the system at 4 MHz. Frequency synthesizer part (1 st part) and the Local Oscillator (4.5 MHz) and 4 MHz gated *RF* generator unit (3rd part) circuits respectively are shown in figures 2.6 and 2.7, while the gate pulse circuit remains same. The 4.0 MHz system is used for probing the ionospheric F-region during evening and nighttime because of the acute broadcast noise encountered on 5.0 MHz at these times at Kodaikanal.

2.2.2. Transmitter.

A C-4 type broad band pulse transmitter is used for transmitting the 100 μsec width pulses at a repetition frequency of 50 Hz. The peak power of the transmitter is 2 KW. Initially a carrier frequency (f) of 5 MHz is used for daytime observations of equatorial ionosphere. The pulse transmitter used in the system is a conventional master oscillator power amplifier (MOPA) arrangement with associated power supplies. It consists of a keyer section and *RF* section. Negative pulse of 100 μ sec width with 50 Hz pulse repetition frequency and 5 MHz gated *RF*, generated in the frequency synthesizer unit, are fed as inputs to the transmitter. The transmitter (Fig 2.1), however, can be operated on any frequency in the range 2-20 MHz. In the keyer section the negative TTL keyer pulse from the frequency synthesizer is amplified in three stages. 6SN7GT and 6J5 valves are employed for the amplification of the keyer pulse. The amplified pulse is then fed to a string of five cathode followers made up of 6L6 valves, the outputs of which are fed to the various amplifier stages of the transmitter. The pulsed RF signal of 5V peak to peak is also amplified in three stages. 6AG7 and 3E29 valves are used for the purpose of preamplification, while 4PR60B electronic valves are used in both the intermediate and final power amplifier stages. The push-pull type final power amplifier output is capacitatively coupled through an open parallel wire feeder to a 600 Ω impedance three element folded dipole type of antenna which is installed at an height of about $\frac{\lambda}{4}$ (wavelength λ for the carrier frequency of 5 MHz is 60 mt) from the ground. Since the transmitter can be operated at any frequency in the range 2-20MHz, no modifications are needed in the unit to operate

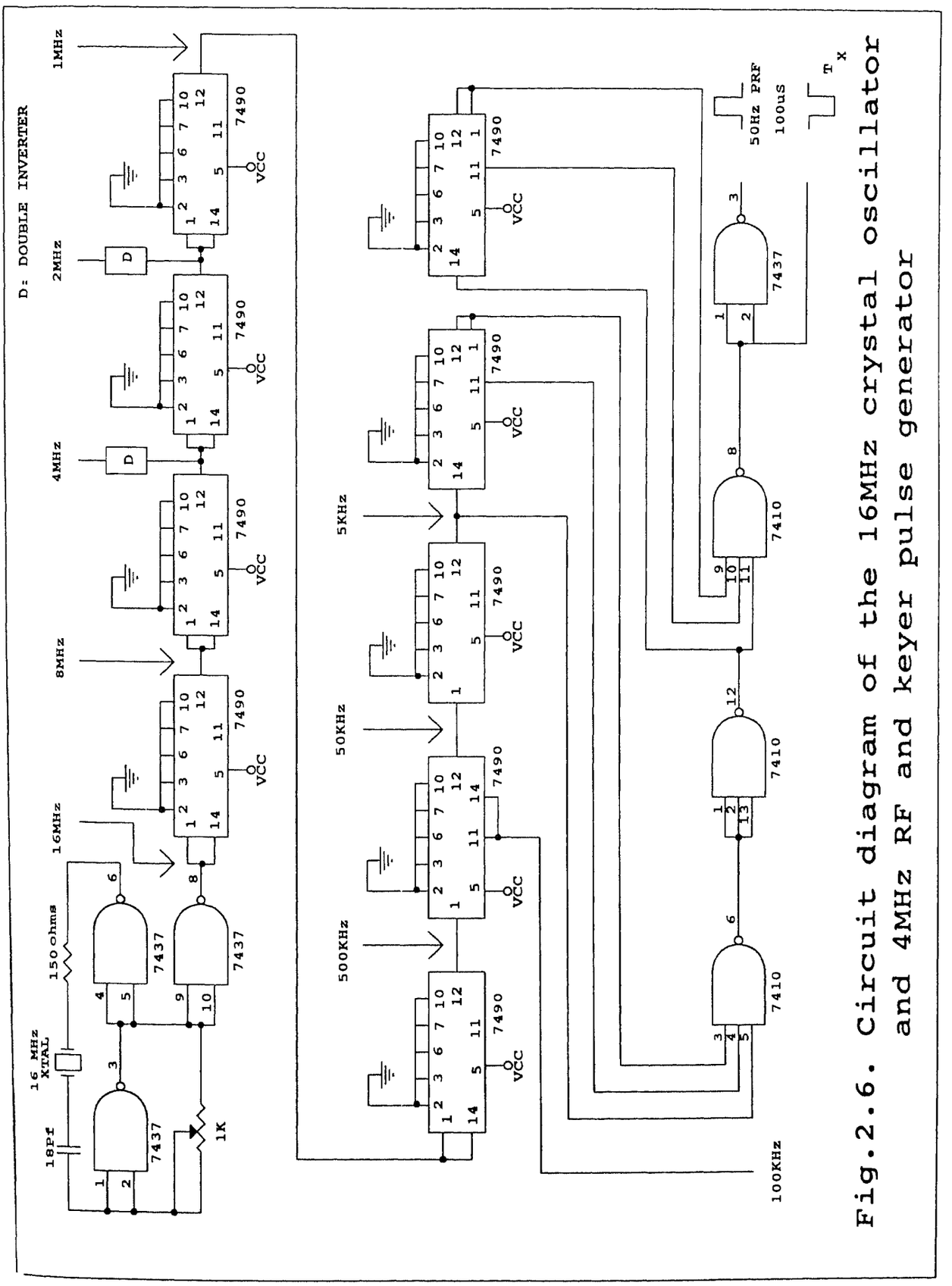

Fig.2.6. Circuit diagram of the 16MHz crystal oscillator and 4MHz RF and keyer pulse generator

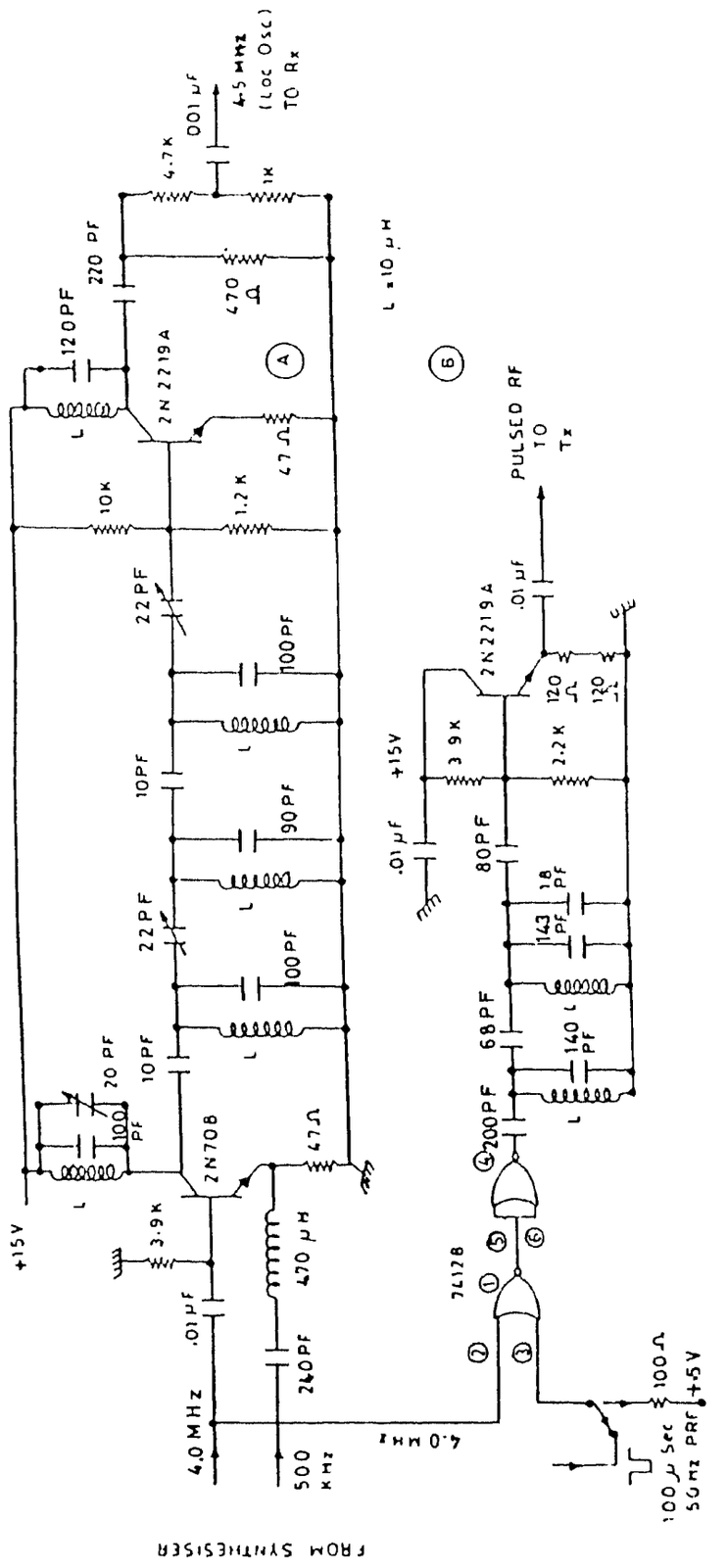

Fig.2.7. Circuit diagram of 4.5 MHz Local Oscillator frequency and 4 MHz pulsed RF generators.

the transmitter on 4 MHz. However, a transmitting antenna is installed with the dimensions corresponding to the operating frequency of 4 MHz.

2.2.3. Receiver.

The pulsed RF after reflection from the ionosphere is received by a half wave dipole type of receiving antenna which is installed co-linearly with transmitting antenna. A 1:1 balun converts the balanced output of the antenna to unbalanced input for the wide band pre-amplifier. The balun and the pre-amplifier are housed in a weather proof box which is mounted at the top of a wooden post placed at the centre of the receiving antenna. RG 8 A/U co-axial cable is used to carry the *RF* output of the pre-amplifier to the receiver. The same cable carries the +15 V d.c. required for the pre-amplifier from the receiver.

The block diagram of the receiver is shown in Fig. 2.1. The receiver comprises of a conventional mixer and IF amplifier, IF being 500 KHz. The local oscillator (LO) frequency (f + IF) for the mixer which is generated in the frequency synthesizer is fed to the receiver externally. The 2 MHz TTL pulses which are also generated in the frequency synthesizer unit are fed to the receiver where they are frequency divided to yield two square outputs in phase quadrature at 500 KHz. The signal IF in the receiver is then phase compared against the two reference IF signals in two separate phase detectors. The output of the two phase detectors are separately amplified and band limited using active low pass filters. A gate pulse of 10μ sec width which is generated in the frequency synthesizer unit and whose delay with respect to the transmitter pulse can be varied is fed to the receiver to activate the sample and hold (S/H) circuits in the two quadrature channels. The filtered output in the quadrature channels are thus sampled and held for a period for 20 ms. The two quadrature channel outputs I and Q can be identified as the respective Acosϕ and Asinϕ components, A being the instantaneous amplitude and ϕ the instantaneous carrier phase of the received signal. From the quadrature outputs the two parameters A and ϕ can be computed. By selecting the time delay of the gate pulse, phase path variations corresponding to specific altitude regions in the ionosphere can be recorded. The height resolution corresponding to the gate pulse width of 10 μsec is 1.5 km.

The phase coherent receiver used in the system enables measurement of phase of the carrier signal in the band 2-20 MHz. The receiver does not contain any internal local oscillator. Instead, an appropriate local oscillator signal corresponding to the operating frequency is to be fed to the receiver. The unit also needs an external source of 2 MHz TTL pulses for phase detection at IF. To compensate for changes in the input signal level to the receiver due to changing ionospheric conditions, a 10 position front-panel controlled attenuator is incorporated before the mixer to provide attenuation from 0 to 40 db in steps of 5db. The IF bandwidth of the receiver is 40 KHz which is wide enough to handle pulses of 50 μ sec width and larger. The dc output of the quadrature channels is in the range 0 - 10 V and can be adjusted by the potentiometers provided on the front panel of the receiver unit. Provision is also available to check for the presence of dc off-sets in the quadrature channel outputs and to null them. Among the four input signals of the receiver, the ionospheric signal and the local oscillator are the two variable signals depending on the frequency at which the systems is operated, while the other two namely, the 2 MHz TTL pulses and 10 μ sec width delay gate pulse are same for any operating frequency. For probing the ionosphere on 5 MHz (4 MHz) 5.5 MHz (4.5 MHz) LO signal is used in the present work.

2.2.4. Logic for inferring sense of changes in Phase Path.

Strip chart recording of the quadrature outputs of the receiver permits evaluation of the phase path variations to an accuracy of about $\lambda/10$ (λ being the wavelength of the probing wave). Manual scaling of the data, however, becomes laborious and highly time consuming particularly when the data is acquired for long durations. Therefore, a logic scheme is developed to infer the sense of changes in phase path in units of a wavelength of the probing wave. This scheme essentially identifies the $2n\pi$ (n is an integer, positive or negative) phase condition using both the quadrature outputs of the receiver and gives out a positive (negative) spike when the phase path is increasing (decreasing) through one λ. The spike output is recorded on the strip chart.

The circuit diagram of the logic scheme adopted to sense and record the changes in phase path in units of λ is shown in Fig. 2.8, and the waveforms that appear at different stages of the logic scheme are illustrated in Fig. 2.9. The quadrature outputs are fed to two comparators employing LM 311 chips. The comparator (B) to which the SINE channel (Q) is fed is referenced to ground while the comparator (A) to which COSINE channel (I) is fed is referenced to a positive dc voltage of about 70% of the maximum expected amplitude. Inverted pulses (O) required for the analog gate are subsequently obtained on passing positive pulses (K) through an inverter employing 7404 IC. The comparator A gives a positive gate pulse (K) for the duration when the input to it exceeds the reference level. In otherwords the comparator A gives out a positive gate pulse when the phase angle of the received signal is close to $2n\pi$. The comparator B, on the otherhand, gives a wide positive pulse (L) of width equal to the time interval when $A\sin\phi$ is positive $[2n\pi < \phi < (2n+1)\pi]$. The leading edge of the pulse (L) occurs when the phase angle is $2n\pi$ and $A\sin\phi$ swings through zero from negative to positive while the trailing edge of the pulse (L) occurs when the phase angle is $(2n+1)\pi$ and $A\sin\phi$ swings through zero from positive to negative. The broad pulses (L) on passing through a differentiator yields a train of positive and negative spikes (M) corresponding, respectively, to the leading and trailing edges of the pulses (L). The analog gate (DG181) allows the spike output (M) to pass through only when it occurs in coincidence with the gate pulse (K), a situation that corresponds to the phase angle around $2n\pi$ as may be seen from the wave forms illustrated in Fig. 2.9. The output of the analog gate (N) is amplified in a μA741 linear operational amplifier and fed to a centre zero strip chart recorder. The output of the logic scheme are thus a series of positive and negative spikes, the positive (negative) spikes representing the increase (decrease) of phase path in units of a wave length (λ) of the probing radio wave. The changes in phase path thus recorded are practically insensitive to amplitude changes as the 2π condition is identified from changes in both the quadrature outputs of the receiver. The logic has been extensively tested under actual operational conditions and found to give reliable data as may be seen from the portion of a test record reproduced in Fig.2.10. The reference level for the comparator in the COSINE channel is judiciously chosen on individual occasion to minimize the errors due to fading.

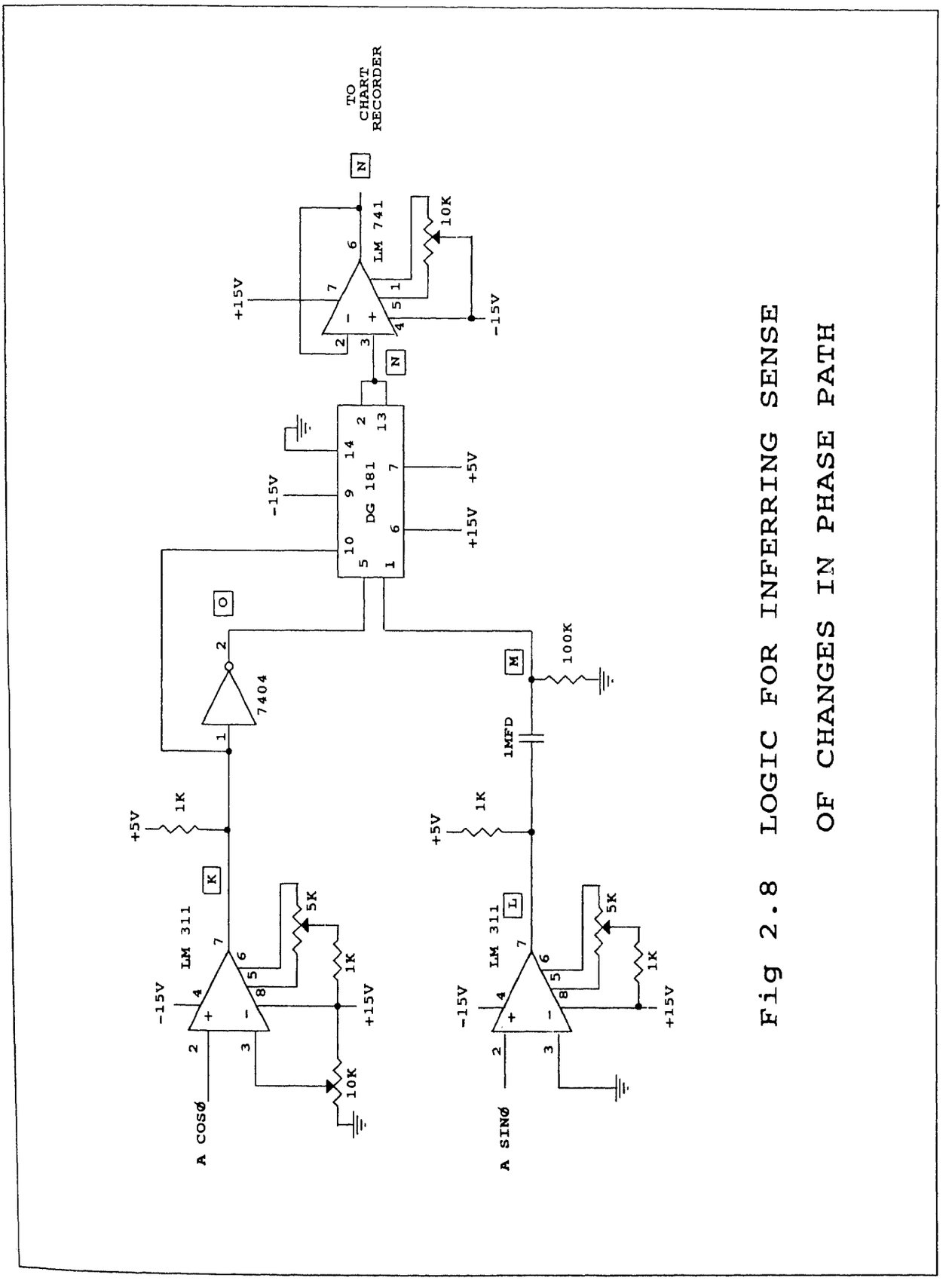

Fig 2.8 LOGIC FOR INFERRING SENSE OF CHANGES IN PHASE PATH

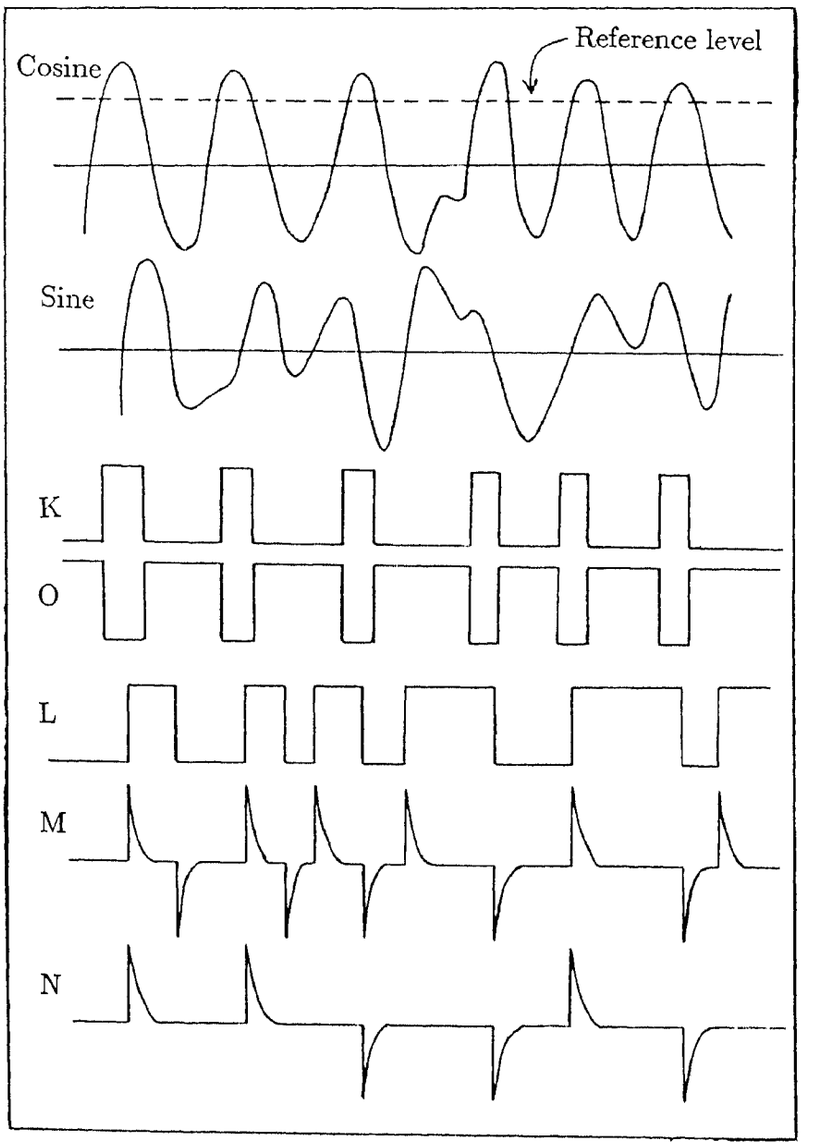

Fig.2.9. Waveforms of the logic scheme for recording phase path changes in units of λ.

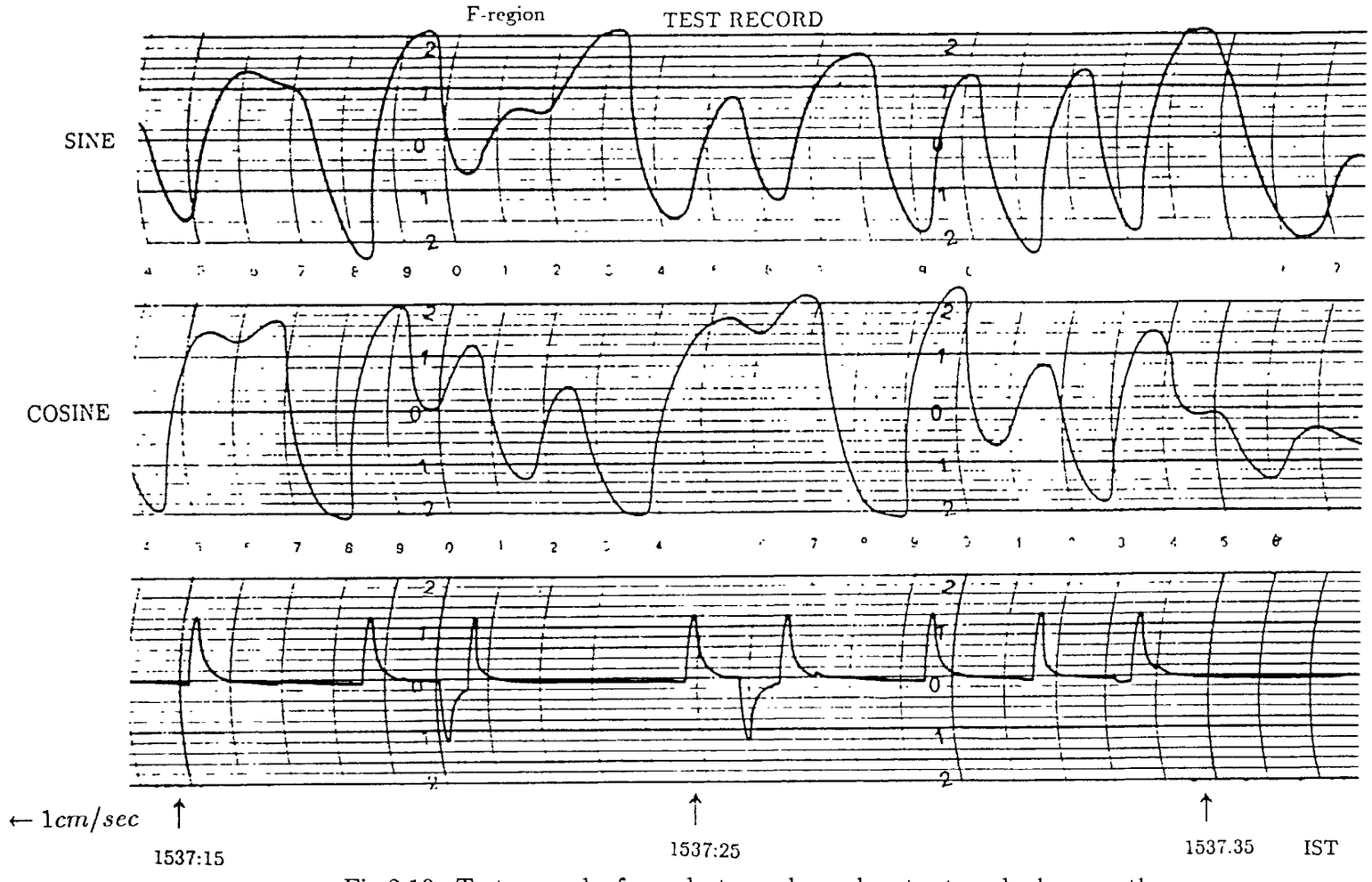

Fig.2.10. Test record of quadrature channel output and phase path changes in units of λ of reflection from F-region.

2.2.5. Scheme for simultaneous recording of phase path of ionospheric reflections from two heights.

To record the changes in phase path of ionospheric reflections simultaneously from two discrete heights, the system has been augmented with another receiver and by duplicating the sample and hold gate pulse circuit and logic scheme to infer sense of changes in phase path. The second gate pulse circuit, however, is incorporated in the synthesizer unit itself. The unbalanced signal of the receiving antenna is taken in parallel through two preamplifiers followed by two individual receivers. Local oscillator and 2 MHz signal fed to the two receivers are drawn from the same source while sample and hold signals are fed to the receivers from two S/H circuits with delays corresponding to two discrete echo levels. The quadrature signals are fed to two separate logic schemes to infer sense of changes in phase path of the radio wave returned from two ionospheric levels. The spike outputs of the two logic circuit units are recorded on the multi-channel strip chart recorder.

2.3. METHOD OF OBSERVATIONS AND DATA ANALYSIS.

The present thesis is primarily based on the observations of phase path of ionospheric F-region reflections made at Kodaikanal (10°N, 77°28'E, dip 3° N) in the Indian equatorial region. Daytime observations have been made on the probing frequency of 5 MHz while those of nighttime on 4 MHz. One of the characteristic features of the daytime equatorial ionosphere is the appearance of sporadic E (Esq). Observations from a co-located ionosonde show that under normal ionospheric conditions, the blanketing frequency of the equatorial sporadic E (f_bE_s) is in the range of 2.5 to 3.5 MHz. Under strong electrojet conditions f_bE_s is found to exceed even 4.0 MHz. Therefore for the observations of daytime bottomside F-region the operating frequency is judicially chosen as 5.0 MHz. During evening and nighttimes the Esq layer disappears and therefore lower frequencies in the HF band can conveniently be used to probe the bottomside F-region. Also in the later part of the night, the critical frequency of the F-region at times falls below 5.0 MHz and, therefore, lower frequencies are generally adopted for the purpose. However, the physical dimensions of the

folded dipole type antenna increase as the probing frequency is decreased. Therefore as a compromise a frequency of 4.0 MHz has been chosen for probing the bottomside F-region during evening and nighttime periods.

The method adopted for recording the changes in phase path of reflections from discrete levels of ionosphere and the data reduction procedures are as follows. The quadrature outputs of the receiver(s) (before the S/H circuits) are monitored on a dual beam oscilloscope and the RF attenuation is adjusted so as to give a dc output of about 3 to 5 V in both the channels. The channel outputs are also checked for the presence of dc off-set. The delay of the S/H gate pulse is adjusted to select the altitude region of interest and is made to coincide with the ionospheric echo maximum. Continuous monitoring of the channel outputs is done throughout each data run to observe the prevailing ionospheric conditions and to make adjustments of the RF attenuation and gate pulse delay, if required. The chart speed used for recording the phase path of F-region reflections is 10cm/sec, while for recording phase path of Esq, which generally shows fast fadings, a chart speed of 1 cm/sec is used. The data are scaled by simply counting the total number of pulses (each pulse corresponding to a phase path change of 1λ) that occurred during a specified time intervals of 6 sec or 1 sec, depending on the speed of the chart used, by taking into account the sign of the pulses. The algebraic sum of the spikes gives the change in phase path (ΔP) in the given time interval and the cumulative sum of ΔP gives as the temporal variation of total phase path P.

The phase path of F-region reflections (on 5.0 MHz operating frequency) during day light hours shows a general decrease in the forenoon period and a general increase in the afternoon period, typical examples of which are shown in the upper panels of Figs 2.11 and 2.12 respectively. During forenoon period the decrease in phase path is due to the fall of reflection level as the production of ionization dominates. There could also be contribution to phase path changes from the changing electron density profile resulting in changes of refractive index of the medium well below the reflection level. During afternoon and evening times the production of ionization decreases while the loss processes increases

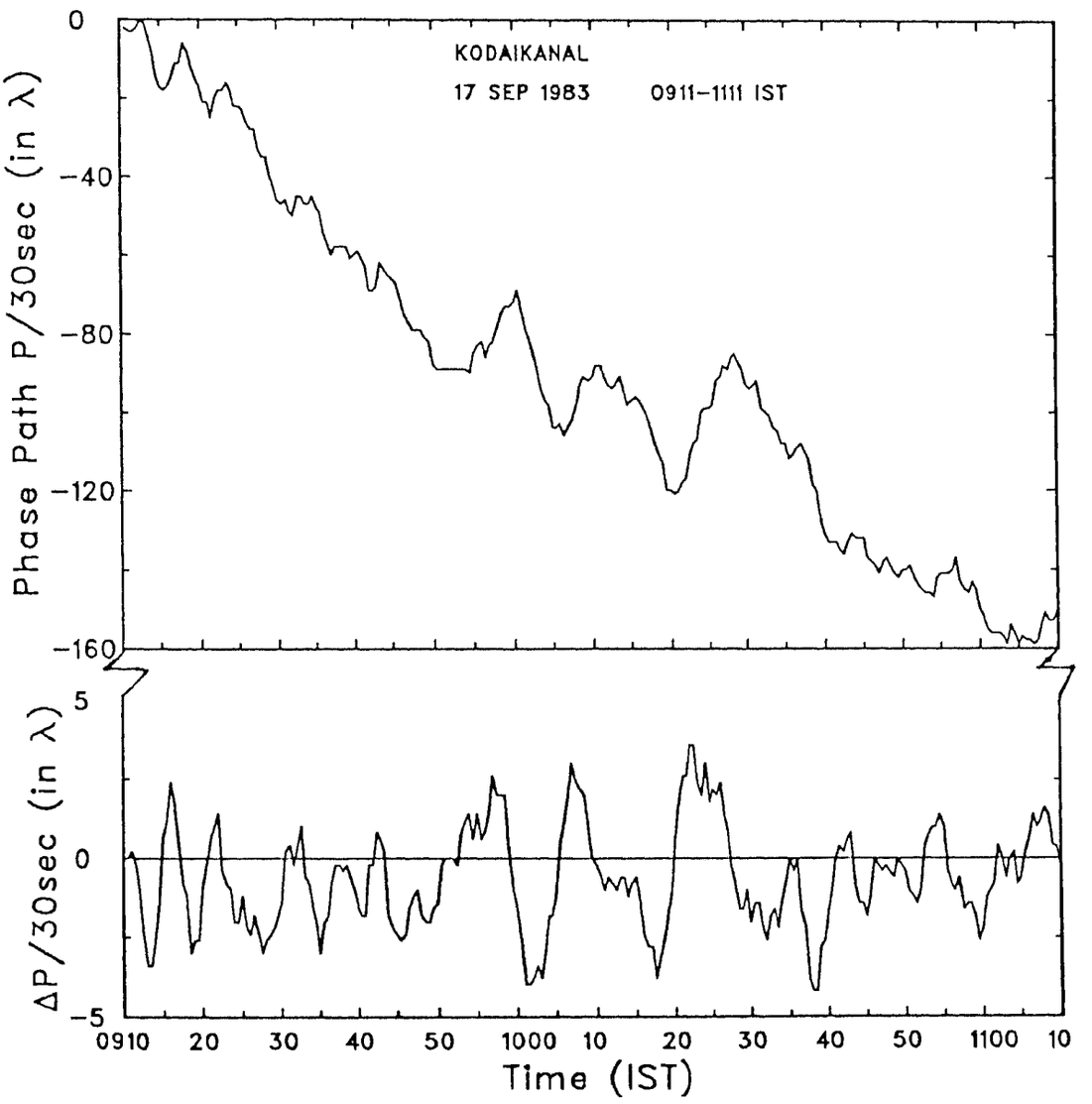

Fig.2.11. Top Panel : Variation of phase path (P) with time of reflection from F-region over Kodaikanal during prenoon hours.

Bottom Panel : Variation of 5 point running means of phase path change (ΔP) per 30 sec with time.

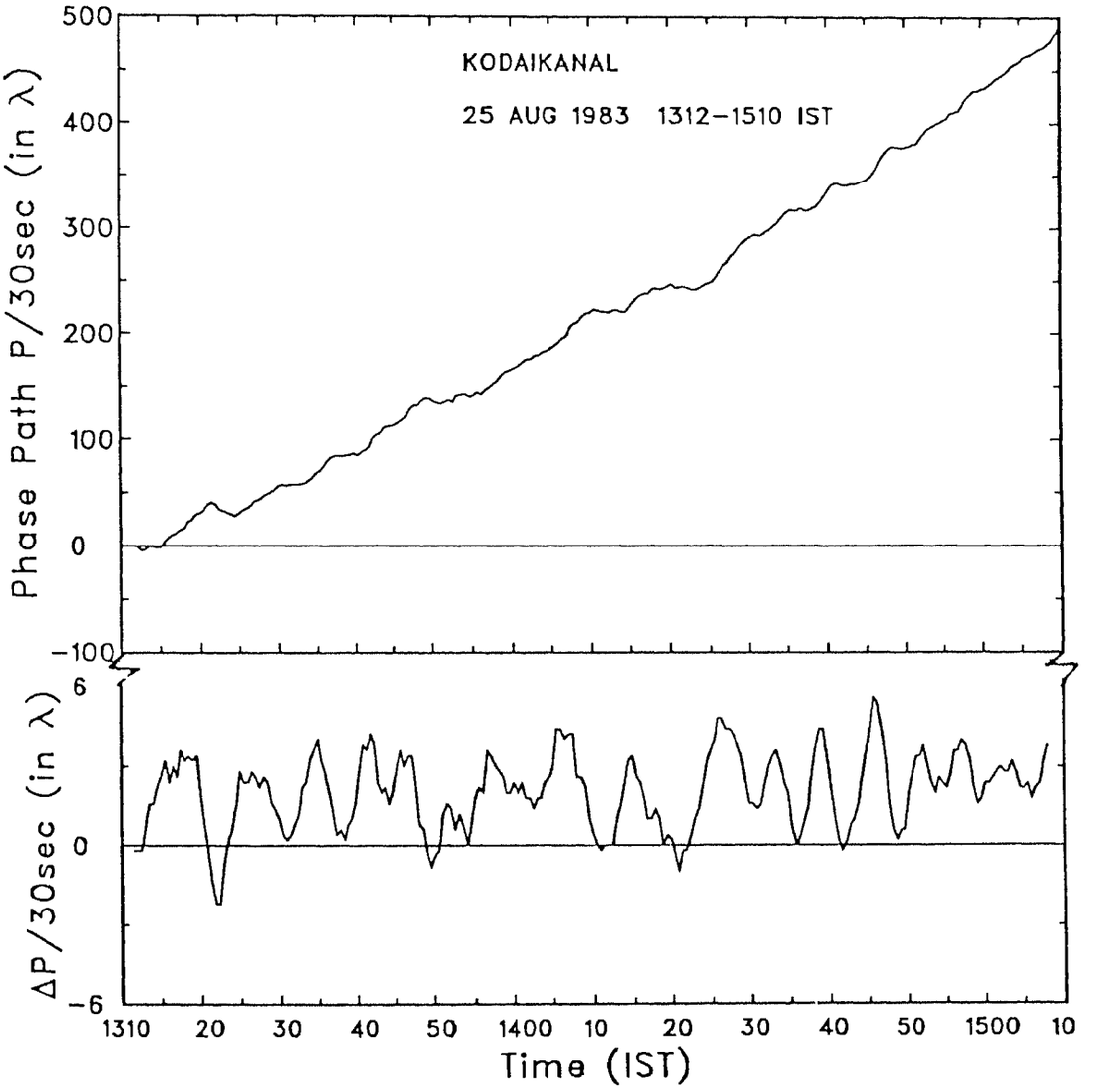

Fig.2.12. Top Panel : Variation of phase path (P) with time of reflection from F-region over Kodaikanal during afternoon hours.

Bottom Panel : Variation of 5 point running means of phase path change (ΔP) per 30 sec with time.

and the overall reduction in ionization is responsible for the general increase of phase path. Besides production and loss of ionization due to photoionization and recombination processes, there are other mechanisms such as vertical plasma drifts which can affect the electron density at all levels of the ionosphere. The vertical drift is particularly important at low dip latitude stations like Kodaikanal.

Another interesting feature observed in the daytime phase path data is the manifestation of small scale oscillations superposed on the steadily decreasing (increasing) phase path in the forenoon (afternoon) hours. To bring out these small scale fluctuations more clearly, the phase path (P) *versus* time curve is differentiated to obtain the rate of change of phase path (ΔP) per unit time. Running mean method with properly chosen window has been employed to supress the noise-like very high frequency fluctuations in ΔP. Typical examples of the fluctuation in ΔP obtained from this procedure are shown in the lower panels of Figs 2.11 and 2.12. The smoothed ΔP values are then subjected to spectral analysis using the standard fast Fourier Transform (FFT) method to infer the spectral content of the small scale fluctuations. The power spectra of the data presented in Figs 2.11 and 2.12 are shown in Fig 2.13. Simultaneous observations of phase path of ionospheric returns from Esq and F-region have been made on several occasions during daytime. A typical example of such observations is shown in Fig. 2.14. The lower and upper panels of Fig. 2.14 represent smoothed values of ΔP of Esq and F-regions respectively. Results of a detailed study made of the short-period fluctuations in phase path of daytime F-region reflections are presented in the 3rd chapter.

Evening and nighttime observations of the phase path of ionospheric F-region reflections are made on the probing frequency of 4 MHz for the present work. A typical example of the changes in phase path (ΔP) of ionospheric F - region reflections during night time (1600 to 0600 hrs IST) is shown in Fig 2.15. The changes in phase path ΔP or Doppler velocity (V_D) is positive during evening hours and negative during nighttime, the reversal occurring after the sunset. Before the reversal from positive to negative a sharp enhancement in ΔP is observed as a regular feature and is known to be due to the action

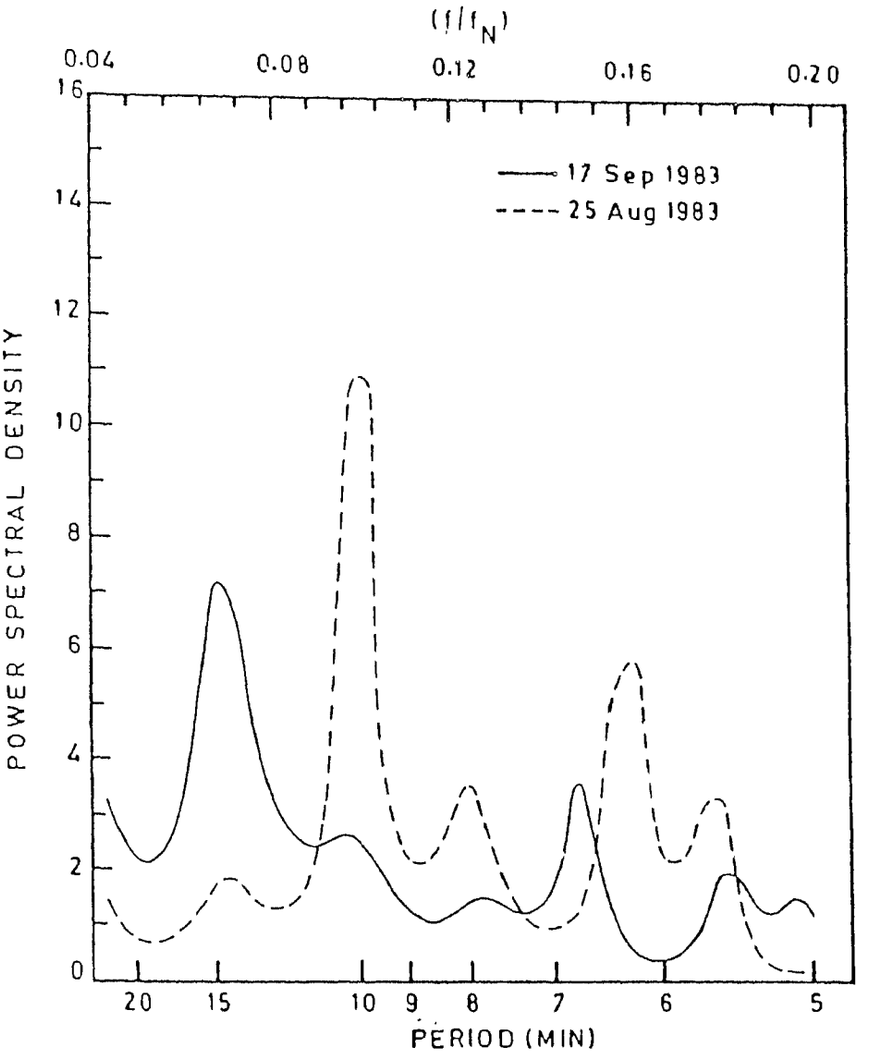

Fig.2.13. Power spectra of ΔP corresponding to records of Figs. 2.11 and 2.12.

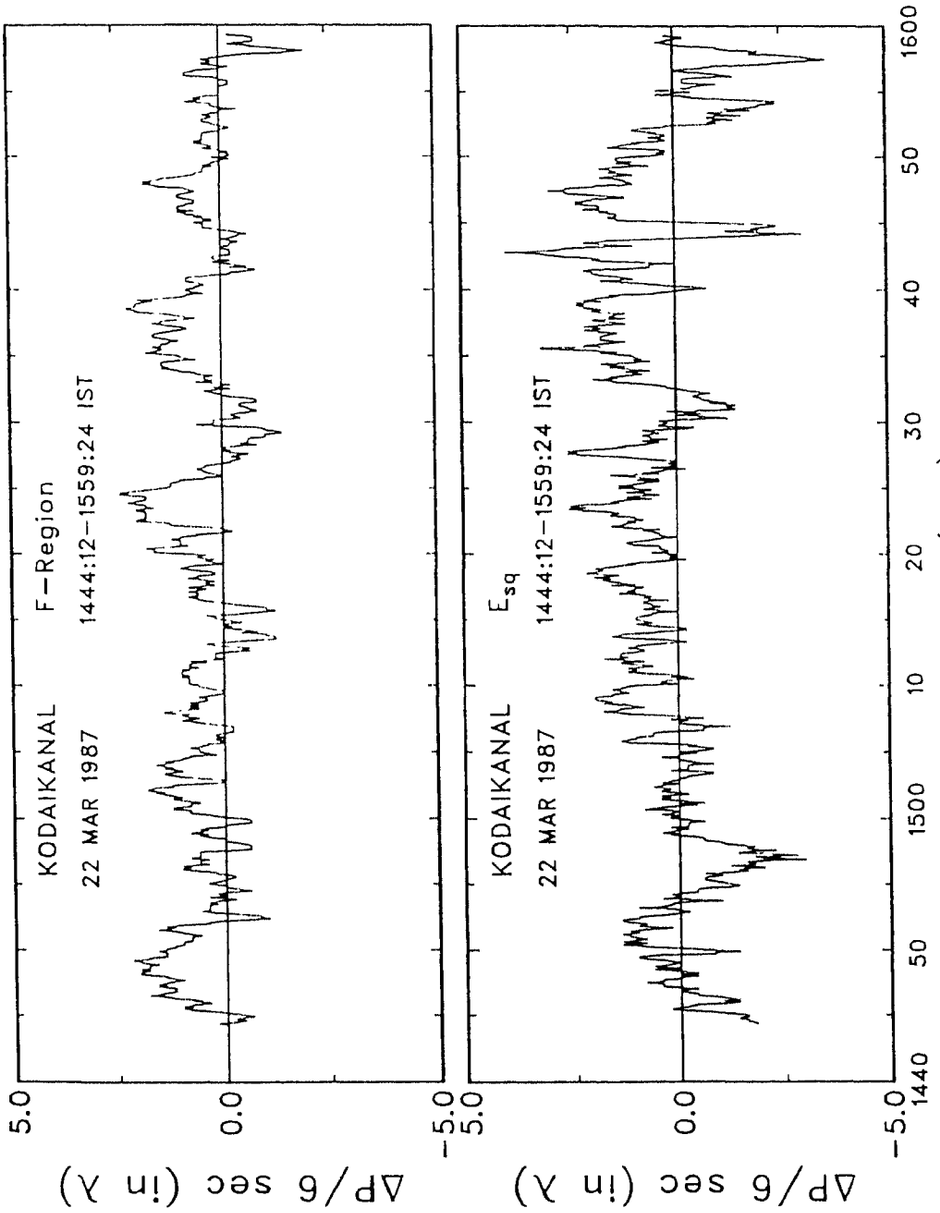

Fig.2.14. Simultaneous recording of changes in phase path of F-region and E_{sq} reflections at Kodaikanal.

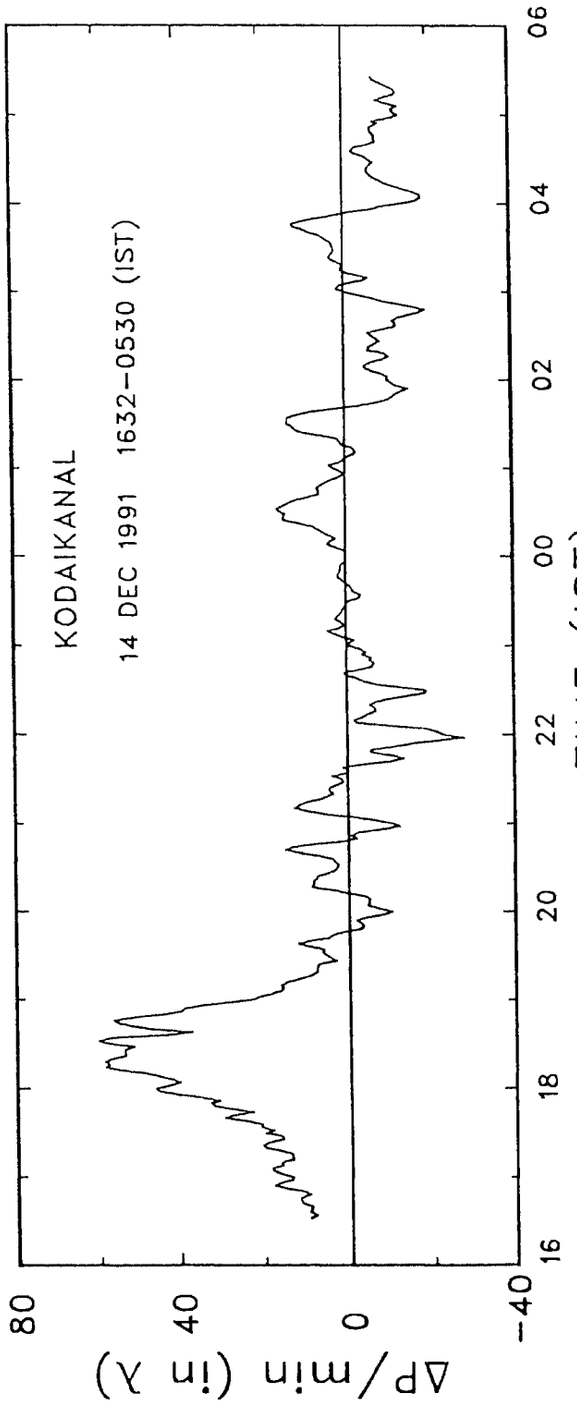

Fig.2.15. Changes in phase path of reflections from F-region over Kodaikanal during evening and nighttimes. These measurements are made with 4 MHz.

of F-region dynamo induced EXB drift which becomes operative around sunset time at equatorial latitudes. The nighttime negative ΔP is indicative of downward EXB plasma drift induced by the westward electric field of E-region dynamo origin. The details of the morphological features of the F-region vertical plasma drifts over Kodaikanal deduced from the changes in phase path of F-region reflections, and the characteristics of the fluctuations in F-region Doppler velocity, V_D observed during an event of geomagnetic micropulsation activity are presented in the 4th Chapter.

CHAPTER 3

STUDIES ON PHASE PATH VARIATIONS OF F-REGION REFLECTIONS DURING DAYTIME

3.1 INTRODUCTION

A pulsed HF phase path sounder, the details of which are described in the second chapter, is regularly operated at Kodaikanal (10°14'N, 77°28'E, dip 3°N) to investigate ionospheric dynamics in the equatorial electrojet region. Phase path of ionospheric reflections at vertical incidence is highly responsive to changes in reflection height caused by vertical plasma drift, and such vertical plasma drifts do commonly prevail in the vicinity of the dip equator as a result of the interaction of largescale east-west electric field (E) of dynamo origin with the nearly horizontal north-south geomagnetic field, B there (see review of Fejer, 1981). The vertical EXB plasma drift, in fact, effectively governs the structure and dynamics of the equatorial ionosphere and is a vital experimental input for quantitative modelling of the low latitude ionosphere (see for example, Anderson, 1981; Sastri, 1990 and references therein). Our phase path sounder which provides information on the changes in the phase path of ionospheric reflections with a temporal resolution of 1 to 6 sec is, therefore, well suited for studies of temporal fine structure in the equatorial electric field (see for e.g., Patel and Lagos, 1985) and signatures of penetration of magnetospheric electric fields during storm-time conditions (see for example Fejer, 1986; and Earle and Kelley, 1987), especially, at times of storm sudden commencements (e.g., Sastri et al., 1993). It is to be noted, however, that the phase path of F-region reflections during daytime at electrojet locations could be influenced by the refractive index variations associated with the electrojet irregularities and their motions that prevail at E-region altitudes in the proximity of the dip equator. Careful assessment of plausible electrojet modulation of F-region phase path during daytime at electrojet locations must there be made to derive reliable information on the F-region vertical plasma drift from HF phase path measurements. An attempt made to quantify the modulations, if any, in F-region phase path caused by the electrojet irregularities is presented in this Chapter.

3.2. OBSERVATIONS OF SMALL SCALE VARIATIONS (30-600 sec).

Recordings of the variations in phase path, P of F-region reflections with 5 MHz operating frequency are carried out on a number of occasions during daytime interval 08-16 IST. The length of the data run in the acquired data sample varied from 2 to 4 hrs on individual occasions. The chart speed used for these observations is 10 cm/min so that the temporal resolution of the data available is 6 sec. In the first instance a total of $\sim$ 90 hrs of data were analysed. Reductions of ionograms obtained from a co-located ionosonde for all the days and for the time interval during which phase path data were acquired showed the true height of reflection for 5 MHz to vary from 210 to 265 km. Therefore the phase path data analysed here pertain essentially to the lower F-region. Data were scaled following the procedure described in the previous chapter.

Reductions of the data showed the regular diurnal changes in P i.e. a steady decrease in the forenoon hours and a steady increase in the afternoon hours. Small-scale variations, superimposed on the regular diurnal trends are found to manifest on almost all the days. To facilitate a study of the small scale variations in P which are masked by the large and often rapid diurnal changes, the time rate of change of phase path, $\dot{P}$ was computed from the first difference of the original P *versus* time record, separated by the sampling interval of 6 sec, i.e., the P-t curve was differentiated. The resulting $\dot{P}$ time series was smoothed with a 30 sec width window to reduce noise like fluctuations of very short time scales. A typical example of the $\dot{P}$ time series during daytime is shown in Fig.3.1.

Perusal of the $\dot{P}$ time histories on individual days revealed a persistent and regular occurrence of fluctuations in $\dot{P}$ with quasi-periods in the range 60-600 sec (see Fig 3.1). The spectral content is felt to be composed of two rather overlapping domains viz., the shorter-period components with periods less than 240 sec and the longer-period components with periods greater than 300 sec with characteristic behaviour. The 6 sec interval $\dot{P}$ data were therefore further processed to bring out the characteristics of the variations in the two spectral domains in a quantitative way.

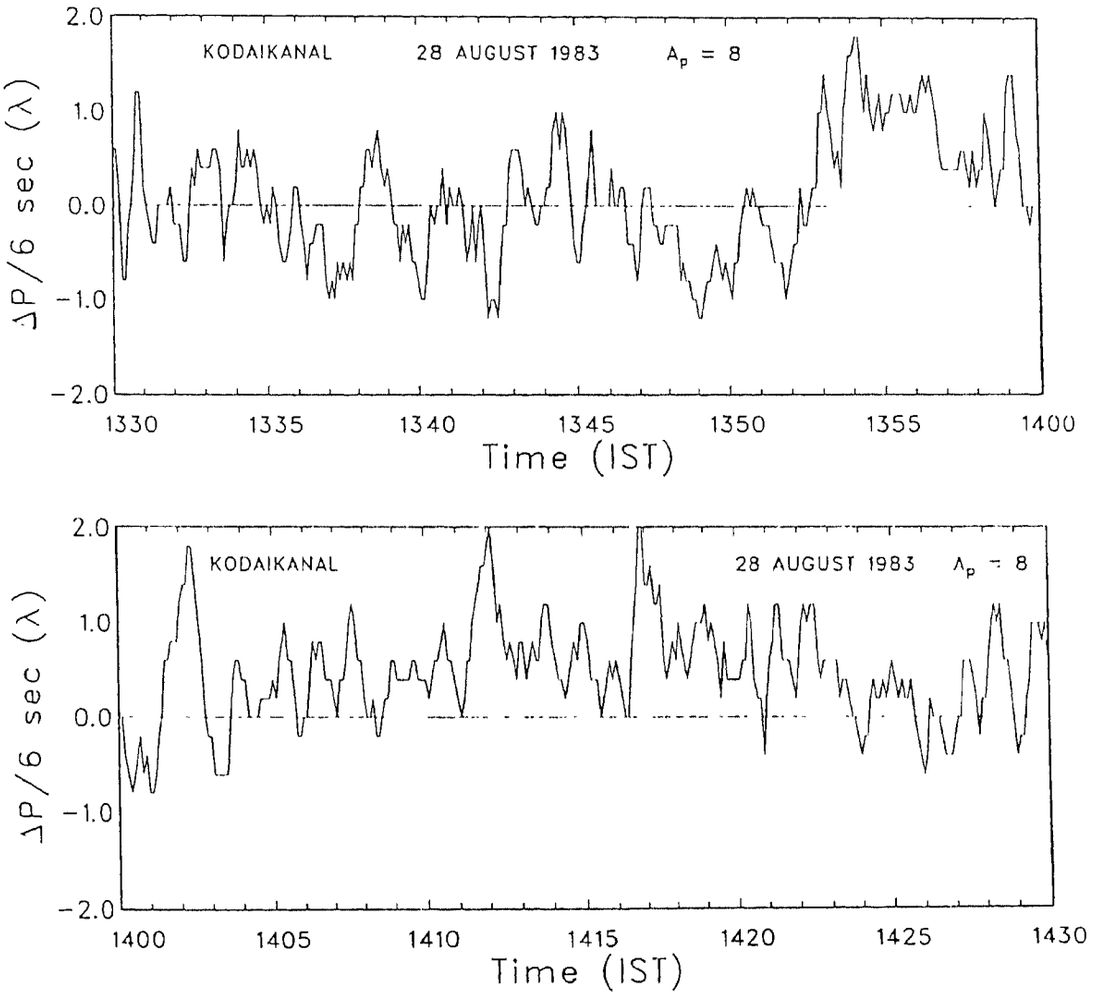

Fig.3.1. Typical example of $\Delta P/6$ sec time series during daytime depicting the occurrence of 60-600 sec period fluctuations.

3.3. LONG-PERIOD OSCILLATIONS (300-600 sec).

To study the longer period (T > 300 sec) components of the fluctuations, the P-t curve is differentiated at 36 sec intervals. This particular sampling rate was chosen because, besides being appropriate, it corresponds to the time resolution of the geomagnetic data as it will be explained later in this chapter. The $\dot{P}$ time series thus obtained was smoothed with 180 sec width window to suppress the contribution of shorter period fluctuations. The resultant $\dot{P}$ time series was then subjected to spectral analysis using the fast Fourier Transform (FFT) technique. In computing the power spectra of the longer-period fluctuations, whenever the data length fell short of the required 2^n data points, the time series was suffixed with zeros at the end.

Temporal variations of $\dot{P}$ (ΔP/36 sec) and the corresponding power spectrum shown in Fig. 3.2 demonstrate the occurrence of longer-period (300-600 sec) quasi-periodic fluctuations in phase path of F-region reflections. These fluctuation in $\dot{P}$ manifest at all time during daytime (08-16 hrs LT) with peak-to-peak amplitudes of 15-30 ms^{-1} in $\dot{P}$ (0.25 to 0.5 Hz in $\Delta f = -\frac{f}{c}\frac{\Delta P}{\Delta t}$). The spectral content of the fluctuations exhibits variability not only from day-to-day but also during the course of a data run, i.e., on time scales of an hour. A systematic dependence of these fluctuations on the ambient electrojet strength and related ionospheric conditions such as disappearance of Esq on ionograms, was not found.

Temporal variation in the rate of change of phase path, $\dot{P}$ of ionospheric reflections at vertical incidence can be caused by perturbations in the reflection height due to vertical up and down movement of the ionosphere as a whole and/or changes in the total electron content below the reflection level (Davies and Baker, 1966, Georges, 1967). The single frequency data presented here are inadequate to unambiguously assess the relative contribution of the two mechanisms to the observed quasi-periodic variations in $\dot{P}$. It is well established in earlier studies, however, that under vertical propagation and non-solar flare conditions, plasma motions near the reflection level are most effective in causing phase

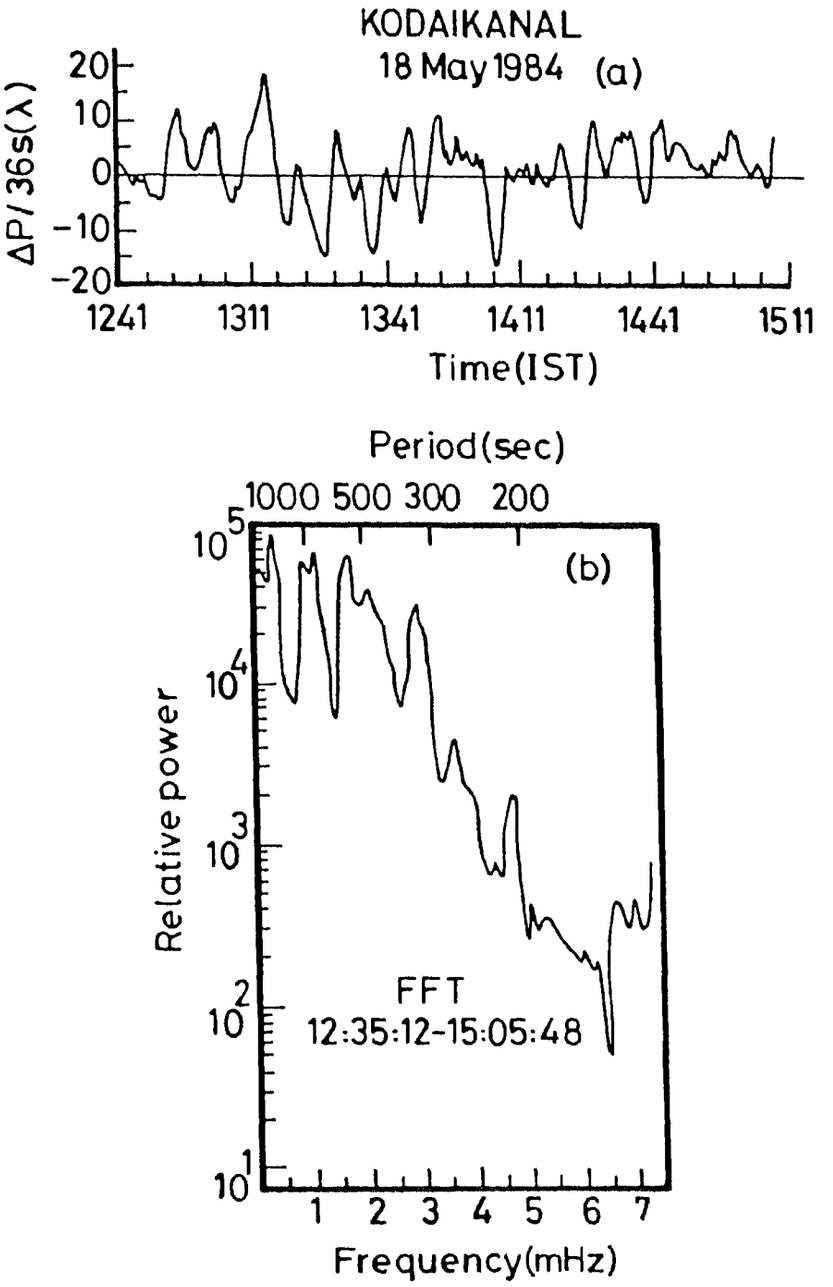

Fig.3.2. Typical example of the longer-period (300-600 sec) quasi- periodic fluctuations in $\Delta P/36$ sec of lower F-region reflections during daytime over Kodaikanal (Top panel) and the corresponding power spectrum (Bottom panel).

path variations (Davies and Baker, 1966, Georges, 1967). For vertical propagation the total path length is twice the reflection height and the rate of change of phase path $\dot{P}$ ($\Delta P/\Delta t$) is equal to twice the rate of change of height of reflection, i.e., $\frac{\Delta P}{\Delta t} = 2\frac{\Delta h}{\Delta t}$ or $\dot{P}$=2V_z. Under this assumption the peak-to-peak amplitude of the causative fluctuations in vertical plasma drift (V_z) will then be in the range 7.5 to 15 ms^{-1}. These values are reasonable compared to the ambient V_z value of $\sim$ 15 ms^{-1} around 200 km derived from incoherent scatter radar measurements (Balsley et al., 1976b). It is also known that the F-region plasma close to the dip equator is subjected to the electrodynamic drift ($\frac{EXB}{B^2}$) during daytime. Therefore the inferred fluctuations in V_z could be arising from changes in E or B or in both.

Geomagnetic micropulsations which are hydromagnetic waves with an oscillating magnetic field that propagate in the ionosphere from above can cause vertical motions of F-region plasma. The inferred fluctuations in $\dot{P}$ fall in the range of Pc4 and Pc5 type of micropulsations which cover the period range from 45 to 600 sec. Pc4 and Pc5 type micropulsations are observed during daytime in the vicinity of the dip equator with a characteristic morphology (e.g., Jain, 1977). Inquiry into the occurrence of inferred $\dot{P}$ fluctuations concurrent with Pc5 micropulsations is therefore quite logical. An experimental set-up to monitor geomagnetic pulsations of 45 - 600 sec periods is in operation at Trivandrum (8°29′N, 76°57′E, dip 0.6°S) since 1978. The micropulsation recording set-up (Jain and Iyengar, 1978) has a sensitivity of 0.2nT/mm in H-field and a temporal resolution of 36 sec. The data from this experiment are thus adequate for quantitative studies of Pc5 (150-600sec) pulsations.

Consultation of geomagnetic pulsation data at Trivandrum showed the availability of data simultaneous with the phase path data at Kodaikanal for $\sim$ 52 hours spread over 19 days. To assess the relationship of the longer period (300-600 sec) fluctuations in $\dot{P}$ with Pc5 micropulsations, the analogue record of H-field data was digitized at 36 sec intervals. The deviations of H-field from the mean value, H-$\bar{H}$ were computed and smoothed with a 180 sec width window to bring out the fluctuations in the Pc5 range. Careful scrutiny of

the temporal patterns of simultaneous $\dot{P}$ and H-$\bar{H}$ on the 19 days indicated the absence of an apparent relationship between the two parameters for most of the time. To substantiate this visual impression, the two sets of data were subjected to cross correlation analysis. This analysis, however, has been carried out by dividing the data on each day into segments of 55.2 min length. Use of a short data window of about 1 hr is felt desirable in view of the influence of the variable ionospheric conductivity on the phase relationship between pulsation signatures in the magnetometer and phase path data. The statistical details of the relationship noticed between the fluctuations in $\dot{P}$ and H-$\bar{H}$ is presented in Table 3.1. Only those correlation coefficients which are significant at ρ (level of significance) $\geq$ 0.01 level are shown in the table. It is clear from Table 3.1 that 80% of the data do not show statistically significant relationship between the two parameters. Even in the remaining 9 segments the correlation coefficients, although statistically significant, were not high enough to be considered as conclusive evidence of a link of the fluctuations in $\dot{P}$ with geomagnetic micropulsation activity. A typical example of the non existence of the relationship between $\dot{P}$ and H-$\bar{H}$ is illustrated in Fig. 3.3. The correlation did not improve significantly even when the starting point of the data window was advanced or delayed. The correlation analysis is repeated for the entire data sample with a shorter data window of 43.2 min length. Such an analysis also yielded more or less similar results. Geomagnetic micropulsations of Pc5 type thus do not seem to be the dominant source of the evidenced 300-600 sec fluctuations in $\dot{P}$ during daytime, though are occasionally found to coincide with similar variations in H-$\bar{H}$ over time spans of 15-30min.

Electric field variations associated with neutral atmospheric waves can cause perturbations in F- region vertical plasma drift. Acoustic waves could be one possible source of neutral atmospheric wave which can be communicated to ionospheric plasma through plasma-neutral coupling processes as the acoustic cut-off period at 200 km is about 10.5 min (Fig. 3.4). Acoustic waves propagate upward at speeds of 500-600 ms $^{-1}$ and are subjected to substantial absorption in the atmosphere mainly by viscosity (Hargreaves, 1979). Acoustic waves are therefore not commonly seen at F-region heights. Experimental evidence so far reported in the literature for acoustic wave signatures at F-region altitudes,

Table 3.1. Statistical details of the relationship between the fluctuations (T > 300 s) in $\dot{P}$ of lower F-region reflections over Kodaikanal (dip 3°N) and in the horizontal component of geomagnetic field at Trivandrum (dip 0.6°S) in the Indian electrojet belt.

Date	Geomagnetic index (A_p)	Correlation coefficients γ			
4 May 1984	13	-	-	-	-
7 May 1984	4	0.37	-	-	-
12 May 1984	12	-	-	-	-
14 May 1984	12	-	-	-	-
17 May 1984	32	-	-	-	-
18 May 1984	12	-	0.61	-	-
22 May 1984	32	-	-	-0.33	-
15 June 1984	24	-	-	-	-
18 June 1984	27	-	-	-	-
14 July 1984	40	0.28	-	-	-
15 July 1984	25	0.35	-	-	-
16 July 1984	25	-	-	-	-
21 July 1984	8	-	-	-	-
4 Sept 1984	59	-0.27	-	-	-
6 Sept 1984	12	-	-	-	-
9 Sept 1984	12	-	-	-	-
11 Sept 1984	17	-	-	-	-
13 Sept 1984	11	-	-0.59	-	-
25 Sept 1984	10	-	0.35	-	0.32

Notes : γ : Correlation coefficient;
All the values of γ are significant at $\rho > 0.01$;

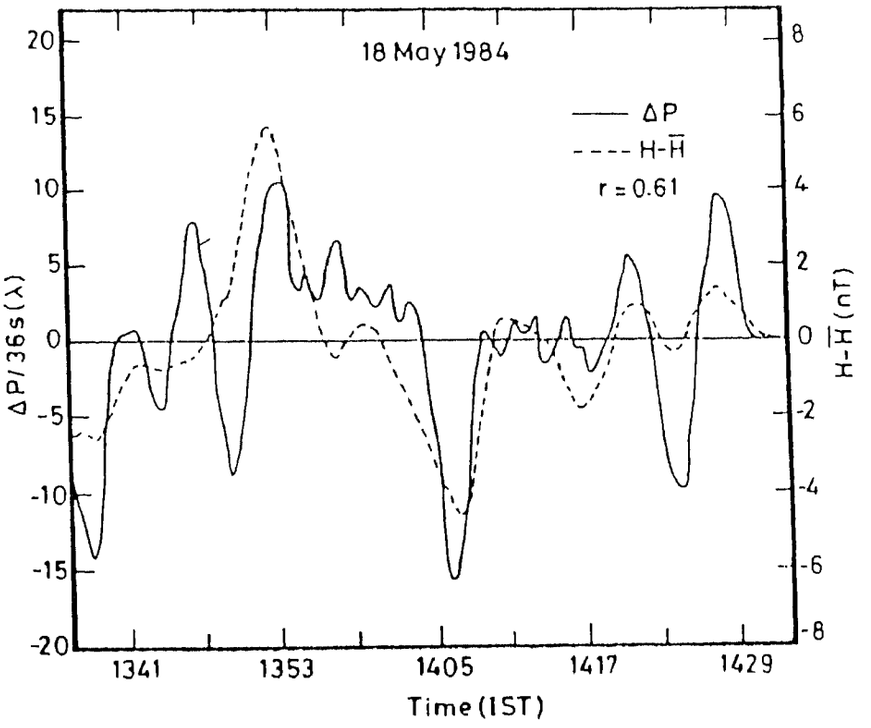

Fig.3.3. Plots of simultaneous data of $\Delta P/36$ sec at Kodaikanal and horizontal component of geomagnetic field (deviation from the mean, $H-\bar{H}$) at Trivandrum depicting the absence of one-to-one correspondence between them in the early part of the data segment.

in fact, consistently shows that they manifest exclusively in association with energetic events, both natural and man-made such as severe thunderstorms, nuclear explosions and earthquakes (Georges, 1967, 1973; Baker and Davies, 1969; Davies and Jones, 1971, 1973; Prasad et al., 1975; Raju et al., 1981; Tanaka et al., 1984; Okuzwa et al., 1986). The inferred fluctuations in $\dot{P}$, though match with acoustic wave periodicities, are present almost all the time during daylight hours unlike the events associated with energetic phenomena. It is, therefore, unlikely that the acoustic waves are the sources of the observed 300-600 sec fluctuations in $\dot{P}$ of F-region reflections during daytime at Kodaikanal near the dip equator.

It is well known that the gravity waves are an important source of electric field fluctuations in the ionosphere (e.g., Prakash and Pandey, 1979; Reddy and Devasia, 1981; Anandarao and Raghavarao, 1987; Earle and Kelley, 1987). Gravity waves are primarily a phenomenon of the neutral air and the neutral motions are communicated to the ionization through collisions. The response of the ionization to gravity waves depends on altitude. At the lower levels, where ion-neutral collision frequency is grater than the ion gyrofrequency, the ionization moves with the neutral air. At higher altitudes, where the ion-neutral collision frequency is much smaller than their gyrofrequency, the ion motion across the geomagnetic field is inhibited, and the ionization will respond only to the component of the wave that acts parallel to the field. At F- region heights the Brunt-Vaisala period, a characteristic parameter of the gravity waves is longer than 10-15 min (Fig. 3.4). The Brunt- Vaisala periods at 110 km and 200 km are approximately 5.1 and 11.6 min respectively. Therefore, the observed fluctuations (300-600 sec) in $\dot{P}$ of F-region reflections fall within the range of periods for propagating gravity waves only at E-region levels. Also unlike large scale waves which are associated with geomagnetic storms, the medium scale waves characterized by periods with few minutes to few tens of minutes, are common in their occurrence at mid and low-latitudes (e.g., Rottger, 1973, Francis, 1975). Thus the internal gravity waves, at E-region levels (90-130 km) which are free of absorption in the atmosphere unlike acoustic waves, seem to be the likely cause of the commonly occuring $\dot{P}$ fluctuations of F-region reflections. According to this understanding, electric field flu-

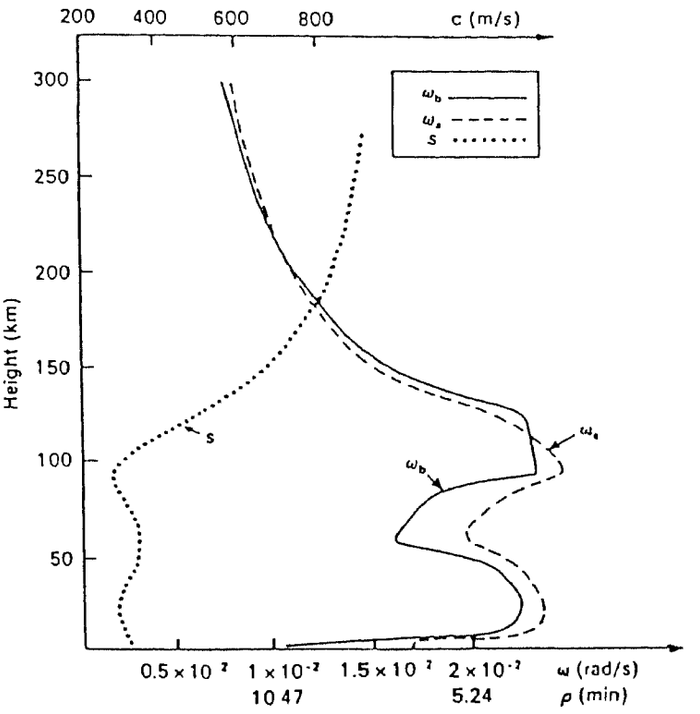

Fig.3.4. Height profiles of the speed of sound (s), the Brunt frequency (ω_b) and the acoustic cut-off frequency (ω_a) in a realistic atmosphere. (After I. Tolstoy and P. Pan, J. Atmos. Sci., 27, 31, 1970)

ctuations associated with E-region internal gravity wave activity at the magnetic link latitudes (outside the electrojet belt) of the F-region over Kodaikanal are responsible for the fluctuations in vertical plasma drift at F-region levels over Kodaikanal, having been communicated there along the magnetic field lines.

3.4. SHORT-PERIOD OSCILLATIONS (30-300 sec).

This sub section is devoted to the study of short period (60-240 sec) oscillations observed during daytime in the phase path of ionospheric F-region reflections. The following procedure is followed to study the short-period fluctuations. As was explained earlier, the rate of change of phase path $\dot{P}$ (ΔP), is obtained by differentiating the phase path data at 6 sec intervals. The resulting $\dot{P}$ time series was smoothed with a 30 sec width window to reduce noise like fluctuations of very short time scales. A running mean computed with a 306 sec (51 point) width window was subtracted from the 30 sec smoothed $\dot{P}$ values to render them relatively free from longer periods (T>5min) and to provide information on the shorter period components of fluctuations. Thus the data has been subjected first to 5 point (30 sec) running mean filter and then to a 51 point (306 sec) running mean filter. The residual $\dot{P}$ data obtained with the above procedure is then subjected to spectral analysis using the fast Fourier Transform (FFT) technique to obtain the spectral content of the changes in $\dot{P}$. The raw spectra were then smoothed with "Hanning" weights. The frequency spectra were computed by dividing each day's data into segments of 51.2min length as FFT requires 2^n points. In the present case the number of points fed to FFT is 512 corresponding to a data length of 51.2 min, the sampling interval being 6 sec.

A typical example of the short-period (T< 240 sec) fluctuations in $\dot{P}$ evidenced in our observations of phase path of F-region reflections over Kodaikanal is shown in middle panel of Fig 3.5. The data corresponds to August 28, 1983 which is a geomagnetically quiet day with Ap = 8. The top panel in Fig. 3.5 shows the horizontal component (H) of earth's magnetic field recorded at Kodaikanal with the Lacour magnetic variometers. The H-field shows the usual build-up and decay of the equatorial electrojet during daytime.

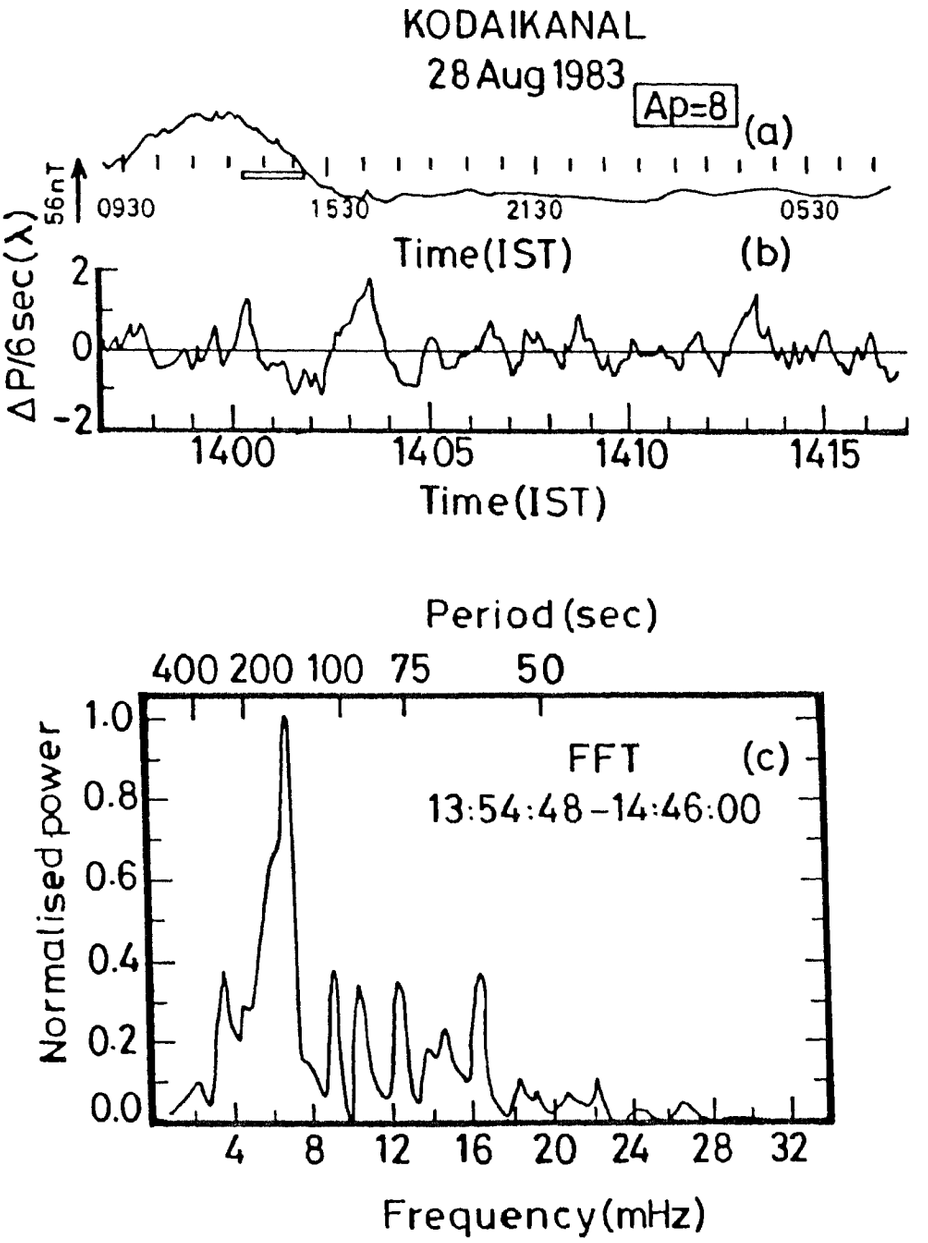

Fig.3.5. Top Panel : Magnetogram (Horizontal component) of Kodaikanal to indicate the usual build-up and decay of the equatorial electrojet during daytime. The solid rectangle indicates the time span of the data run on the day.

Middle Panel : Typical example of the shorter-period (T<240 sec) quasi-sinusoidal fluctuations in $\Delta P/6$ sec of lower F-region reflections over Kodaikanal on 28 Aug 1983.

Bottom Panel : Power spectrum of the data shown in the middle panel.

The ionospheric conditions are also quite normal on this day. The ionograms obtained from a co-located ionosonde showed the presence of equatorial sporadic- E (Esq) for most of the daytime. Perusal of the $\dot{P}$ plot (middle panel of Fig.3.5) and the power spectrum of the corresponding data segment (bottom panel of Fig. 3.5) shows the presence of variations with quasi-periods in the range 60-240 sec and with prominent spectral peaks around 146 sec, 110 sec, 80 sec and 61 sec. A total of $\sim$ 90 hrs of $\dot{P}$ data are analysed to derive the occurrence and spectral characteristics of the short-period fluctuations in $\dot{P}$ the salient features of which are as follows:

(a) The fluctuations in $\dot{P}$ manifest at all times during daytime from 08 to 16 LT with peak-to-peak amplitudes in the range 6-18 ms^{-1} (0.1-0.3 Hz in Δf).

(b) The spectral content of the fluctuations exhibits variability not only from day-to-day but also during the course of a data run, i.e., on time scales of an hour. During the data run, on any given day, the relative amplitudes of the spectral peaks change while the positions of the spectral peak do not change significantly. On the other hand, the day-to-day variability of the spectral content is characterized by shifts in the position of the spectral peaks in the period range 60-240 sec.

(c) The occurrence of short-period fluctuations seem to depend on the ambient electrojet strength and related ionospheric conditions. *They seem to practically disappear during the times of absence of Esq on bottomside ionograms.* Five "no-Esq" events have been noticed in the data sample analysed. Four of them have occurred on quiet days and correspond to partial counter-electrojet conditions, i.e., although Esq was absent, the H-component of the geomagnetic field was not below the mean night time level. Fig 3.6 shows $\dot{P}$ fluctuations and H-field at Kodaikanal for 14 May 1984 which is a quiet day with Ap = 12. The filled rectangle above the H-field trace indicates the time span of the data run on the day. The hatched rectangle above the H-field trace indicates the time span of the absence of Esq on Kodaikanal ionograms. The data in Fig 3.6 amply demonstrate the near absence of short-period fluctuations in $\dot{P}$. This trend is

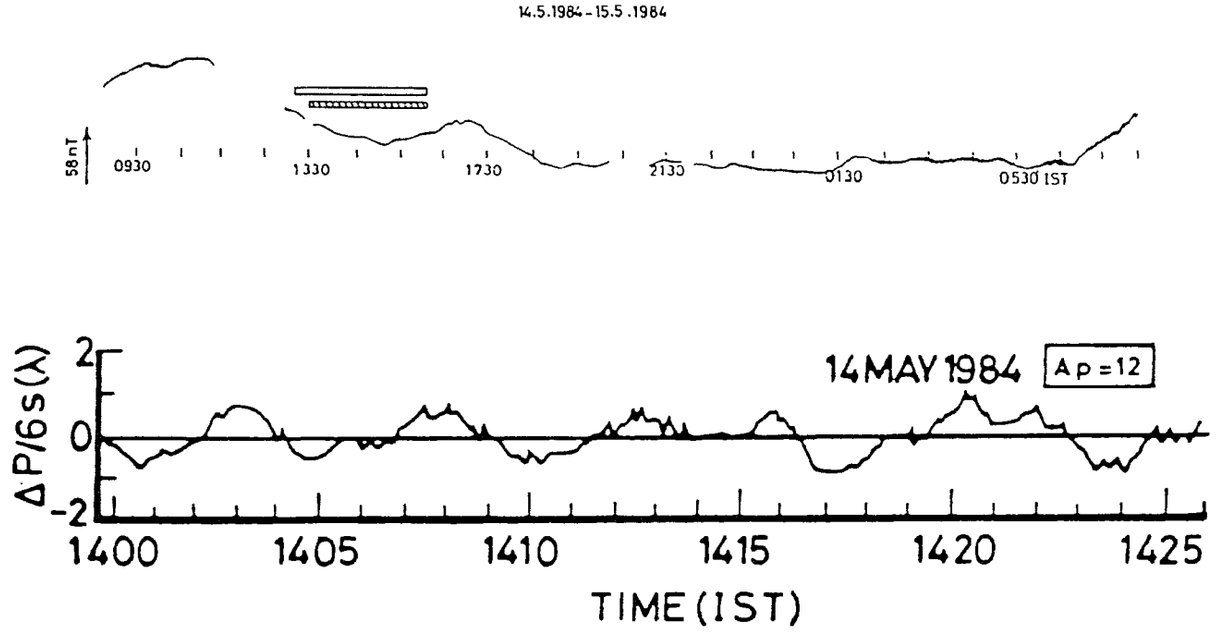

Fig.3.6. Example of $\Delta P/6$ sec illustrating the near absence of short period fluctuations during the time of disappearance of E_{sq} on ionograms on a magnetically quiet day. The magnetogram of Kodaikanal with the time span of the data run (open rectangle) and the time span of near absence of E_{sq} (hatched rectangle) on ionograms is also shown in the top panel.

consistently noticed on the remaining three quiet days under 'no-Esq' conditions. The fifth "no-Esq" event corresponds to 22 May 1984 which is magnetically disturbed day with Ap = 32. $\dot{P}$ fluctuations and H-field data for this day are shown in Fig. 3.7. The electrojet conditions for this day couldn't be assessed due to non- availability of H-field data from a station outside the electrojet belt. However the disappearance of Esq (duration is shown in hatched rectangle above H-field plot) on ionograms on this day during 1400-1545 hr IST is clearly seen. $\dot{P}$ data on this day during the absence of Esq on Kodaikanal ionograms again demonstrate the near absence of short-period fluctuations.

As mentioned earlier, the temporal variations in rate of change of phase path $\dot{P}$ of ionospheric reflections at vertical incidence can be caused by perturbations in the reflection height due to a vertical up and down movement of the ionosphere as a whole and/or changes in the ionization below the reflection level (Davies and Baker, 1966, Georges, 1967). Since during daytime the F-region plasma close to the dip equator is subjected to $\frac{EXB}{B^2}$ vertical drift, and if the changes in $\dot{P}$ are to be due to vertical up and down movement of the F-region plasma, then, the inferred fluctuations in $\dot{P}$ could be due to the changes in E or B or in both.

Pulsations in geomagnetic field that propagate in the ionosphere from above can cause variations in V_z and hence in $\dot{P}$. The inferred fluctuations in $\dot{P}$ (60-240 sec) fall in the period range of Pc4 (45-150 sec) and partly Pc5 (150-600sec) type micropulsations. To assess the relationship of short period (60-240 sec) fluctuations in $\dot{P}$ with Pc4 micropulsations, 19 days of simultaneous $\dot{P}$ data at Kodaikanal and geomagnetic micropulsation data at Trivandrum were examined. From the visual scrutiny of the two data sets it was found that in 18 out of 19 days Pc4 activity was absent. Only on one occasion Pc4 activity was evident. In Fig. 3.8 is reproduced the simultaneous H- field data of Trivandrum and $\dot{P}$ data of Kodaikanal for the day when Pc4 activity was evident, to indicate the temporal correspondence between the Pc4 pulsations activity and the 60- 240 sec $\dot{P}$ fluctuations. The absence of one-to-one correspondence between the two parameters strongly suggests that the short period fluctuations in $\dot{P}$ are not related to Pc4 micropulsations.

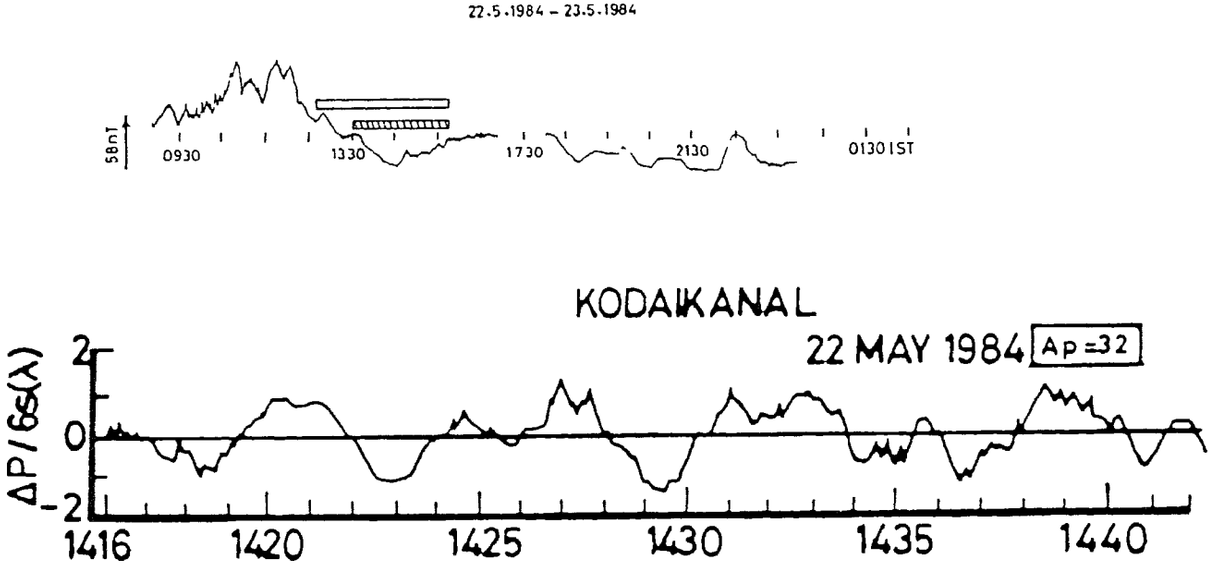

Fig.3.7. Example of $\Delta P/6$ sec illustrating the near absence of short period fluctuations during the time of disappearance of E_{sq} on ionograms on a magnetically disturbed day. The magnetogram of Kodaikanal with the time span of the data run (open rectangle) and the time span of near absence of E_{sq} (hatched rectangle) on ionograms is also shown in the top panel.

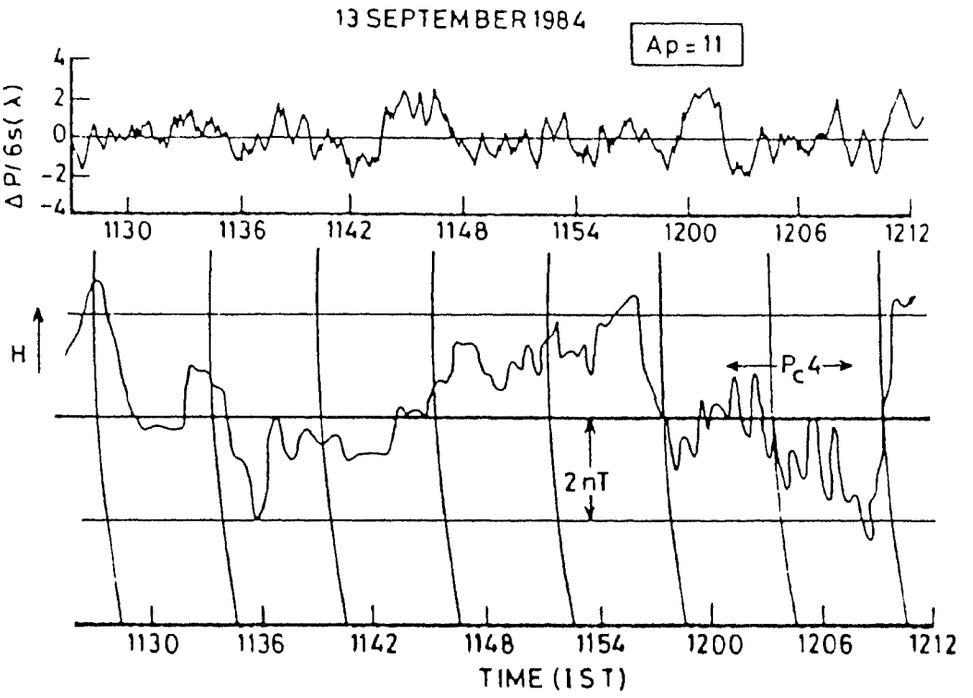

Fig.3.8. Simultaneous data of $\Delta P/36$ sec at Kodaikanal and geomagnetic field (H-component) at Trivandrum illustrating the lack of correspondence between the short-period (60-240 sec) pulsations in ΔP and Pc4 micropulsations in the geomagnetic field.

Changes in the zonal electric field (E) can impose fluctuations in phase path of F-region reflections through the action of EXB plasma drift which in the equatorial ionosphere is approximately vertical under the influence of the east-west electric field. Esq is widely considered to be due to scattering from the irregularities arising from the gradient drift plasma instability mechanism in the equatorial electrojet region (Balsley, 1976b). The short-period fluctuations in $\dot{P}$ are found to cease rather systematically during the disappearance of Esq traces on ionograms. It is therefore reasonable to assume that the causative mechanism(s) responsible for the short period fluctuations in $\dot{P}$ is rooted in the E- region and is related to plasma turbulence in the electrojet. The short- period fluctuations in $\dot{P}$ could be due to electric fields associated with electrostatic drift waves generated by the gradient drift plasma instability mechanism at E-region levels outside the electrojet belt, and communicated along field lines to F-region levels over Kodaikanal. This process, however, cannot be expected to be very effective because the incidence of Esq is rather low at non-electrojet latitudes, particularly outside the local summer months (Knecht and McDuffie, 1962), while the short period fluctuations are very common in the phase path of F-region reflections at Kodaikanal.

3.4.1. Dependence on Strength of the Electrojet.

Signatures of the cessation of the short-period fluctuations in $\dot{P}$ during the disappearance of Esq on ionograms provided the impetus for studying the dependence of these fluctuations on the strength of the equatorial electrojet which is known to be responsible for Esq. On the other hand the electrojet irregularities are partially transparent to reflections from higher altitudes in the HF band. Therefore measurements of phase path of F- region echoes during daytime at electrojet locations could contain a significant high frequency component due to the phase path changes produced by the refractive index variations associated with the electrojet irregularities and their motion. Fig. 3.9 shows the location of Kodaikanal with reference to that of the equatorial electrojet in the Indian sector and a schematic of the ionospheric conditions commonly obtained during daytime at such locations (adopted from Balsley, 1977).

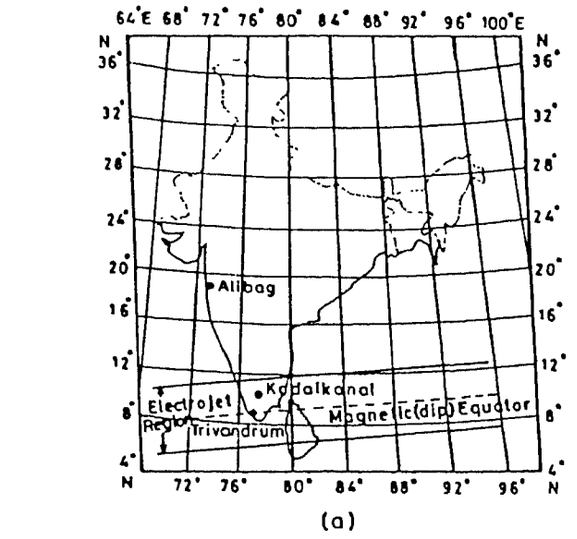

(a)

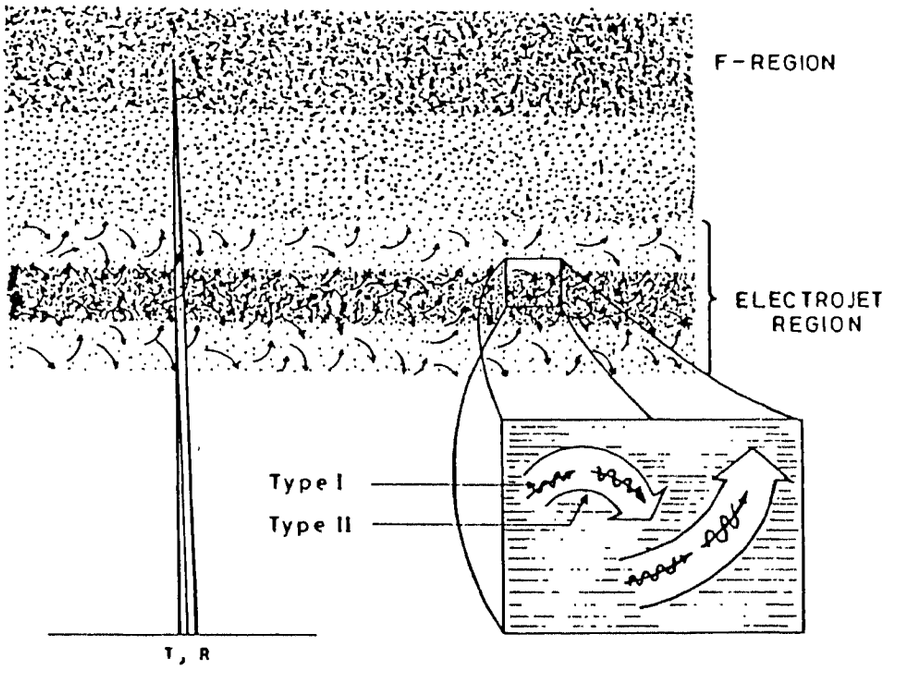

(b)

Fig.3.9. (a) Map showing the location of Kodaikanal and the equatorial electrojet region in the Indian sector. The location of the magnetometer stations, Trivandrum and Alibag, whose H-field data are used to compute the equatorial electrojet strength are also shown. (b) Schematic illustrating the ambient ionospheric conditions corresponding to the daytime F-region phase path measurements at Kodaikanal (not to scale). Note that the F-region phase path may be influenced by the convective motions of the irregularities in the electrojet medium (type I and type II), except during partial counter electrojet conditions when the favourable conditions for the irregularity penetration do not exist. (The concept of the irregularity structure is taken from Balsley, 1977).

In order to analyse the short-period fluctuation activity in relation to the strength of the electrojet, a total of 380 hours of data covering 116 days during the months May-October in 1983, 1984 and 1986 spanning the daytime interval 08-16 hrs IST (Indian Standard Time = UT + 5.5 hrs) are used. The phase path data analysed pertain essentially to the lower F-region reflections in the height range of 210-265 km as mentioned earlier.

The strength of the electrojet is estimated following the procedure introduced by Kane (1973). The strength of the electrojet can be estimated from the H-field data of a station in the equatorial region by eliminating the contributions to it from the magnetospheric effects. Kane (1973) proposed that the disturbance daily variation at a nearby low latitude station outside the electrojet influence may be considered as representative of the magnetospheric effects for the equatorial region also and hence defined the quantity Sd_I for an equatorial station as

$$Sd_I = H_E - H(\theta) + Sq(\theta) \tag{3.1}$$

where Sd_I is the ionospheric contribution for H at the equatorial station, H_E is the horizontal component of the magnetic field at the equatorial station, H (θ) is the horizontal component of magnetic field at a low latitude station outside the influence of the electrojet, Sq (θ) is the quiet day average for the same low latitude station and θ is the geomagnetic latitude.

The parameter ΔSd_I, defined as the deviations of Sd_I from its mean midnight level, is taken to represent the electrojet strength, and is given by

$$\Delta Sd_I = Sd_I - Sd_I < 00, 01, 02 \quad LT > \tag{3.2}$$

In the present study the published hourly H-field data of Trivandrum (8°29′N, 76°57′E, dip 0.6′S), an equatorial station and Alibag (18°38′N, 72°52′E, dip 9°26′N), a low latitude station well outside the influence of the electrojet are used to evaluate the parameter ΔSd_I. This pair of stations (locations of which with reference to electrojet region in the Indian sector are shown in Fig 3.9a) in the Indian sector are well suited for the estimation of electrojet strength (e.g., Rastogi and Patel, 1975; Bhargava et al., 1980., Sastri 1988a).

From the data of individual days, strings of $\dot{P}$ data spanning 1 hr intervals centred on the full hours of IST are taken up for spectral analysis using FFT technique. This criteria is adopted as the published magnetic data provide hourly averages of H- field centred on 30 min of UT or full hours of IST (IST = UT + 5.5hr). Moreover, a window of 51.2 min centred on the full hours of IST is in effect used with $\dot{P}$ data as the FFT needs 2^n points as explained earlier. The omission of 8.8 min data is felt not to vitiate the spectral estimates, as we are primarily concerned here with $\dot{P}$ variations with periods less than 300 sec. To quantify the level of quasi-periodic variations in $\dot{P}$ in the period range 30-300 sec, a reverse FFT is then performed by setting the power to zero outside the frequency range of interest, to restore the data to the time domain. The lower cut-off of 30 sec chosen here is to restrict the contributions to noise-like components at very high frequency end of the spectrum. The higher cut-off of 300 sec chosen is to restrict the contributions from the fluctuations with periods greater than 300 sec at the low frequency end of the spectrum. The pass band chosen (30-300 sec) is, therefore, considered wide enough to include the period regime, T $<$ 240 sec that was noticed to respond to ambient electrojet conditions. The variance (σ^2) of the 51.2 min $\dot{P}$ data segments thus synthesized are taken to represent the spectral content of the 30-300 sec quasi-periodic fluctuations for the central hour (in IST) of the data span.

A total of 281 hours of data with 110 hours of data in the forenoon period (0900-1300 hr IST) and 171 hours of data in the afternoon period (1400-1600 hr IST) became available for study. The data studied covered a wide range of electrojet conditions from strong electrojet with ΔSd_I = 138 nT at one end, and weakened/reversed electrojet accompanied by the absence of Esq on ionograms at the other end. Careful scrutiny of the original $\dot{P}$ data and the corresponding FFT spectra, the synthesized time series of $\dot{P}$ (representing mainly the 30-300 sec fluctuations) and its variance (σ^2) in relation to electrojet strength indicated the inhibition of short-period fluctuations in $\dot{P}$ when Esq was absent on ionograms (i.e. under partial/complete counter electrojet conditions). Fig 3.10 depicts the occurrence and the subsidence of the short-period fluctuations in $\dot{P}$ respectively on 5 Sept 1986 and 2 Sept 1986 along with the profiles of the strength of the electrojet on both the days. 5 Sept 1986

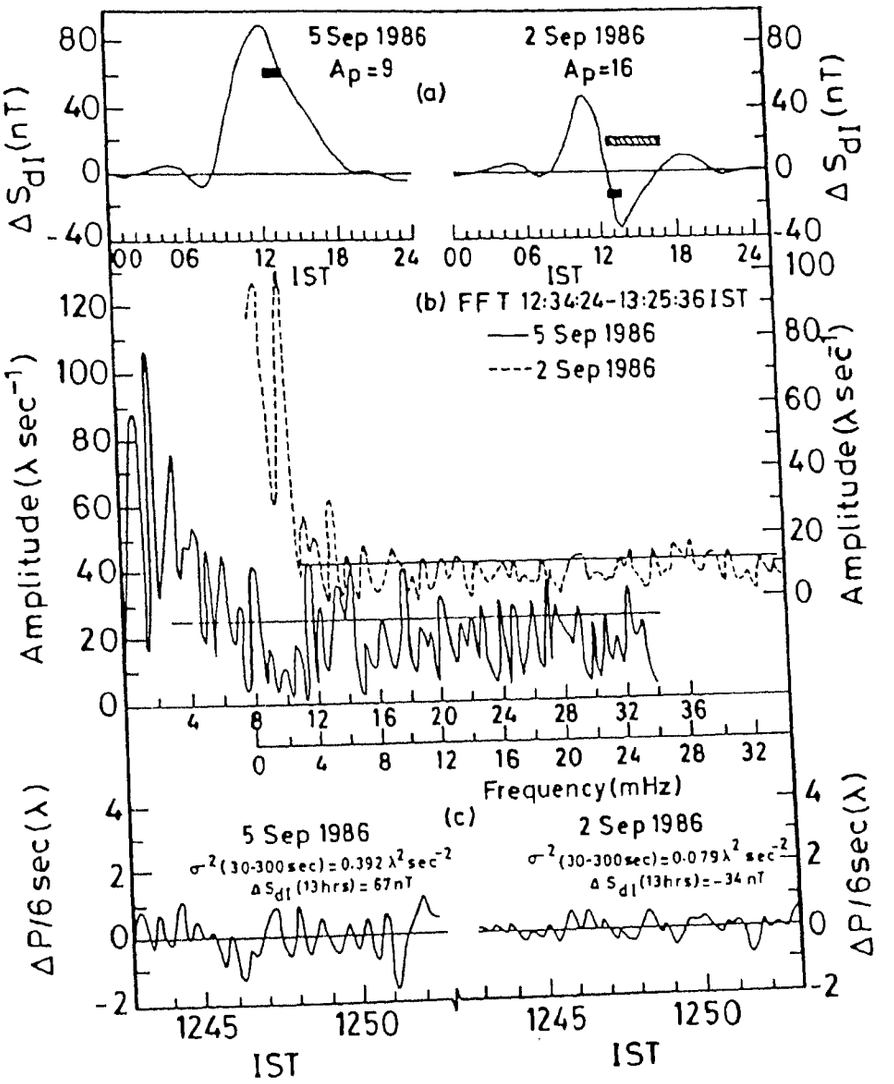

Fig.3.10. Composite figure illustrating the dependence of the short-period (30-300 sec) fluctuations in ΔP (Doppler frequency shift) of lower F-region reflections over Kodaikanal. The details are given in the text.

is a geomagnetically quiet day (Ap = 6) with a normal growth and decay of the electrojet during the course of the day as can be seen from the diurnal pattern of ΔSd_I shown in top left panel of the figure. The ionospheric conditions were also normal on this day with the Esq present on Kodaikanal ionograms for most of the daytime. The solid rectangle on ΔSd_I plot indicates the 1 hr span (1230-1330 hr IST) of the data. The frequency spectrum of the original $\dot{P}$ data pertaining to a 1-hr slot centred on 13 h IST is shown in the middle left panel of the figure. The frequency spectrum indicates the presence of significant variations in the period range 30-300 sec with spectral peaks around 192, 123, 85, 70 and 56 sec. The synthesized time series of $\dot{P}$ is shown in the bottom left panel of the figure. The plot of synthesized $\dot{P}$ time series and its high level of variance ($\sigma^2 = 0.392\ \lambda^2/\text{sec}^2$) clearly show the presence of short-period fluctuations in the period range of 30-300 sec. Right panel of Fig. 3.10 illustrates the subsidence of the short-period fluctuations on a counter- electrojet day. In the top right panel of Fig. 3.10 is shown the diurnal profile of ΔSd_I on 2 September 1986. The solid rectangle on ΔSd_I plot indicates the 1 hr span (1230-1330 hr IST) of the data. In the middle and bottom right panels are shown, the frequency spectrum of original data for 1 hr slot centred at 13 hrs IST and the corresponding synthesized time series of $\dot{P}$ respectively. 2 September 1986 is a slightly disturbed day with Ap = 16. Unambiguous counter-electrojet conditions prevailed on this day starting around 1230 hr IST when ΔSd_I became negative accompanied by the disappearance of Esq on Kodaikanal ionograms (the hatched rectangle indicates the period of the absence of Esq on Kodaikanal ionograms on 2 Sept 1986). The electrojet recovered to the more or less normal level by about 1700 hr IST but Esq did not reappear during the day. In response to this reversed electrojet situation, the level of wave activity in $\dot{P}$ in the band 30-300 sec was markedly reduced as can be seen from the amplitude spectrum of original $\dot{P}$ data (middle panel) and the variance ($\sigma^2 = 0.079\ \lambda^2/\text{sec}^2$) of the synthesized $\dot{P}$ data (bottom panel) presented in Fig 3.10. The numerical values, in fact, show a reduction by a factor of 5 in the variance of the $\dot{P}$ fluctuations when ΔSd_I changed from 67 to -34 nT between the two days in the same local time interval. The two examples shown in Figs 3.10 correspond to the two extreme forms of the normal day-to-day variability of the electrojet. In order to check the validity of the relationship found between the level of the short-period fluctuations in $\dot{P}$ and the

strength of the electrojet, correlation analysis of the paired hourly values of σ^2 and ΔSd_I has been carried out. it is revealed that a highly significant linear relationship indeed exists between the level of 30-300 sec wave activity in $\dot{P}$ and the strength of the electrojet. This can be seen from the mass plot of σ^2versus ΔSdI presented in Fig. 3.11. The line of best fit is also shown in the figure. The correlation analysis is repeated by dividing the data base into that of forenoon (0900-1300 hr IST) and afternoon (1400-1600 hr IST) sectors. The statistical results which are summarized in Table 3.2 validate the linear relationship of 30-300 sec wave activity in $\dot{P}$ with the strength of the electrojet both for the forenoon and afternoon periods.

With a view to infer whether the evidenced dependence of the 30-300 sec variations in $\dot{P}$ on the electrojet strength is a characteristic feature over the entire period range (i.e., whether there is any narrow band regime that is more responsive to electrojet than the others), the variance and correlation analyses are repeated by splitting the original pass band into three sub-bands of 90 sec width viz., 30-120, 120-210 and 210-300 sec. Fig 3.12 depicts the dependence of the variance (σ^2) of the fluctuations in $\dot{P}$ in the sub-bands 30-120, 120-210 and 210-300 sec on the electrojet strength (ΔSdI). The lines of best fit for the three sub-bands are also shown in the figure. The statistical details are given in Table 3.2. Following are the conclusions drawn from Fig. 3.12 and Table 3.2.

a. The response of variance of the fluctuations in $\dot{P}$ to changes in electrojet strength is not uniform over the period range 30-300 sec. The sensitivity, in fact, is highest for the sub-band 30-120 sec and decreases, in general, with the increase of the range of periodicity as can be seen from Fig 3.12 and the numerical values of the correlation coefficient (γ) and the slopes of the regression line (b) listed in Table 3.2. The reduction in sensitivity is, however, not uniform between the sub-bands and is significant only between the sub-bands 30-120 and 120-210 sec.
b. For a given strength of the electrojet, the variance is, in general, higher in the sub-band 30-120 sec compared to the other two sub-bands.
c. The differences in the level of variance between the three sub-bands increase in general

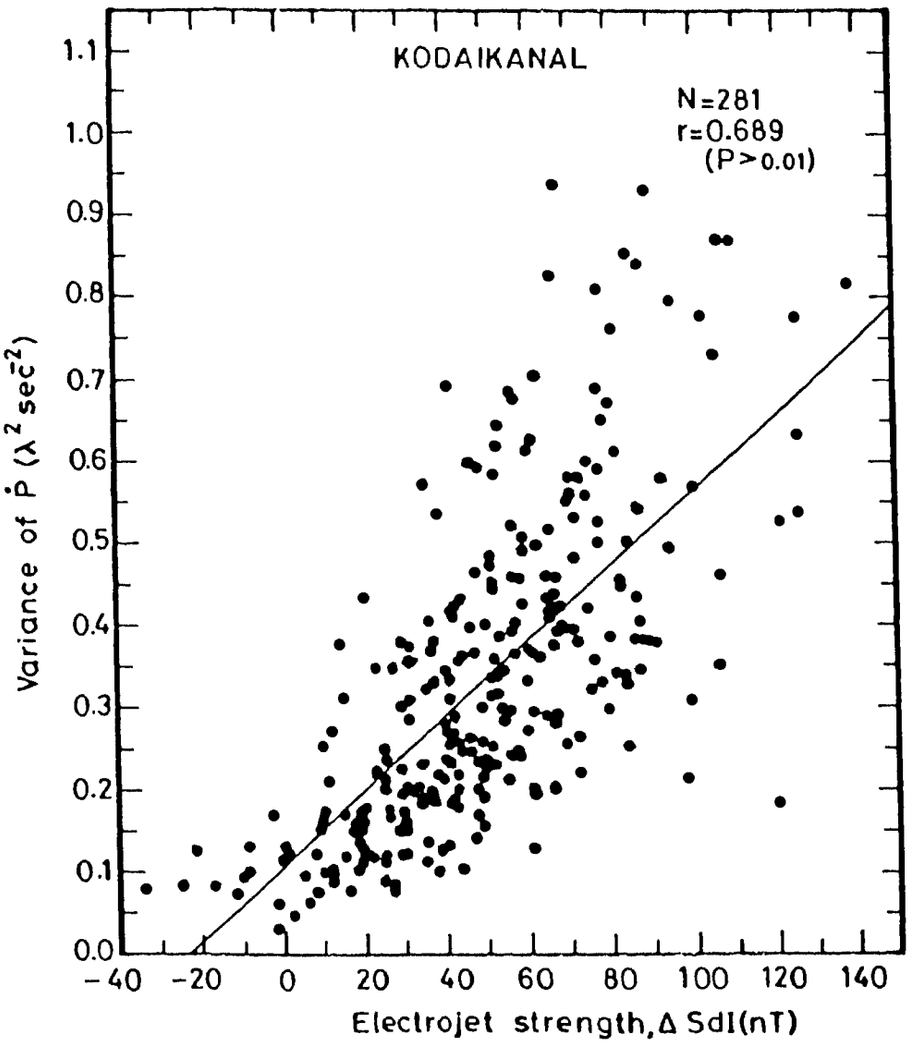

Fig.3.11. Mass plot depicting the relationship of the variance (σ^2) of the 30-300 sec fluctuations in $\dot{P}$ to the ambient strength of the equatorial electrojet ($\Delta S\, d_I$). The solid line represents the line of best fit to the data. Statistical details are also given at the top of the figure.

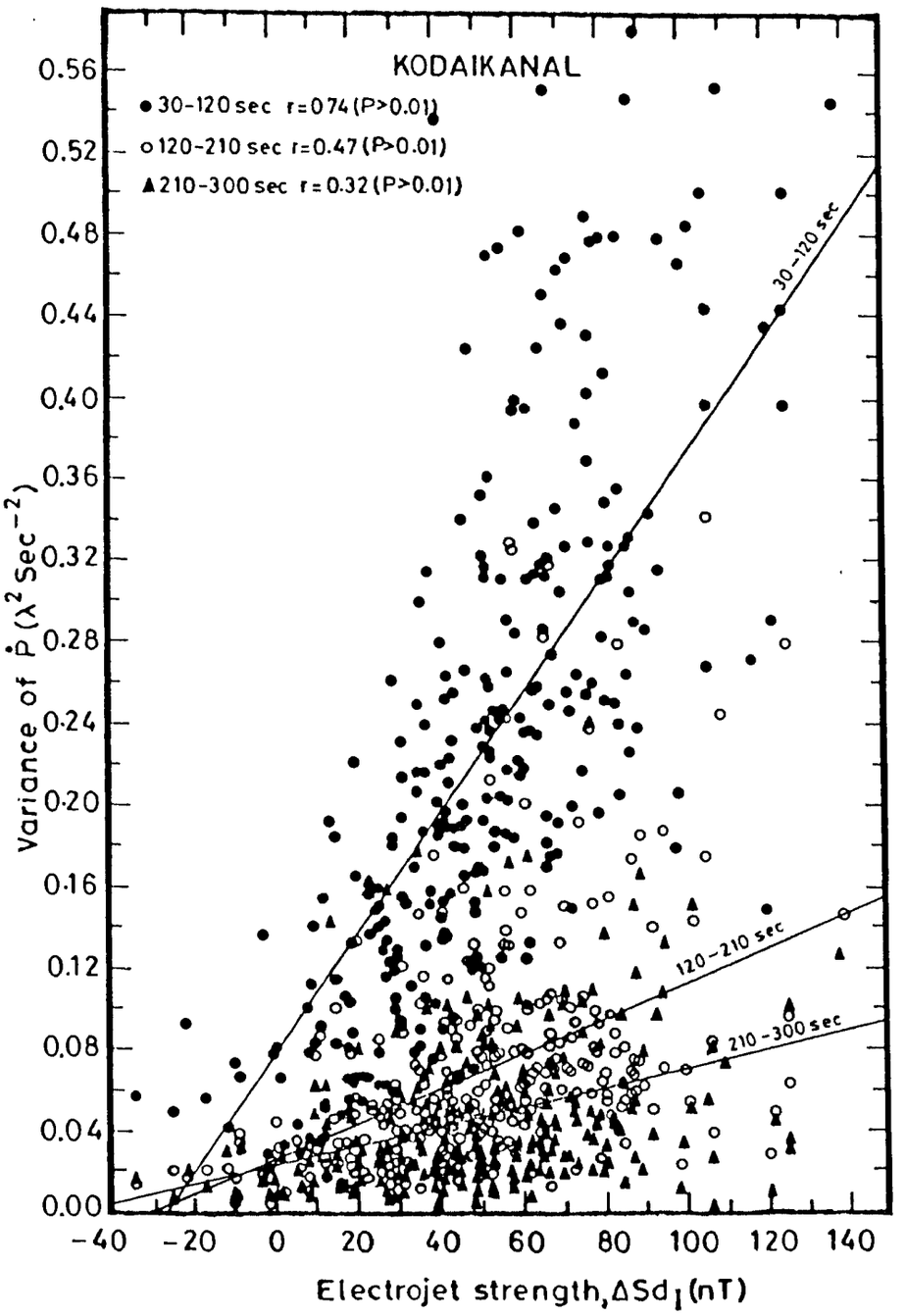

Fig.3.12. Mass plot depicting the relationship of the variance (σ^2) of the fluctuations in $\dot{P}$ in the sub-bands 30-120, 120-210 and 210-300 sec to the ambient strength of the equatorial electrojet (ΔSd_I). The solid lines represents the line of best fit to the data. Statistical details are also given at the top of the figure.

Table 3.2. Statistical details of the relationship between the Variance (σ^2) of quasi-periodic variations in the period band 30-300 sec and sub-bands 30-120, 120-210 and 210-300 sec in the rate, of change of phase path $\dot{P}$ of lower F-region reflections over Kodaikanal (dip 3°N) and the equatorial electrojet strength (ΔSd_I).

Time slot	Number of Data Points (N)	Period Band							
		30-300 s		30-120 s		120-210 s		210-300 s	
		γ	b	γ	b	γ	b	γ	b
Forenoon 09-13 hr IST	110	0.615	0.0044	0.673	0.0031	0.430	0.0009	0.221	0.0004
Afternoon 14-16 hr IST	171	0.652	0.0051	0.715	0.0036	0.449	0.0010	0.249	0.0004
All data 09-16 hr IST	281	0.689	0.0046	0.740	0.0032	0.472	0.0009	0.323	0.0005

Notes : γ : Correlation coefficient ; All the values of $|\gamma|$ are significant at $\rho > 0.01$;
b : slope of the line of best fit.

with increase in the electrojet strength. This feature is again prominent only between the sub-bands 30-120 sec and 120-210 sec.

Taken together these statistical trends imply that as the strength of the electrojet increases, although the level of quasi-periodic fluctuations in $\dot{P}$ increases in the entire period range 30- 300 sec, there occurs a preferential increase in the sub-band 30-120 sec. In otherwords, with the increase in electrojet strength the spectral characteristics change so as to render the higher frequency components in $\dot{P}$ more prominent.

3.4.2. Model calculations of influence of electrojet irregularities on F-region phase path.

The main experimental result that emerged from the above detailed study is that the ambient strength of the equatorial electrojet exerts a marked control on the manifestation and spectral characteristics of the short period (30- 300 sec) fluctuations in $\dot{P}$ of lower F-region reflections during daytime in the electrojet region. As mentioned earlier vertical plasma motions near the reflection level can cause changes in the phase path of echoes at normal incidence, under non-flare conditions. Electron density irregularities close to the reflection level are however also known to cause pronounced effects on the phase path of the radio waves due to rapid variations in the refractive index (μ) near the reflection point (Booker, 1955, Fooks, 1962; Paul et al., 1974., Robinson and Dyson, 1975). The model calculations of Robinson and Dyson (1975) in particular showed that the net phase path change (ΔP) produced by an ionospheric irregularity critically depends on its location with reference to the reflection level, its strength (Δn/n) and the background ionization gradient, and not so much on its thickness. Moreover, for a given gradient of the background ionization, irregularities of greater strength can produce substantial changes in ΔP even if they are well below the reflection height i.e., for lower values of X = f_N^2/f^2, where f is the sounding frequency and f_N is the plasma frequency corresponding to the peak of the irregularity.

Robinson and Dyson (1975) studied the effects of irregularities on the phase path using specific (triangular) model irregularities. The change in phase path between transmitter

and reflection point due to an irregularity of intensity 'A' introduced between the heights h_1, and h_3 (Fig 3.13) at time t_2, over the background profile of arbitrary shape prevailing over the time t_1, is given by

$$\Delta P = \Big(\int_o^h \mu dh\Big)_{t_2} - \Big(\int_o^h \mu dh\Big)_{t_1} \tag{3.3}$$

where h_r is the height of reflection. If the height of reflection is unaltered by the irregularity then equation 3.3 reduces to

$$\Delta P = \Big(\int_{h_1}^{h_3} \mu dh\Big)_{t_2} - \Big(\int_{h_1}^{h_3} \mu dh\Big)_{t_1} \tag{3.4}$$

It follows from equation 3.2 that a change in $\dot{P}$ due to a change in the electron density profile is dependent only on that part of the profile that is actually effected. The above equation may be rewritten in the following way by changing the variable of integration to X as μ (x) is profile independent and also by splitting the range of integration at h_2 to avoid difficulty in the case of non-monotonic profiles.

$$\Delta P = \int_{x_1}^{x_2+A} \mu(x)\Big(\frac{dh}{dx}\Big)_{t_2} dx + \int_{x_2+A}^{x_3} \mu(x)\Big(\frac{dh}{dx}\Big)_{t_2} dx - \int_{x_1}^{x_3} \mu(x)\Big(\frac{dh}{dx}\Big)_{t_1} dx \tag{3.5}$$

where $X = \frac{f_N^2}{f^2}$. Equation 3.5 is valid for a monotonic profile at time t_1 in the rage X_1 to X_3, and profile dependence is now contained in dh/dx terms. Modified versions of equation 3.5 for non-monotonic profiles when the height of reflection is altered by the irregularity are given by Robinson and Dyson (1975). They have also discussed the merits and demerits of this model in detail. This method is adopted to evaluate ΔP for the conditions relevant to the measurements made at Kodaikanal and to compare the model estimates with the observations of phase path of ionospheric F-region reflections made during daytime at Kodaikanal.

The plasma frequency (f_N) corresponding to the seat of the electrojet irregularities at E-region altitudes varies in the range 3.3 - 4.0 MHz over the interval 09-16 hr IST. The parameter X = f_N^2/f^2 corresponding to this range of plasma frequencies and the probing frequency (f) of 5.0 MHz used here ranges from 0.43 to 0.64. These values of X are lower than those that are found from model studies of Robinson and Dyson (1975) to have pronounced effects on phase path (X around 0.9). It is to be noted, however, that the model calculations of Robinson and Dyson (1975) refer to irregularities of intensity of 1-5%, where as the electrojet irregularities are much stronger with intensity of 5-15% and, as already mentioned, for irregularities of greater strength significant phase path changes can occur even at lower values of X. Moreover, although the work of Robinson and Dyson (1975) showed that in general irregularities have little effect on the phase path until X $\sim$ 0.9, this effect is less prominent when the probing frequency (f) is well above the gyro frequency (f_H) since, then, the refractive index (μ) just approaches $\sqrt{1-\mathrm{X}}$. For the vertical soundings at Kodaikanal where the magnetic field is practically horizontal, μ for the ordinary ray is always described by $\sqrt{1-\mathrm{X}}$, so that one mode will not show the sudden onset of an increase of μ as X approaches 1 even when f is not well above f_H. The sounding conditions thus favour the argument that the turbulent motions of the electrojet irregularities may be an effective source of phase path fluctuations of F-region echoes over Kodaikanal. To ascertain the validity of this assessment of the physical situation, model calculations of the effect of irregularities on the phase path of radio waves reflected at normal incidence are carried out using the generalized approach of Robinson and Dyson (1975) assuming a straight line background profile and irregularities of triangular shape (Fig. 3.13). The intensity and thickness of the irregularity are assumed to correspond to the known characteristics of the equatorial electrojet irregularities (Basu et al,, 1977). Following are the input parameters used in the model computations of the effect of electrojet irregularity on F-region ΔP which are relevant to the measurements made at Kodaikanal.

(i) Probing frequency (f) = 5.0 MHz.

(ii) Dip angle of Kodaikanal (θ) = 3°.N.

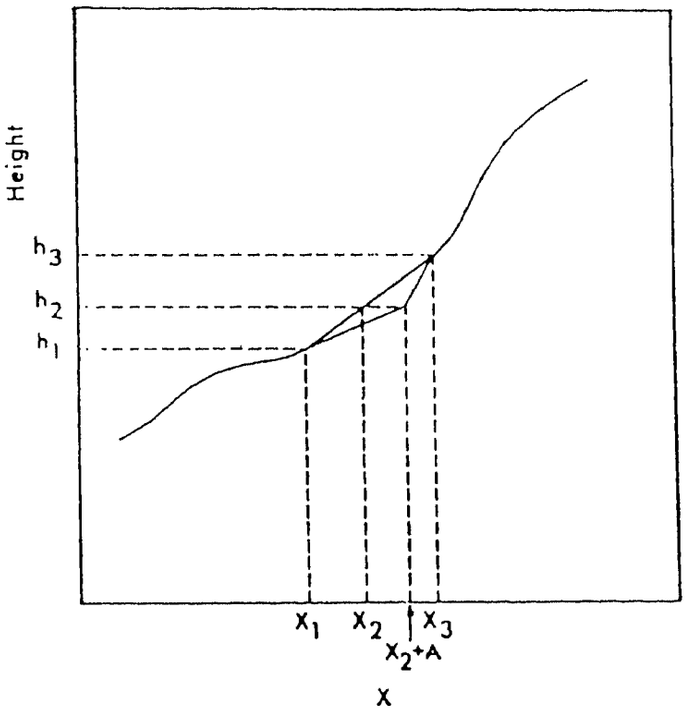

Fig.3.13. A model irregularity of triangular shape superposed on a background profile which is a straight line in the vicinity of the irregularity.

(iii) Electron gyro frequency (f_H) = 1.0 MHz.

(iv) Irregularity thickenss (dh) = 5km.

(v) Intensity range of irregularities (A) = 5-15%.

(vi) Background gradient of the ionosphere ($\frac{dh}{dX}$) = 20 km.

The refractive index μ was calculated from the Appleton-Hartree equation using Doupnik's trigonometric transformation (Jackson, 1967) and to avoid computer round-off errors, the integrations were carried out using three point Gaussian quadrature method.

The results of the model calculations are presented in Fig 3.14 wherein the change in phase path, ΔP is plotted as a function of X_2, the value of X at the centre of the irregularity. The calculations are made for values of X_2 in the range 0.24 -0.88, that is, for the situation when the irregularity is essentially below the level of reflection as is the case in our measurements. Fig 3.14 clearly shows that for vertical soundings near the dip equator, the electrojet irregularities can produce appreciable changes in phase path (ΔP) of F-region reflections even though the irregularities are well below the reflection height. For a given value of X_2 the magnitude of ΔP produced by the irregularities increases with increase in their amplitude. Moreover, the calculated magnitudes of ΔP ($< 2\ \lambda$) are in good agreement with the peak-to-peak amplitudes of the short-period fluctuations in $\dot{P}$ of F-region reflections as can be seen from bottom panel of Fig. 3.10. *The electrojet irregularities thus seem to effectively modulate the phase path of F- region echoes during daytime at electrojet stations.* According to this interpretation, then, as the electrojet strength increases the amplitude and frequency of the $\dot{P}$ fluctuations of reflections from the F-region are to increase due to the increase in drift speed and the strength of the irregularities. This point is quite clear from: (a) the significant linear relationship of the variance of $\dot{P}$ fluctuations with the electrojet strength, (b) the more or less comparable values of variance in the three sub-bands under weak electrojet conditions ($\Delta Sd_I \leq 10$ nT) (see Fig 3.12) and (c) the higher sensitivity of the $\dot{P}$ fluctuations in the lower period band (30-120 sec) compared to the other two sub-bands evidenced in the present study. Fig 3.12 also shows another interesting feature, namely, the rapid increase in the variance

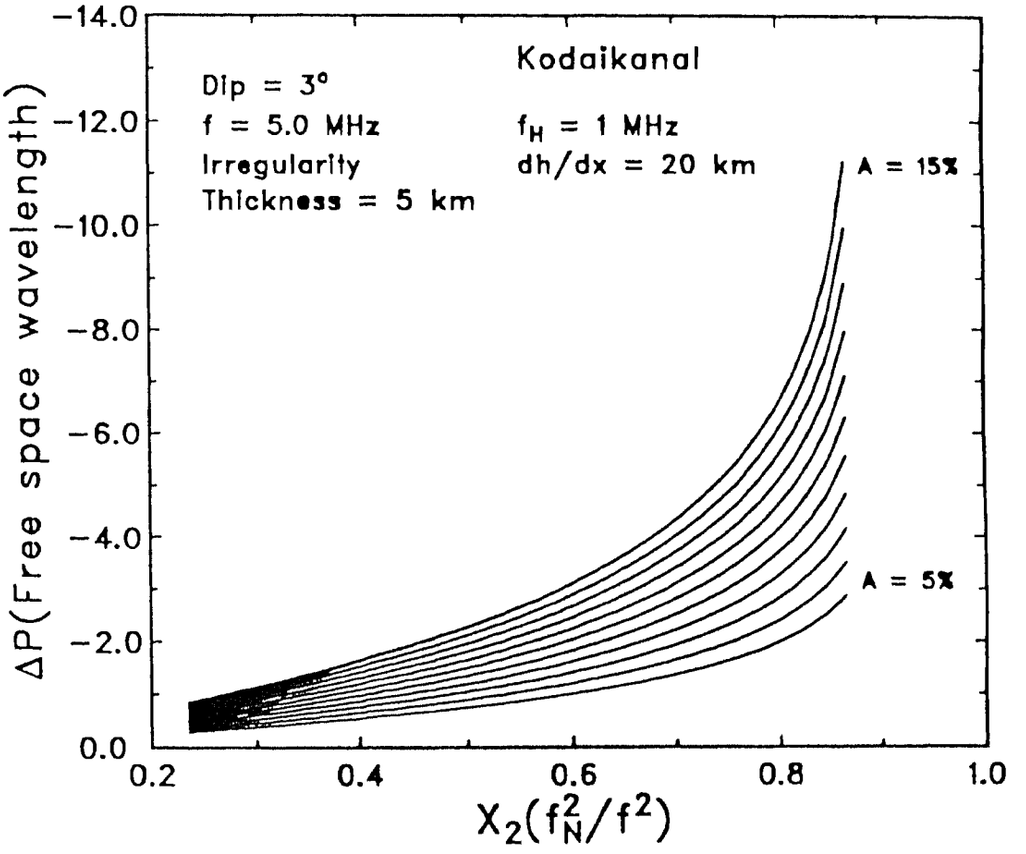

Fig.3.14. Model calculations of the change in phase path (ΔP) as a function of the amplitude of the irregularities (A, expressed as a percentage of X_2) and the value of X_2 at the center of the irregularity. The background gradient of the ionosphere ($\frac{dh}{dx}$) and the irregularity thickness assumed are also indicated.

(σ^2) of the 30-120 sec fluctuations in $\dot{P}$ for the electrojet strength above 30-40 nT. This suggests that Type I irregularities are probably the major contributor to the 30-120 sec fluctuations in $\dot{P}$, because they are much shorter in wave length compared to the Type II irregularities (Fig 3.9) and form when the electrojet is rather strong. Simultaneous measurements of phase path of F-region reflections on two or more probing frequencies are required to verify the frequency dependence of the amplitude of the short period (30-300 sec) fluctuations in $\dot{P}$ attributed to the convective motions of electrojet irregularities due to the changes in the relative locations of the irregularities and the reflection point as the probing frequency is varied. The amplitudes is to be maximum at lower frequencies ($\sim$ 3.5 MHz) corresponding to the plasma frequency of the seat of the irregularities, and has to decrease as the sounding frequency is increased well beyond 5.0 MHz. Infact, the simultaneous measurements of phase path of Esq and F-region reflections made on limited number of occasions on 5.0 MHz show that the variance (σ^2) of Esq is higher than those of F-region reflections (Fig 3.15) particularly for 30-120 sec period band. It is to be remembered, however, that the F-region echoes are due to specular reflections while those from Esq are enhanced echo returns from the intense electrojet irregularities.

3.4.3. Influence of electrojet irregularities on the Phase Path of F-region reflections - observational evidence.

In this section is presented the direct observational evidence for the influence of electrojet irregularities on the short period (30-300 sec) fluctuations in phase path of day time F-region reflections at electrojet locations and for the inference drawn from Fig 3.12, namely, the presumed dependence of 30-120 sec period oscillations on the Type I electrojet irregularities. Simultaneous measurements of phase path of F-region reflections at Kodaikanal (10°14′N, 77°29′E, dip 3°N) and the phase velocities of electrojet irregularities with the VHF backscatter radar at Thumba (8°29′N, 76°57′E, dip 0.6°S) are used for the purpose.

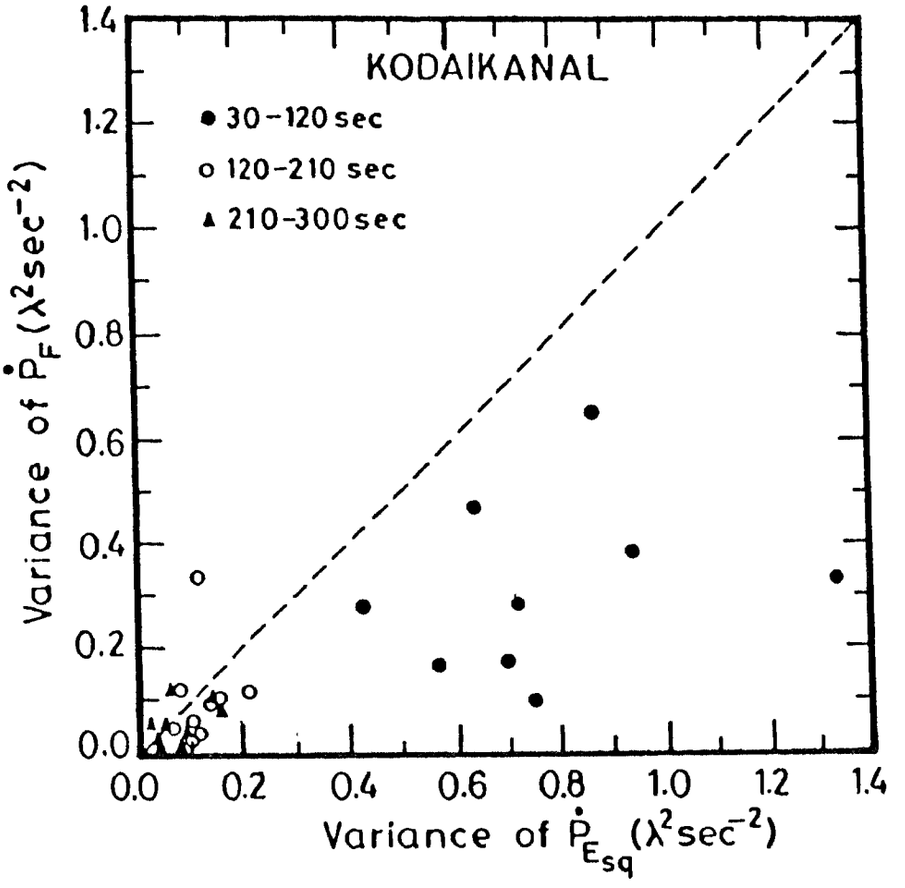

Fig.3.15. Scatter plot showing the relative magnitudes of the variance of $\dot{P}$ fluctuations in the three spectral bands, 30-120, 120-210 and 210-300 sec of echoes from E_{sq} ($\dot{P}_{E_{sq}}$) and lower F-region ($\dot{P}_F$) recorded simultaneously on the same frequency (5 MHz). The dashed line represent the line of unit slope. Note the higher values of variance of $\dot{P}$ from E_{sq}, particularly in the band 30-120 sec.

The analysis of simultaneous data of F-region phase path at Kodaikanal and of equatorial electrojet with the VHF backscatter radar at Thumba (dip 0.6°S) facilitates evaluation of the influence of electrojet irregularities on the short-period oscillations in $\dot{P}$ of F-region reflections over Kodaikanal. This is because the radar experiment provides direct and important information on the nature of the irregularities (Type I/II or combination) and their horizontal phase velocities (V_p). It is to be noted that Kodaikanal (dip 3°N) is in the northern half of the electrojet belt, while Thumba (dip 0.6°S) is south of dip equator at a latitudinal separation of ~150 km from Kodaikanal. The comparative study of the F-region phase path at Kodaikanal with that of electrojet at Thumba is, nevertheless, justified because the primary zonal electric field (E_y) of global wind dynamo origin as well as the secondary enhanced vertical polarization electric field (E_p) generated by it and which is responsible for the electrojet current pervades the entire electrojet belt and E_p drops off rapidly only beyond 4° geomagnetic latitude (e.g., Forbes, 1981). The close association between the parameters of daytime F-region (height of constant electron density and semi-thickness) over Thumba and E_y (deduced from groundlevel H-field data of Thumba) found by Sengupta and Krishnamurthy (1973) indicates, infact, that the scale of E_y producing the changes in F-region must extend by atleast 10° in latitude, because the F-region at Thumba would be linked to the dynamo region at a magnetic latitude of $\sim$ 10°. The strength of the electrojet and the phase velocity (V_p) of electrojet irregularities depend on E_y. The characteristics of the electrojet irregularities at Kodaikanal will not, therefore, be substantially different from those at Thumba both the stations being in the electrojet belt.

The VHF backscatter radar at Thumba operates on a frequency of 54.95 MHz with a peak power of 12 kW. Yagi arrays are used both for tansmission and receiption. For each signal pulse received from the electrojet the phase quadrature components of the receiver outputs are low-pass filtered, digitized, and stored on a magnetic tape. The Doppler power spectrum is computed from off-line processing of recorded data using a fast Fourier Transform (FFT) algorithm. The horizontal phase velocity (V_p) of the electrojet irregularities is computed from the observed Doppler shift (f_D) using the relation

$$V_p^{\theta} = \frac{\lambda}{2} f_D \tag{3.6}$$

where λ is the radar wavelength and θ is the elevation angle of the radar beam. For Type I spectra arising from two-stream plasma instability the Doppler frequency corresponding to the peak value of the spectrum is commonly used to compute V_p. In the case of Type II spectra arising from gradient drift instability the mean Doppler frequency, $\bar{f}_D$ is used as a measure of the mean phase velocity of the irregularities in the sampled volume. The value of $\bar{f}_D$ is computed from

$$\bar{f}_D = \frac{\int f_D P(f_D) df_D}{\int P(f_D) df_D} \tag{3.7}$$

with the integration usually done from - 200 to + 200 Hz for $\bar{f}_D$. The error in $\bar{f}_D$ so computed is typically $\pm$ 1 Hz which for the radar geometry at Thumba corresponds to an error of $\pm$ 2.7 ms^{-1} in V_p. The overall uncertainty in the absolute heights assigned to each range gate sampled spectrum is $\pm$ 1.5 km on average. Complete details of the system are available in the literature (Reddy et al., 1987).

Out of 116 days of phase path data used for the present study, simultaneous VHF backscatter radar data of Thumba are available only for 7 days because of operational problems and absence of preplanning of observational schedules at Kodaikanal and Thumba. As the data sample available is rather limited in size, the analysis of variance *versus* strength of the electrojet described in the previous section is repeated to check the reliability of using the 7 days of data. A total of 16 hours of simultaneous measurements are available over the 7 days. The paired hourly values of the variance (σ^2) of 30-300 and 30-120 see fluctuations in $\dot{P}$ and the strength of the electrojet (ΔSd_I) for the 16 hours of data is subjected to correlation analysis. Lower and upper panels of Fig 3.16 depict respectively the dependence of the variance (σ^2) of the 30-300 sec and 30-120 sec fluctuations in $\dot{P}$ on the ambient electrojet strength. The lines of best fit to the mass plots and the correlation

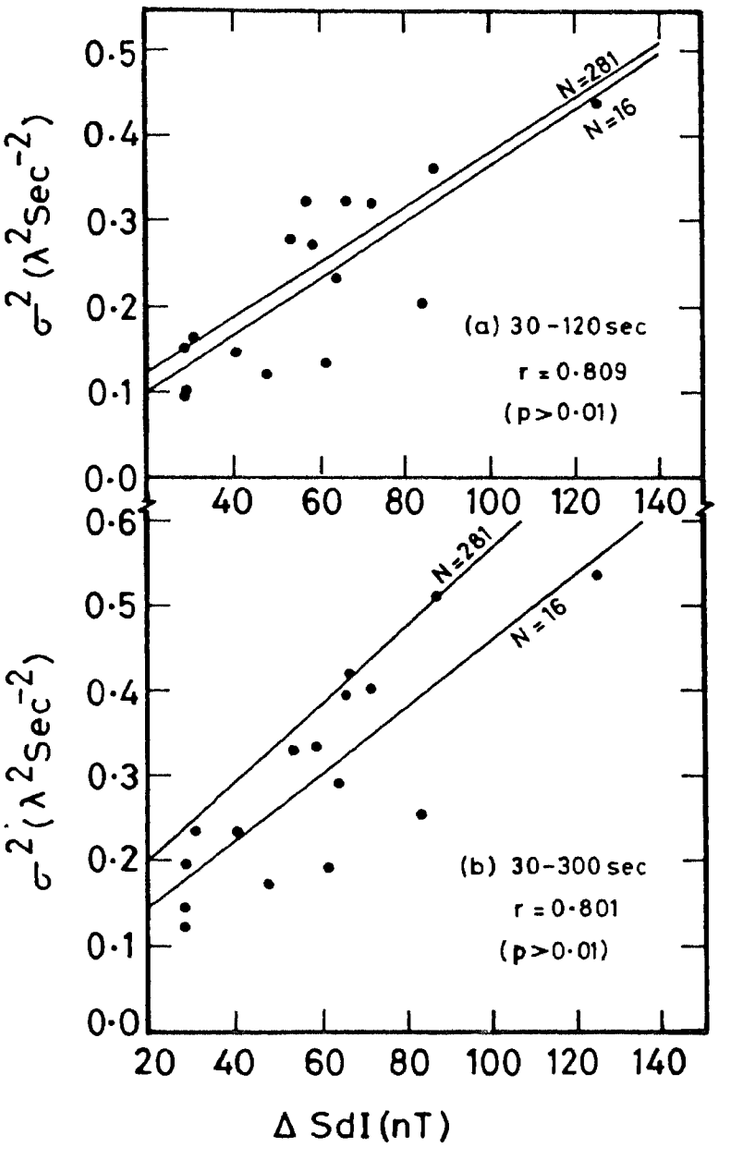

Fig.3.16. Plot showing the relationship of the variance (σ^2) of 30-300 sec and 30-120 sec fluctuations in $\dot{P}$ with ΔSd_I for the limited data sample (N=16) for which the simultaneous V_p data became available. Solid line represent the line of best fit of the data. The line of best fit obtained with large data sample (N=281) is also shown in the figure for comparison.

co-efficients are also shown in the figure. The lines of best fit characterising the σ^2 - ΔSd_I relationship evidenced in the large data sample (N=281) is also shown in the Fig 3.16 to facilitate comparison. The results of the statistical analysis such as correlation co-efficient, slope and intercept of the line of best fit for both limited (N = 16) and large (N = 281) data samples are given in Table 3.3. The σ^2 - ΔSd_I relationship is studied only for the 30-120 sec sub-band because, as already presented, this period range responds very sensitively to changes in electrojet strength compared to the other two sub-bands (120-210 sec and 210-300 sec), and its variance contributes substantially to the variance of the entire band 30-300 sec. It is quite evident from Fig. 3.16 that the linear relationship of σ^2 to Δ Sd_I holds good even for the 16 hours of data for which simultaneous data from the HF phase path sounder at Kodaikanal and the VHF backscatter radar at Thumba are available. In fact, the value of σ^2 for the 30-120 sec fluctuations calculated from the lines of best fit of the 16 hours data sample differs from that of the large data sample (N=281) by $\sim$ 13 percent at Δ Sd_I = 30 nT and by $\sim$ 3 percent at Δ Sd_I = 120 nT. The corresponding figures for the 30-300 sec band are $\sim$ 24 and 18 percent respectively. These numerical values show that the 7 day's observations available describe adequately the dependence of the short-period fluctuations (particularly in the sub-band 30-120 sec) in $\dot{P}$ on the electrojet conditions, and hence form a suitable data base for further studies to understand the physical mechanism(s) responsible for the fluctuations in $\dot{P}$.

In Figures 3.17 and 3.18 is illustrated the dependence of the spectral content of the short-period fluctuations in $\dot{P}$ on the phase velocities (V_p) of the electrojet irregularities and type of the irregularities regime. The daytime variation of V_p at 99 and 104 km (based on 5-min interval VHF radar data) is shown in figures 3.17 and 3.18 for two successive days in October 1983 and two nearby days in October 1984 respectively. The hourly values of the electrojet strength, ΔSd_I, and levels of variance (σ^2) of the 30-120 sec and 30-300 sec $\dot{P}$ fluctuations are also shown in the figure. Since the relationship between σ^2 and ΔSd_I is period dependent, the scales of ΔSd_I (also V_p) and σ^2 in figures 3.17 and 3.18 are arbitrarily chosen for convenience in plotting the relevant data, and do not conform to the statistical relationships evidenced in the study between the parameters. The scales of

Table 3.3. Statistical Relationship of the Variance of Quasi-Periodic Fluctuations with ΔSd_I and V_p

Parameters	Number of Data Points	Period Band					
		30-300 s			30-120 s		
		γ	b	a	γ	b	a
σ^2 versus ΔSdI	281	0.689	4.596×10^{-3}	1.0772×10^{-1}	0.740	3.246×10^{-3}	5.822×10^{-2}
σ^2 versus ΔSdI	16	0.801	3.934×10^{-3}	6.729×10^{-2}	0.809	3.334×10^{-3}	3.473×10^{-2}
σ^2 versus V_p (99 km)	16	0.766	3.743×10^{-3}	-6.088×10^{-2}	0.753	3.085×10^{-3}	-6.548×10^{-2}
σ^2 versus V_p (104 km)	14*	0.829	1.887×10^{-3}	-2.303×10^{-2}	0.855	1.732×10^{-3}	-5.95×10^{-2}

Details of the statistical relationship of the variance (σ^2) of quasi-periodic fluctuations (30-300 and 30-120 s) in the time rate of change of phase path, P (Doppler frequency shift) of lower F region reflections during daytime at Kodaikanal (dip 3° N) with the equatorial electrojet strength ΔSdI and the phase velocity (V_p) of electrojet irregularities measured with the VHF coherent backscatter radar at Thumba (dip 0.9° S).

Notes: γ, correlation coefficient. All values of γ significant > 99% level; a,b, Intercept and slope of the lines of best fit.

* Intervals with type I spectra in radar data are excluded.

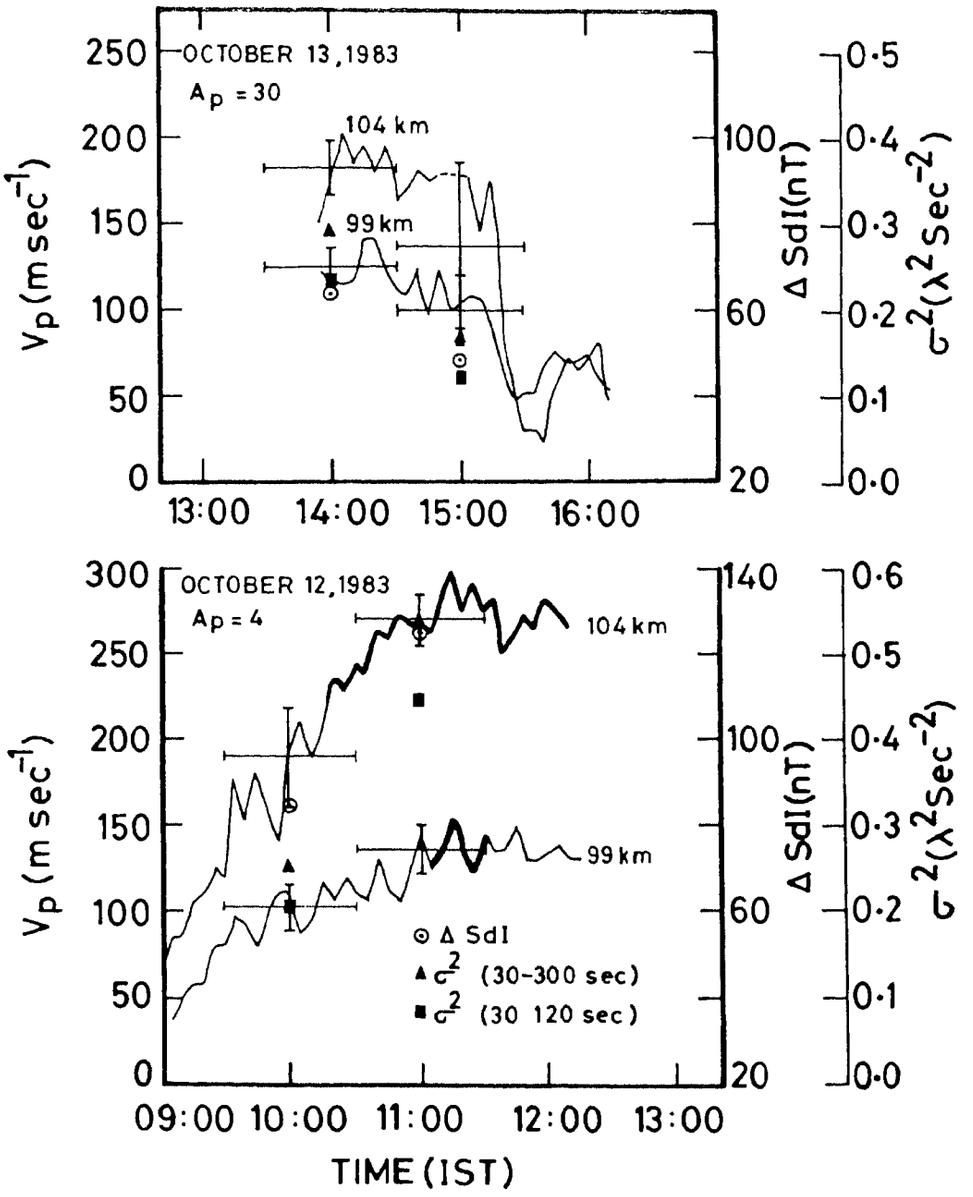

Fig.3.17. Temporal variation of V_p of electrojet irregularities at 99 and 104 km on October 12, 1983 and October 13, 1983. The heavy line indicates the interval when type I spectra prevailed at 104 km. The average value of V_p and its standard deviation over 1 hr intervals centered on full hours of IST are shown by horizontal and vertical bars, respectively. The corresponding hourly values of ΔSd_I and σ^2 of the 30-300 sec and 30-120 sec fluctuations in $\dot{P}$ are shown.

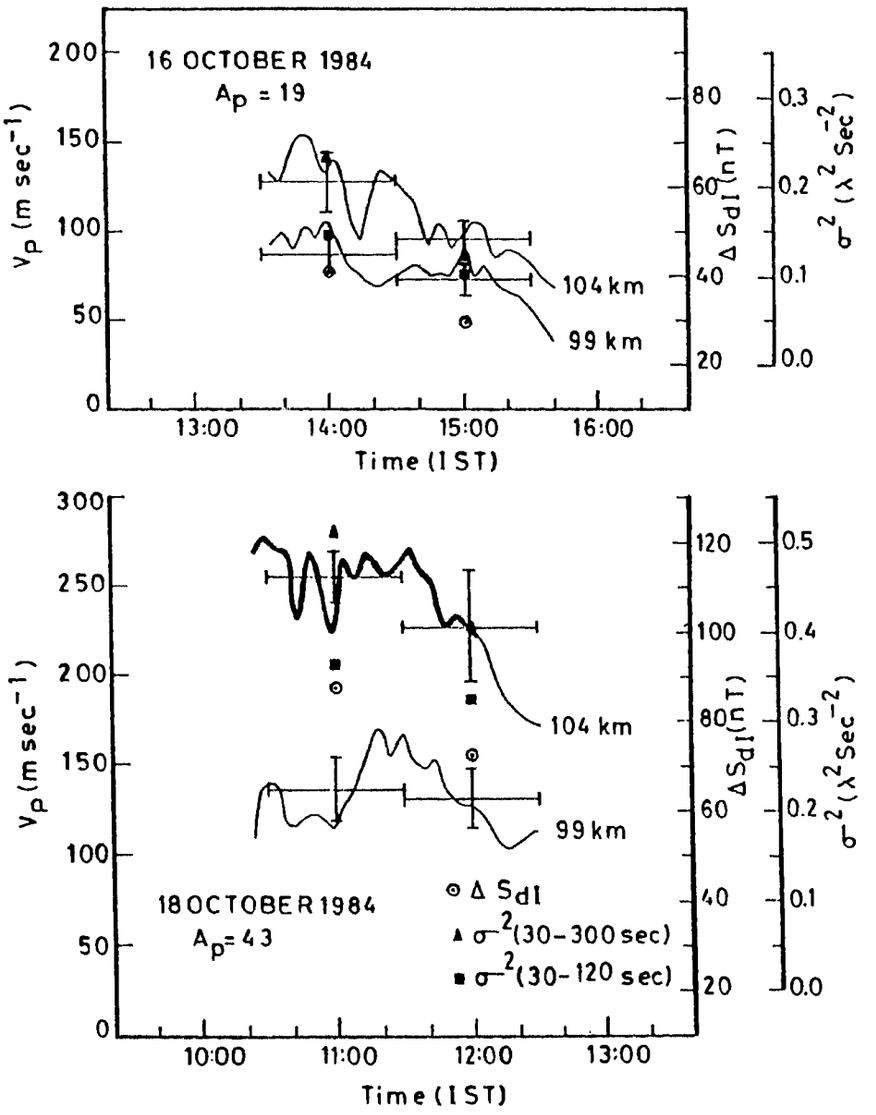

Fig.3.18. Temporal variation of V_p of electrojet irregularities at 99 and 104 km on October 16, 1984 and October 18, 1984. The heavy line indicates the interval when type I spectra prevailed at 104 km. The average value of V_p and its standard deviation over 1 hr intervals centered on full hours of IST are shown by horizontal and vertical bars, respectively. The corresponding hourly values of ΔSd_I and σ^2 of the 30-300 sec and 30-120 sec fluctuations in $\dot{P}$ are shown.

ΔSd_I and σ^2 are such that 20nT in ΔSd_I correspond to 0.1 λ^2 sec^{-2} in σ^2 irrespective of period, while the corresponding value of σ^2 expected from the statistical relationship (for N = 16) is 0.0667 λ^2 sec^{-2} for the 30-120 sec band and 0.0787 λ^2 sec^{-2} for the 30-300 sec band. The thick lines in the Figures 3.17 and 3.18 indicates the intervals when type I spectra prevailed in the VHF radar data. The average value of V_p and its standard deviation over 1 hour intervals centred on full hours of IST are shown by horizontal and vertical bars respectively.

On October 12, 1983, a geomagnetically quiet day (Ap = 4), the normal build up and decay of the electrojet strength was apparent during daytime. Strong electrojet conditions prevailed around noon as can be seen from the values of ΔSd_I and V_p for the forenoon period presented in the bottom panel of Fig 3.17. In fact, Type I spectra were seen in radar data at 104 km height from 1025 to 1130 IST, while at the lower height of 99 km Type I contamination is evident only for a short period from 1105 hrs to 1130 hrs IST. It is known that the Type I irregularities manifest under strong electrojet conditions when the electric field that drives the electrojet current renders the electron drift speed relative to the less mobile ions exceed the ion-acoustic speed in the electrojet. On the other hand, Type II irregularities occur even when the electrojet is weak (i.e., for electron drift speed $\geq$ 30ms^{-1}) and are longer in wave length compared to Type I irregularities (Fig 3.9). Moreover, Type II usually prevail at heights below 101 km although the height at which Type I contribution begins to contaminate Type II spectra significantly is rather variable from day to day. It is quite evident from Fig 3.17 that the level of variance (σ^2) of the short period fluctuations in $\dot{P}$ closely followed the enhancement of the electrojet strength as well as V_p during the forenoon on October 12, and was high around noon when Type I irregularities prevailed in the electrojet medium. Similar high values of σ^2 were also noticed on October 18, 1984 (Ap = 43) when Type I irregularities were seen at 104 km under strong electrojet conditions in the forenoon (1030 -1230 hr IST) as may be seen from Fig 3.18. In contrast, on October 13, 1983, a day of moderate geomagnetic activity (Ap = 30), only weak electrojet conditions were evidenced during the day, although the usual build up and decay of the electrojet strength was seen. VHF radar data, in fact,

showed the presence of only Type II spectra both at 99 and 104 km. In response to this physical state of the electrojet medium the levels of variance (σ^2) of the short period (30-300 and 30-120 sec) fluctuations in $\dot{P}$ remained low and closely followed the decrease of the electrojet strength (ΔSd_I) as well as V_p during the afternoon hours as can be seen from the top panel of Fig 3.17. A similar pattern of variation in V_p, ΔSd_I, and σ^2 under weak electrojet conditions ($\Delta Sd_I \leq 41$ nT) during which the Type II spectra at both 99 and 104 km prevailed, was also evidenced in the afternoon (1330 - 1530 IST) of October 16, 1984 (Ap = 19), as may be seen from the top panel of Fig 3.18.

The well-correlated temporal variations in σ^2, ΔSd_I and V_p described above are seen in all the 7 days of observations studied. To establish this feature, hourly averages of V_p at 99 and 104 km are calculated and cross correlation analysis of paired hourly values of σ^2 and average V_p is performed. It is known from the characteristics of the electrojet irregularities that the phase velocities of Type I irregularities remains constant and gets saturated at the ion-acoustic velocity and is thus not proportional to the electron drift speed, while Type II irregularities more or less move with the electron drift speed. Therefore the hourly data intervals when Type I spectra are seen at 104 km are excluded in the correlation analysis. This limitation has reduced the number of paired values of σ^2 and average V_p (at 104 km) from 16 to 14. The results of the correlation analysis are displayed in Fig 3.19 and are also summarized in Table 3.3. It is quite evident that the variance levels of 30-300 sec as well as 30-120 sec fluctuations in $\dot{P}$ exhibit a statistically significant linear relationship with V_p both at 99 and 104 km.

From the linear theory of plasma instabilities in the electrojet and VHF radar observations it is known that the increase in drift speed and the strength of the irregularities are the result of an enhancement in the electrojet strength (e.g., Reddy and Devasia, 1976; Farley, 1985). According to the inferences drawn from the present correlative studies of variance (σ^2) of short period (30-300 sec) fluctuations in $\dot{P}$ of F-region reflections and the strength of the electrojet (ΔSd_I), and the model calculations on the effect of electrojet irregularities on the phase path of F-region reflections performed, the amplitude and fre-

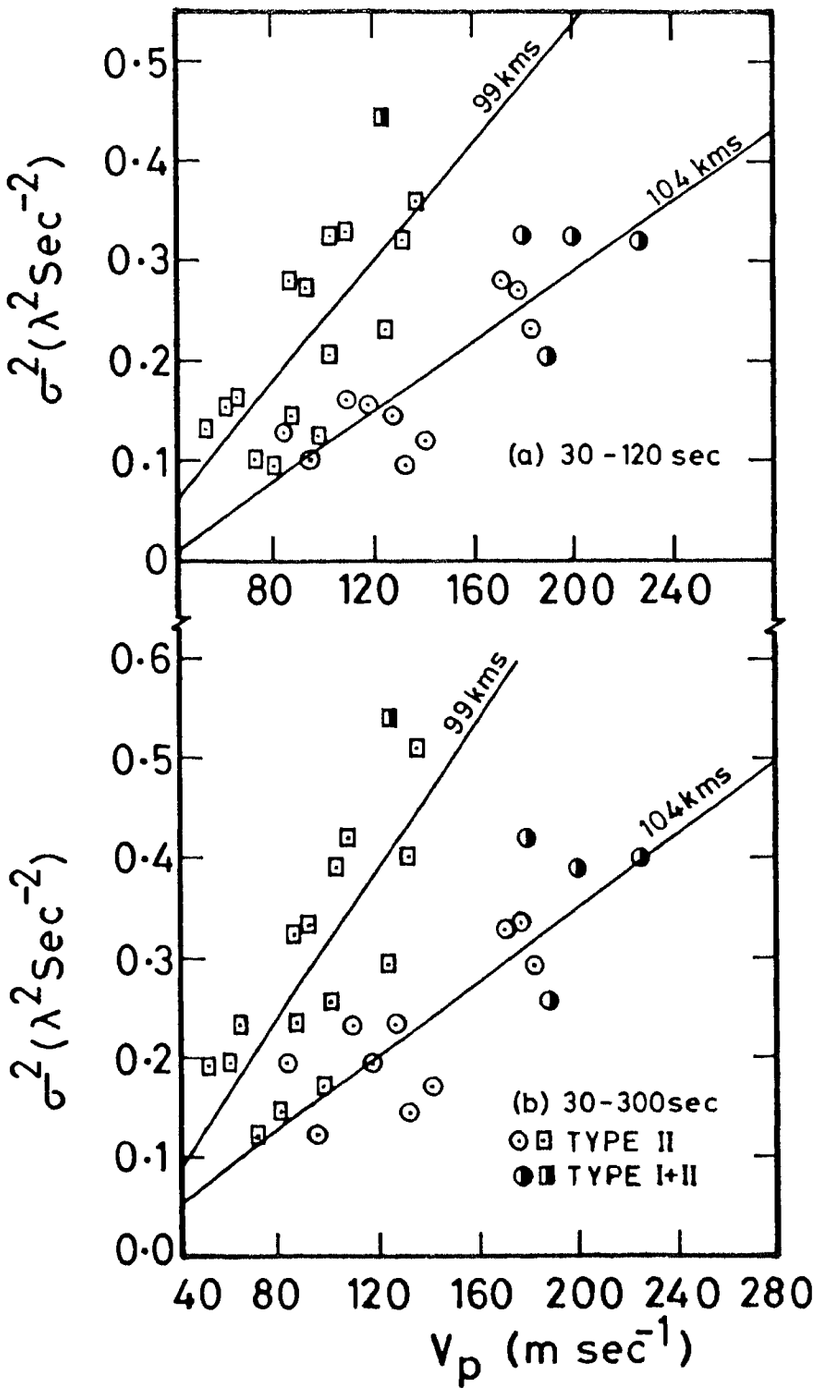

Fig.3.19. Plots showing the dependence of σ^2 of 30-300 sec and 30-120 sec fluctuations in $\dot{P}$ on V_p at 99 (squares with dots) and 104 km (circles with dots). The nature of the Doppler power spectrum (type II/combination of type I and II) from which V_p is deduced is also indicated.

quency of the $\dot{P}$ fluctuations of F-region echoes (i.e. level of variance) should increase with the drift speed and the strength of the irregularities. That is, a positive relationship between the level of variance of $\dot{P}$ fluctuations and the horizontal phase velocity of electrojet irregularities is expected. Moreover, under strong electrojet conditions when Type I irregularities are generated in the electrojet, the variance level of the shorter period (30-120 sec) segment of the $\dot{P}$ fluctuations is to be high because these irregularities are shorter in wave length compared to Type II irregularities and move with higher speed (though saturated at the ion acoustic speed). Both of these features are clearly seen in the results of the analysis of simultaneous measurements of F-region phase path and the VHF radar measurements of phase velocities of the electrojet irregularities. *It is interpreted, therefore, that the turbulent state of the equatorial electrojet plasma is the primary cause of the short-period (30-300 sec) fluctuations commonly observed in rate of change of phase path ($\dot{P}$) of lower F-region reflections at electrojet locations during daytime.*

The equatorial electrojet modulation of lower F-region phase path variations at Kodaikanal, if confirmed by multifrequency phase path measurements, will find two important and immediate applications. First, because of their sensitivity to ambient electrojet conditions the high-frequency component of F-region phase path variations hold the promise of providing indirect information on the regime of the electrojet irregularities and their phase velocities. The later forms the primary data from which the equatorial electric field is estimated (see Reddy et al,, 1987). Second, the daytime phase path data can be used to derive reliable and valuable data on F-region vertical plasma drift (V_z) at electrojet stations like Kodaikanal by adopting appropriate filtering techniques to minimize the contribution due to electrojet irregularities below the reflection level. This is warranted because the peak-to-peak amplitude of the Doppler velocity variations due to electrojet irregularities (6-18ms^{-1}) are comparable to those associated with the normal vertical plasma drifts (10-30ms^{-1}) during daytime (see for e.g., Fejer, 1981).

CHAPTER 4

STUDIES ON PHASE PATH VARIATIONS OF F-REGION REFLECTIONS DURING NIGHTTIME

4.1. INTRODUCTION

Vertical drifts of ionospheric plasma in the dip equatorial region play a dominant role in determining the structure and dynamics of the low latitude ionosphere and hence constitute an important input parameter for quantitative modeling studies (see recent reviews of Sastri,1990; Stenning,1992). The east-west electric field responsible for the vertical drifts of F-region are generated through the dynamo mechanism operative at E-region altitudes. This electric field is eastward by day causing an upward vertical drift and reverses its direction at night causing a reversal in the ionization drift to downward. Before its reversal to downward, the F-region vertical drift undergoes an enhancement giving rise to a characteristic prereversal or postsunset maximum. The postsunset or prereversal enhancement of F-region vertical drift is widely considered to be caused by polarization electric fields produced in the F-region by the action of upper thermospheric winds (Rishbeth,1971; Heelis et al., 1974; Farley et al., 1986). These F-region dynamo electric fields are shorted out effectively during the day by the large E-region conductivity and begin to gain importance from around sunset when the conductivity in the lower ionosphere is reduced. The incoherent scatter radar measurements at Jicamarca (76.87°W, 11.95°S, dip 2°N) have made singular contribution to our current knowledge of the diurnal pattern of equatorial F-region vertical plasma drift (V_z) and its dependence on season and levels of geomagnetic and solar activity (see Fejer et al., 1991 and references therein).

Richmond et al (1980) developed an empirical model of quiet time solar minimum ionospheric electric fields at low and middle latitudes based on incoherent scatter radar measurements in the American and European sectors. Walker and Chan (1989) and

Fejer et al. (1991), however, pointed out that the Jicamarca vertical drift data may not be an appropriate input for modelling of the low latitude ionosphere of the Australian/ East Asian longitude zones. One of the motivations for the present work is that detailed experimental specification of the variation of the equatorial F-region vertical drifts with season and solar cycle at different longitudes will help develop realistic emperical models of global electrodynamics and constrain the theoretical models. This kind of data are also needed to ascertain the presence of any systematic and significant longitudinal dependence of V_z and, if present, to understand its origin and to assess its role for example, in the pronounced longitudinal differences observed in the development of equatorial ionization anomaly (Walker, 1981).

What is avilable at the moment is limited information on the evening V_z patterns at stations in the Brazilian and Indian sectors [Fortaleza (38°W, dip 2°S); Kodaikanal (77°28'E, dip 3°N) and Trivandrum (8° 29'N, 76° 57'E, dip0.6°N)] derived from ionosonde data for specific periods, some of which with particular reference to phenomenon of equatorial spread F, ESF (Abdu et al., 1981; Sastri, 1984; Batista et al., 1986; Goel et al., 1990). First-order information on F-region vertical drifts at Trivandrum in the Indian sector has been derived recently for moderate to low solar activity conditions (1984-89) using the HF Doppler radar technique (Namboothiri et al., 1989; Balachandran Nair et al., 1993). These studies however used a rather small data sample. The results of a detailed study of the characteristics of the evening and nighttime F-region vertical plasma drifts at the dip equatorial station, Kodaikanal about 200 Km north of Trivandrum are presented in this chapter. The study is based on a large sample of F-region vertical drift measurements made with the HF phase path sounder (Doppler radar) during a 25-month period of moderate to high solar activity.

Temporal fine structure in V_z and its response to electric field disturbances arising out of dynamic/electrodynamic coupling of high latitude and low latitude ionospheres at times of geomagnetic sudden commencements, geomagnetic micropulsations, sub-

storms/storms is another important aspect of the ionospheric dynamics (e.g., Patel and Lagos, 1985; Early and Kalley, 1987, Sastri et al., 1993). As presented and discussed in chapter 3, measurements of phase path of F-region reflections during daytime near dip equator show severe wave activity in the period band 30-600 sec. The fluctuations in $\dot{P}$ (or Doppler velocity, V_D) in the range of 30-300 sec band are interpreted as the modulations caused by the refractive index variations associated with convective motions of electrojet irregularities at E-region altitudes. Measurements of phase path of F-region reflections on the lower frequency of 4 MHz during evening and nighttime have distinct advantages over the daytime observations on 5 MHz as they are relatively free from the modulation due to electrojet irregularities. Therefore, the estimation of vertical plasma drift (V_z) from Doppler velocity, V_D is relatively straight forward. The variations in F-region Doppler velocity (V_D) with periods of 300-600 sec which are commonly observed at Kodaikanal during daytime (0800-1600 IST) are interpreted as the signatures of gravity waves related changes in the E-region zonal electric field at the magnetic link latitude of the F-region over Kodaikanal. Dependence of 300-600 sec fluctuations in $\dot{P}$ (V_D) of daytime F-region reflections on Pc5 (150-600 sec) micropulsation activity is not seen in the correlation analysis of the simultaneous data of F-region phase path at Kodaikanal and groundlevel pulsations at Trivandrum.

We hold the view that the absence of a clearcut association during daytime (0800-1600 IST) between the 300-600 sec fluctuations in F-region Doppler velocity at Kodaikanal and Pc5 pulsations could be due to the dominance of the ever-present gravity wave activity. The amplitude and occurrence of Pc5 micropulsations near the dip equator are known to exhibit a local time pattern similar to the growth and decay of the electrojet current during the day (Jain, 1977). This feature indicates a significant influence of ionospheric conductivity in the manifestation of pulsations in the groundlevel magnetic data. The ionospheric electric fields associated with pulsations of a given amplitude at groundlevel are, therefore, to be much larger at night than during daytime because, the reduced E-region Pederson and Hall conductivities at night require

larger electric fields to produce E -region currents sufficient enough to maintain the amplitude of groundlevel magnetic pulsations. The model calculations of Sutcliffe and Poole (1990), in fact, demonstrate the remarkable influence of E region conductivity changes between day and night on the amplitude of the pulsation-related ionospheric Doppler velocity variations at vertical incidence . For a typical midlatitude location with an inclination (I) of +60° and background magnetic field (B) of 30000 nT, while the field-aligned component of the magnetic pulsation field (b_p) associated with Pc3 pulsations (T=20 sec) of 1 nT amplitude at groundlevel remains the same between day and night , the east-west component of the ionospheric electric field (E_y) is larger by a factor of 10-50 at night than during the day depending on altitude. The increase in the relative amplitudes of electric and magnetic fields at night leads to larger amplitudes of ionospheric Doppler velocity for groundlevel magnetic pulsations of a given magnitude. This physical situation also reflects in the fact that the early reports of pulsation-related Doppler velocity variations were for night time conditions (e.g., Duffus and Boyd,1968; Klostermeyer and Rottger, 1976) and the association for daytime has been documented only in recent times with the use of sensitive techniques (e.g., Lathuillere et al., 1981; Menk et al., 1983; Tedd et al., 1989). It follows, therefore, that the detectability of signatures of micropulsations in F region Doppler velocity near the dip equator (where the plasma transport at F region heights is essentially controlled by the electromagnetic EXB drift) will, in general, be higher in the local evening and night time periods than during daytime.

In this chapter are presented the results of a detailed study made in respect of the morphological features of the evening and nighttime equatorial F-region vertical drifts (V_z) based on a large sample of phase path data of F-region echoes acquired at Kodaikanal. The occurrence of remarkable fluctuations in evening F-region Doppler velocity, V_D at Kodaikanal in association with Pc5 type micropulsations is also demonstrated through a case study.

4.2. MORPHOLOGICAL STUDIES OF F-REGION VERTICAL PLASMA DRIFTS NEAR GEOMAGNETIC EQUATOR.

4.2.1. Observations and Data analysis

The present work is based on measurements made on 410 days over the period February 1991 through February 1993. The data run varied from 3 to 14 hours on individual days over the time interval 1600 - 0600 hrs IST (IST = UT + 5.5 hrs). The observations are more or less uniformly distributed over the three seasonal groups of months during the two year period. The number of days of observations for the two years viz., 1991-92 (Feb 1991 to Feb 1992) and 1992-93 (Mar 1992 to Feb 1993) are 201 and 209 respectively. The number of days of observations available for the three seasons viz., summer (May, June, July and August), winter (November, December, January, and February) and equinox (March, April, September and October) are 133, 152, and 125 respectively. During the 25 month period of our observations the 10.7cm solar flux ($F_{10.7}$) varied in the range 97.8 to 296.6 flux units with an average of 215.1 and 136.7 flux units for the years 1991-92 and 1992-93 respectively. The variation in monthly averages of $F_{10.7}$ flux pertaining to the phase path observations of these two years are shown in Fig.4.1. The monthly averages of 10.7cm solar flux are shown in bar diagrams while the total number of days of observations for the corresponding month is shown in rectangle above each bar diagram. Geomagnetic conditions varying from quiet (A_p = 2) to highly disturbed (A_p = 179) were encountered. The monthly distribution of phase path data over the two years under consideration as a function of the prevailing level of geomagnetic activity is shown in Fig.4.2. The inner bar diagrams show the minimum A_p value and the hatched bar diagrams show the maximum A_p value encountered during the corresponding month. The numbers shown in rectangles on the top of each bar diagram indicate the total number of days of observations available for the corresponding month.

For each night, the time rate of change of phase path or Doppler velocity, V_D of the F-region reflections is calculated at 1 min intervals and then converted to vertical

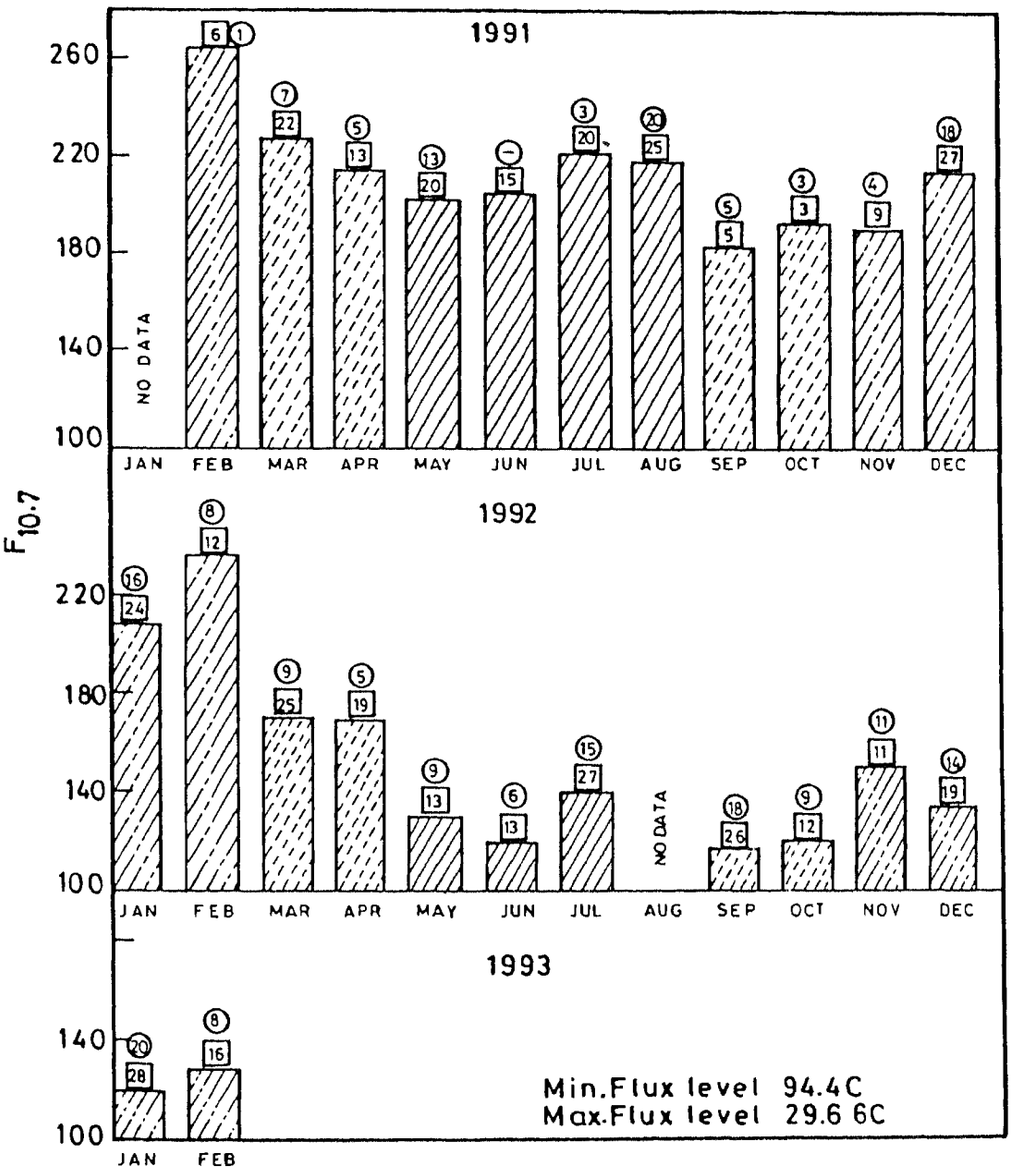

Fig.4.1. Monthly averages of 10.7 cm solar flux (solar flux for the days when the phase path observations are available only are considered) for the duration February 1991 to February 1993 are shown in bar diagrams. Numbers shown in rectangles and circles above the bar diagrams correspond respectively to the number of days of phase path data available in that month and the number of days for which the peak of the prereversal enhancement (V_{zp}) is available.

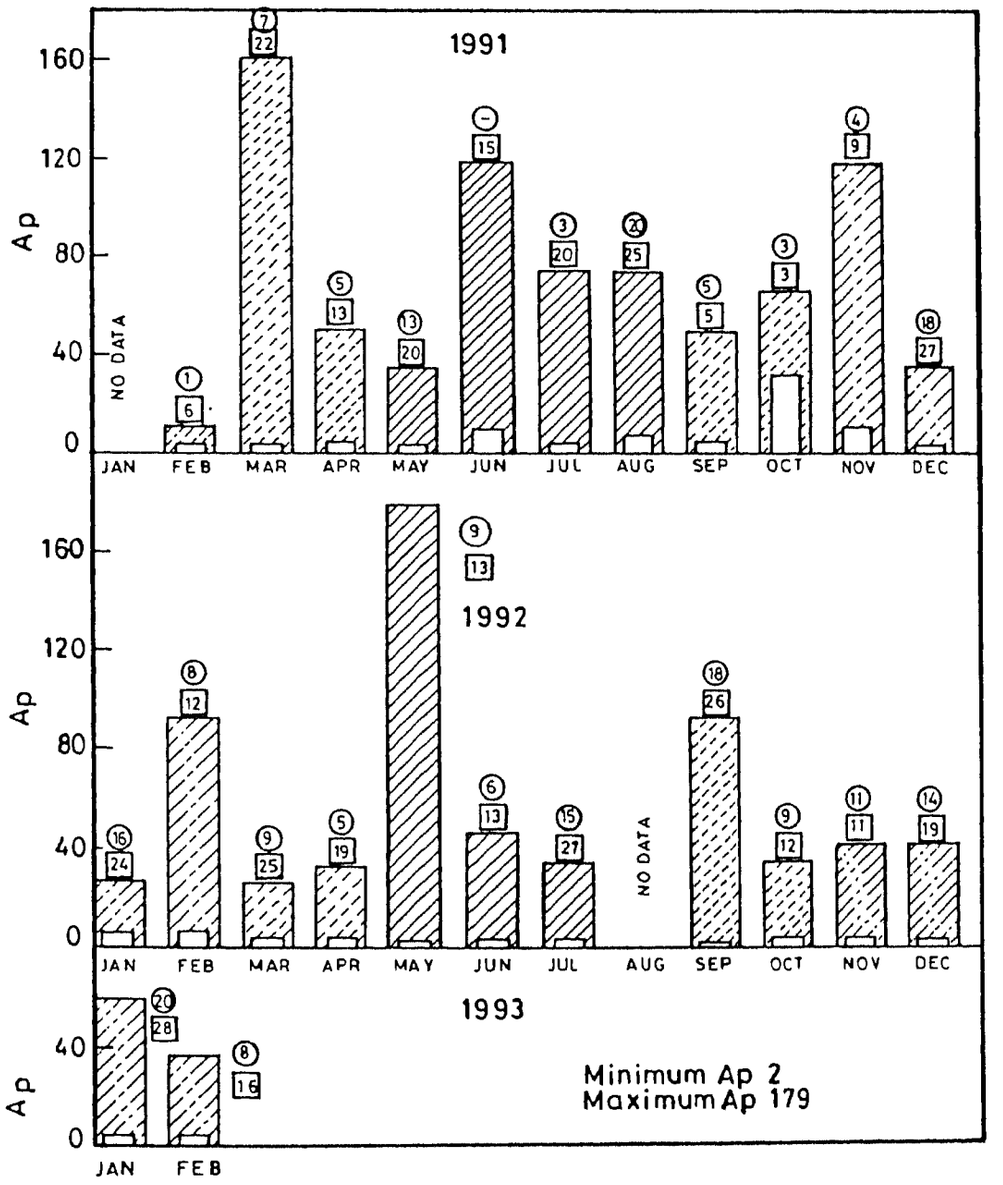

Fig.4.2. Monthly range (minimum and maximum) of A_p encountered during the span of phase path observations used in the present work are shown in bar diagrams. Numbers shown in rectangles and circles are same as those shown in Fig.4.1.

plasma drift,V_z ($= \frac{V_p}{2}$). The data are analysed for information on steady vertical drift by computing the running averages of 1min interval V_z with a 65 min window. This is done in order to suppress noise-like fluctuations and also the large amplitude fluctuations of periods less than 1hr which are known to prevail quite commonly in the F-region vertical drift near the dip equator during the evening hours (Balachandran Nair et al., 1992; Subbarao and Krishnamurthy,1994). This exercise is repeated with windows of 55 min, 45 min and 25 min widths to check for any significant underestimation of V_z due to the smoothing process. It is found that the average V_z patterns (for example as a function of season) are not significantly affected by the width of the window (in the range 25-65 min) chosen for the smoothing process (the change in the magnitude of the prereversal peak in average V_z is found to be 2-3m/sec). The peak of the prereversal enhancement in V_z (V_{zp}) is determined for each night for studies of its dependence on season and solar and geomagnetic activity. It is to be mentioned here that V_z could not be ascertained with any certainty on some of the nights, particularly during equinoctial and summer months due to the frequent occurrence of equatorial spread F conditions. This limitation has reduced the number of nightly V_{zp} values to 227. Seasonal separation of V_{zp} data yielded 36(30), 47(53)and 20(41) nightly values for the year 1991-92.(1992-93) for summer, winter and equinoctial months respectively. Number of V_{zp} values available for each month are shown in circles above the bar diagram of monthly averages of $F_{10.7}$ (A_p) in Fig 4.1 (Fig 4.2).

4.2.2. Seasonal variation

Figure 4.3 shows the scatter plots of the nocturnal variation of F-region V_z over Kodaikanal for the three seasonal groups of months based on a total of 245 days of data for the period February 1991 through April 1992. This limited data base has been used in the first instance as the h'F (height of bottomside F-region) data from a co-located ionosonde were available during whole night only for these 245 days. Fig.4.4 shows the mean pattern of the nocturnal variation of F-region V_z for the data presented in Fig.4.3.

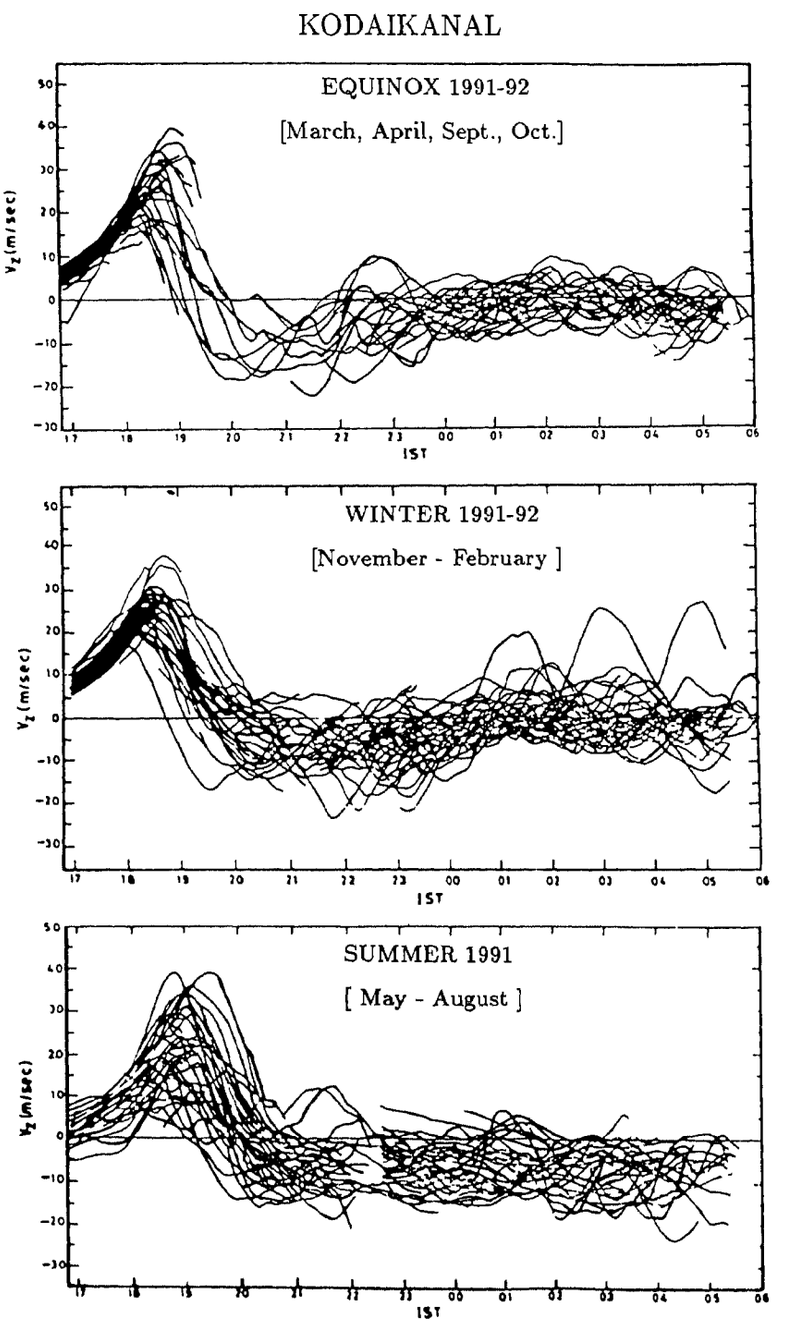

Fig.4.3. Scatter plots of nighttime F-region vertical drifts (V_z at Kodaikanal (dip 3°N), during summer, winter and equinoctial months over the period February 1991 - April 1992.

Also shown in Fig.4.4 is the average nighttime pattern of h'F derived from 1 hr interval h'F data of individual nights.

Bittencourt and Abdu (1981) have shown that the effect due to layer decay on the vertical drifts arising from chemical loss is significant at times of the reflecting layer remaining below 300 km. The seasonal changes in the nocturnal F-region height at Kodaikanal (see Fig.4.4) clearly indicate that (a) the V_z pattern derived from Doppler data is reliable in all seasons for the premidnight period during high solar activity period because h'F remained above 300km in that local time period and (b) the absence of sizeable downward drift in the postmidnight hours (the local time period when h'F remained below 300km) during winter and equinoxes is due to swamping of the ambient downward V_z by upward drift induced by chemical loss. The derived V_z data for individual days in winter and equinoxes are still be useful as they can be corrected for the effects due to layer decay through the use of neutral atmospheric models such as MSIS-86 and ionosonde data for the electron density scale length (Somayajulu et al., 1991).

A larger data base of 410 days covering the period February 1991 through February 1993 is used to derive the seasonal pattern of F-region vertical drift (V_z) over the time interval 1600 - 0600 IST. The height of bottomside F-region (h'F) scaled from the ionograms of a co-located ionosonde, is found to be less than 300 km during the evening period on only 80 days out of the total 410 days. 11 out of these 80 days belonged to the category with h'F $\leq$ 250km for which the correction to V_z due to chemical loss is $\geq$ 7ms^{-1}. For the remaining 69 days with 250km $<$ h'F $\leq$ 300km the corrections to V_z is $<$ 7ms^{-1}. Explicit corrections for the effects of chemical loss are, therefore, not made in determining gross features of V_z like the average seasonal patterns.

Fig.4.5 shows the average pattern of the nocturnal variation of F-region vertical plasma drift, V_z over Kodaikanal for the three seasons of both high (Feb 1991 through Feb 1992) and moderate (March 1992 through Feb 1993) solar activity epochs. The

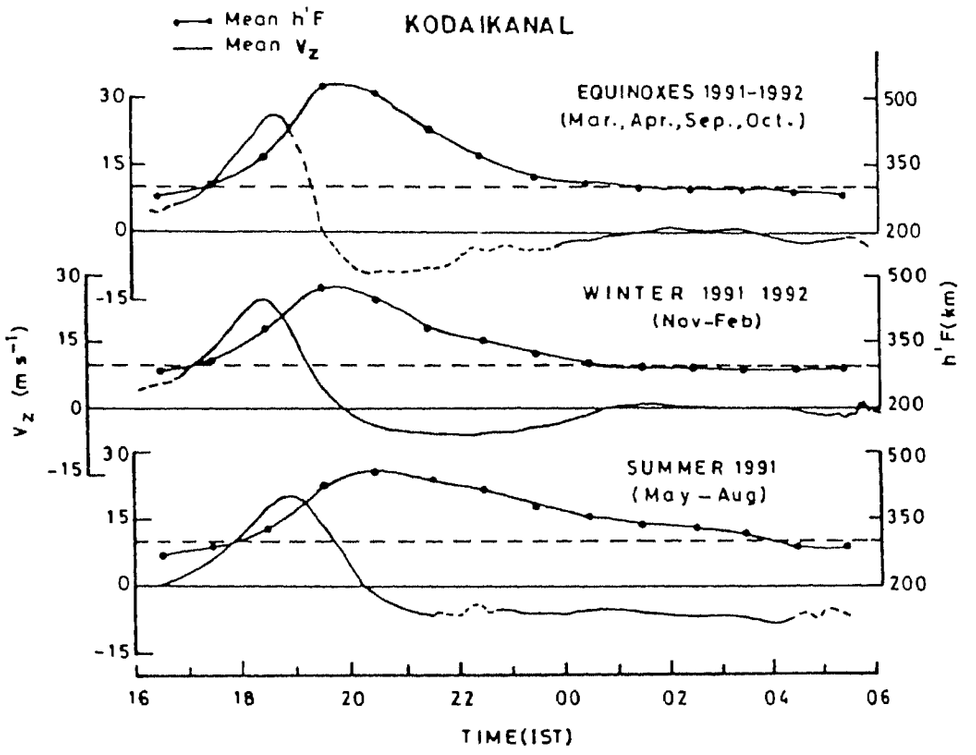

Fig.4.4. Average patterns of vertical drifts (V_z) for the data shown in Fig.4.3. Average pattern of height of bottomside F-region (h'F) is also shown. The horizontal line on h'F plot correspond to an height of 300 km.

statistical results of the behaviour of the prereversal peak (V_{zp}) obtained from the average V_z patterns shown in Fig.4.5 are given in Table 4.1 It is quite evident from Fig.4.5 that the postsunset or prereversal enhancement is the dominant feature of the nighttime pattern of F-region vertical drift near the dip equator. The prereversal peak in average V_z is higher in equinoxes and local winter than in local summer for both high and moderate solar activity conditions. The same seasonal trend is also seen when the analysis is done exclusively for quiet days ($A_p \leq 14$) of both high and moderate solar activity periods. The reduction in V_{zp} from equinox to summer is by a factor of 1.3 and 1.5 for high and moderate solar activity conditions respectively. The corresponding reduction factors for quiet days alone are 1.3 and 1.8. In contrast to this behaviour at Kodaikanal, the V_{zp} at Jicamarca is, on the average, higher in equinoxes and local summer than in local winter (see Fig.1 of Fejer et al., 1991). The reduction in V_{zp} from equinox to local winter at Jicamarca is by a factor of 2.8 and 2.5 for magnetically quiet ($K_p < 2^+$) conditions of high and moderate solar activity respectively. The minimum value of V_{zp} at Jicamarca during local winter months and at Kodaikanal during local summer months are, however, of the same magnitude. The seasonal behaviour of V_{zp} is thus markedly different at dip equatorial stations in the Indian and American sectors for both high and moderate solar activity conditions. It is to be borne in mind, however, that the Jicamarca drift data correspond to the height interval 200 to 800 Km, whereas the data at Kodaikanal correspond to the reflection height of the F-layer which varies with local time and from day-to-day. Comparison of the V_{zp} patterns at Kodaikanal with those reported earlier for Trivandrum (Namboothiri et al., 1989) for moderate solar activity conditions showed that though the seasonal behaviour is same (i.e., higher V_{zp} in equinoxes and winter than in summer), the values of V_{zp} at Kodaikanal are smaller than those at Trivandrum (see Table 4.1). The difference is striking in equinox when the average V_{zp} at Kodaikanal for quiet days is less by a factor of ≈ 1.6 compared to that at Trivandrum. During equinoxes the V_{zp} values for high solar activity at Kodaikanal are found to be less than those of V_{zp} at Trivandrum for moderate solar activity. This is rather puzzling because V_{zp} is known to increase with solar flux irrespective of season

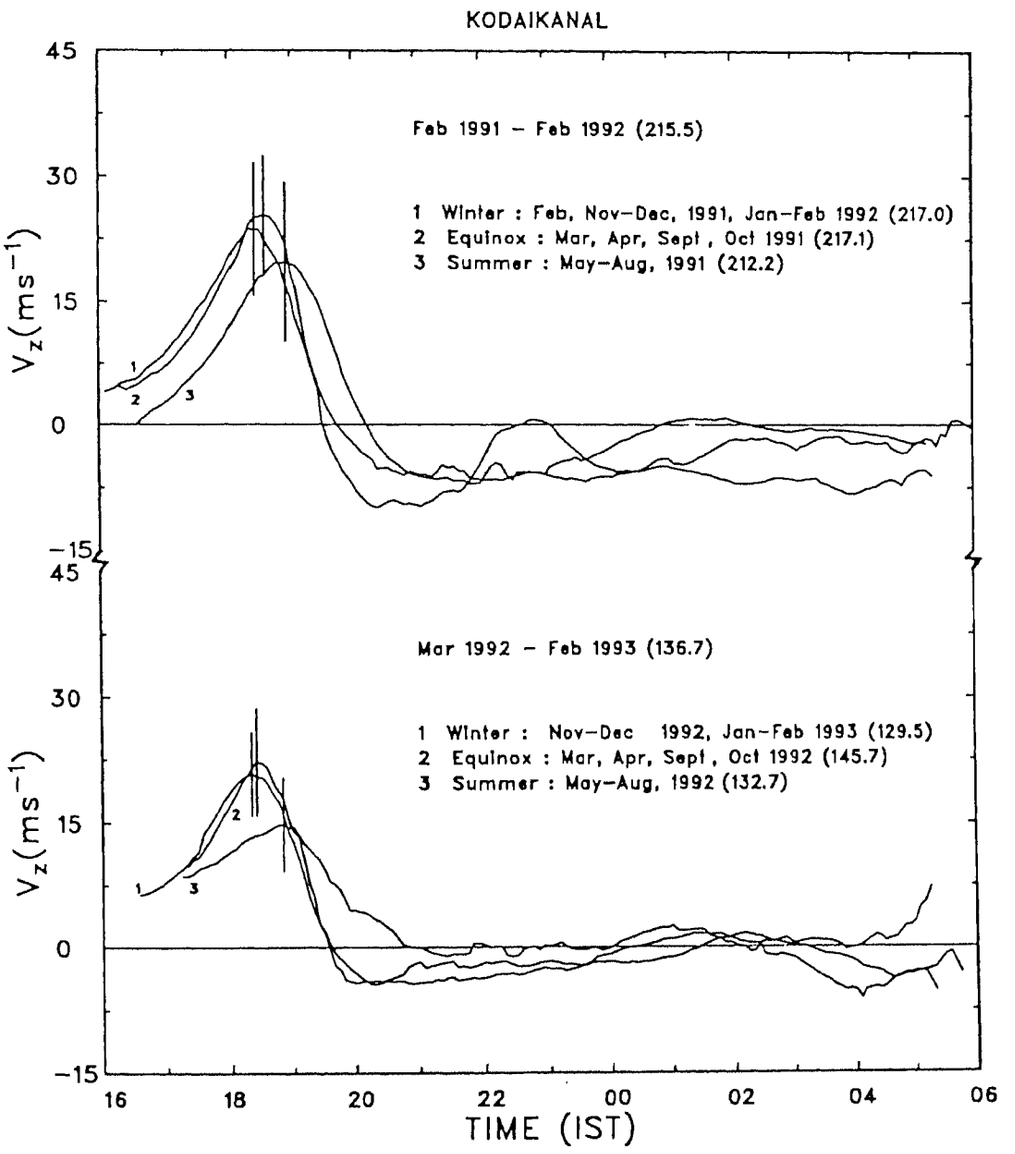

Fig.4.5. Average patterns of nighttime V_z at Kodaikanal during summer (May - August), winter (Nov - Feb) and equinoctial (March, April, Sept and Oct) months. The patterns are shown for periods of high solar activity(Feb 1991 - Feb 92) as well as moderate solar activity (Mar 1992 - Feb 1993). Numbers in parentheses indicate the average solar 10.7cm flux for the seasonal groups of months. The vertical bars represent the standard deviations near the peak of the prereversal enhancement in average V_z pattern for each season.

Table 4.1. Statistical details of V_zp at Kodaikanal (India) for high and moderate solar activity conditions. Similar details of V_{zp} at Jicamarca (Peru) and Trivandrum (India) are also given for comparison.

Station			Equinox		Winter		Summer		Reference
			High Solar Act.	Moderate Solar Act.	High Solar Act.	Moderate Solar Act.	High Solar Act.	Moderate Solar Act.	
Kodaikanal	All Days	N	43	82	78	74	80	53	Current Work
		V_{zp}	26.0	22.2	25.0	20.8	20.0	14.8	
		cv	0.28	0.28	0.22	0.24	0.48	0.37	
	Quiet $A_p \leq 14$	N	20	47	43	47	28	38	
		V_{zp}	26.3	24.9	25.0	20.0	20.7	14.2	
		cv	0.26	0.23	0.17	0.22	0.50	0.40	
Jicamarca	Quiet $K_p < 2^+$	V_{zp}	~50	~25	~17	~10	~38	~25	Fejer et al., 1991.
Trivandrum	Quiet $A_p \leq 14$	N	-	7	-	6	-	9	Balachandran Nair et al., 1992.
		V_{zp}	-	~40	-	~25	-	~17	

Notes: V_{zp} : Peak of the prereversal velocity enhancement obtained from average V_z profiles, in ms^{-1}.
cv = Sd/mean, Sd: Standard deviation.
Station Coordinates : Kodaikanal : 77°28′E, 10°14′N, dip 3°N.
Jicamarca : 76.87°W, 11.95°S, dip 2°N.
Trivandrum : 76°57′E, 8°29′N, dip 0.6°S.

at Jicamarca (Fejer et al., 1991). It is to be noted, however, that the prereversal enhancement in V_z exhibits marked day-to-day variability even on quiet days (Fejer, 1991), and that the equinox V_z pattern at Trivandrum was derived from a limited data base (see Fig. 2a of Namboothiri et al., 1989). Moreover, the V_z patterns at Trivandrum were obtained from spot measurements of V_z at 5 min intervals using a 1 min sampling interval, and were not smoothed for short-period variations as in the present work. The day-to-day variability in V_{zp} at Kodaikanal as represented by the coefficient of variation ($cv = sd/mean$) is highest in summer and lowest in winter (Table 4.1). This pattern of day-to-day variability persists even on quiet days of both high and moderate solar activity epochs.

The monthly averages of prereversal peak in vertical drift obtained by averaging the V_{zp} values of individual days of each month are shown in Fig.4.6 for both high and moderate solar activity conditions. The vertical bars on the two curves represent the standard deviations ($\pm\sigma$). The seasonal variation in V_{zp} with higher values in equinoxes and local winter than in local summer mentioned earlier can clearly be seen from Fig.4.6. It is interesting to note here that during summer months the average V_{zp} undergoes a significant reduction from the high solar activity epoch (1991-92) to the moderate solar activity epoch (1992-93).

4.2.3 Solar cycle variation.

Fig. 4.7a shows the mass plot of the variation of V_{zp} with the daily 10.7cm solar flux ($F_{10.7}$) in our entire data sample. The data points shown in triangles represent V_{zp} values for which the h'F values are less than 300km. The line of best fit for V_{zp} *versus* $F_{10.7}$ is also shown in the figure. The values of V_{zp} for individual days are, however, determined after applying the correction for the effects of layer decay. The correction term V_β is given by the following expression

$$V_\beta = \beta L \tag{4.1}$$

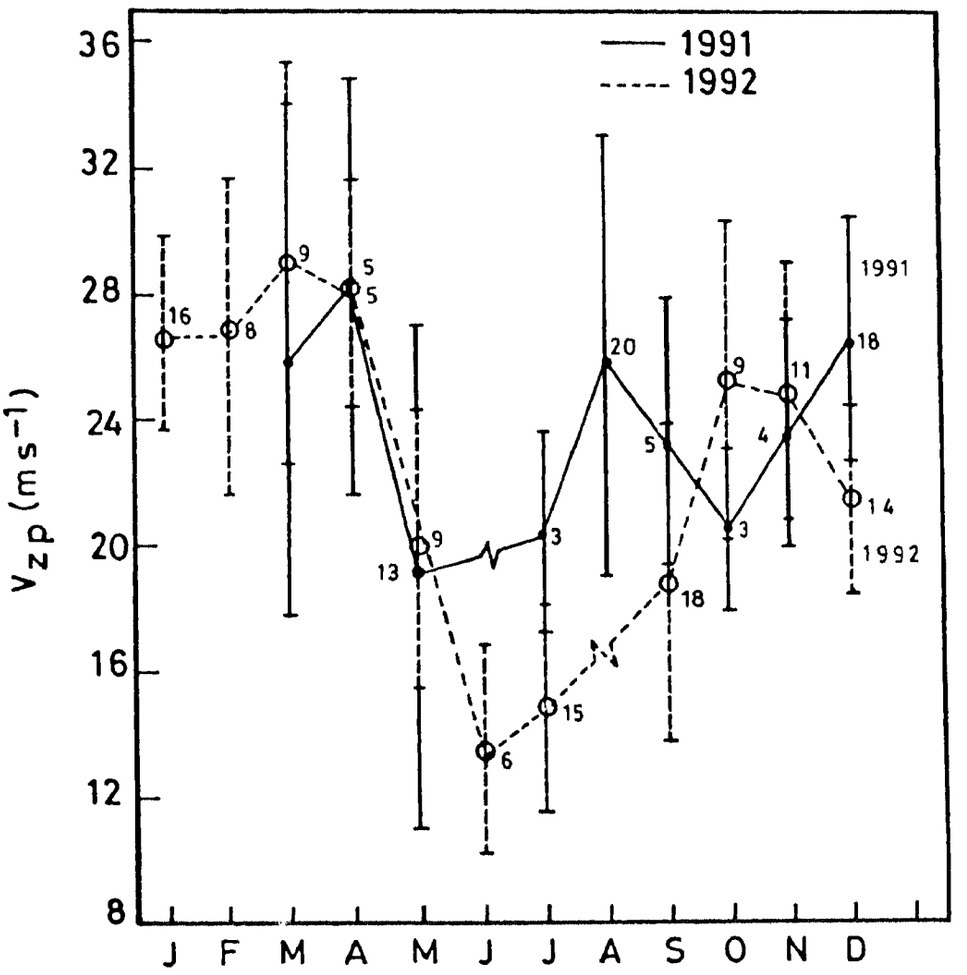

Fig.4.6. Monthly averages of V_{zp} for high and moderate solar activity periods. Vertical bars represent the standard deviations. The total number of nightly values of V_{zp} used for obtaining the monthly average V_{zp} are also shown.

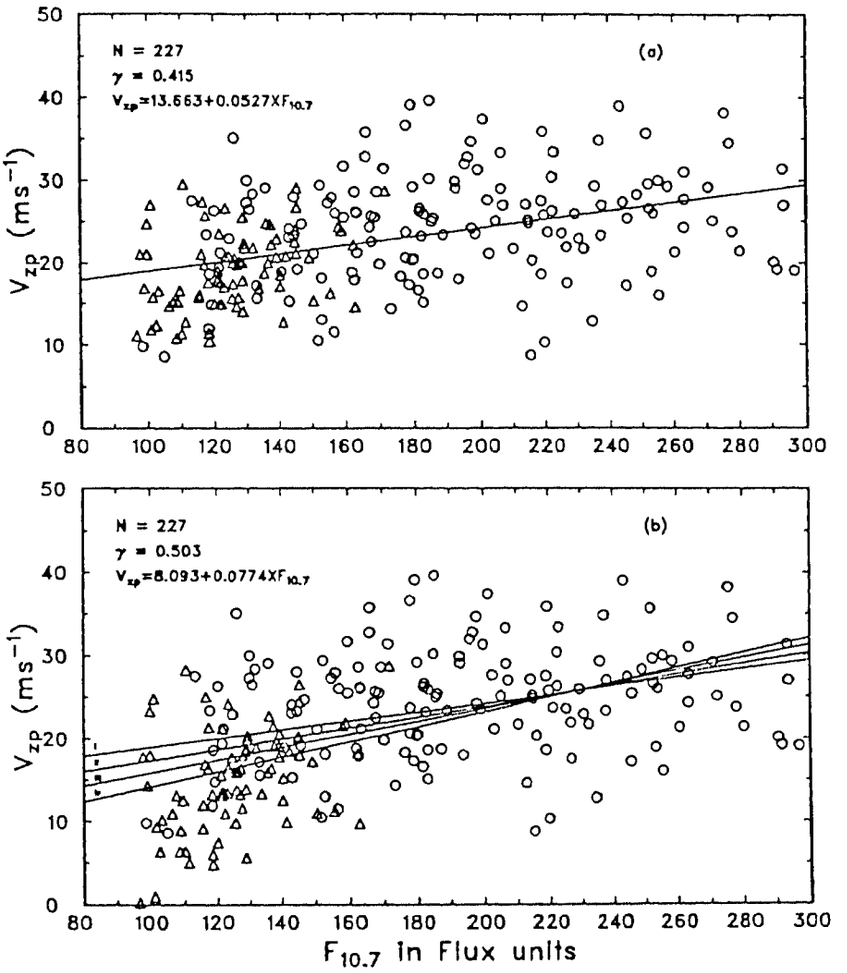

Fig.4.7. Dependence of peak prereversal velocity (V_{zp}) on the solar 10.7cm flux. (a) Data points with triangles show the V_{zp} values corresponding to the days with h'F <300 Km for which corrections due to layer decay are not made . The line of best fit to the data is also shown. (b) Values of V_{zp} with h'F <300 km corrected for layer decay with a scale length (L) of 10 km are shown in triangles. The regression lines in the lower panel are for all the data uncorrected for layer decay and corrected for layer decay (on 80 days) with electron density scale length (L) of 5 Km, 10 Km and 15 Km.

where L is the plasma density scale length and β is the chemical loss rate coefficient (Titheridge and Buonsanto, 1983) and are given by

$$L = \frac{1}{N_e}\frac{dN_e}{dz}^{-1} mts. \tag{4.2}$$

and

$$\beta = 5.4 \times 10^{-19}([N_2] + 23[O_2])s^{-1} \tag{4.3}$$

In the above expressions N_e is the electron concentration, $[N_2]$ and $[O_2]$ are the concentration of molecular nitrogen and oxygen respectively. $[N_2]$ and $[O_2]$ are derived from the MSIS-86 thermospheric model (Hedin, 1987) for the relevant geophysical conditions and are in turn used in the expression 4.3 to evaluate β. The correction term V_β for the vertical drifts is then computed for an assumed electron density scale length (L) of 10 Km. The ideal approach of course would be the use of actual values of L derived from the electron density (N-h) profiles obtained from ionogram reductions. But this is a laborious and time consuming process particularly when a large data base of phase path measurements is to be treated as is the case here. The resultant pattern of V_{zp} *versus* $F_{10.7}$ is shown in Fig. 4.7b. In the process of applying corrections for V_{zp} the electron density scale length (L) was assumed to be 10km. A sensitivity check, however, is made by applying corrections for V_{zp} with different values of L. The linear- fitted curves for L values of 5 Km,10 Km and 15 Km are also shown in Fig 4.7b. It can be seen that the sensitivity of V_{zp} to 10.7cm solar flux does not depend critically on the L value used. Therefore a L value of 10 km is adopted throughout in applying corrections to V_{zp} for the effects of layer decay whenever the height of the reflecting layer is below 300 Km. The scatter plot as well as the linear fitted curves of Fig. 4.7 demonstrate that at Kodaikanal the prereversal peak in F-region vertical drift V_{zp} increases with solar activity.

The plausible seasonal changes in the variation of V_{zp} with solar activity are studied by binning V_{zp} values for the 10.7cm flux levels of 80-100, 100-120, 120-140, 140-160,

160-180, 180-200, 200-220, 220-240, and 240-260 flux units. Fig.4.8 shows the variation of V_{zp} with the 10.7cm solar flux obtained with this procedure separately for the three seasons. The standard deviations of the average values of the 10.7cm flux and V_{zp} are indicated by horizontal and vertical bars respectively. The linear and quadratic fitted curves are also shown in the figure. Bins in which the total number of paired values of V_{zp} and $F_{10.7}$ are less than 3 are not considered for the regression analysis but are shown in the figure for completeness. Statistical details of the relationship between V_{zp} and $F_{10.7}$ are summarized in Table.4.2. Published results on the relationship between V_{zp} at Jicamarca and $F_{10.7}$ are also given in Table.4.2 to facilitate a comparative study of the dependence of V_{zp} on solar activity at the dip equatorial stations in the Indian and American sectors. It is quite obvious from Fig.4.8 that at Kodaikanal V_{zp} increases linearly with the solar flux during equinox. On the other hand, the summer and winter data show a better fit to a quadratic curve and V_{zp} seems to saturate for the values solar flux $>$ 230 units. The absence of saturation during equinox may be due to the lack of V_{zp} data for very high flux levels in our data sample. Similar seasonal trends in the dependence of V_{zp} on solar flux are seen even when the daily values of V_{zp} and $F_{10.7}$ are analysed instead of binning the data according to the solar flux level (not shown here). In contrast at Jicamarca the prereversal peak velocity is reported to saturate for flux levels $>$ 170 flux units during local winter and to increase linearly during local summer and equinoxes (see Fig.3. of Fejer et al., 1991). It is clear from Fig.4.8 and Table.4.2 that the sensitivity of V_{zp} with solar flux as represented by the slope of the lines of best fit is higher at Jicamarca than at Kodaikanal irrespective of season (see also Fig. 3 of Fejer et al., 1991).

4.2.4. Variation with Geomagnetic Activity

Correlation analysis of daily values of V_{zp} and the geomagnetic activity index, A_p showed the absence of a systematic relationship between them. Seasonal and solar activity dependence of the relationship between V_{zp} and A_p is also evaluated by separa-

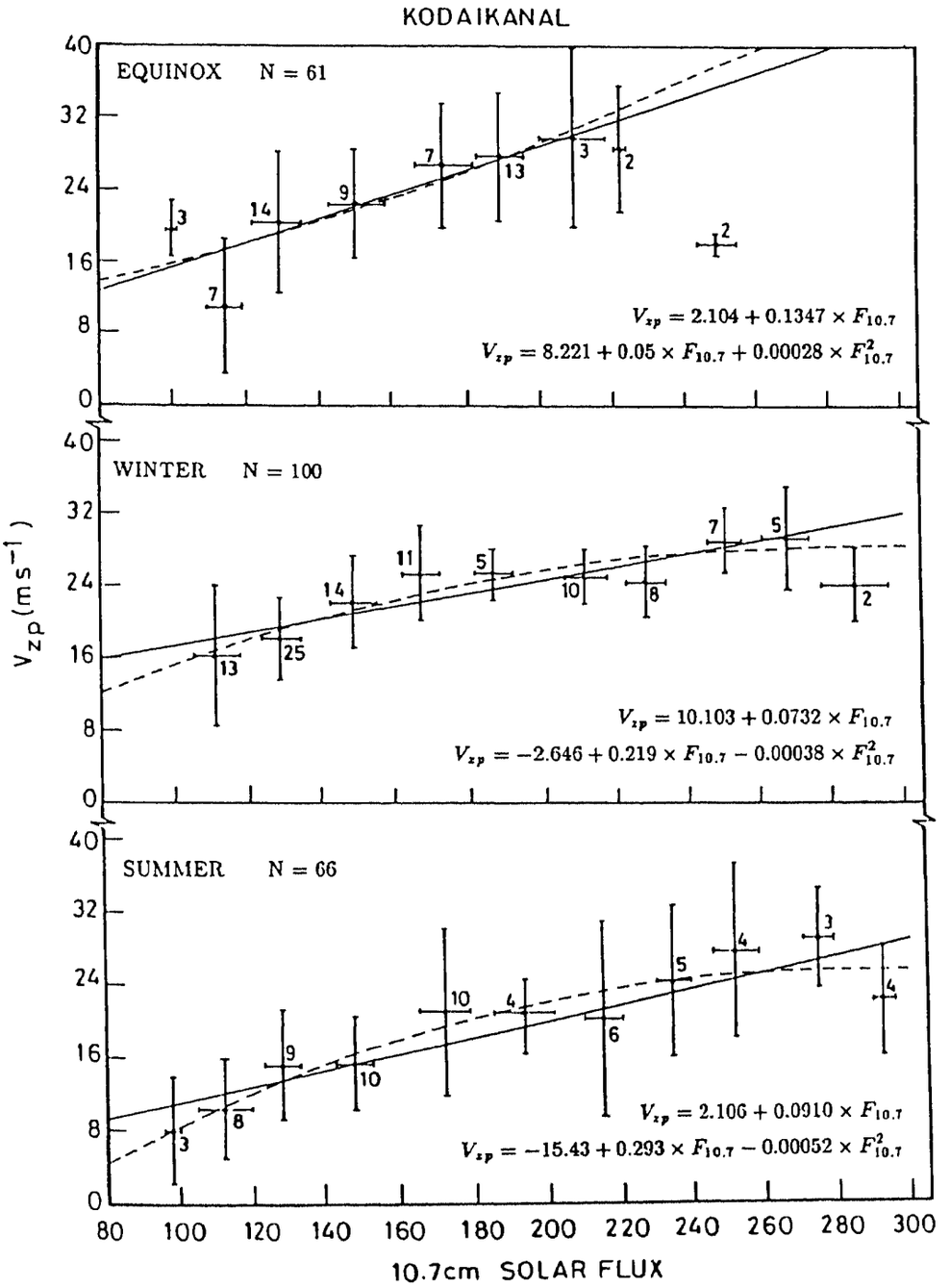

Fig.4.8. Variation of the average preversal peak velocity (V_{zp}) with the solar 10.7cm flux ($F_{10.7}$). The horizontal and vertrical bars represent standard deviations of solar flux and V_{zp} respectively.

Table 4.2. Statistical details of the Variation of V_{zp} at Kodaikanal (India) with $F_{10.7}$. Similar details of variation of V_{zp} of Jicamarca (Peru) with $F_{10.7}$ is reproduced for comparison.

Station	Coefficients	Equinox		Winter		Summer		Reference
		Linear	Quadratic	Linear	Quadratic	Linear	Quadratic	
Kodaikanal	A	2.104	8.221	10.103	-2.646	2.106	-15.430	Current work
	B	0.1347	0.0500	0.0732	0.2187	0.0910	0.2933	
	C	-	0.00028	-	-0.00038	-	-0.00052	
Jicamarca	A	-4.650	-	-	-51.375	-4.450	-21.507	Fejer et al., 1991
	B	0.2900	-	-	0.8010	0.2500	0.5050	
	C	-	-	-	-0.0021	-	-0.000805	

Notes: Linear - $y = A + Bx$. Quadratic - $y = A + Bx + Cx^2$.

$F_{10.7}$: 10.7cm Solar flux

Station Coordinates :

Kodaikanal : 77°28′E, 10°14′N, dip 3°N.

Jicamarca : 76.87°W, 11.95°S, dip 2°N.

ting the V_{zp} data according to season and the level of solar activity and the results are presented in Fig.4.9. The scatter plots of V_{zp} *versus* A_p and the corresponding correlation coefficients shown in Fig.4.9 amply demonstrate the absence of any significant relationship between the two parameters. The singular exception is the significant negative relationship evidenced during equinox of the year 1992 corresponding to moderate solar activity conditions. The correlation between V_{zp} and A_p for the other seasons did not change even when V_{zp} values corrected for layer decay (80 days with h'F < 300km) are considered. It is pertinent to mention here that the A_p is a gross index of geomagnetic activity obtained by averaging the 3-hourly a_p index for a given day. In the recent times the time weighted accumulations of a_p, $a_p(\tau)$ is considered to be a better index of geomagnetic activity for studies of the ionospheric response to geomagnetic activity (Wrenn, 1987). The attenuation factor, τ representative of the response time of F-region to geomagnetic activity is found to be 0.75 (Wrenn,1987). We have, therefore, calculated the three- hourly $a_p(\tau)$ values from the 3-hour K_p index values following the procedure introduced by Wrenn (1987). The correlation analysis is repeated with paired values of V_{zp} corrected for layer decay with a scale length of 10 Km and $a_p(\tau)$ for the 3-hour block corresponding to the time of prereversal enhancement in V_z. The outcome of this analysis is found to be the same as with A_p , namely, there is no significant relationship of V_{zp} at Kodaikanal with geomagnetic activity in any of the seasons except during the equinoctial months of moderate solar activity. This can be seen from Fig.4.10 which depicts the relationship of V_{zp} with $a_p(\tau)$ (lower panel) for equinox of moderate solar activity when a significant correlation between them is apparent. Scatter plot of V_{zp} (corrected for layer decay with L = 10km) *versus* A_p and the corresponding regression line are also shown in Fig.4.10 (upper panel) for comparison. The effect of magnetic activity on V_{zp} at Kodaikanal thus seems to be quite different from that at Jicamarca, where the average V_{zp} was reported to decrease with enhanced geomagnetic activity during equinoxes and increase in local winter at solar maximum (Fejer et al., 1989). An increase of the prereversal velocity enhancement with magnetic activity during local winter is recently found to be the situation for low solar flux levels

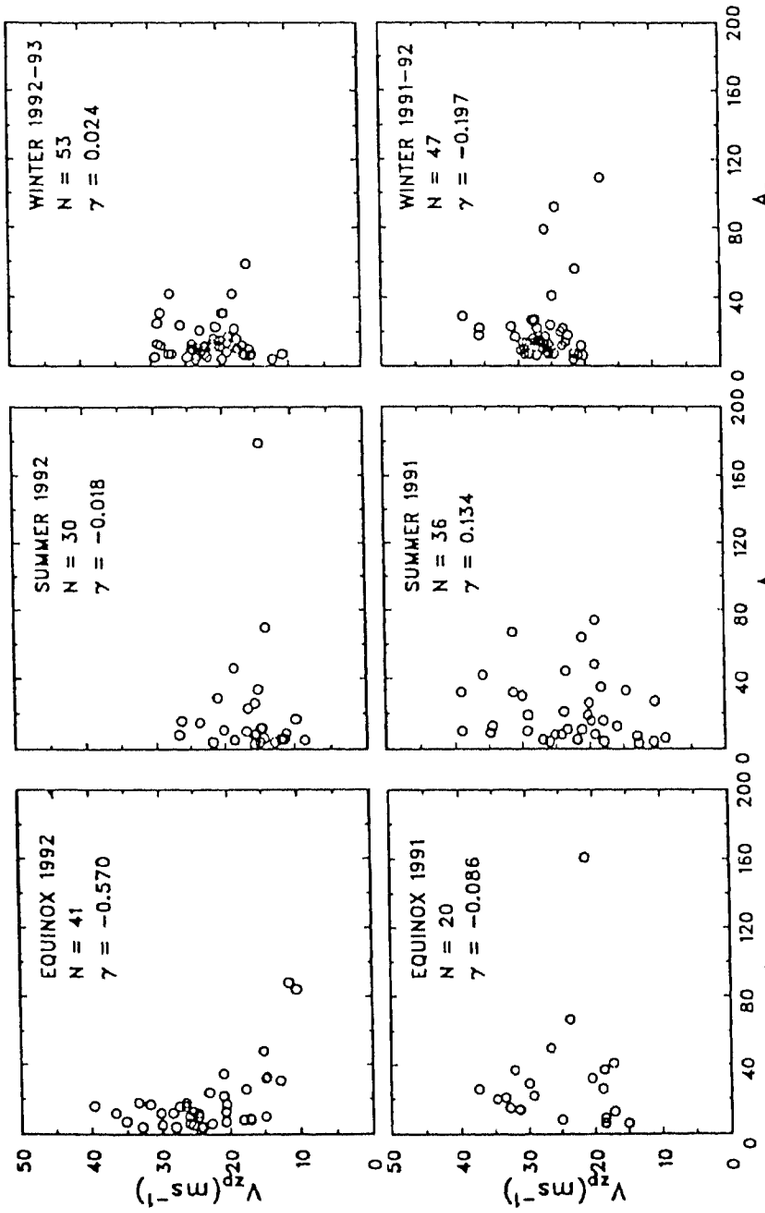

Fig.4.9. Variation of V_{zp} with the geomagnetic activity index, A_p during the three seasons of the years 1991-92 and 1992-93. N and γ represent the number of values and the correlation coefficient respectively.

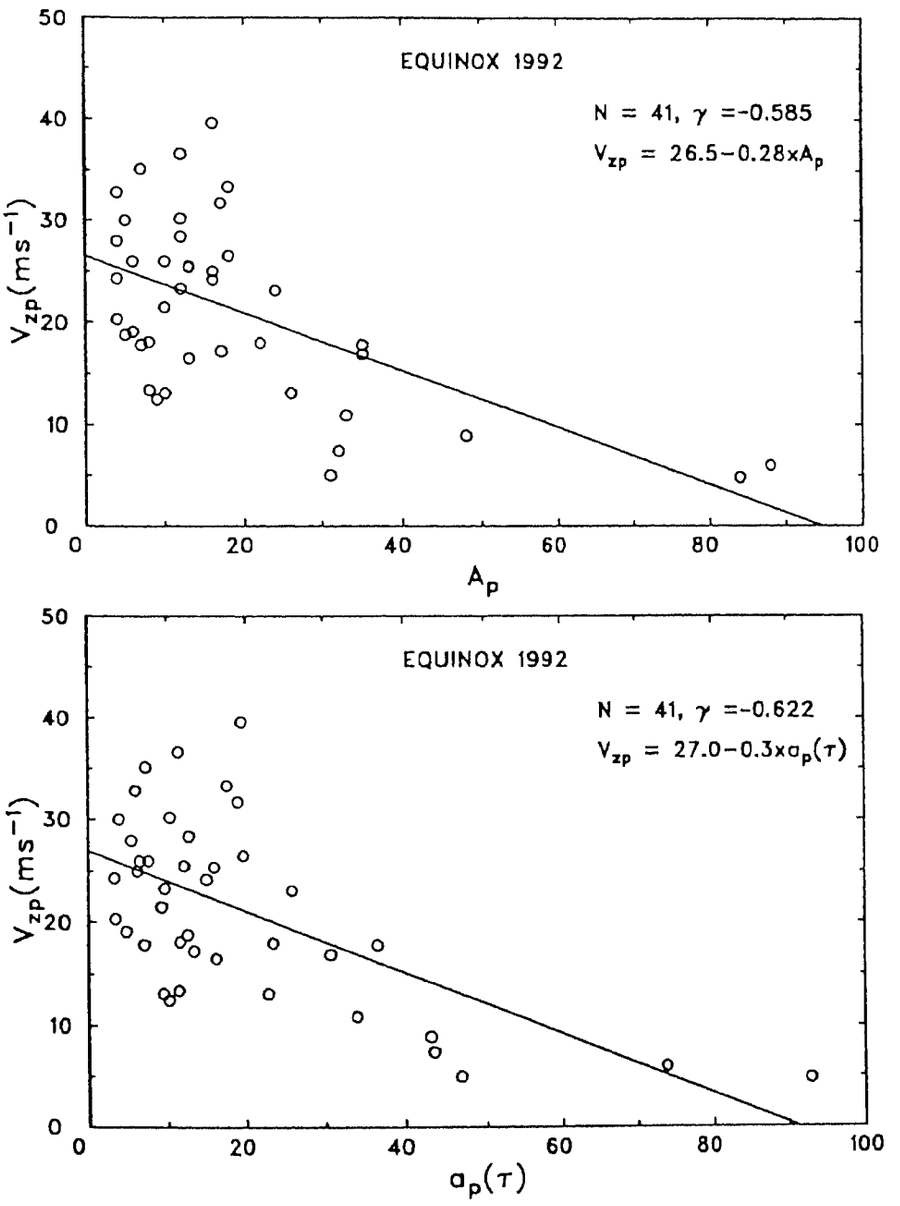

Fig.4.10. Variation of (V_{zp}) with geomagnetic indicies A_p and $a_p(\tau)$ during the equinoctial months of moderate solar activity. V_{zp} values are corrected for layer decay with a scale length (L) of 10km. N and γ represent the number of values and the correlation coefficient respectively.

also at Jicamarca (Fejer et al.,1991). Fejer et al, however, opined that the scatter in the data (see Fig.4 of their paper) does not allow them to give much significance to the noticed trends in the variation of V_{zp} with magnetic activity at Jicamarca. The earlier results from the Doppler radar observations at Trivandrum indicate a decrease of the prereversal velocity enhancement as magnetic activity changes from quiet to moderate conditions (A_p about 15-20), but an increase well above the quiet time values for high magnetic activity (Namboothiri et al.,1989).

4.2.5 Discussion

As mentioned earlier, the postsunset enhancement of the vertical drift of F-region plasma at dip equatorial latitudes is widely considered as due to enhanced electric fields generated by the F-region dynamo mechanism (Rishbeth, 1971; Heelis et al., 1974; Farley et al., 1986). According to the model of Farley et al (1986), a number of factors contribute to the prereversal enhancement of F-region vertical drift. These include the F-region zonal wind, the ratio of E to F-region conductivity, E-region dynamo whose contribution may not always be negligible to that of the F-region dynamo, the lack of symmetry between the hemispheres and non-coincidence of the geographic and dip equators. Batista et al. (1986) demonstrated a strong influence of the declination angle and the thermospheric zonal winds on the amplitude of the prereversal peak in F-region vertical drift at equatorial stations. Goel et al (1990) suggested the increase of the E-region conductivity gradient near the dusk meridian from solar minimum to maximum as partly responsible for the increase of the prereversal enhancement with solar activity. We hold the view that variations in the thermospheric zonal winds may be responsible for the day-to-day and seasonal variability in V_z noticed at Kodaikanal. This will remain a speculation due to the glaring absence at the moment of simultaneous data on F-region zonal winds.

During magnetically quiet conditions electric fields due to E and F region dynamos are primarily responsible for the vertical drifts of equatorial F-region. During mag-

netically disturbed conditions electric fields of magnetospheric/high latitude origin and those generated by the " disturbance dynamo" mechanism gain prominence. Sudden and prominent transitions in the orientation of the north-south (B_z) component of interplanetary magnetic field (IMF) and attendant changes in the electric potential across the polar cap and auroral electrojets (AE index) often result in short-lived (1-2 hr) global electric field disturbances (see review of Fejer, 1991). The amplitude and frequency of occurrence of the transient electric field disturbances associated with sudden northward turning of IMF manifest quite frequently at all local times with maximum amplitudes in the midnight-dawn sector, while those associated with sudden southward turning of IMF manifest only occasionally with a preference for the midnight-noon sector with largest amplitudes just before sunrise (see Fejer,1986 and references therein). Because of being transient and strongly local time dependent, vertical drifts due to these electric fields tend to cancel out in the average patterns obtained as function of season or level of solar flux. On the otherhand, persistent (several hours duration) perturbations in the equatorial zonal electric field with delays of 13-24 hr with reference to the causative geomagnetic disturbances are also known to occur at all local times in phase opposition to the quiet time fields (Fejer et al., 1983; Sastri, 1988a). These slowly-varying and delayed electric field disturbances are generated by the modifications in the global thermospheric circulation induced by the storm-time energy input to high latitude ionosphere-thermosphere system i.e., through the ionospheric "disturbance dynamo" mechanism (Blanc and Richmond, 1980). During geomagnetically disturbed conditions significant perturbations in the equatorial cross-field plasma drifts may therefore be expected. The present statistical study, nevertheless, showed a significant relationship of V_{zp} at Kodaikanal with geomagnetic activity only during the equinoctial months of moderate solar activity.

4.3 DOPPLER VELOCITY FLUCTUATIONS ASSOCIATED WITH ULF GEOMAGNETIC PULSATIONS - A CASE STUDY.

As mentioned briefly in the later part of the introduction to this chapter, the probability of detecting the signatures of micropulsation-related perturbations in F-region Doppler velocity (changes in time rate of change of phase path) near dip equator is, in general, higher in local evening and night time periods than during daytime. This gave us the impetus to search for such perturbations in our evening - night time phase path data. The H-field data of geomagnetic field routinely acquired with the IZMIRAN magnetometer systems at Trivandrum (08° 29′N, 76° 57′E, dip 0.6°S) and Alibag (18° 38′N, 72° 52′E, dip 24.5°N) are used for the identification of geomagnetic pulsation activity. The quartz magnetic sensors of the IZMIRAN system possess very good long-term stability as they are practically immune to temperature and humidity effects. The sensitivity in the H-component is 2.27 nT/mm and 1.68 nT/mm at Trivandrum and Alibag respectively, and the time resolution is better than 45 sec. The IZMIRAN magnetometer data are thus adequate for quantitative studies of the Pc5 pulsations as shown earlier by Jain (1977).

Careful scrutiny of our evening-night time phase path data did provide clear-cut evidence for oscillations in F-region Doppler velocity, V_D concurrent with groundlevel magnetic pulsations for one case, namely, the prominent Pc5 type event that occurred on 24 March 1991, a geomagnetically disturbed day (Ap=161, $\Sigma K_p = 54$). The record of geomagnetic storms for March 1991, infact, shows that a storm started with a sudden commencement (SC) at 0341-42 UT (0911-12 IST) on 24 March and lasted for about three days (Prompt reports of Solar-Geophysical Data, NOAA,USA). Fig.4.11 (top panel) shows the variations in the geomagnetic H-component (above the base level) at Trivandrum and Alibag over the time interval 1620-1843 IST on 24 March 1991 based on 1-min interval sampling of raw data. The presence of pulsations with dominant periods in the band 7-10 min is quite obvious particularly from 1700 IST onwards. The pulsations abruptly ceased by 1910 IST and this feature is not shown in Fig 4.11 for

lack of simultaneous ionospheric data. Though the dominant period (~8 min) of the pulsations is of the right order, the amplitude (half of the peak-to-peak amplitude) of the pulsations (4-20 nT at Trivandrum, 4-16 nT at Alibag) are higher than those of Pc5 that manifest near the dip equator around dusk time (~2.5 nT) (see Figs 1 and 5 of Jain, 1977). The pulsations may tentatively be classified as Psc5 as for now because of their association with the SC, large amplitudes and the damped-type wave forms (see Saito, 1978 and references therein). The amplitude damping can clearly be seen in the H-component at Trivandrum in the intervals 1700-1725 IST, 1745-1805 IST, and 1815-1835 IST. It is to be recalled here that the characteristics of Psc5 bear a similarity to those of Pc5, and this feature is also seen here in the amplitudes of pulsations which are of the same order at Trivandrum (under the electrojet) and Alibag (outside the electrojet belt)- a known feature of Pc5 at equatorial latitudes (Jain and Srinivasacharya, 1975).

The ionospheric response at Kodaikanal to the Pc5 pulsation event as seen in measurements of Doppler velocity (V_D) of F-region reflections at vertical incidence is shown in the bottom panel of Fig.4.11 The dashed line on the V_D plot represents the smoothed variation of V_D obtained by subjecting the original V_D data (1- min sampling) first to a running mean filter of 5- min width and then a running mean filter of 31- min width. The twice- filtered values of $V_D/2$ reflect the temporal pattern of background vertical plasma drift (V_z) which at a location like Kodaikanal corresponds to that in the zonal electric field with a small contribution from layer decay as mentioned earlier. From a theoretical comparison of real and apparent vertical plasma drifts in the dusk-time equatorial F-region, Bittencourt and Abdu (1981) showed that the upward drift due to layer decay is insignificant provided the height of the reflecting region is above a threshold altitude of 300 km. This physical condition was indeed met at Kodaikanal at the time of the geomagnetic pulsations on 24 March. Values of h'F (minimum vertical height of bottomside F-region) scaled from the ionograms of a co-located ionosonde were greater than 300 km from 1630 IST onwards on 24 March. The temporal pattern of V_D

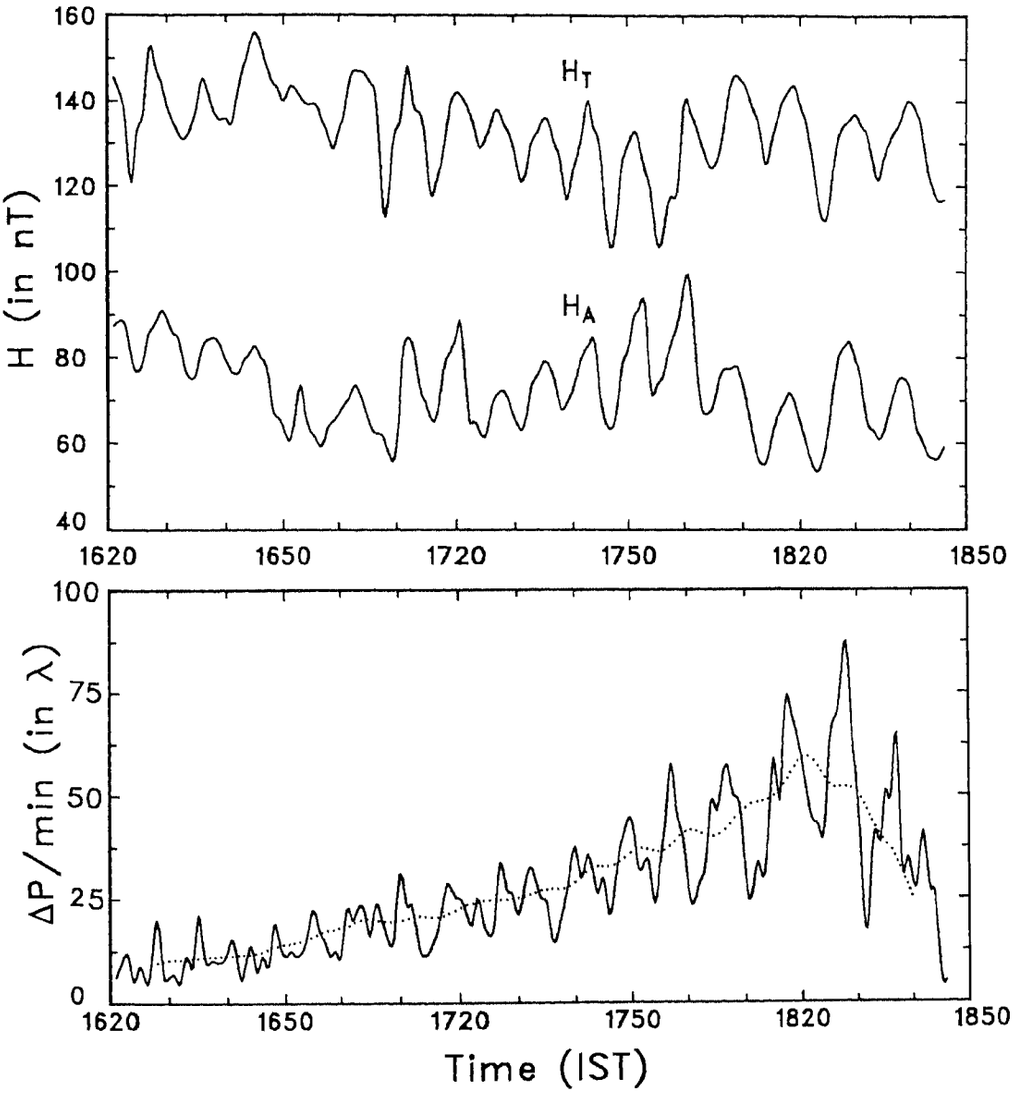

Fig.4.11. Variation of the geomagnetic H-component (above the base level) at Trivandrum, H_T (dip 0.6° S) and Alibag,H_A (dip 24.5° N) on 24 March 1991 showing the Psc5 type micropulsations(top panel).The variation of Doppler velocity,V_D of F-region reflections at Kodaikanal (dip 3°N) is also shown (bottom panel). The dashed curve on the V_D plot represents the smoothed variation of V_D.

shown in Fig.4.11, therefore, corresponds essentially to that of vertical plasma drift V_z (= $V_D/2$) under the influence of the zonal electric field . The data of Fig.4.11 display two noteworthy features. The first one is the characteristic sunset enhancement of V_z near the dip equator which is widely considered to be due to the build up of F-region polarization electric fields (see Fejer,1991 and references therein) . The peak value of V_z of $\simeq$30 ms^{-1}, though of the right order of magnitude for the prevailing solar activity conditions (monthly mean $F_{10.7}$ = 227.6 units; on 24 March $F_{10.7}$ = 260.5 units), seems to be on the low side because the value of V_{zp} corresponding to the flux level of 260.5 is $\sim$ 37ms^{-1} (estimated from the linear relationship of V_{zp} with $F_{10.7}$ for equinox; V_{zp} = 2.104 + 0.01347 x $F_{10.7}$; see Table 4.2). The calculated V_{zp} value corresponding to the value of 260.5 flux units may be an overestimation as the linear relationship deduced between V_{zp} and $F_{10.7}$ is mainly based on the data with $F_{10.7}$ < 220 flux units (see Fig 4.8). However, the observed value of V_{zp} on the day of our interest is approximately equal to the average V_{zp} (26.0 ms^{-1}) of the equinoctial months of high solar activity conditions. The second feature is the occurrence of large amplitude oscillations of 7-10 min periods in V_D concurrent with the geomagnetic pulsations, especially from 1710 IST, i.e. over 11 cycles. Shorter-period fluctuations of 4-6 min are also present in the V_D data superposed on the longer-period components associated with micropulsations. The amplitude damping effect seen in the magnetic pulsations is however not seen in V_D, instead , the pulsations steadily grew in amplitude till about 1830 IST, i.e. in consonance with the background V_D (see dashed curve of Fig.4.11). The peak-to-peak amplitude of the pulsation-related oscillations in V_z varied in the range 6.2 - 33.1 ms^{-1} which corresponds to 0.25 - 1.3 mV/m in the east-west electric field.

Since the V_D spectrum is not monochromatic but showed periodic fluctuations in two distinct bands of 4-6 min and 7-10 min, the raw data are filtered to ascertain the temporal association of the longer-period variations in V_D with groundlevel magnetic pulsations. For this purpose a unit gain rectangular filter in the period range 6.4 - 10.67 min is applied to the FFT spectra of raw data and reverse FFT is performed. The

filtered time series of the relevant physical parameters shown in Fig.4.12 illustrate the concurrence of the pulsations in H-component at Trivandrum and Alibag with those in V_D at Kodaikanal. To provide an overview of the relationship between the geomagnetic and ionospheric pulsations the raw data are also subjected to spectral analysis. Figs.4.13 and 4.14 show the FFT spectra of the H-component at Trivandrum and Alibag and V_D at Kodaikanal for the interval 1629-1837 IST and for the sub-intervals 1629-1733 IST and 1734-1837 IST respectively. The spectral analysis is restricted to these specific time slots because FFT needs 2^n points ($\Delta t = 1$ min, n=64/128, T=64/128 min). The frequency spectra of Figs. 4.13 and 4.14 clearly show the presence of significant power in the period band 7-10 min in all the parameters and the growth of the amplitude of the pulsations in V_D with a period of $\sim$ 8 min between the intervals 1629-1733 IST and 1734-1837 IST. During the interval 1734-1837 IST the phase difference between the H-component at Trivandrum (Alibag) and V_D at Kodaikanal is 137 ° (159°) at the dominant period of 8 min. The FFT spectra of V_D also indicate the presence of low-amplitude fluctuations in the band 4-6 min as evident in the time variation of V_D shown in Fig. 4.11.

The results of the present case study demonstrate a close association between the Doppler velocity of F-region reflections at normal incidence and geomagnetic pulsations of Psc5 type near the dip equator in the local dusk period. Since the magnetic pulsations at groundlevel arise from E-region currents (Hughes,1974), it would be interesting to enquire whether any E-region effects are observed for the pulsation event under discussion. Signatures of pulsation electric fields at E-region altitudes have indeed been reported for this event from measurements of drift velocities of electrojet irregularities with the VHF backscatter radar at Trivandrum (Sudha et al.; abstract of paper presented in National Space Science Symposium ,PRL, Ahmedabad, India, March 1992). The vertical polarization electric field computed from the drift velocities showed fluctuations of 8-10 min periods at the altitudes of 99 km, 104 Km and 109 Km. over the interval 1730-1930 IST on 24 March.

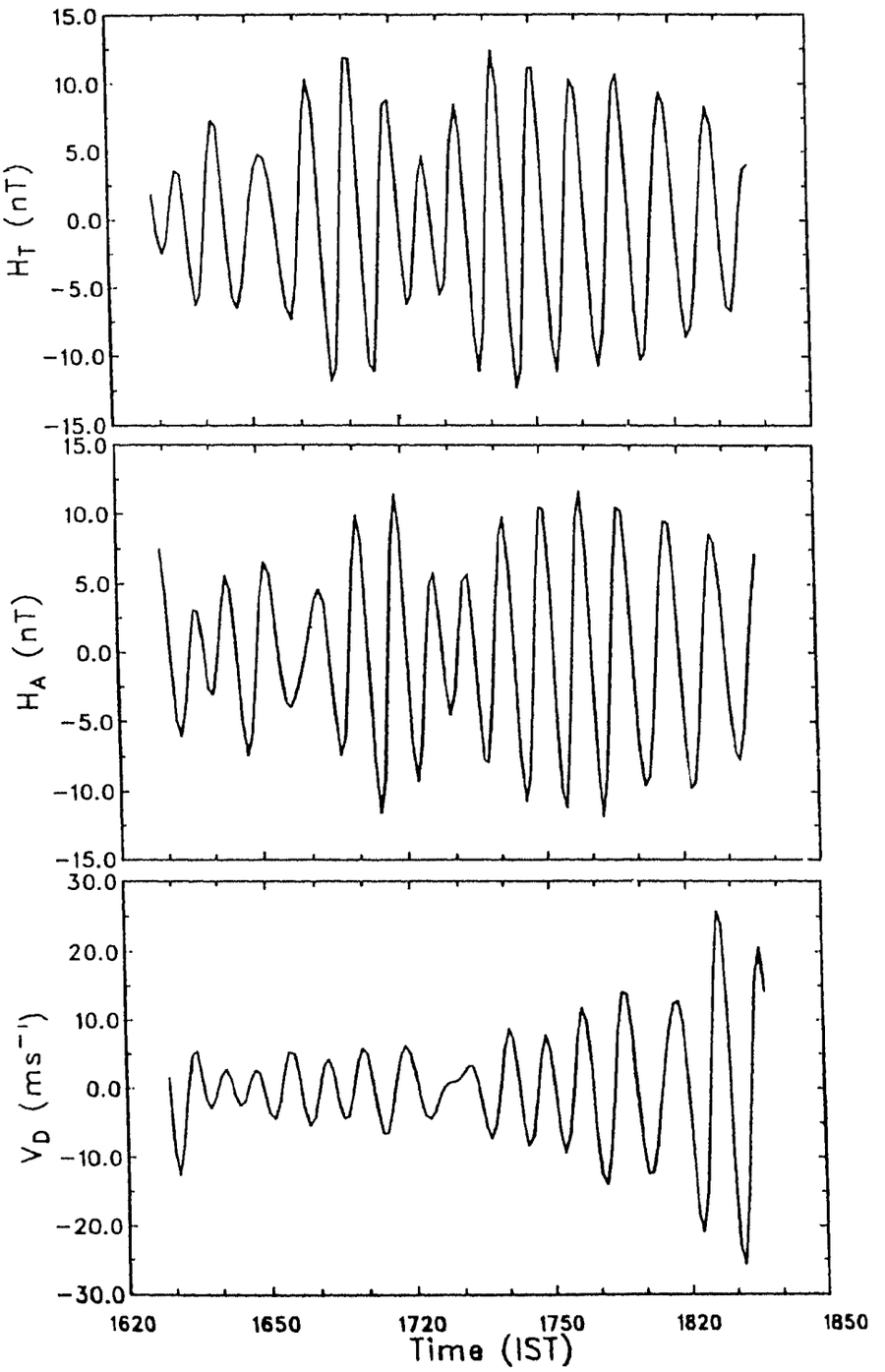

Fig.4.12. Variation in H-component of geomagnetic field at Trivandrum (H_T) and Alibag (H_A) and the Doppler velocity (V_D), filtered in the band $6.4 < T < 10.67$ min.

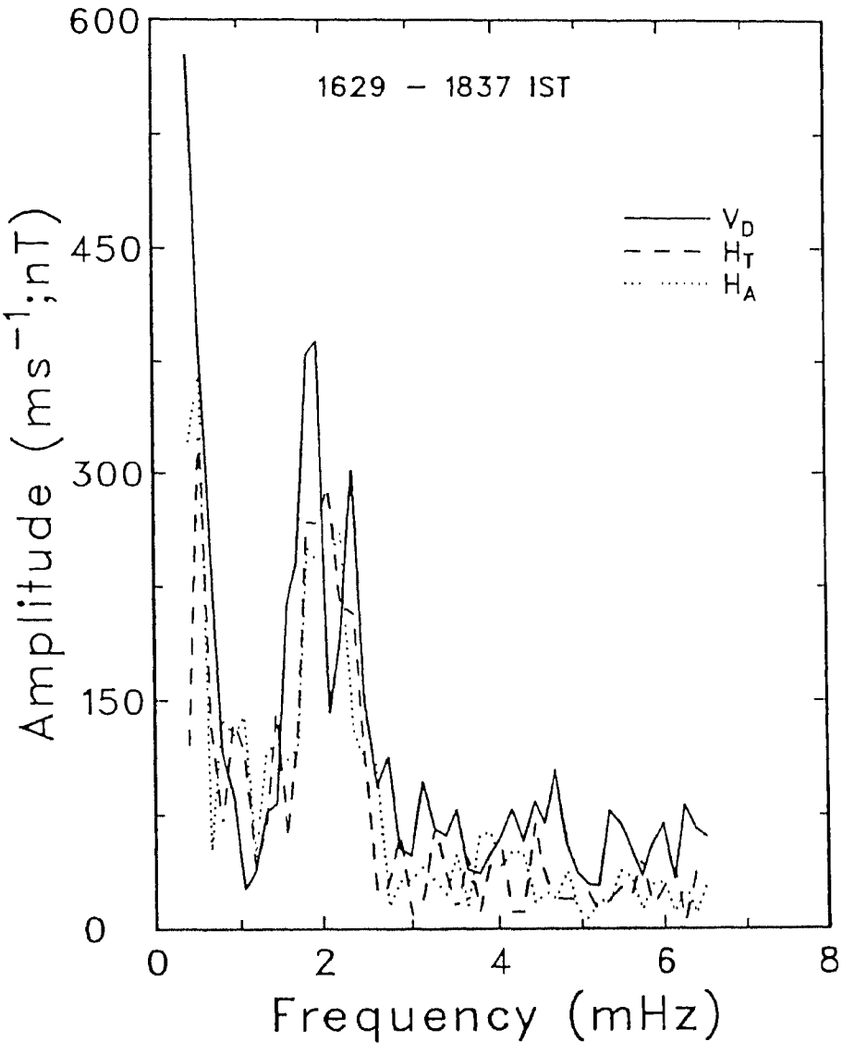

Fig.4.13. Frequency spectra of H-component at Trivandrum and Alibag and Doppler velocity (V_D) at Kodaikanal for the interval 1629-1837 IST.

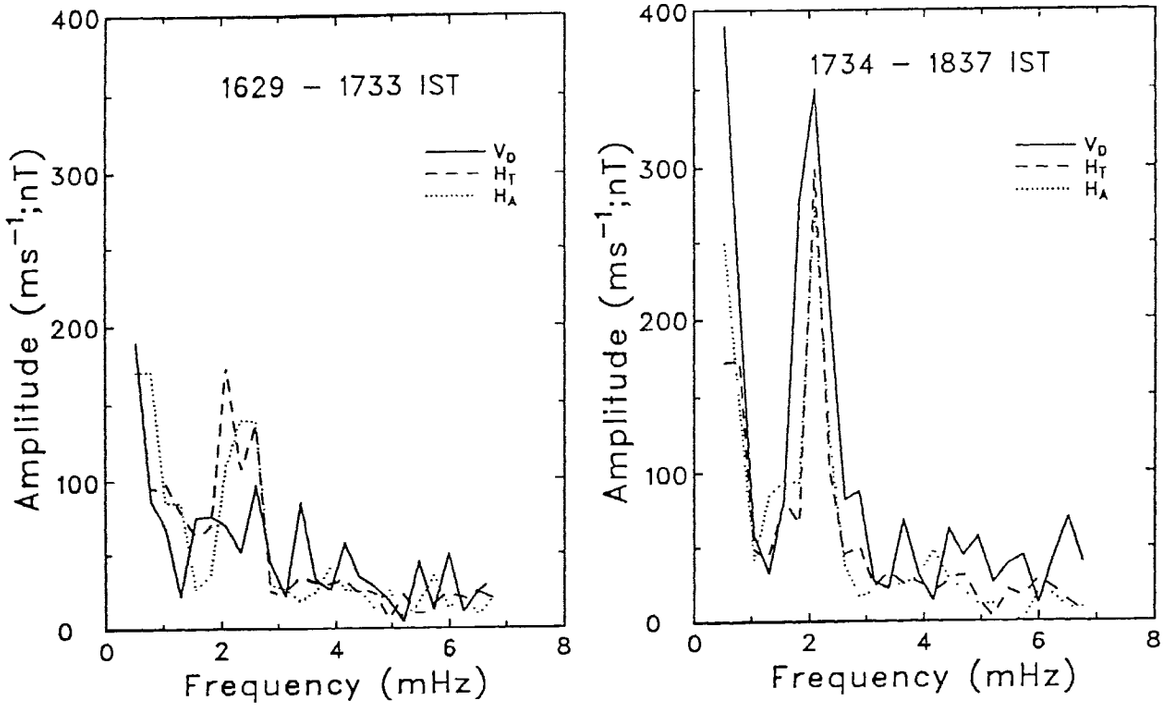

Fig.4.14. Frequency spectra of H-component at Trivardrum and Alibag and Doppler velocity (V_D) at Kodaikanal for the sub-intervals 1629-1733 IST and 1734-1837 IST.

It is necessary to recall here that wave activity in the period range 300-600 sec attributable to gravity waves is a common feature of the temporal pattern of V_D at electrojet locations in the dusk sector (Sastri et al., 1988). The question thus arises as to the uniqueness of the association between the pulsations in V_D at Kodaikanal and H-component at Trivandrum and Alibag . Since the sources of gravity waves are diverse in nature, the large amplitude oscillations in V_D on 24 March could as well be due to intensification of any particular source or reduced attenuation of gravity wave energy in propagating to ionospheric heights from tropospheric sources. To establish the association of V_D oscillations with geomagnetic pulsations, the level of variance (σ^2) of fluctuations in V_D in the band 6.4-10.7 min (see Fig.4.12) is computed for the interval 1629-1837 IST for 24 March and for nineteen other days in the same month when Pc5 type pulsations were absent in the specified time interval in the Indian equatorial region. Because the amplitude of the oscillations in V_D grew with time on 24 March, the variance levels are also calculated for the sub-intervals 1629-1733 IST and 1734-1837 IST. The results presented in Fig.4.15 show that the level of wave activity in V_D is indeed well above the range of variability encountered on days without Pc5 pulsation activity. This is particularly so for the interval 1734-1837 IST (1629-1837 IST) for which the variance (σ^2) on 24 March is 4.28 (3.77) times higher than the average for days without pulsations. The absence of such a feature for the interval 1629-1733 IST (Fig.4.15) supports our point that it is rather difficult to detect the Pc5 pulsation-related variations in V_D for daytime conditions due to the dominance of fluctuations associated with atmospheric sources. It is only when the pulsation electric fields are strong as at night and at dusk due to reduced E-region conductivity that their manifestation in ionospheric parameters in general becomes apparent.

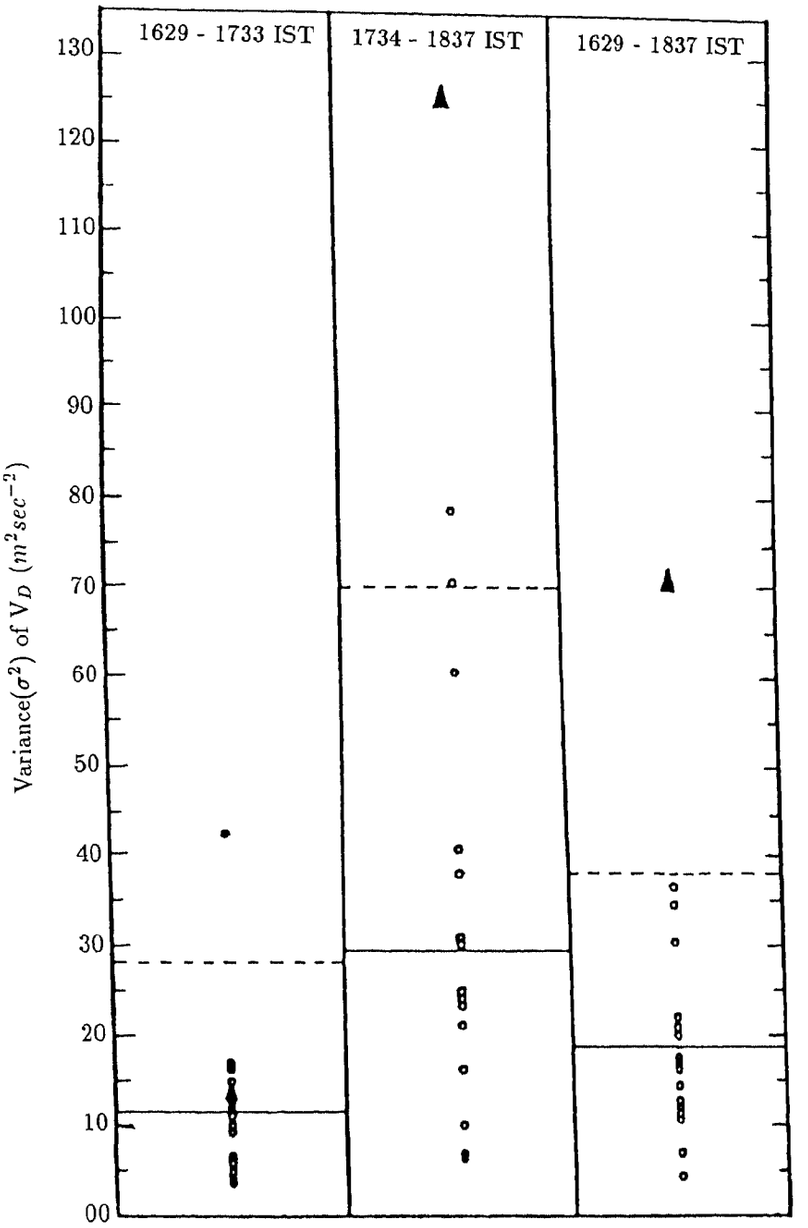

Fig.4.15. Levels of variance (σ^2) of fluctuations in the band 6.4-10.67 min in V_D at Kodaikanal on 24 March 1991 (▲) and 19 other days in March when geomagnetic pulsations were not seen (○). Variance values are shown for the interval 1629-1837 IST and for the sub-intervals 1629-1733 IST and 1734-1837 IST separately. The horizontal solid and dashed lines represent the mean value of variance for the 19 days without pulsations and the level corresponding to twice the standard deviation above the mean respectively.

CHAPTER 5

SUBSTORM RELATED TRANSIENT COMPOSITE ELECTRIC FIELD DISTURBANCES IN THE EQUATORIAL IONOSPHERE

5.1. INTRODUCTION.

It is well known that the daytime equatorial F-region ionization moves upward due to the EXB drift arising from the eastward electric field induced by the E-region dynamo. This electric field is reversed at night causing also a reversal in the ionization drift velocity (V_z) to downward. Perturbations in electric fields and currents are known to occur in the sub-auroral ionosphere during geomagnetic substorms/storms (e.g., Fejer, 1986; Reddy, 1989; Ganguly et al., 1987; Senior and Blanc, 1987; Sastri,1988a; Mazaudier and Venkateswaran, 1990; Reddy et al., 1990 a, b; Fejer et al., 1990 a,b). In the dip equatorial region the transient perturbations (typical duration $\sim$ 2 hr) in the electric fields are caused by the penetration of magnetospheric/high latitude electric fields to low latitudes at times of sudden transitions in north-south component of interplanetary magnetic field (IMF B_z) and attendant changes in polar cap potential drop (ϕ_{pc}), auroral substorm activity and asymmetric ring current (e.g., Sastri,1988b; Fejer, 1991; Reddy and Nishida, 1992; Batista et al., 1991; Somayajulu et al., 1991). The polarity of the zonal electric field disturbances associated with swift northward B_z turnings is westward (eastward) during day (night) i.e., in phase opposition to the S_q-field pattern, and these tend to occur during the recovery phase of auroral substorms triggered by the rapid northward turning of B_z. Transient disturbances in-phase with the S_q-field pattern (eastward by day and westward by night) are also sometime observed in association with sudden southward swings in IMF B_z. The amplitude and frequency of occurrence of the electric field disturbances are strongly dependent on local time in that, while those associated with northward IMF turnings and substorm recovery phase onsets manifest quite frequently and at all times with maximum amplitudes in the midnight-dawn sector. Those associated with southward IMF B_z turnings manifest only occasionally with a preference for the midnight-noon sector with largest amplitudes just before sunrise (see Fejer, 1986 and references therein). The response of

the equatorial zonal electric field to changes in IMF B_z and substorm activity is thus quite asymmetric.

Recent theoretical studies of the electrodynamical coupling between high latitude and low latitude ionospheres have been fairly successful in explaining the basic characteristics of penetration electric fields such as the diurnal patterns of their amplitude and polarity and latitudinal variation (e.g., Senior and Blanc, 1984; Spiro et al., 1988; Fejer et al., 1990b). They correctly predict, for example, the diurnal pattern of the amplitude and polarity of the penetration electric fields associated with decrease as well as increase in polar cap potential, in particular, the maximum amplitude of zonal electric field perturbations near the dip equator in the midnight-dawn sector associated with decrease in polar cap potential. The predicted latitudinal variation of the penetration electric fields is also in reasonable agreement with observations (Fejer et al., 1990a, b). There are, nevertheless, some areas of substantial discrepancy between theory and observations (see for e.g., Reddy et al., 1990a, b) as well as several ill-understood features of the morphology of penetration electric fields. The models cannot explain, for example, the highly asymmetric response of the equatorial zonal electric field to sudden changes in polar cap potential, i.e., higher sensitivity to decrease in polar cap potential than to increase mentioned earlier. The model results of Spiro et al.(1988) and Fejer et al. (1990b) show that following a sharp increase in the polar cap potential, the zonal electric field experiences an eastward (westward) perturbation by day (at night) at all latitudes with largest amplitudes before dawn at 0400 MLT (= UT - 5hrs). But the penetration electric field decays very fast with a time constant of $\sim$ 15-20 min. The infrequent observation of penetration electric fields near the dip equator due to increase in magnetospheric convection (even in the predawn sector) is generally attributed to inadequate temporal resolution of the experimental data. The SUNDIAL-86 campaign results from the Jicamarca (dip 2°N) radar data (basic time resolution 1 min) do not, however, supports this view. (Fejer et al., 1990b). The model cannot also fully account for the persistence (typical duration $\sim$ 2hr) of the zonal electric field perturbations associated with decreases in magnetospheric convection (Fejer et al., 1990b).

Another aspect of transient electric fields at equatorial latitudes that has not received due attention so far is the observation that they tend to appear either with an increase in high latitude convection around the onset of a substorm associated with southward turning of IMF B_z or with a decrease in convection during its recovery phase associated with northward turning of IMF B_z *but not both* (Fejer et al., 1979b). This mutually exclusive nature of substorm phase-related electric field perturbations is rather disconcerting because, typically in any substorm increase in convection around its onset will be followed by a decrease in recovery phase and the effects of both are to prevail, at least in principle. In fact, the calculations of Spiro et al., (1988) and Fejer et al, (1990b) simulate the effects of sharp increase in polar cap potential, θ followed by a sharp decrease as in a substorm (the abrupt changes assumed in the models are, of course, idealised version of the natural situation). Explicit observational evidence for the occurrence of the composite effect at equatorial latitudes due to an increase and a subsequent decrease in convection in a single substorm event has not been reported so far. In this chapter is presented the unambiguous evidence for the occurrence of such a pattern of transient composite electric fields in the midnight-dawn sector near the dip equator during a substorm, based on equatorial ionosonde data and high latitude magnetograms.

5.2. DETERMINATION OF F-REGION VERTICAL DRIFT (V_z).

Perturbations in electric fields and currents in the sub-auroral ionosphere associated with changes in magnetospheric convection can be studied through their effects on F-region plasma drift patterns and ground level geomagnetic field variations. An eastward (westward) electric field near the dip equator that causes F-region plasma to move upward (downward) through EXB drift can effectively be detected by incoherent scatter radar measurements of F-region vertical plasma drifts (e.g., Woodman, 1970). In the absence of incoherent scatter radar facility an alternative and indirect approach to derive information on electric fields would be the use of ground-based ionogram data, in particular those of h'F, the minimum virtual height of bottomside F-layer. At nighttime the time derivative of h'F $[\frac{d(h'F)}{dt}]$ has been shown to accurately represent the F-region vertical plasma drift

and hence of the east-west electric field that causes it (e.g., Bittencourt and Abdu, 1981, Sastri, 1984, Batista et al., 1986). This method of estimating vertical plasma drift near the dip equator provides reliable and valuable information provided the F-layer is above a threshold height of 300 km (Bittencourt and Abdu, 1981). Bittencourt and Abdu (1981) demonstrated from theoretical considerations that for heights less than 300 km, the time rate of change of h'F deviates significantly from the vertical EXB drift velocity due to the increasing dominance of the recombination process (βN) at the lower heights. This, however, is not a major limitation if the primary requirement is not absolute values of the vertical plasma drift but the changes in it. Also due to the ionization below the reflection height, h'F tends to be higher than the true height of bottomside of F-region by 15-20 km depending on the time of the night, but $\frac{d(h'F)}{dt}$ which is proportional to the vertical plasma drift induced by the east-west electric field, is unlikely to be affected by the underlying ionization. Keeping these limitations in mind h'F data have been used here for studying the perturbations in equatorial ionosphere which occurred in the wake of isolated substorm activity.

5.3. EVENT OF 29-30 AUGUST 1957.

Careful study of h'F data scaled from 5-min interval ionograms recorded at Kodaikanal (10°14'N, 77°29'E, geomag. lat. 0.6°N) in the Indian equatorial belt provided clear-cut evidence for the occurrence of a transient electric field perturbation of composite nature during one specific substorm. This electric field disturbance occurred on the night of 29-30 August 1957 in the midnight- dawn period. In Fig. 5.1 (top panel) is shown the time variation of h'F at Kodaikanal based on 5 min interval ionograms on the night of 29-30 August 1957 together with the monthly median pattern (30-min values) superposed for reference. The middle and lower panels of Fig. 5.1 show the time histories of the auroral electrojet (AE) index and the equatorial D_{st} index during the night.

It is well known from the extensive measurements of the F-region plasma vertical drift at Jicamarca (dip 2°N) that the F-region plasma drifts upward during day due to EXB

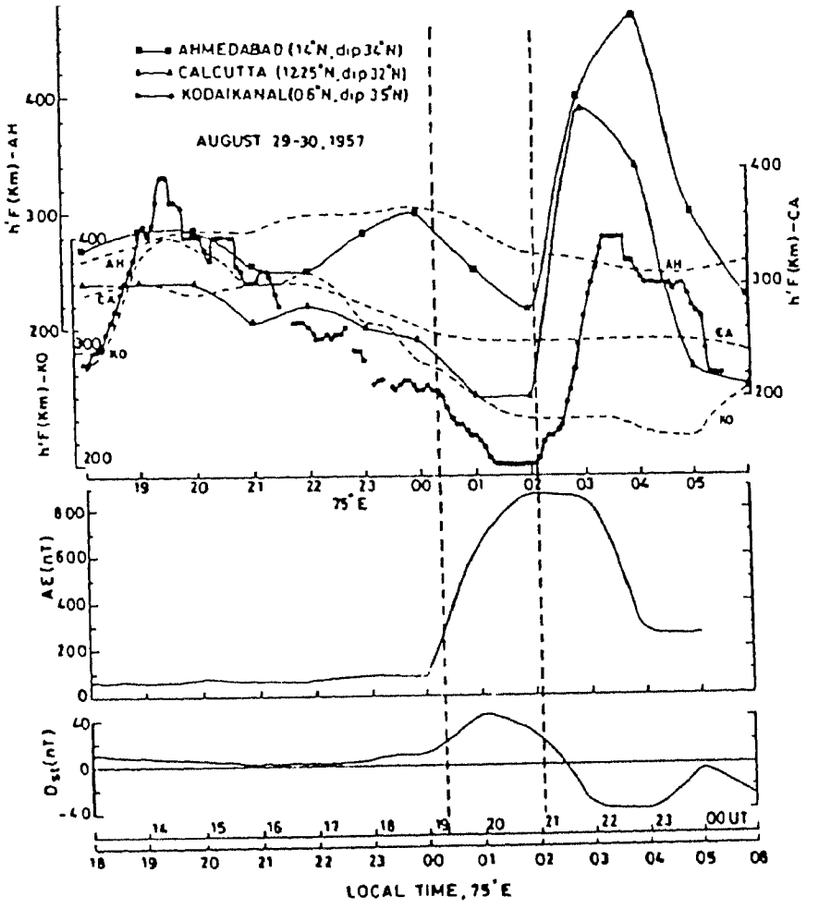

Fig 5.1. In the top panel are shown the temporal variation of the minimum virtual height (h'F) of F-region at three stations, namely Kodaikanal (KO), Calcutta (CA) and Ahmedabad (AH), in the Indian equatorial region on the night of 29-30 August 1957. In the middle and bottom panel are shown respectively, the time histories of the auroral electrojet (AE) index and the equatorial Dst index.

drift arising from the eastward electric field generated by the global E-region dynamo. The electric field is westward at night causing a downward plasma drift. Before its reversal from daytime upwards to nighttime downward the F-region vertical drift undergoes a rapid enhancement in the post-sunset hours. The post-sunset enhancement, which manifests prominently during high sunspot years, is widely considered to be due to F-region dynamo electric fields. This behavior of equatorial F-region is briefly discussed earlier in section 1.4.3. In Fig. 5.2 is shown the time variation of the vertical drift $[\frac{d(h'F)}{dt}]$ for the night of 29-30 August 1957 along with the median pattern of $\frac{d(h'F)}{dt}$ for that month. Though the basic time resolution available is 5 min for the event under examination, $\frac{d(h'F)}{dt}$ is derived from 30 min interval h'F data to facilitate comparison with the median behavior. The monthly median pattern of h'F at Kodaikanal and in particular, that of its time derivative reflect the typical behavior of F-region vertical drift at sunspot maximum, namely, an enhancement in the upward drift during post-sunset hours and downward drift through the remainder of the night until sunrise, as can be seen from Fig. 5.2.

On the night of 29-30 August 1957, h'F at Kodaikanal underwent the common post-sunset enhancement (Fig. 5.1) although the absolute values of h'F as well as the time derivatives of h'F before and at the peak (at 1930 LT) were slightly higher than the monthly median values. This indicates the occurrence of higher values of upward drift as well as longer duration of its postsunset enhancement (Fig. 5.2). After reaching the maximum, h'F rapidly decreased and went through sharp changes until about 2200 LT. Fig. 5.2 also depicts the rapid changes in vertical plasma drift after its reversal to downward with the strong vertical downward plasma drift over the median values, following the post-sunset enhancement. Absolute values of h'F (Fig. 5.1) were also lower than the median values during this period. Between 2200 LT and midnight h'F closely followed the median pattern though absolute values were lower than the median values. The time derivative of h'F displayed in Fig. 5.2 indeed shows the close agreement of the vertical drift with the median pattern both in amplitude and polarity. The deviations in the behaviour of h'F from the median pattern noticed in the pre-midnight period on 29-30 August are not surprising and are rather to be expected, because the F-region vertical drift is well known

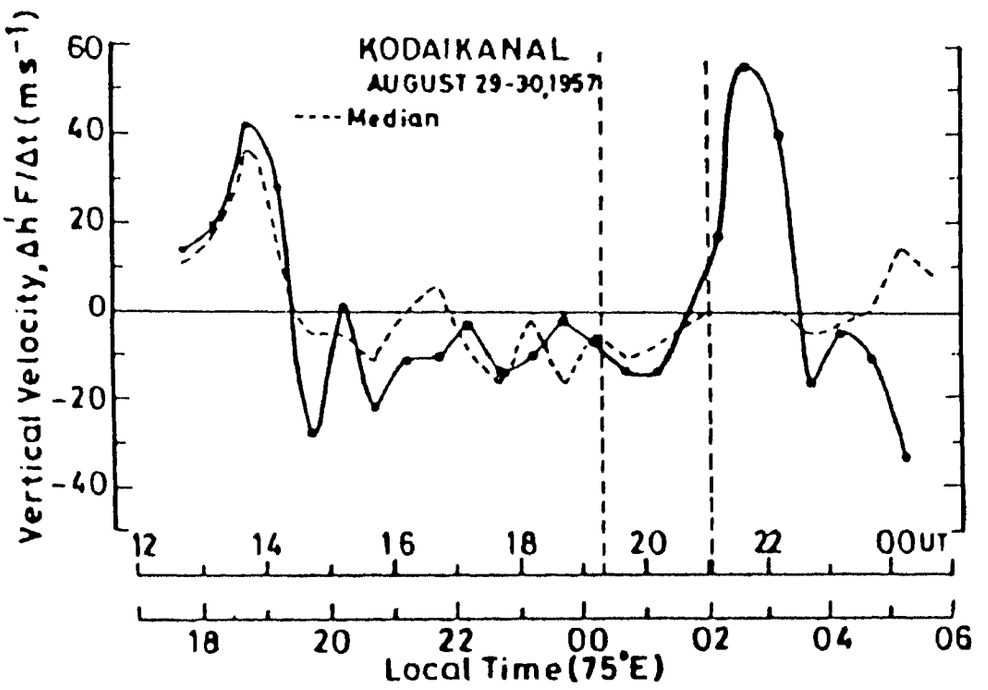

Fig 5.2. Vertical plasma drift velocities derived from the Kodaikanal ionogram data (30-min interval) on the night of 29-30 August 1957. the monthly median pattern is also shown for reference. The vertical dashed line indicate the time of the transient anomalous decrease and subsequent increase in h'F noticed in 5-min interval h'F data (Fig.5.1) and the corresponding disturbance in the verticl drift velocity is indicated by the heavy line.

to exhibit considerable day-to-day variability even on quiet days especially in the postsunset period (see Fejer, 1981, and Chapter IV of this thesis). The deviations are unlikely to be of external influences such as those associated with high-latitude and magnetospheric phenomena driven ultimately by the solar wind, since they occurred under very quiet geomagnetic conditions as can be seen from the temporal behaviour of AE and D_{st} indices presented in Fig. 5.1. The values of the 3-hour K_p index, 2° and 1^{+} for the local premidnight interval and in the range 1 to 2^{+} for the whole 12 hour period also indicate the prevelance of quiet geomagnetic activity conditions on the night of 29-30 August 1957.

In contrast to the above mentioned pre-midnight situation, a sudden reduction in h'F is evident just after midnight at 0020 LT (1920 UT, UT=LT-5hrs). The decrease in h'F from 265 km at 0020 LT to as low as 200 km by 0120 LT (2020 UT) i.e., a decrease of 65 km in 60 min corresponds to a downward drift velocity of 18 ms^{-1}. $\frac{d(h'F)}{dt}$ evaluated from 30 min interval data (Fig. 5.2) showed a downward drift velocity of 14ms^{-1} for about an hour, while the median pattern showed smaller down ward drift of 11 ms^{-1}. It is to be highlighted here that the values of the downward plasma drift derived from the time derivative of h'F constitute under estimates because, for altitudes below 300 km the height increase due to chemical loss counteracts the height decrease caused by the westward electric field. This physical situation of increase of height due to layer decay contaminating the downward plasma drifts caused by the westward electric field at times when h'F $\leq$ 300 km was predicted by Bittencourt and Abdu (1981). This effect is also demonstrated by Batista et al (1986) by comparing the direct measurements of F-region vertical drift with the incoherent scatter radar with those estimated from ionogram data. It is apparent in the present case that the downward drifts of 14-18ms^{-1} prevailed when the h'F was in the range 200-265 km. Otherwise, in the absence of increase of height due to chemical loss the downward drifts would have assumed much higher values. Thus the prevalence of significant downward drifts at times of h'F $\leq$ 300 km indicates the presence of intense westward electric fields after midnight on the night of 29-30 August 1957. This is particularly so as downward plasma diffusion due to the gradient of plasma density and the gravitational acceleration is very ineffective near the geomagnetic equator.

Following the rapid decrease just after midnight, the F-region height at Kodaikanal experienced another more conspicuous perturbation in the form of a rapid and substantial increase in h'F from 200 km at 0205 LT (2105 UT) to 400 km at 0320 LT (2220 UT). This sudden increase in h'F as can be seen from Fig. 5.1, is about 200 km in 75 min which corresponds to an upward drift of about $45 ms^{-1}$. The vertical velocities estimated from the time derivative of h'F indeed show the presence of significant upward drifts for about 90 min starting from 0205 LT, in sharp contrast to the median pattern as may be seen from Fig 5.2. The estimates of the upward vertical drift represent the correct values except for the brief interval 0205-0250 LT, when h'F was below 300 km, when they get over estimated due to the contribution of height increase induced by a chemical loss as mentioned earlier. The entire sequence of a rapid decrease followed by a prominent increase in h'F manifested over a time span of just about 3 hours which, incidentally, is the typical duration of a magnetospheric substorm. The estimates of vertical drift are corrected for the upward drift due to chemical loss, V_β given by equation 4.1. The loss coefficient β is determined from the expression 4.3, while the required concentrations of neutral species are determined from the MSIS-86 thermospheric model for the relevant geophysical conditions. However, since N_e is proportional to the square of the plasma frequency (f_o), equation 4.2 becomes

$$L = \frac{f_o}{2}\frac{\Delta f_o}{\Delta h'} \tag{5.1}$$

L is then determined from the above expression, while the required values of f_o and h' are scaled from the ionograms. The use of h' from ionograms instead of the real height in the expression 5.1 will introduce only a negligible effect in the final value of L, since the underlying ionization in the later part of the night is very small. Moreover, for small changes in f_o, the difference between h and h' remain nearly the same i.e., $\Delta h' \approx \Delta h$. The vertical drifts are then corrected for the influence of chemical loss using the expression.

$$V = \frac{d(h'F)}{dt} - V_\beta \tag{5.2}$$

The corrected values of V showed that the maximum amplitude of the westward as well as eastward electric field perturbation is $\approx$ 2mV m^{-1}. These observations constitute clear-cut evidence for the occurrence of a prominent transient disturbance in the F-region vertical plasma drift and hence in the east-west electric field at Kodaikanal in the post-midnight period on the night of 29- 30 August 1957.

The rapidity of the evidenced changes in the vertical drift in the post-midnight period strongly suggest that the electric field disturbance is of external origin rather than due to perturbations in the wind dynamo process which by their very nature are to be relatively slower in development. Also it is well established that the equatorial zonal electric field responds very sensitively to high latitude processes during enhanced geomagnetic activity conditions, particularly in the midnight-dawn period (Fig. 1.17). Examination of hourly values of auroral electrojet (AE) index, infact, showed the prevalence of an isolated substorm of moderate strength on the night of 29-30 August 1957. The time histories of AE index indicated the beginning of the substorm at 0000 LT (1900 UT) which is in excellent temporal coincidence with the evidenced transient disturbance in the equatorial F-region height in the post-midnight hours. This feature is clearly seen from Fig. 5.1 in which the vertical dashed line at 1920 UT (0020 LT) indicates the near-simultaneous onset time of the substorm and the beginning of the perturbation in h'F. The substorm which lasted until 0400 LT (2300 UT) is characterized by a slower development (1900-2100 LT) and a faster recovery. It is quite interesting to see that the rapid decrease in h'F just after midnight, indicative of a significant prominent westward perturbation in the zonal electric field, occurred during the development phase of the substorm and the subsequent abrupt and conspicuous increase in h'F during the substorm recovery phase. Further the magnetogram data of several high latitude stations are used to define in a much better way the observed temporal relationship between the composite electric field disturbance to the phases of the substorm. Figure 5.3 shows the horizontal component of the earth's magnetic field at three high latitude stations, namely Dixon Island (63°N, 81°E), Tixie Bay (71.6°N, 129°E) and College (64°N, 212°E) on a common scale for the interval 1800-0000 UT. The vertical dashed line in Fig. 5.3 depicts the times of onset of the conspicuous decrease and

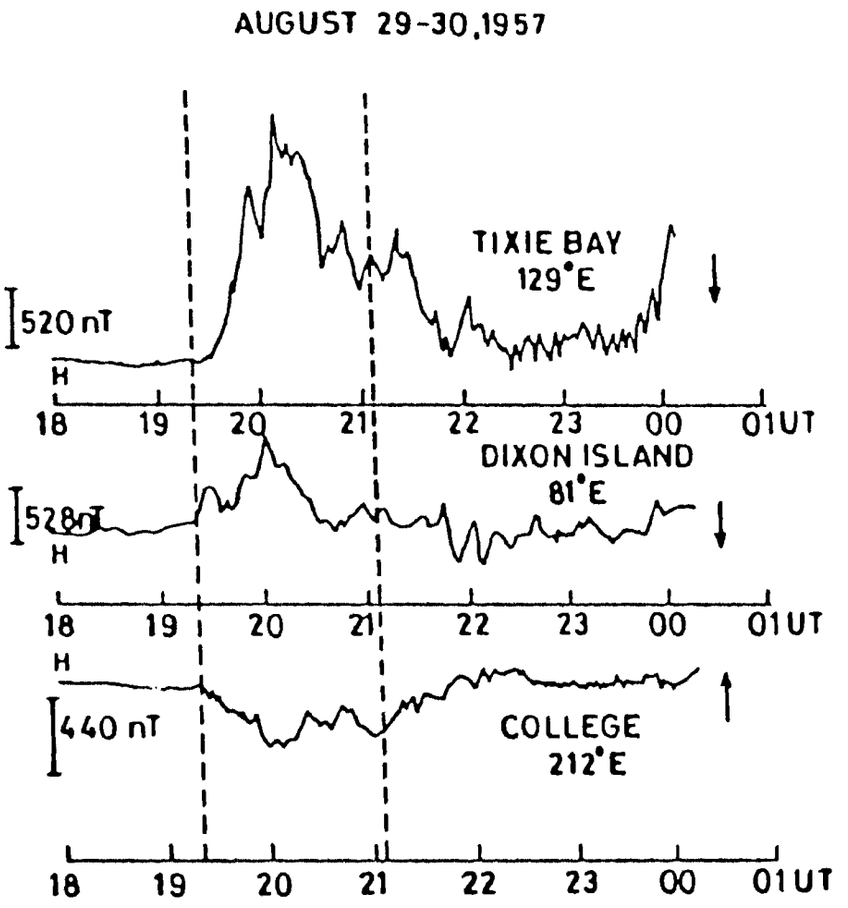

Fig 5.3. Common scale magnetograms (H-comp) of three high - latitude stations namely College, Dixon island and Tixie Bay during 1800-0000 UT on 29-30 August 1957. The vertical dashed lines mark the time of onset of the conspicuous decrease and subsequent increase in h'F at the three equatorial stations shown in Fig.5.1.

subsequent increase in h'F evidenced at Kodaikanal (Fig. 5.1 and 5.2). The magnetogram data of high-latitude stations widely separated in longitude, showed the substorm signature (bay disturbance) at the time of the transient perturbation in the F-region height at Kodaikanal. The bay disturbance was also apparent at Thule (67°N, 291°E) and Cape Chelyuskin (77.7°N, 104° E) though not shown in Figure 5.3. It is quite clear from Fig. 5.3 that the beginning of the rapid decrease in h'F (westward electric field) occurred around the onset of the substorm and the subsequent conspicuous increase in h'F (eastward electric field) during the substorm recovery phase. This close temporal relationship establishes the substorm origin of the composite disturbance in equatorial zonal electric field as evidenced in F-region height at Kodaikanal.

The theoretical modelling results (e.g,. Senior and Blanc, 1984; Spiro et al., 1988; Fejer et al., 1990b) which are discussed briefly in the section 1.7, show that in the midnight-to-morning sector, transient westward electric fields prevail in association with an increase in magnetospheric convection (increase in polar cap potential) and long lasting eastward electric fields at the time of a decrease in convection (decrease in polar cap potential). Therefore, a composite disturbance with westward electric fields around the beginning of a substorm and eastward electric fields in the recovery phase can be expected. The observed transient composite electric field disturbance, whose polarity structure is in good agreement with the predictions of the global convection models, thus finds a logical interpretation in terms of low latitude penetration of substorm associated perturbations in high latitude electric fields. Since the penetration electric fields are global in nature, one would expect to see the similar effects at other locations in the same longitude sector. In order to verify this feature, the published hourly h'F data of two stations in the Indian equatorial region, namely Calcutta, CA (22°58'N, 88°34'E, geomag. lat. 12.25°N) and Ahmedabad, AH (23°01'N, 72°34'E, geomag. lat. 14°N) are examined. The profiles of hourly values of h'F along with the monthly median values of these two stations are shown in top panel of Fig. 5.1. Sudden decrease in h'F just after local midnight (1900 UT) at both the stations contrary to their respective median pattern is quite evident. At Calcutta the decrease in h'F is by about 65 km in 1 hr corresponding to an apparent downward drift of about 14

ms^{-1} while at Ahmedabad the decrease in h'F is by about 85 km in 2 hr corresponding to an apparent downward drift of about $11.8ms^{-1}$. The decrease was followed by an abrupt and substantial increase beginning at 0200LT (2100 UT) by as much as 250 km in 1 hr with an upward drift of $69.4ms^{-1}$ at Calcutta and 185km in 1 hr with an upward drift at $51.4ms^{-1}$ at Ahmedabad. The downward and upward drift values at the two stations, derived from the time derivative of h'F, are gross underestimates because of the inherent low-time resolution of the data used. The height increase due to chemical loss also contributes to the under estimation of the downward drift velocities because h'F reached as low as 225 to 200 km at the two stations after midnight (Fig.5.1). These features amply demonstrate the presence of a transient disturbance in F-region height at the two stations near simultaneous with the one seen at Kodaikanal and of the same nature. The occurrence of the same type of transient disturbance in F-region height simultaneous at three stations spanning a latitudinal range of about 14° and in excellent coincidence with the onset of an isolated geomagnetic substorm, confirms its interpretation as a clear-cut signature of a substorm-related electric field disturbance. This feature also rules out the possible contribution of substorm-generated neutral wind disturbance, to the observed changes in F-region height, because such effects will normally manifest with a delay of a couple of hours, depending on the speed of the wind disturbance, from the start of the auroral substorm.

5.4. EVENT OF 24-25 MARCH 1971.

Transient electric field perturbation which occurred on the night of 29-30 August 1957 indicates that the westward and eastward perturbation in the night time equatorial electric fields during substorm development and recovery phases respectively can occur in a single substorm event and need not be exclusive as indicated by earlier studies (Fejer, 1979b). As a support to this inference, another event of composite electric field disturbance that manifested in the wake of an auroral substorm event is found from the earlier published work. The event is evidenced in the F-region vertical drift measurements made at Jicamarca (12°S, 76.9°W, dip 2°N) on the night of 24-25 March 1971 and figures in the review

of Fejer (1986). The Jicamarca vertical drift data (from Fig. 9 of Fejer, 1986) coupled with those of the auroral electrojet (hourly values of AU/AL) are reproduced in Fig. 5.4. Fig. 5.4 depicts the variation in the F-region vertical drift over a 24 hr period starting from 1300 UT (0800hr, 75°W) of 24 March 1971 along with the quiet day pattern superposed for reference. On the night of 24-25 March 1991, the upward vertical drift at Jicamarca exhibited the common postsunset enhancement and reversed direction thereafter. Though there is a large gap in data for about 4 hrs from about 1900 LT, downward vertical drift around midnight is quite evident. Beginning at about 0100 LT the downward drift experienced a rapid increase and recovered to quiet day values by about 0300 LT (the break in data forbids assessment of the complete temporal structure of the perturbation). This was immediately followed by an anomalously large upward drift with a maximum (> 20 ms^{-1}) around 0400 LT. The pronounced downward and upward perturbation in vertical drift bears a close temporal relationship to southward and northward turning B_z respectively as can be seen from the top panel of Fig. 5.4. This event, in fact, was discussed by Fejer (1986) in the context of the occurrence of B_z related disturbance in the night time vertical drift near the dip equator. The time history of the auroral electrojet indices (AU/AL) clearly shows that an isolated substorm prevailed for about 4 hours starting around 0600 UT (in the interval 0100-0500 LT, 75°W). Further the occurrence of downward drift perturbation during the development phase of the substorm and the subsequent upward drift perturbation in the substorm recovery phase are quite evident. This is not unexpected because B_z is well known to bear a significant correlation to substorm activity (e.g., Arnoldy, 1971, Foster et al 1971). But the composite nature of the disturbance in vertical drift and the relationship of its polarity structure to substorm phase were not studied and emphasized by Fejer (1986). Disturbances in F-region height (h'F) of the type reported here are also found very recently to occur near-simultaneously at middle and low latitude stations (in Japanese sector) during some substorms, and are interpreted as signatures of substorm-related electric fields after detailed analysis of data and careful assessment of the role of other competing processes such as the height changes due to substorm-generated winds and waves (Reddy and Nishida, 1992).

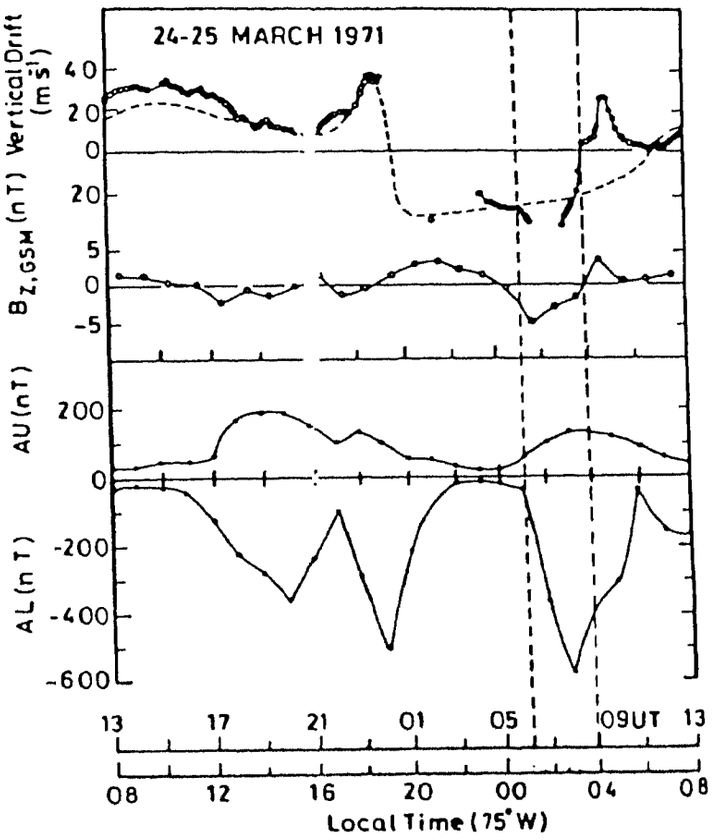

Fig 5.4. The variation of F-region vertical drift at Jicamarca (Dip 2°N) and IMF Bz over a 24-hr period in March 1971 . The dashed curve represents the quite time vertical drift pattern. The bottom panel shows the time histories of the auroral electrojet indices (AU/AL) for the corresponding period. The middle panel shows the IMF Bz in GSM coordinates. The vertical dashed line mark the beginning of the rapind increase in downward drift and the subsequent swing of the vertical drift to upward direction (After Fejer, 1986).

5.5. DISCUSSION.

It is clear from the present case study that the equatorial zonal electric field perturbations of composite nature associated with substorms are not as uncommon as one is led to infer from the literature available on the subject to date. They are, however, not as common as the eastward perturbations during midnight-dawn sector that occur with substorm recovery phase triggered by northward turning of IMF B_z. Two main reasons are considered for the lack of information and discussion of the substorm-related composite disturbances in the sub-auroral electric fields during nighttime. First one is an obvious selection effect arising from the use of h'F. It is easy to detect increases in h'F that predominantly occur during decay phase of substorms triggered by the northward turning of B_z, because they are usually prominent and more importantly, are anomalous being in phase opposition to the normal diurnal pattern. On the other hand, decrease in h'F that are to occur in the substorm development phase can at best be of only moderate amplitude due to the opposing effect of the height increase induced by chemical loss and occur superposed on the normal diurnal pattern. They are not readily noticeable but can be recognised once noticed as demonstrated in the present study.

The second and more important reason is our current inadequate understanding of the subtle aspects of magnetospheric phenomena and the apparently complex magnetosphere-ionosphere interactions. For example, it is found recently that the westward auroral electrojet current in the midnight-to-morning sector is much stronger, larger in spatial extent and more uniform in longitudinal spread than the eastward electrojet in the evening-to-midnight sector, and that it undergoes intensification over from an increase in ionospheric conductivity due to particle precipitation than from an enhancement of the driving electric field(s) (Kamide and Vickery, 1983). It is known and also shown from the present study that the transient disturbances in F-region vertical drift/height in the postmidnight period are associated with an enhancement in the westward electrojet. A prominent increase in h'F/upward vertical drift delayed with reference to the onset of substorm only will prevail if the westward electrojet intensification is predominantly caused by intense particle precipitation, and the enhancement of the auroral ionospheric electric fields occurs after

the maxima in particle precipitation, conductivity and probably the field aligned currents. Extensive and detailed case studies of simultaneous data of IMF B_z, particle fluxes, high latitude magnetic field variations and h'F/vertical drifts at low/equatorial latitudes are needed to further our knowledge of penetration electric fields that manifest in association with substorms.

CHAPTER 6

SUMMARY OF THE RESULTS AND FURTHER WORK

6.1 SUMMARY OF THE RESULTS

The main aim of the present work is to understand the physical mechanisms responsible for some of the dynamical properties of the equatorial ionosphere. The major ones are the small scale structures in the daytime vertical drifts of ionospheric F-region in the vicinity of the dip equator, variation in the nighttime vertical drifts with season and levels of solar and geomagnetic activity and the perturbations in them in the wake of magnetospheric substorms. The HF phase path sounder (Doppler radar) installed at Kodaikanal (dip 3°N), an equatorial station in the Indian longitude zone is used for these studies, because of the known sensitivity of the phase path of ionospheric reflections at vertical incidence to changes in reflection height caused by the vertical plasma drifts. When aided by other experiments such as ionosondes, VHF backscatter radar, etc., the HF phase path sounder can help understand several of the unanswered questions related to the dynamics of the ionospheric F-region particularly in the dip equatorial region. The results of the present study the details of which are presented in various chapters of this thesis are summarized below.

In *chapters 1 and 2* are given the background for the present work and the design aspects of the phase path sounder respectively.

Chapter 3

Observations of phase path (P) of lower F region reflections (true height of reflection $\sim$ 225 km) during day time at Kodaikanal revealed the regular presence of quasi-sinusoidal fluctuations in the time rate of change of phase path, $\dot{P}$ (or Doppler frequency shift) with periods in the range 30-600 sec and peak-to-peak amplitudes of 6-30 ms^{-1} in $\dot{P}$ (0.1-0.5 Hz in Δf). The ambient state of the electrojet and associated ionospheric conditions were

found to influence the spectral content of the $\dot{P}$ fluctuations in that, while the longer-period segment of the oscillations (T > 300 sec) persist almost all the time, the shorter-period components tend to cease at times of absence of Esq configuration on bottomside ionograms. The spectral content of the fluctuations changes significantly not only from day to day at a given local time but also from hour to hour on a given day.

The absence of a systematic relationship of 30-600 sec fluctuations in $\dot{P}$ with Pc4/Pc5 micropulsations, indicated that hydromagnetic (HM) waves are not the primary source of the Doppler fluctuations. The association of the fluctuations in $\dot{P}$ with acoustic waves is discounted on logical grounds as these fluctuations are commonly seen in the $\dot{P}$ data of Kodaikanal, while those associated with acoustic waves are well known to appear with energetic events such as earthquakes, thunderstorms, ... etc.

The longer-period (300 < T < 600 sec) fluctuations in $\dot{P}$ observed at Kodaikanal are attributed to gravity waves-related perturbations in the zonal electric field of the conjugate E region levels outside the electrojet belt and mapped along the field lines to F-region altitudes over Kodaikanal.

The shorter-period (T < 300 sec) Doppler oscillations seem to appear at all times during the day time with small peak-to-peak amplitudes of 6-18 ms^{-1} in $\dot{P}$ (0.1-0.3 Hz in Δf) and tend to practically disappear quite consistently (particularly variations with T < 180 sec) when Esq is absent on ionograms, i.e., during partial/complete counterelectrojet conditions.

The level of wave activity in $\dot{P}$ in the period range 30-300 sec (quantified in terms of variance computed at $\sim$ 1-hour intervals) bears a significant linear relationship to the ambient strength of the equatorial electrojet estimated from groundbased magnetometer data.

$\dot{P}$ fluctuations in the range 30-120 sec are most sensitive to changes in electrojet strength and dominate, in general, the spectral content of $\dot{P}$ in the range 30-300 sec (variance of 30-120 sec fluctuations constitutes, on the average, 65 percent of the variance of 30-300 sec fluctuations).

Model calculations showed that for vertical soundings on 5.0 MHz at Kodaikanal the electrojet irregularities can produce appreciable changes in the phase path of F region reflections, even though the irregularities are located well below the reflection height. The model estimates of the net change in phase path ΔP ($<2\lambda$) have been found to be in good agreement with the peak-to-peak amplitudes of the 30-300 sec fluctuations noticed in Kodaikanal $\dot{P}$ data.

A high degree of correlation is found between the level of variance of short period fluctuations in $\dot{P}$ of F-region reflections at vertical incidence over Kodaikanal (10°14′N, 77°28′E, dip 3.0°N) and the horizontal phase velocity of equatorial electrojet irregularities determined from the VHF backscatter radar at Trivandrum (8°29′N, 76°56′E, dip 0.6°S) .

On the basis of these experimental and modeling results the short-period fluctuations (30-300 sec) in the Doppler frequency (Δf) of lower F region echoes over Kodaikanal have been interpreted in terms of phase path changes imposed on F region echoes by the refractive index variations associated with the convective motions of electrojet irregularities.

Chapter 4

On the basis of a detailed study the evening- nighttime F-region vertical drift (V_z) pattern derived from phase path observations is shown to be reliable in all seasons for the premidnight period during high solar activity period because h′F remained above 300km in that local time period. The absence of sizeable downward drift in the postmidnight hours (the local time period when h′F remained below 300km) during winter and equinoxes is explained as due to swamping of the ambient downward V_z by upward drift induced by chemical loss. It is suggested that the derived V_z data for individual days in winter and equinoxes can effectively be used if corrected for the effects due to layer decay through the

use of neutral atmospheric models such as MSIS-86 and ionosonde data for the electron density scale length.

The postsunset or prereversal enhancement is found to be the dominant feature of the nighttime pattern of F-region vertical drift at Kodaikanal near the dip equator. The prereversal peak in average V_z is higher in equinoxes and northern winter than in northern summer for both high and moderate solar activity conditions. This seasonal variation is less pronounced than at Jicamarca (76.87°W,11.95°S, dip 2°N) in the American sector. The same seasonal trend is seen for quiet days ($A_p \leq 14$) of both high and moderate solar activity periods.

The monthly averages of prereversal peak in vertical drift obtained by averaging the V_{zp} values of individual days showed that during summer months the average V_{zp} undergoes a significant reduction from the high solar activity epoch (1991-92) to the moderate solar activity epoch (1992-93).

The prereversal peak in F-region vertical drift V_{zp} increases with solar activity. At Kodaikanal, V_{zp} increases in all seasons with the solar flux but seems to saturate for the values of solar flux > 230 units during summer and winter months. The sensitivity of V_{zp} with solar flux is higher at Jicamarca than at Kodaikanal irrespective of season. It is speculated that variations in the thermospheric zonal winds may be responsible for the day-to-day and seasonal variability in V_z noticed at Kodaikanal. Direct information on F-region zonal winds for the Indian sector are needed to verify the tentative interpretation.

V_{zp} at Kodaikanal does not seems to depend on geomagnetic activity (A_p) when the entire data base is considered. Also it does not seem to depend on geomagnetic activity in any of the seasons except during equinoctial months of moderate solar activity conditions. Similar trends are seen even with $a_p(\tau)$ which is considered as a better index of geomagnetic activity over A_p. The effect of magnetic activity on V_{zp} at Kodaikanal is, therefore, different from that at Jicamarca (76.87°W,11.95°S, dip 2°N) where the average V_{zp} was reported to decrease with enhanced geomagnetic activity during equinoxes of high

solar activity and increase in local winter during both high and low solar flux epochs. It is to be noted that the earlier results from the Doppler radar observations at Trivandrum (8°29'N,76°57'E, dip 0.6°S) in Indian sector indicated a decrease of the prereversal velocity enhancement (V_{zp}) as magnetic activity changes from quiet to moderate conditions (A_p about 15-20) and an increase well above the quiet time values for high magnetic activity.

The postsunset enhancement of upward vertical drifts at Kodaikanal exhibits remarkable day-to-day variability which is a maximum in summer months during the epoches of both high and moderate solar flux. *The morphology of the evening F-region vertical drifts in the Indian dip equatorial region is different in its details from that in the American region.*

Experimental evidence is presented to show that on 24 March 1991 (A_p =161) the Doppler velocity of F-region reflections at vertical incidence over Kodaikanal is influenced around sunset by MHD waves, the magnetic effects of which are detected on the ground and tentatively identified as Psc5 micropulsations. The evidenced Doppler velocity oscillations are attributed to fluctuations in vertical plasma drift induced by the zonal component of time-varying electric fields associated with the magnetic pulsations. The peak-to-peak amplitude of the pulsations in zonal electric field is estimated to be in the range 0.25-1.3 mV/m. The case study indicates the potential of evening-nighttime HF phase path data for studies of ionospheric effects of geomagnetic pulsations in the dip equatorial region.

Chapter 5

Perturbations in height of equatorial F-layer (h'F) over Kodaikanal in the midnight-dawn period with a rapid decrease (with h'F reaching as low as 200-225 km) followed by an abrupt and substantial increase during the course of an isolated geomagnetic substorm of moderate strength is presented and discussed. The perturbations in h'F were near simultaneous at a meridional network of stations spanning the geomagnetic latitude range of 0.6° - 14°N. The marked decrease in h'F occurred during the development phase of the substorm and the subsequent anomalous increase during the substorm recovery phase. The

perturbations in F-region height are interpreted as a clear-cut signature of a transient composite disturbance in the equatorial zonal electric field caused by the prompt penetration of high latitude electric fields into the equatorial ionosphere. The polarity pattern of the electric field disturbance (westward fields in the substorm development phase followed by eastward fields in the substorm recovery phase) is in good agreement with the predictions of the currently available models of penetration electric fields in the subauroral ionosphere. The possibility that the occurrence of transient composite disturbance in equatorial zonal electric fields at times of substorm activity may not be very rare is indicated by bringing into light the evidence for the presence of such a disturbance in the direct measurements of F-region vertical drift with the incoherent radar at Jicamarca reported in the literature.

6.2. SCOPE FOR FURTHER WORK

Vertical drifts of F-region near geomagnetic equator provide a great deal of information on equatorial zonal electric fields. It is clear from the present study (*Chapter 3*) that at and around dip equator the daytime vertical drifts of F-region obtained from phase path technique can be contaminated by the short period fluctuations in the period range 30-300 sec with amplitudes comparable to vertical drifts of F-region. Caution is, therefore, to be exercised in estimating the vertical drifts during daytime near dip equator with the phase path technique. The short- period fluctuations are interpreted in terms of the phase path variations imposed on F-region reflections by the refractive index variations associated with convective motions of the electrojet irregularities. Multifrequency measurements of phase path (preferably near simultaneous) are nevertheless needed to establish the interpretation because they enable verification of the dependence of the spectral content of the short-period Doppler fluctuations on the probing frequency (f). As the probing frequency is varied the relative locations of the irregularities and the reflection level vary such that the amplitude of the Doppler fluctuations is a maximum at frequencies corresponding to the plasma frequency of the seat of the irregularities ($\sim$ 3.5 MHz) and decreases as the sounding frequency is raised well beyond 5.0 MHz. Coordinated measurements of phase path of F-region reflections and the phase velocities (V_p) of electrojet irregularities with

the VHF backscatter radar if made extensively will then help establish the relationship of 30-300 sec and in particular 30-120 sec fluctuations with V_p which is shown here with a limited but valid data base.

The morphological features of nighttime equatorial F-region vertical drifts have been brought out by using phase path data obtained at Kodaikanal during high and moderate solar activity periods (see §4.2). Similar kind of studies, however, are needed for low solar activity conditions to have a clear picture of the long-term variations of the F-region vertical drifts in the Indian equatorial region. Observations of the thermospheric zonal winds (for example measurements with the Fabry-Perot interferometric technique or through the spaced receiver method with phase path technique) would help understand the origin of day-to-day seasonal and solar cycle variations of F-region vertical drift. Case studies of the disturbed-time behaviour of F-region vertical drifts would throw light on the magnetosphere - equatorial ionosphere coupling processes.

The large amplitude quasi-periodic variations in Doppler velocity (V_D) of F-region reflections at vertical incidence over Kodaikanal which occurred on 24 March 1991 in association with Psc5 geomagnetic micropulsations are attributed here to fluctuations in the F-region vertical plasma drift caused by the zonal component of time-varying ionospheric electric fields (peak-to-peak amplitude (0.25-1.3 mV/m) associated with the ULF geomagnetic pulsation activity. It is only when the pulsation electric fields are strong as at night and at dusk due to reduced E-region conductivity that the manifestation of pulsation activity in ionospheric parameters seems to become apparent. The present study (see §4.3) also raises the question whether the clear-cut relationship between geomagnetic and ionospheric Doppler velocity oscillations evidenced on 24 March 1991 is because of the ambient disturbed geomagnetic conditions. In other words, whether such unambiguous ionospheric response can be seen with Pc5 pulsations that occur during quiet days and with other types of pulsations (Pc3-4 and Pi2) is to be assessed. This is quite logical because earlier studies showed that near the dip equator, the amplitude of Pc5 pulsations increases with geomagnetic activity, K_p (Jain,1977) and that the zonal electric field fluctuations (T<5

hrs) associated with magnetospheric sources dominate those due to atmospheric sources for $K_p > 3$ (Earle and Kelley,1987). Analysis of the extensive nighttime Doppler data at Kodaikanal is, therefore, needed to seek answer(s) to this important question concerning magnetosphere - equatorial ionosphere coupling.

It is known and also shown in the present thesis (*Chapter* 5) that the transient disturbances in F-region vertical drift/height in the post-midnight period are associated with an enhancement in the westward auroral electrojet. A prominent increase in h'F/upward vertical drift delayed with reference to the onset of substorm (which is what is commonly noticed and widely reported in the literature) only will prevail if the westward electrojet intensification is predominantly caused by intense particle precipitation, and the enhancement of the auroral ionospheric electric fields occurs after the maxima in particle precipitation, conductivity and probably the field-aligned currents. Detailed case studies of simultaneous data of IMF B_z, particle fluxes, high latitude magnetic field variations and h'F/vertical drifts are needed to further our knowledge concerning magnetosphere - ionosphere interactions.

References

Abdu, M.A., J.A. Bittencourt, and I.S. Batista, J. Geophys. Res., **86**, 11443-11446, 1981.

Abdu, M.A., G.O. Walker, B.M. Reddy, J.H.A. Sobral, B.G. Fejer, T. Kikuchi, N.B. Trivedi, and E.P. Szuszczewicz, Ann. Geophys., **8**, 419-430, 1990.

Aksofu, S.I. and S. chapman, J. Geophys. Res., **66**, 1321, 1961.

Akasofu, S.I., Planet. Space. Sci., **12**, 273, 1964.

Aggson, T.L., N.C. Maynard, F.A. Herrero, H.G. Mayr, L.H. Brace and M.C. Liebrecht, J. Geophys, Res., **92**, 311, 1987.

Anandarao, B.G., and R. Raghavarao, J. Geophys. Res., **92**, 254, 1987.

Anderson. D.N., J. Atmos. Terr. Phys., **43**, 753, 1981.

Anderson, D.N. and R.G. Roble, J. Atmos. Terr. Phys., **43**, 835, 1981.

Anderson, D.N., M. Mendillo and B. Herniter, Radio Sci., **22**, 292, 1987a.

Anderson, D.N., R.A. Heelis, and J.P. McClure, Ann. Geophys., **5**, 435, 1987b.

Appleton, E.V. and M.A.F. Barnett, Proc. Roy. Soc., A109, 621, 1925.

Appleton, E.V., Nature, **157**, 691, 1946.

Arnoldy, R.L., J. Geophys. Res., **76**, 5189, 1971.

Baker, W.G. and D.F. Martyn, Philos, Trans. R. Soc. London, Ser. A., **246**, 281-294, 1953.

Baker,D.M., and K. Davies, J. Atmos. Terr. Phys., **31**, 1345-1352, 1969.

Balachandran Nair, R., N. Balan, G.J. Bailey, and P.B. Rao, Planet. Space Sci., **40**, 655-662, 1992.

Balachandran Nair, R., B. Jayachandran, P.B Rao and N. Balan. Ind. J. Radio & Space Phys., **22**, 89-93, 1993.

Balan, N., V.N. Nandakumar,, S. Chandrasekhar, K.N. Iyer, P.B. Rao and A. Sridhar, Ind. J. Radio & Space Phys., **8**, 289,1979.

Balan, N., B. Jayachandran, R. Balachandran Nair, S.P. Namboothiri, G.J. Bailey and P.B. Rao, J. Atmos. Terr. Phys., **54**, 1545-1554, 1992.

Balsley, B.B., J. Geophys. Res., **74**, 2333-2347, 1969.

Balsley, B.B. and D.T. Farley, J. geophys. Res., **76**, 8341, 1971.

Balsley, B.B., D.A. Carter, and R.F. Woodman, J. Geophys. Res., **81**, 1296, 1976a.

Balsley, B.B., A.Rey, and R.F. Woodman, J. Geophys. Res., **81**, 1391-1396, 1976b.

Balsley, B.B., J. Atmos. Terr. Phys., **39**, 1087, 1977.

Basu, S., J. Aarons and B.B. Balsley, J. Geophys. Res., **82**, 5262, 1977.

Batista, I.S., M.A. Abdu, and J.A. Bittencourt, J. Geophys. Res., **91**, 12055-12064, 1986.

Batista, I.S., M.A. Abdu and R.A. Medrano, Ann. Geophys., **8**, 357-364, 1990.

Batista, I.S., E.R. DePaula, M.A. Abdu, and N.B. Trivedi, J. Geophys. Res., **96**, 13943, 1991.

Berger, C., M. Ill, and F. Barlier, Ann. Geophys., **6**, 541, 1988a.

Berger, C., F. Barlier and M. Ill, Phys. Scrip., **37**, 421, 1988b.

Bhargava, B.N., N.S. Sastri, B.R. Arora and R. Rajaram, Ann. Geophys., **36**, 231-240, 1980.

Biondi, M.A. and D.P. Sipler, Planet. Space Sci., **33**, 817, 1985.

Biondi, M.A. and J.W. Meriwether, Geophys. Res. Lett., **12**, 267, 1985.

Biondi, M.A. and J.W. Meriwether, B.G. Fejer, S.A. Gonzales and D.C. Hallenback, J. Geophys. Res., **96**, 15917, 1991.

Bittencourt, J.A., and M.A. Abdu, J. Geophys. Res, **86**, 2451-2454, 1981.

Bittencourt, J.A., and Y. Sahai, J. Atmos. Terr. Phys., **40**, 669-676, 1978.

Bittencourt, J.A., and Y. Sahai, J. Atmos. Terr. Phys., **41**, 1233, 1979.

Blanc, M., and A.D. Richmond, J. Geophys. Res., **85**, 1669, 1980.

Blanc, M., J. Geophys. Res., **88**, 235, 1983.

Booker, H.G., J. Atmos. Terr. Phys., **7**, 343, 1955.

Booker, H.G., J. Atmos. Terr. Phys., **41**, 501, 1979.

Bourdillon, A., J. Delloue, and J. Parent, Radio Sci., **24**, 183, 1989.

Breit, G. and M. Tuve, Phys. Rev., **28**, 554, 1926.

Buneman, O., Phys, Rev. Lett., **10**, 285, 1963.

Burnside, R.G., F.A. Herraro, J.W. Meriwether Jr. and J.C.G. Walker, J. Geophys. Res., **86** 5532, 1981.

Butcher, E.C., and K.H. Joyner, Planet. Space Sci., **20**, 613-616, 1972.

Carter, D.A., B.B. Balsley, and W.L. Ecklund, J. Geophys. Res., **81**, 2786, 1976.

Chan, K.L., D.P. Kanellakos, and O.G. Villard. Jr, J.Geophys. Res., **67**, 2066, 1962.

Chan, H.F. and G.O. Walker, J. Atmos. Ter. Phys., **46**, 1103, 1984a.

Chan, H.F. and G.O. Walker, J. Atmos.Terr. Phys., **46**, 1113, 1984b.

Chapman, S., Arch. Meteorol. Geophys. Bioklimatal, Ser. A, **4**, 368, 1951.

Chen, L. and A. Hasegawa, J. geophys, Res, **79**, 1024-1032, 1974.

Chiu, Y.T., J. Atmos. Terr. Phys., **37**, 1563, 1975.

Cohen, R., and Bowles, K.L., J. Geophys. Res., **72**, 885, 1967.

Coley, W.R. and R.A. Heelis, J. Geophys. Res., **94**, 6751, 1989.

Coley, W.R., J.P. McClure, and W.B. Hanson, J. Geophys. Res. **95**, 21285, 1990.

Cowling, T.G., Mon. Not. R. Astron. soc., **93**, 90-98, 1933.

Cowling, T.G. and R. Borger, Nature, **162**, 143, 1948.

Crochet, M., J. Atmos. Terr. Phys., **39**, 1103, 1977.

Cummings, W.D., P.J. Coleman, and G.L. Siscoe, J. Geophys. Res., **76**, 926, 1971.

Davies, K., and D.M., Baker, Radio Sci., **1**, 545, 1966.

Davies, K., and G.K. Hartman, J. Geophys. Res., **81**, 3431, 1976.

Davies, K., and T.B. Jones, J. Atmos. Terr. Phys., **28**, 254-262, 1971.

Davies, K., and T.B. Jones, J. Atmos. Terr. Phys., **35**, 1737-1744, 1973.

Deminov M.G., N.A. Kochenova and S. Yu. Sitnov, Geomag. & Aeron., **28**, 57, 1988.

Desai, J.N., P.D. Bhavasar, R. Raghavarao, and M.S. Narayanan, Space Res., XV, 267, 1975.

Doupnik, J.H., A, Brechkem and P.M. Banks, J. Geophys. Res., **82**, 499, 1977.

Duffus, H.J., and G.M. Boyd, J. Atmos. Terr. Phys., **30**, 481, 1968.

Dungey, J.W., The Structure of the exposure or adventures in velocity space, in Geophysics, The Earth's Environment, edited by C.Dweitt, 537 pp, Gorden and breach, New York, 1963.

Earle, G.D. and M.C. Kelley, J. Geophys. Res., **92**, 213, 1987.

Farley, D.T., J. Geophys. Res., **68**, 6083, 1963.

Farley D.T., J. Atmos. Terr. Phys., **47**, 729, 1985.

Farley, D.T., E. Bonelli, B.G. Fejer, and M.F. Larsen, J. Geophys. Res., **91**, 13723, 1986.

Fejer, B.G., D.T. Farley, B.B. Balsley, and R.F. Woodman, J. Geophys. Res., **80**, 1313, 1975.

Fejer, B.G., D.T. Farley, B.B. Balsley, and R.F. Woodman, J. Geophys. Res., **81**, 4621, 1976.

Fejer, B.G., D.T. Farley, R.F. Woodman and C. Calderon, J. Geophys. Res., **84**, 5792, 1979a.

Fejer., B.G., C.A. Gonzales, D.T. Farley, M.C. Kelley and R.F.Woodman, J. Geophys. Res., **84**, 5797, 1979b.

Fejer, B.G., and M.C. Kelley, Reviews of Geophys. Space Phys. **18**, 401, 1980.

Fejer, B.G., J. Atmos. Terr. Phys., **43**, 377-386, 1981.

Fejer, B.G., M.F. Larsen and D.T. Farley, Geophys. Res. Lett., **10**, 537, 1983.

Fejer, B.G., Equatorial Ionospheric electric fields associated with magnetospheric disturbances, in Solar Wind-Magnetosphere Coupling (Edited by Kamide, Y. and J.A. Slavin), P. 519, Terra, Tokyo, 1986.

Fejer, B.G., E.R. De Paula, I.S. Batista, E. Bonelli, and R.F. Woodman., J. Geophys. Res., **94**, 12049-12054, 1989.

Fejer ,B.G., M.C. Kelley, C. Senior, O. De La Beaujardiere, J.A. Holt, C.A. Tapley, R. Burnside, M.A. Abdu, J.H.A. Sobral, R.F. Woodman, Y. Kamide, and R. Lepping, J.Geophys. Res., **95**, 2367, 1990a.

Fejer, B.G., R.W. Spiro, R.A. Wolf and J.G. Foster, Ann. Geophys., **8**, 441, 1990b.

Fejer, B.G., J. Atmos. Terr. Phys., **53**, 677-693, 1991.

Fejer, B.G., E.R. DePaula, S.A. Gonzales, and R.F. Woodman, J. Geophys. Res., **96**, 13901-13906, 1991.

Findlay, J.W., J. Atmos. Terr. Phys., **1**, 353-366, 1951.

Fooks, G.F., J. Atmos. Terr. Phys., **24**, 937, 1962.

Forbes, J.M., Rev. Geophys. Space Phys., **19**, 469-504, 1981.

Forbes, J.M. and R. S. Lindzen, J. Atmos. Terr. Phys., **38**, 879, 1976a.

Forbes, J.M. and R. S. Lindzen, J. Atmos. Terr. Phys., **38**, 911, 1976b.

Forbes, J.M. and R. S. Lindzen, J. Atmos. Terr. Phys., **38**, 1369, 1976c.

Forbes, J.M. and R. S. Lindzen, J. Atmos. Terr. Phys., **39**, 1369, 1977.

Foster, J.C., D.H. Fairfield, K.W. Ogilvie and T.G. Rosenberg, J. Geophys. Res., **76**, 6971, 1971.

Francis, S.H., J. Atmos. Terr.Phys., **37**, 1011, 1975.

Fukumishi, H., and L.J. Lanzerotti, J. Geophys. Res., **79**, 142-158, 1974.

Ganguly, S., and R.A. Behnke, J. Geophys. Res., **87**, 261-264, 1982.

Ganguly, S., R.A., Behnke and B.A. Enery, J. Geophys. Res., **92**, 1199, 1987.

Georges, T.M., ESSA. Tech. Rep., IER 57-ITSA 54, U.S. Department of Commerce/ ESSA, Boulder, 1967.

Georges, T.M., J. Atmos. Terr. Phys., **30**, 735-746, 1968.

Georges, T.M., Rev. Geophys., **11**, 571-594, 1973.

Glangeaud, F., C. Lathuillere, M. Lambert and Z. Zhao, J. Geophys. Res., **90**, 8319, 1985.

Goel, M.K., S.S. Singh and B. C. N. Rao, J. Geophys. Res., **95**, 6237-6246, 1990.

Gonzales, C.A., M.C. Kelley, B.G. Fejer, J.F. Vickrey, and R.F. Woodman, J. Geophys. Res., **84**, 5803, 1979.

Gonzales, C.A., M.c. Kelley, R.A. Behnke, J.F. Vickrey, R.Wand and J. Holt, J. Geophys. Res.**88**, 9135, 1983.

Gouin, P. and P.N. Mayaud, Ann. Geophys., **23**, 41-47, 1967.

Gul'yel'mi, A.V., Space Science Rev., **16**, 331, 1974.

Gupta, J.C., Ann. Geophys., **110**, 2076-2084, 1973.

Hanuise, C., and M. Crochet, J. Atmos. Terr. Phys., **39**, 1097, 1977.

Haerendel, G. and J.V. Eccles, J. Geophys. Res., **97**, 1181, 1992.

Hargreaves, J.K., The Upper atmosphere and Solar-Terrestrial relations, Van Nortrand Reinhold Co. ltd., England, 1979.

Hedin, A.E., J. Geophys. Res., **92**, 4649, 1987.

Heelis, R.A., D.C.Kendall, R.J. Moffett, D.W. Windle, and H. Rishbeth, Planet. Space Sci., **22**, 743-756, 1974.

Heelis, R.A., Rev. Geophys. Space Phys., **25**, 419, 1987.

Hughes, W.J., Planet. Space Sci., **22**, 1157,1974.

Hutton, R. and J.O. Oyinloye, Annls. Geophys., **26**, 921, 1970.

Ijima, T., and T. Nagata, Planet. Space Sci., **20**, 1095, 1972.

Jacchia, L.G., Special Report, **375**, Smithsonian Astrophys. Obs., Cambridge, Mass.. (USA), 1977.

Jacobson, A.R., R.C. Carols, and E. Blanc, Radio Sci., **23**, 820-830, 1988.

Jacobson, A.R., and R.C. Carols, J. Atmos. Terr. Phys., bf 51, 297-309, 1989.

Jain, A.R., J. Atmos. Terr. Phys., **39**, 843, 1977.

Jain, A.R., and K.G. Srinivasacharya, J. Atmos. Terr. Phys., **37**, 1477, 1975.

Jain, A.R., and R.V. Iyengar, Ind. J. Radio & Space Phys., **7**, 128, 1978.

Jackson, J.E., Proc. IEEE, **57**, 960, 1967.

Jarvis, M., and H. Gough, Planet. Space Sci., **36**, 733, 1988.

Kamide Y, and S. Matsushita, J. Atmos. Terr. Phys., **43**, 411, 1981.

Kamide, Y., and J.F. Vickery, J. Geophys. Res, **88**, 7989, 1983.

Kane, R.P., J. Atmos. Terr. Phys., **35**, 1565-1567, 1973.

Kane, R.P., Space Sci. Rev., **18**, 413-540, 1976.

Kane, R.P., J. Geophys. Res., **83**, 2671, 1978.

Kelley, M.C., B.G. Fejer and C.A. Gonzales, Geophys. Res. Lett., **6**, 301, 1979.

Kelley, M.C., The Earth's Ionosphere, chapter 3, Page 65-110, 1989, Academic Press, San Diego, California, 92101.

Kikuchi, T., and T. Araki, J. Geophys. Res., **90**, 12195-12200, 1985.

Klostermeyer, J., and J. Rottger, Planet. Space Sci., **24**, 1065, 1976.

Knecht, R.W and R.E. McDuffie, Ionospheric Sporadic-E (Edited by E.K. Smith and S. Matsushita), p.215, Pergamon Press (1962).

Krishnamurthy, B.V., C. Raghava Reddy, K.S.V. Subbarao, R. Raghavarao and P. Sharma, J. Geophys. Res., **81**, 705, 1976.

Krishnamurthy, B.V., S.S. Hari and V.V. Somayajulu, J. Geophys. Res., **95**, 4307, 1990.

Lathuillere, C., F. Glangeaud, J.L. Lacoume and Lejeune, J. Geophys. Res., **86**, 7669, 1981.

Lewis. T.J. Can. J. Phys., **45**, 1549, 1967.

Martyn.D.F., Proc. Roy. Sci. (Lond), A 219, 214, 1947.

Martyn, D.F., Nature **162**, 142-143, 1948.

Matsushita, S., J. Geomag. Geoelec., **3**, 44-46, 1951.

Matsushita.S., J. Geomag. Geoelectr. **31**, 287, 1979.

Matsushita.S., and B.B. Balsley, Planet. space. Sci, **8**, 1259, 1972.

Matuura, N., J. Geophys. Res., **79**, 4679, 1974.

Maynard, N.C., T.L. Aggson, F.A. Herrero and M.C. Liebrecht, J. Geophys. Res., **93**, 4021, 1988.

Mazaudier, C., R. Bernard, and S.V. Venkateswaran, J. Geophys. Res., **90**, 2885, 1985.

Mazaudier C. and S.V. Venkateswaran, Ann. Geophys., **8**, 511, 1990.

Menk, F.W., K.D. Cole and J.C. Devlin, Planet. Space Sci., **31**, 569, 1983.

Moffett, R.J., Fund. Cosmic Phys., **4**, 313, 1979.

Meriwether, J.W., J.W. Moody, M.A. Biondi, and R.G. Roble, J. Geophys. Res., bf 91, 5557, 1986.

Mozer, F.S., Rev. Geophy. space. Phys., **11**, 755, 1973.

Nagpal, O.P., A.B. Gupta, and C.S.G.K. Setty, Ann. Geophys., **29**, 293-300, 1973.

Namboothiri., S.P., N. Balan, and P.B. Rao, J. Geophys. Res., **94**, 12055-12060, 1989.

Nishbeth, J.S., M.J. Miller and L.A. Carpenter, J. Geophys. Res., **83**, 2647, 1978.

Nishida A., N. Iwasaki and T. Nagata, Ann. Geophys., **22**, 478, 1966.

Okuzawa. T., and K. Davies, J. Geophys. Res., **86**, 1355, 1981.

Okuzawa, T., T.Shibata, T. Ichniose, K. Takagi, C. Nagasawa, I. Nagano, M. Mambo, M. Tsutsui and T. Ogawa, J. Geomagn. Geoelectr., **38**, 239-266, 1986.

Onwumechilli, C.A., Geomagnetic variations in the equatorial zone, in Physics of Geomagnetic Phenomena, edited by S. Matsushita and W.H. Campell, pp 425-507, Academic, New York, 1967.

Onwumechille, A., K. Kawasaki, and S.I. Akasofu, Planet Space Sci., **21**, 1, 1973.

Orr, D., T. Atmos. Terr. Phys., **35**, 1, 1973.

Patel, V.L., J. Geophys. Res., **83**, 2137, 1978.

Patel, V.L., and P. Lagos, Nature, **313**, 559, 1985.

Paul, A.K., J.W. Wright, and L.S. Fedor, J. Atmos. Terr. Phys., **36**, 193, 1974.

Pfister, W., J. Atmos. Terr. Phys., **33**, 999-1025, 1971.

Pingree, J.E., and B. G. Fejer, J. Geophys. Res., **92**, 4763, 1987.

Poole, A.W.V. and P.R. Sutcliffe, J. Atmos. Terr. Phys., **49**, 231, 1987.

Poole, A.W.V., P.R. Sutcliffe and A.D.M. Walker, J. Geophys. Res., **93**, 14656, 1988.

Prakash, S., B.H. Subbaraya, and S.P. Gupta, Ind. J. Radio Space Phys., **1**, 72, 1972.

Prakash, S., and R. Pandey, Proc. Ind. Acad. Sci., **88A**, 229, 1979.

Prasad, S.S., L.J. Schneck, and K. Davies, J. Atmos. Terr. Phys., **37** 1357-1363, 1975.

Raghavarao, R., and B.G. Anandarao, Geophys. Res. Lett., **7**, 357, 1980.

Raghavarao, R., and B.G. Anandarao, Ind. J. Radio & Space Phys., **16**, 54, 1987.

Raghavarao, R., S.P. Gupta, R. Sekar, R. Narayanan, J.N. Desai, R. Sridharan, V.V. Babu, and V. Sudhakar, J. Atmos. Terr. Phys., **49**, 485, 1987.

Raghavarao, R., R. Sridharan, J.H. Sastri, V.V. Agashe, B.C.N. Rao, P.B. Rao, and V.V. Somayajulu, The Equatorial Ionosphere, WITS Hand book, **1**, 48, 1988.

Rajaram, T.N., J.N. Desai, S.S. Degaonkar, Proc. Ind. Acas. Sci., **88**, 69, 1979.

Raju, D.G.K., M.S. Rao, B.M. Rao, C. Jogulu, C.P. Rao, and R. Ramachandran, J. Geophys. Res., **86**, 5873-5880, 1981.

Rastogi, R.G., H. Chandra and S.C. Chakravarty, Proc. Ind. Aca. Sci.,**74**, 62-67, 1971.

Rastogi, R.G., Ann. Geophys., **28**, 717, 1972.

Rastogi, R.G., Planet. Space Sci., **21**, 1355, 1973.

Rastogi, R.G. and V.L. Patel, Proc. Indian Acad. Sci., **82A**, 121, 1975.

Reddi, C.R., and B.R. Rao, Radio Electronic Engrs., **34**, 53, 1967.

Reddi, C.R., Ph.D. Thesis, Andhra Univ., 1969.

Reddi, C.R., and B.R. Rao, J. Atmos. Terr. Phys., bf 33, 251, 1971.

Reddi, C.R., B.V.K. Murthy, K.S.V. Subbarao, K.P. Khosla, P.B. Rao, N. Balan, VSSC Tech. Rep. **46**, 1980.

Reddy, C.A. and C.V. Devasia, Nature, **261**, 396, 1976.

Reddy, C.A. and C.V. Devasia, J. Geophys. Res., **82**, 125, 1977.

Reddy, C.A., V.V. Somayajulu, and C.V. Devasia, J. Atmos.Terr. Phys., **41**, 189, 1979.

Reddy, C.A. and C.V. Devasia, J. Geophys. Res., **86**, 5751, 1981.

Reddy, C.A., B.T. Vikram Kumar and K.S. Viswanathan, J. Atmos. Terr. Phys., **49**, 183-191, 1987.

Reddy, C.A., PAGEOPH, **131**, 485, 1989.

Reddy, C.A., S. Fukao, T. Takami, M. Yamamota, T. Tsuda, T. Nakamura and S. Kato, J. Geophys. Res., **95**, 21077, 1990a.

Reddy, C.A. A. Nishida, S. Fukao, and V.V. Somayajulu, Geophys. Res. Lett., **17**, 2333, 1990b.

Reddy, C.A., and A. Nishida, J. Geophys. Res., **97**, 3039-3061, 1992.

Richmond, A.D., S. Matsushita, and J.D. Tarpley, J.Geophys, Res., **81**, 547, 1976.

Richmond, A.D., J. Geomag. Geoelectr., **31**, 287, 1979.

Richmond, A.D., M. Blanc, B.A. Emery, R.H. Wand, B.G. Fejer, R.F. Woodman, S. Ganguly, P. Amayenc, R.A. Behenke, C. Calderon and J.V. Evans, J. Geophys. Res., **85**, 4658, 1980.

Rigger, E.J. MPi/PAE -extraterr. 49/70, Max-Planck Institute for Physik and Astrophysik, Sep. 1970.

Rishbeth, H., and O.K. Garriott, Radio Sci. **68D**, 339, 1964.

Rishbeth, H. and O.K. Garriott, An Introduction to ionospheric physics, Int. Geophys. Ser., **14**, Academic Press, New York & London, Pages 199 - 204, 1969.

Rishbeth, H., Planet. Space Sci., **19**, 263-267, 1971.

Rishbeth, H., J. Atmos. Terr. Phys, **39**, 1159-1168, 1977.

Robinson, I., and P.L. Dyson, J. Atmos. Terr. Phys., **37**, 1459, 1975.

Rostoker, G., S.I. Akasofu, J. Foster, R.A. Greenwald, Y. Kamida, K. Kawasaki, A.T.Y. Lui, R.L. Mc Pherron, C.T. Russel, J. Geophys. Res., **85**, 1663-1668, 1980.

Rottger, J., J. Atmos. Terr. Phys., **35**, 1195, 1973.

Russell, C.T. and Fleming, B.K., J. Geophys. Res., **81**, 5882, 1976.

Sahai, Y., J.A. Bittencourt, H. Takahashi, N.R. Teixeira, B.A. Tinsley, and R.P. Rohr baugh, J. Atmos. Terr. Phys., **52** 749, 1990.

Sahai, Y., H. Takahashi, P.R. Gufundes, B.R. Clemesha, N.R. Teixeira and J.A. Bittencourt, Planet. Space Sci., **40**, 767, 1992.

Samson, J.C., J.A., Jacobs, and G. Rostoker, J. Geophys. Res., **76**, 497, 1971.

Sastri, J.H. and B.S. Murthy, J. Geomag. Geoelectr., **29**, 497, 1977.

Sastri, J.H., Ind. J. Radio & Space Phys., **9**, 209, 1980.

Sastri, J.H., Ann. Geophys., **2**, 353, 1984.

Sastri, J.H., Ann. Geophys. **6**, 635-642, 1988a,

Sastri, J.H., Planet.Space. Sci., **36**, 785-790, 1988b.

Sastri, J.H., K.B. Ramesh, D.R.K. Rao and J.V.S.V. Rao, Phys. Scri., **37**, 501-505, 1988.

Sastri, J.H., Planet.Space. Sci., **37**, 1403, 1989.

Sastri, J.H., Ind. J. Radio & Space Phys., **19**, 225, 1990.

Sastri, J.H. and H.N.R. Rao, J. Atmos. Terr. Phys., **56**, 775-782, 1994.

Sastri, J.H., J.V.S.V. Rao, and K.B. Ramesh, J. Geophys. Res., **98**, 17517, 1993.

Sato, T., Phys. Res. Lett., **28**, 732, 1972.

Saito, T., Space Sci. Rev., **21**, 427, 1978.

Schieldge, J.P., S.V. Venkateswaran and A.D. Richmond, J. Atmos. Terr.Phys., **35**, 1045, 1973.

Schrader, D.H., and A.D. Fraser, J. Atmos. Terr. Phys., **37**, 429-438, 1975.

Sengupta, K. and B.V. Krishnamurthy, Planet. Space Sci., **21**, 2227, 1973.

Senior, C. and M. Blanc., J. Geophys. Res., **89**, 1984.

Senior, C. and M. Blanc., Ann. Geophys., **5**, 405, 1987.

Sipler, D.P., and M.A. Biondi, Geophys. Res. Lett., **5**, 373-376, 1978.

Sipler, D.P., M.A. Biondi and R.G. Roble, Planet. Space Sci., **31**, 53, 1983.

Sleeper, A.M., and J. Weinstock, Phys. Fluids, **15**, 1507, 1972.

Smith, E.K., and S. Matsushita, (eds) Ionospheric Sporadic E, Int. Ser. of monographs on Electromagnetic waves, **2**, Pergamon Press, New York, 1962.

Sojka, J.J. and Schunk, R.W., J. Geophys. Res., **90**, 5285, 1985.

Somayajulu, V.V., C.A. Reddy, and K.S. Viswanathan, Geophys. Res. Lett., **12**, 473, 1985.

Somayajulu, V.V., C.V. Devasia, C.A. Reddy and K.S. Viswanath, Geophys. Res.Lett., **14**, 876, 1987.

Somayajulu, V.V., B.V.K. Murthy, and K.S.V. Subbarao, J. Atmos. Terr. Phys., **53**, 965-976, 1991.

Southwood, D.J., Planet Space Sci. **22**, 483-491, 1974.

Spencer, N.W., H.B. Niemann and G.R. Carignan, Radia Sci., **8**, 284, 1973.

Spiro, R.W., R.A. Wolf and B.G. Fejer, Ann. Geophys., **6**, 39, 1988.

Sridharan, R., S. Gurubaran, R. Raghavarao and R. Suhasini, J. Atmos. Terr. Phys., **53**, 515-519, 1991.

Srivastava, S.K., S.M. Pradhan, B. Singh, B.A.P. Tantry, Ind. J. Pure & Appl. Phys., **9**, 609, 1971.

Stening, R.J., J. Atmos. Terr. Phys., **39**, 1071, 1977.

Stening, R.J., J. Geophys. Res., **94**, 1525, 1989.

Stening, R.J., J. Atmos. Terr. Phys., **54**, 1387, 1992.

Subba Rao, K.S.V. and B.V. Krishnamurthy, Ind. J. Radio & Space Phys., **12**, 94, 1983.

Subbarao, K.S.V., and B.V. Krishnamurthy, J. Atmos. Terr. Phys., **56**, 59-65, 1994.

Sudan, R.N., J. Akiurimisi and D.T. Farley, J. Geophys. Res., **78**, 240, 1973.

Sudan, R.N., J. Geophys Res., **88**, 4853, 1983.

Sugiura, M. and J.C.Cain. J. Geophys. Res., **71**, 1869-1877, 1966.

Sugiura, M. and D.J. Poros, J. Geophys. Res., **74**, 4025, 1969.

Sutcliffe, P.R., and A.W.V. Poole, Geophys. Res. Lett., **11**, 1172, 1984.

Sutcliffe, P.R., and A.W.V. Poole, Planet. Space Sci., **38**,1581, 1990.

Takeda, M., and H. Maeda, J. Geophys. Res., **85**, 6895, 1980.

Tanaka, T., T. Ichinose, T. Okuzawa, T. Shibata, Y. Sato, C. Nagasawa and T. Ogawa, J. Atmos. Terr. Phys., **46**, 233-245, 1984.

Tedd, B.L., K.D. Cole and P.L. Dyson, Planet. Space Sci., **37**, 1079, 1989.

Tolstoy, I., and P. Pan, J. Atmos. Sci., **27**, 31, 1970.

Titheridge, J.E., and M.J. Buonsanto, J. Atmos. Terr. Phys., **45**, 683-696, 1983.

Tsutsui, M., T. Horikawa and T. Ogawa, J. Atmos. Terr. Phys., **46**, 233-245, 1984.

Tsutsui, M., T. Ogawa, Y. Kamide, H.W. Kroehl, and B.A. Hausman, Radio Sci., **23**, 119-128, 1988.

Vasyliunas, V.M., Earth's magnetospheric processes (ed. McCormac, B.M.), Page 29, D. Reidal, Dordrecht, 1972.

Vincent, R.A., J. Atmos. Terr. Phys., **34**, 1881, 1972.

Viswanathan, K.S., B.T. Vikramakumar and C.A. Reddy, J. Atmos. Terr. Phys., **49**, 193, 1987.

Wadlock, J.A., and T.B. Jones, J. Atmos. Terr. Phys., **48**, 245-260, 1986.

Walker, A.D.M., R.A. Greenwald, W.F. Stauart and C.A. Green, J. Geophys. Res., **84**, 3373, 1979.

Walker. G.O., J.H.K. Ma, R.G. Rastogi, M.R. Deshpande, and H. Chandra, J.Atmos. Terr. Phys., **42**, 629, 1980.

Walker G.O., J. Atmos. Terr. Phys., **93**, 763-774, 1981.

Walker, G.O., and H.F. Chan, J. Atmos. Terr. Phys., **51**, 953-974, 1989.

Walton. E.K., and A. Bowhill, J. Atmos.Terr. Phys., **41**, 937-950, 1979.

Watermann, J., J. Geophys., **61**, 39, 1987.

Watts, J.M., and K. Davies, J. Geophys. Res., **65**, 2295-2301, 1960.

Wolf R.A., R.W. Spiro and G.A. Mantjoukis, Adv. Space. Res. **6**, 177, 1986.

Woodman, R.F., J.Geophys. Res., **75**, 6216-6259, 1970.

Wrenn, G.L., J. Geophys. Res., **92**, 10125-10129, 1987.

Yomoto, K., K. Takahashi, T. Ogawa and T. Watanabe, J. Geomag. Geoelect., 41, 871, 1989.

Zamay, S.S., Geomag. Aeron., **29**, 104, 1989.